Linkage between catalytic mechanism and conformational dynamics in $(\beta\alpha)_8$-barrel enzymes at the example of Imidazole Glycerol Phosphate Synthase

DISSERTATION ZUR ERLANGUNG DES
DOKTORGRADES DER NATURWISSENSCHAFTEN (DR. RER. NAT.)
DER FAKULTÄT FÜR BIOLOGIE UND VORKLINISCHE MEDIZIN
DER UNIVERSITÄT REGENSBURG

vorgelegt von

Enrico Hupfeld

aus Thedinghausen

im Jahr 2020

Das Promotionsgesuch wurde eingereicht am: 12.06.2020

Die Arbeit wurde angeleitet von:

Prof. Dr. Reinhard Sterner

Unterschrift:

A goal is not always meant to be reached.
It often simply serves as something to aim at.

Bruce Lee

This work was done in the period from April 2015 to August 2019 in the group of Prof. Dr. Reinhard Sterner (Biochemistry II, Institute of Biophysics and Physical Biochemistry, University of Regensburg).

Table of contents

List of figures

List of tables

List of acronyms and abbreviations

TS	transition state
TIM	triose phosphate isomerase
NMR	nuclear magnetic resonance
MD	molecular dynamics
ProFAR	N'-[(5'-phosphoribosyl)-formimino]-5-aminoimidazole-4-carboxamide ribonucleotide
PrFAR	N'-[(5'-phosphoribulosyl)-formimino]-5-aminoimidazole-4-carboxamide ribonucleotide
ImGP	imidazole glycerol phosphate
AICAR	5-aminoimidazole-4-carboxamide-ribotide
ImGPS	imidazole glycerol phosphate synthase
LDH	lactate dehydrogenase
GDH	glutamate dehydrogenase
NAD	nicotinamide adenine dinucleotide
AMP	adenine monophosphate
GATase	glutamine amidotransferase
(sm)FRET	(single molecule) fluorescence energy transfer
EPR	Electron paramagnetic resonance spectroscopy
PRE	paramagnetic relaxation enhancement
RNA	ribonucleic acid
MCS	multiple cloning site
ORF	open reading frame
fwd	forward (primer)
rev	reverse (primer)
SDS	sodium dodecyl phosphate
PAGE	polyacrylamide gel electrophoresis
(ds)DNA	(double strand) deoxyribonucleic acid
IPTG	isopropyl-β-D-thiogalactopyranosid
LB	lysogeny broth
TB	terrific broth
dNTP	deoxy nucleotide triphosphate
IMAC	immobilized metal ion affinity chromatography
APS	ammonium persulphate
rpm	rotations per minute
UV	ultra violet
PCR	polymerase chain reaction
RT	room temperature
TEV	tobacco etch virus
CouA	L-(7-hydroxycoumarin-4-yl) ethylglycine
IDA	iminodiacetic acid
SEC	size exclusion chromatography
ATP	adenine triphosphate
DTT	dithiothreitol
PRPP	phosphoribosyl pyrophosphate

TEMED	tetramethylethylendiamine
GOX	glutamate oxidase
AAP	amino antipyrine
HRP	horseradish peroxidase
EDTA	ethylenediaminetetraacetic acid
MTSSL	(1-Oxyl-2,2,5,5-tetramethylpyrroline-3-methyl)methanethiosulfonate
M-TEMPO	4-Maleimido-2,2,6,6-tetramethyl-1-piperidinyloxy
RCT	rotational correlation time
TROSY	transverse relaxation optimized spectroscopy
TOCSY	total correlation spectroscopy
UAA	unnatural amino acid
ITC	isothermal titration calorimetry
RMSD	root mean square deviation

Abstract

Imidazole glycerol phosphate synthase (ImGPS) is a bienzyme complex from histidine biosynthesis, which consists of the cyclase subunit HisF and the glutaminase subunit HisH. In HisH, glutamine is hydrolysed to glutamate and ammonia, which is channelled through an intramolecular tunnel to the HisF active site, where it reacts with N'-[(5'-phosphoribulosyl)-formimino]-5-aminoimidazole-4-carboxamide ribonucleotide (PrFAR) to form imidazole glycerol phosphate (ImGP), a precursor of histidine, and 5-aminoimidazole-4-carboxamide-ribotide (AICAR), which is salvaged in purine biosynthesis. The two reactions are tightly coupled: HisH is strongly activated by the binding of PrFAR to HisF by a V-type allosteric mechanism to limit unproductive glutamine hydrolysis.

HisF adopts a $(\beta\alpha)_8$-barrel fold, the most common and versatile single domain fold in nature. Proteins with this fold are of particular interest to study fundamental principles of enzyme catalysis. One of these aspects is the connection between conformational dynamics and catalytic function. In the last few decades, this connection has become a major field of research and many examples have been found in which motions have a central role in the catalytic cycle of the respective enzyme.

The first part of this thesis is dedicated to the connection between catalysis and conformational dynamics, in particular of the $\beta_1\alpha_1$-loop (loop1) in HisF, which is in close proximity to the active site. This loop has previously been shown to be important for HisF activity and has been observed to adopt two distinct conformations in X-ray crystal structures called the open and closed conformations. Mutational analysis in this work identified several key amino acid residues within loop1 that are essential for catalysis. Specifically, the mutations G20P, G30P and F23A resulted in a complete loss or a drastic reduction of HisF activity. The two glycine residues appear to serve as hinges on which the loop can move to adopt different conformations. F23 probably serves as a hydrophobic anchor, which fixes the loop in the open conformation. NMR paramagnetic enhancement measurements confirmed that the open conformation is the main conformation in solution, for wild type HisF as well as HisF F23A and HisF G20P. Changes in loop dynamics for these two variants were confirmed with limited proteolysis and electron paramagnetic resonance spectroscopy.

To gain a deeper insight into HisF catalysis, transient ligand binding kinetics were recorded. Since the fluorescence of W156 of HisF proved unsuitable as a binding signal, the unnatural amino acid L-(7-hydroxycoumarin-4-yl) ethylglycine (CouA) was incorporated at position 132. The resulting variant HisF K132CouA showed wild-type like activity and a strong spectroscopic signal upon binding of all used HisF ligands. Stopped-flow measurements allowed for the determination of binding and dissociation rate for all ligands and a kinetic model for the entire ammonia dependent HisF reaction was formulated. The kinetic analysis also revealed an induced-fit type conformational motion upon PrFAR binding. This motions could not be observed for labelled variants carrying the mutations F23A or G20P, indicating that loop1 plays an integral role in this conformational change.

The second part of this thesis is concerned with the allosteric communication within ImGPS, specifically the stimulation of glutaminase activity in the HisH subunit. It was already previously recognized that conformational dynamics are of central importance for the transmission of the allosteric signal in ImGPS. Here, it could be shown that the flexible HisF loop1 has a strong influence on the activation of HisH. Mutations in loop1 that reduced HisF activity also decreased capability of HisF to stimulate HisH activity. Both effects appear to be coupled to the induced-fit type motion of loop1 after PrFAR binding. Moreover, also other residues outside loop1 were identified that play an important role in ImGPS allostery. Specifically, the crystal structure of the

mutant V48A, which was observed to reduce HisH stimulation in a previous study, led to the discovery of conformational changes of I7 and L169, two residues within the ammonia channel of HisF. Mutation of either residue led to a reduction in HisH stimulation.

Previously, two hypotheses have been proposed to explain the strong allosteric activation of HisH catalysis on a molecular level: The formation of the oxyanion hole and increased release of ammonia. A factor that has hitherto not been studied is whether the protonation states of catalytic H178 and C84 in HisH change during allosteric activation. Measurement of the pH-dependency of the HisH reaction allowed for the determination of two pK_a values which most likely correspond to these two residues. This conclusion was supported by measurements of the inactivation kinetics of HisH with the suicide inhibitor acivicin. NMR measurements with $^{13}C\varepsilon$ labelled H178 at physiological pH demonstrated that the catalytic histidine is protonated upon allosteric activation, which in turn stabilizes the deprotonated state of the catalytic cysteine. This change only manifested in the presence of glutamine and the PrFAR analogue ProFAR, indicating that both ImGPS substrates are needed for HisH to adopt the active conformation. It was hypothesized that the HisF residue D98, which is located within the interface with HisH, contributes the change of the protonation state of H178. Indeed, the mutation D98E, which mimics the approximation of the D98 carboxyl group to the active site of HisH led to a significant increase in both basal and ProFAR activated HisH activity. The closer proximity of the carboxyl group in the mutant D98E could be confirmed by X-ray crystallography. In a structure with bound glutamine and ProFAR, E98 shows an alternative conformation, which is an indication that it undergoes a conformational change during allosteric activation. While these results show that the tuning of the protonation of the catalytic residues in HisH is part of the activation mechanism, mutational analysis of V51 and the Ω-loop of HisH support the hypothesis that the correct formation of the oxyanion hole also makes a significant contribution to the stimulation of HisH. Thus, it appears that several factors contribute to HisH stimulation, highlighting the complex nature of allostery in this bienzyme complex.

Finally, measurements of the steady-state concentration of thioester intermediate carrying enzyme showed that both half-reactions, the formation and the hydrolysis of the thioester, are strongly accelerated during allosteric activation of HisH. This further supports the notion that allosteric activation influences a chemical factors that are important for both half-reactions.

In conclusion, the results presented in this thesis have revealed important information on the inner workings of the bienzyme complex ImGPS. Conformational dynamics are clearly of paramount importance both for the reaction catalyzed by HisF as well as for the allosteric activation of HisH. Further study of this intriguing system will undoubtedly increase our understanding of enzyme catalysis and enzyme complexes.

Zusammenfassung

Die Imidazolglycerinphosphatsynthase (ImGPS) ist ein Bienzymkomplex aus der Histidinbiosynthese, welcher aus der Cyclaseuntereinheit HisF und der Glutaminaseuntereinheit HisH besteht. In HisH wird Glutamin zu Glutamat und Ammoniak hydrolysiert, der dann durch einen intramolekularen Kanal zum aktiven Zentrum von HisF gelangt und dort mit N'-[(5'-phosphoribulosyl)-formimino]-5-aminoimidazol-4-carboxamid-Ribonukleotid (PrFAR) reagiert um Imidazolglycerinphosphat, ein Vorläufermolekül von Histidin, und 5-aminoimidazol-4-carboxamid-Ribotid (AICAR) zu bilden. AICAR wird in der Purin-Biosynthese wiederverwertet. Die beiden Teilreaktionen sind strikt gekoppelt: HisH wird durch die Binding von PrFAR in einem V-Typ allosterischen Mechanismus stark aktiviert um unproduktive Hydrolyse von Glutamin zu vermeiden.

HisF nimmt eine $(\beta\alpha)_8$-barrel Faltung an, die am verbreitetsten und vielseitigste einzelne Domänen-Faltung. Proteine mit dieser Faltung sind vom besonderem Interesse in Untersuchungen zu den grundlegenden Prinzipien von Enzymkatalyse. Einer dieser Aspekte ist die Verbindung zwischen konformationellen Bewegungen und der Katalysefunktion von Enzymen. In den letzten Jahrzehnten ist dies ein großes Forschungsgebiert geworden und viele Beispiele wurden gefunden in denen Bewegungen eine zentrale Rolle im katalytischen Zyklus der entsprechenden Enzyme einnehmen.

Der erste Teil dieser Arbeit ist dem Zusammenhang zwischen Katalyse und konformationellen Bewegungen, im Speziellen denen des $\beta_1\alpha_1$-loop (loop1) in HisF, welcher sich in unmittelbarer Nähe des aktiven Zentrums befindet, gewidmet. Es wurde bereits gezeigt, dass dieser *loop* von großer Bedeutung für die Aktivität von HisF ist. In Rötgenstrukturen wurde er in zwei verschiedenen Konformationen beobachtet, die die offene und die geschlossen Konformation genannt werden. In dieser Arbeit konnten mehrere Schlüssel-Aminosäuren durch Mutationsanalyse identifiziert werden. Besonders drastisch waren die Mutationen G20P, G30P und F23A, die zu einem kompletten Verlust oder einer drastischen Reduktion der HisF-Aktivität führten. Die zwei Glycin-Reste scheinen eine Art Scharnier zu bilden, das es dem *loop* erlaubt, unterschiedliche Konformationen einzunehmen. F23 dient vermutlich als hydrophober Anker, der den *loop* in der offenen Konformation fixiert. Durch paramagnetische Relaxationsverstärkung in NMR-Experimenten konnte gezeigt werden, dass die offene Konformation die häufigste Konformation in Lösung ist, sowohl für Wildtyp-HisF, als auch HisF F23A und HisF G20P. Änderungen in konformationeller Dynamik wurden für die zwei Varianten in limitierter Proteolyse und Elektronenspinresonanzspektroskopie nachgewiesen werden.

Um tiefere Einblicke in die Katalyse von HisF zu gewinnen wurden transiente Bindungskinetiken verschiedener Liganden aufgenommen. Da sich die intrinsische Tryptophanfluoreszenz als ungeeignete Sonde für Ligandenbindung erwies, wurde die unnatürliche Aminosäure L-(7-hydroxycoumarin-4-yl) ethylglycin (CouA) in Position 132 eingebracht. Die resultierende Variante HisF K132CouA zeigte wildtypische Aktivität und ein starkes spektroskopisches Signal bei Bindung aller HisF-Liganden. *Stopped-flow* Messungen erlaubten die Bestimmung von Bindungs- und Dissoziationsraten für alle Liganden und ein kinetisches Modell für die gesamte Ammoniak-abhängige HisF-Rekation wurde aufgestellt.

Die kinetische Bindungsanalyse konnte auch eine konformationelle Änderung in Form eines *induced fit* aufdecken. Da diese Bewegung in markierten Varianten mit den Mutationen F23A oder G20P nicht beobachtet werden konnte, liegt es nahe, dass loop1 eine wichtige Rolle in dieser konformationellen Veränderung einnimmt.

Der zweite Teil dieser Arbeit behandelt die allosterische Kommunikation innerhalb der ImGPS, genauer gesagt die Stimulierung der Glutaminase-Aktivität der HisH-Untereinheit. Es wurde schon in früheren Arbeiten gezeigt, dass konformationelle Dynamik von zentraler Bedeutung für

die Weiterleitung des allosterischen Signals in der ImGPS ist. Hier konnte gezeigt werden, dass der flexible loop1 in HisF einen starken Einfluss auf die Aktivierung von HisH hat. Mutationen, die HisF-Aktivität reduzieren, verringern auch die Fähigkeit von HisF, HisH-Aktivität zu stimulieren. Beide Effekte scheinen mit dem *induced fit* von loop1 nach PrFAR-Bindung verbunden zu sein. Darüber hinaus konnten auch andere Reste identifiziert werden, die an der Allosterie in der ImGPS beteiligt sind. Konkret führte die Analyse der Kristallstruktur der Mutante V48A, für die eine geringere HisH-Aktivierung in einer früheren Studie beobachtet wurde, zur Entdeckung von konformationellen Veränderungen in den Resten I7 und L169, zwei Resten im Ammonikkanal von HisF. Die Mutation beider Reste führt zu verringerter HisH-Aktivierung.

Zuvor wurden bereits zwei Hypothesen aufgestellt, die die starke Aktivierung von HisH auf der molekularen Ebene erklären: Die Ausbildung des Oxianionenlochs und eine gesteigerte Freisetzung von Ammoniak. Ein Faktor, der bis jetzt noch nicht betrachtet wurde, ist ob die Protonierungszustände der katalytischen Aminosäurereste H178 und C84 sich während der allosterischen Aktivierung ändern. Die Messung der pH-Abhängigkeit der HisH-Reaktion erlaubte die Bestimmung von zwei pK_S-Werten, die aller Wahrscheinlichkeit nach diesen zwei Resten zugeordnet werden können. Diese Schlussfolgerung konnte durch Messung der Inaktivierungskinetik mit dem irreversiblen Inhibitor Acivicin gestützt werden. NMR-Messungen mit $^{13}C\varepsilon$-markiertem H178 bei physiologischem pH zeigten, dass allosterische Aktivierung zur Erhöhung der Protonierung des katalytischen Histidins führt, was wiederum den deprotonierten Zustand des katalytischen Cysteins stabilisiert. Diese Änderung manifestiert sich nur in der Anwesenheit von sowohl Glutamin als auch dem PrFAR-Analog ProFAR, was ein starker Hinweise darauf ist, dass beide ImGPS Substrate benötigt werden, damit HisH die aktive Konformation ausbilden kann. Es wurde die Hypothese aufgestellt, dass der HisF-Rest D98, welcher sich in der Kontaktfläche mit HisH befindet, zur Änderung der Protonierung von H178 beiträgt. In der Tat konnte für die Mutante D98E, welche eine Annäherung der Carboxylgruppe von D98 an das aktive Zentrum von HisH nachahmt, eine signifikante Erhöhung der basalen als auch der durch ProFAR aktivierten HisH-Aktivität nachgewiesen werden. Die Annäherung der Carboxylgruppe konnte durch Röntgenkristallographie nachgewiesen werden. In einer Struktur mit gebundenem Glutamin und ProFAR zeigt E98 eine alternative Konformation, was zeigt, dass dieser Rest seine Konformation während der allosterischen Aktivierung verändert. Während diese Ergebnisse zeigen, dass die Protonierung der katalytischen Reste in HisH eine wichtige Rolle des Aktivierungsmechanismus sind, stützen Mutationsanalysen des Restes V51 sowie des Ω-loops die Hypothese, dass die korrekte Bildung des Oxianionenlochs einen signifikanten Beitrag zur Stimulierung von HisH leistet. Es scheint daher, dass mehrere Faktoren an der HisH-Stimulierung beteiligt sind, was die komplexe Natur der Allosterie in diesem Bienzymkomplex noch einmal unterstreicht.

Abschließend konnten Messungen der Konzentration an Enzym, welches das Thioester-Intermediat während des *steady-state* trägt, zeigen, dass beide Halb-Reaktionen von HisH, die Bildung des Thioesters und seine Hydrolyse, während der allosterischen Aktivierung stark beschleunigt werden. Dies unterstützt weiter die Annahme, allosterische Aktivierung Einfluss auf einen chemischen Faktor nimmt, der beide Halb-Reaktionen beeinflusst.

Zusammenfassend kann gesagt werden, dass in dieser Arbeit wichtige Informationen zur inneren Funktionsweise des Bienzymkomplexes ImGPS aufgedeckt wurden. Konformationelle Bewegungen sind offensichtlich von außerordentlicher Bedeutung, sowohl für die von HisF katalysierte Reaktion als auch für die allosterische Aktivierung von HisH. Weitere Studien dieses faszinierenden Systems werden mit Sicherheit unser Verständnis von Enzymkatalyse und Enzymkomplexen weiter verbessern.

1 Introduction

1.1 Enzyme catalysis

The catalysis of chemical reactions is one of the key functions of proteins in all living organisms.[1] Chemical reactions progress from the educt(s) (or substrate(s) in enzymatically catalysed reactions) via a transition state (TS) to the product(s). As indicated by the energy difference between substrates and products (Fig. 1), enzyme catalysed reactions are thermodynamically favourable, but are kinetically impaired by the high activation energy $\Delta G^{\ddagger}$, the difference between the substrate ground state and the TS of the reaction. According to transition state theory, the rate enhancement in enzymes (and all other catalysts) is achieved by the stabilization of the TS.[2] Enzymes catalyse the synthesis and degradation the vast plethora of molecules occurring in nature, some of which are chemically extremely challenging, in a region- and enantioselective manner. The most remarkable observation is that they achieve this relying on a minimum of different chemical principles. Most enzymes use general acid-base catalysis[3] or nucleophilic attacks. The use of cofactors allows for hydride[4] or electron transfers[5] and in rare cases, radical reactions.[6] Also, electrostatical factors play an important role, most importantly in enzymes using metal ions as cofactors.[7,8] The catalytic activity of an enzyme is usually measured via its steady state kinetics as it was introduced by Michaelis and Menten.[9] From such measurements the turnover number (k_{cat}), which is the maximum catalytic rate divided by the enzyme concentration, and the Michaelis constant (K_M), which is a first approximation of a measure for substrate affinity, of an enzyme can be determined. The catalytic efficiency is defined as k_{cat} (unit: s^{-1}) divided by K_M (unit: M) and thus has the unit $M^{-1}s^{-1}$.

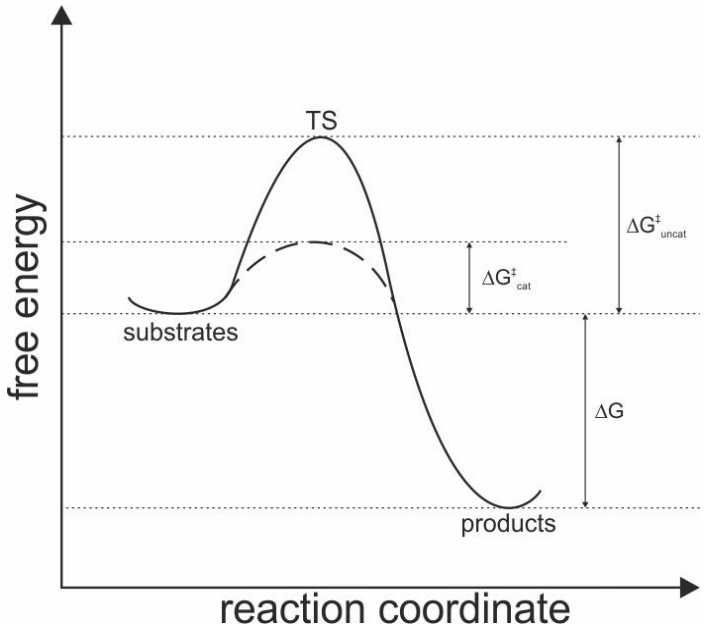

Fig. 1: Energy diagram of a chemical reaction. The substrates have a higher energy than the products, yielding a negative reaction free energy ΔG. The difference from the substrates to the transition state (TS) is called the activation energy $\Delta G^{\ddagger}$. This energy leads to a kinetic barrier. Enzymes (and all other catalysts) enhance the kinetic rate by lowering the activation energy from $\Delta G^{\ddagger}_{uncat}$ to $\Delta G^{\ddagger}_{cat}$.

Enzymes can accelerate chemical reactions by many orders of magnitude.[1] Comparatively simple reactions that also occur spontaneously in solution, such as isomerizations, can reach the diffusion limit, i.e. the diffusion and "meeting" of enzyme and substrate become rate limiting.[10] These enzymes are also known as "perfect enzymes". A prime example of this is triose phosphate isomerase (TIM), which reaches a catalytic efficiency of up to 10^9 $M^{-1}s^{-1}$.[11] Other reactions that are more demanding do not occur spontaneously. For instance, in the biosynthesis of cholesterol, all four cycles of the final product are formed in a single step catalysed by lanosterol synthase.[12] The substrate oxidosqualene is a linear molecule that is "folded" into the right conformation by the enzyme and by general acid/base catalysis a cascade of intramolecular nucleophilic attacks is set in motion, forming four new carbon-carbon bonds and four new steric centres in a highly specific manner.[13] As this is one of the most complex enzymatic reactions known to date, no rate can be determined for the uncatalysed reaction, as it is most unlikely that such a reaction would happen "by accident".

The efficiency of enzymes and their versatility in the synthesis of a vast number of molecules make them a highly interesting target for industrial applications.[14] Most enzymes work at ambient temperature in aqueous solutions at neutral pH and are therefore energy and cost efficient as well as environmentally friendly. While there are already examples of applications of enzymes as commercial catalysts[15,16], the field is still dominated by classical organic chemistry. The main reason for this is that it is still not well understood what exactly makes enzymes such outstanding catalysts and thus the tuning of enzymes for desired reactions is often very difficult. Many reaction mechanisms have been elucidated and factors that enable enzyme catalysis have been identified by structural analysis. However, this has yet to translate into an understanding that is sufficient to rationally design enzymes that are efficient catalysts. *De novo* designs have yielded active enzymes, but their catalytic efficiency is several orders of magnitude lower when compared to natural enzymes.[17–19] Acceptable activity, at least up to date, is only achieved by the randomized approach of directed evolution[20,21], which adds a large experimental effort to the already considerable computational workload. Directed evolution experiments use random mutagenesis either of the entire gene or of specific positions and have produced several enzyme catalysts with activities that rival and sometimes even surpass natural enzymes.[22] Using this process, it could be shown that some proteins can catalyse unnatural reactions and can be optimised to perform them.[23] However, the applicability of these efforts is strongly limited by pre-existing, promiscuous activities and the needed screening effort.

The ultimate goal that has to be achieved in order to effectively apply enzymes as catalysts is the understanding of rate acceleration in such detail that enzymes can be designed for any reaction at will. This goal however is still far off. The lack of understanding of enzyme catalysis stems from the enormous complexity of the systems. In order to better understand the amazing molecular machines that enzymes are we still need to gather more information on the elusive processes within enzymes that are not yet understood.

1.2 Enzymes as dynamical entities

One of the factors in enzyme catalysis that is still subject of considerable research efforts is protein dynamics. If and to which extent dynamics are of relevance to the catalysis of enzymes is still under considerable and highly controversial debate. However, some of these issues appear to root in misunderstandings in terminology and definitions as well as different perspectives and the study of several enzymes showing distinct dynamical behaviour.[24] It should be noted at this point that in the context of this work, all conformational protein motions are referred to as dynamics. Their influence on catalysis is not necessarily meant in the sense of actual chemical catalysis, i.e. the lowering of the activation energy, but also in structural rearrangements that are essential for efficient enzyme function and can thus become rate limiting to the reaction by factors other than lowering the kinetic barrier of the reaction.

Over the last decades, a large amount of structural data on proteins has been gathered.[25] Although this information is indispensable to gain insight into the molecular details of enzyme catalysis and other protein functions, most of this data has been collected in X-ray crystallography experiments that only capture a single snapshot in the "life" of a protein.[26] Also, crystallization is hardly a natural process for most proteins and can lead to structural distortions which in turn may lead to flawed interpretations.[27,28] The static nature of structural information and difficulties in studying dynamic effects on the molecular level have led to protein dynamics being neglected for a long time.[29] It is quite intuitive that proteins, being chains of amino acids that are more or less loosely folded into a 3D structure by non-covalent interactions, are inherently flexible and that this flexibility has implications for protein function. Several theories have been proposed to account for protein dynamics in protein function and, more specifically, enzyme catalysis.

The simplest way to think of enzyme catalysis is in a "lock-and-key" model (Fig. 2), which does not account for protein dynamics.[30–32] This model suggests that the binding site is always perfectly formed for ligand binding. For enzymes, this model is sometimes also called "preorganization".[33] The assumption of this concept is that the active site reduces the activation energy of the reaction by providing a pre-arranged environment ideally suited for catalysis.[34,35] Since this implies that the active site is already ideally formed to perform catalysis, the substrate can transition into the TS quite rapidly after binding, since no further rearrangement is needed. This model is related to the theory of near attack conformations[36], which states that there are reactive conformations of the substrates that are stabilized by the enzyme, thus facilitating the reaction. While this second model accepts a dynamical nature of the substrate, it does not necessarily account for movements of the enzyme.

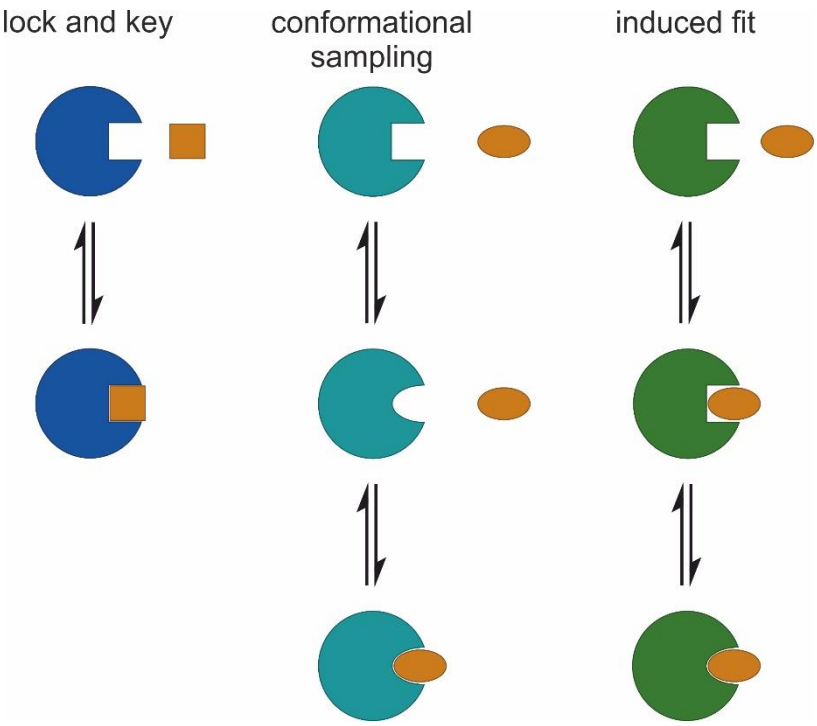

Fig. 2: Schematic representation of ligand binding modes. In the lock-and-key-model, the correct protein conformation is permanently present and can bind the ligand. Induced-fit implies that the protein conformation changes after ligand binding, whereas in conformational sampling, the protein is in a conformational pre-equilibrium with only on ligand binding competent conformation.

The theories mentioned above certainly explain what happens in the moment of actual catalysis and describe some enzyme systems very well. However, in other cases protein motions have to take place in order to enable two or more protein conformations relevant to catalysis. For instance, quite obviously, substrate binding needs the active site to be accessible to solvent in order for the substrate to enter. One requirement for some reactions is however the shielding of the reactive state from solvent. Therefore, closing of the active site after substrate binding can be highly beneficial to the reaction. Different protein conformations relevant for ligand binding can be adopted in one of or a mixture of two mechanisms: Conformational sampling and induced fit (Fig. 2).[37–39] Conformational sampling on the one hand refers to the case that the enzyme always exists in an equilibrium of two states. The substrate can bind to only one conformation, which would constitute the active conformation in enzymes. Induced fit on the other hand, was already proposed by Koshland[37], at a time when it was not even certain that proteins are flexible at all. Put to the extreme, this model suggests that the enzyme is permanently in an open conformation when no substrate is bound and the closed conformation is induced by substrate binding. In both cases, the conformational transition is often rate-limiting for the overall reaction, conformational changes being slow compared to the chemical reaction rates of most enzyme-catalysed reactions. Examples can be found that behave as an ideal for either model, but naturally there are also proteins that behave in a mixture, i.e. there is already a conformational equilibrium and the closed state is stabilized by ligand binding. In the light of the ongoing debate on the relevance of protein dynamics it is important to understand that some researchers consider these motions non-dynamical since they are in equilibrium and as such do not contribute to catalysis in an energetic sense, i.e. that they provide the energy to lower the activation barrier. Still, these effects can undisputedly have a profound impact on the rate of an enzymatic reaction and on the binding affinity of the substrate, due to kinetic restrictions of the rate of movement.

These three theories explain some aspects of enzyme catalysis very well, albeit macroscopically. It has however been observed that the molecular motions of proteins occur on a multitude of size scales and thus over a timescale of several orders of magnitude.[40,41] In some select cases, their functional relevance has been unveiled, which often extends to far more complicated scenarios that the opening or closing of an active site. However, in many proteins, the exact influence of many of these motions is still not well understood and may vary greatly from enzyme to enzyme.

The molecular motions occurring in proteins can be categorized according to the timescale on which they take place (Fig. 3). Motions in the fs–ps range are generally very small motions, such as bond vibrations or vibrations of bond angles (indicated as small energy barriers in Fig. 3A). Motions in the ns–ms range include side chain rotations, movements of small loops or other small conformational rearrangements (intermediate energy barriers in Fig. 3A). Larger movements such as the movement of large loops or even entire domains occur on the scale of µs–ms and even seconds (e.g. interconversion of conformation A and B in Fig. 3A). For each case, these particular motions can be of significant importance for the function of the respective proteins. Bond vibrations for instance limit the rate of chemical reactions in general since the maximal rate for the breaking and reforming of a covalent bond is the rate of the bond vibration. In some enzymes, such as dihydrofolate reductase[42] and cyclophilin A[43] it has been suggested that small vibrations of amino acid residues actually accelerate the rate limiting step of the reaction. This however is a topic under intense debate and is not conclusively resolved to date.[44,45] On the other end of the size scale, larger domain movements can also be beneficial for catalysis. One example is anthranilate phosphoribosyl transferase (TrpD).[46] This enzyme is a prime example of stabilizing near attack conformations, since it does not actually possess any catalytically active amino acid residues, but rather accomplishes catalysis by binding the two substrates, anthranilate and phosphoribosyl pyrophosphate, upon which its two domains close and bring the substrate molecules into close proximity in the correct orientation for the reaction to occur.[47,48]

The experimental study of molecular motions in proteins is often challenging. Fig. 3B gives a rough overview of available methods and the motions they can study. NMR spectroscopy can access many different timescales with the added advantage of a more physiological setting since samples are measured in solution.[49] X-ray crystallography is a very powerful tool and time resolved experiments are in principle not limited in the time scale, however experiments are dependent on protein crystallization, which is in many cases not trivial and provides a less physiological setting.[50] Spectroscopic methods using light absorption or emission are the least complex experiments, but give more limited information, especially in the sense of atomic details and are thus sometimes not straightforward in their interpretation.[51] The highest detail is certainly provided by computational methods like molecular dynamics (MD) simulations. These methods are however strongly limited by available computation power and are thus restricted in both timescale (computational effort) and atomic detail (simplification to enable longer simulation times).[52,53]

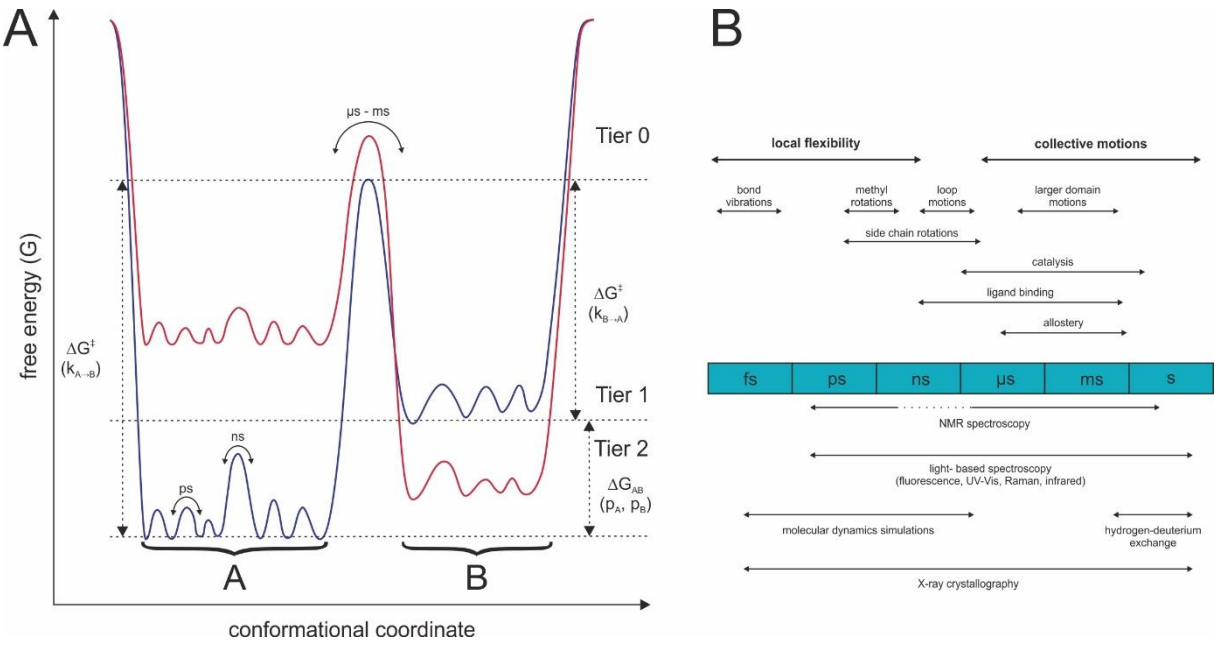

Fig. 3: Schematic representation of the relevant timescales of protein dynamics. (A) One dimensional cross-section of the multi-dimension energy landscape of a protein, categorizing motions into tiers according to their energetic level, which determines their respective rates.[41] The major conformations A and B on tier 0 are minima in the energy landscape. The population of these states (p_A, p_B) follow a Boltzmann distribution and are defined by the energy difference ΔG_{AB}. The kinetic rate of interconversion is determined by the activation energy $\Delta G^{\ddagger}$. Conformational changes on tiers 1 and 2 are smaller fluctuations on the ns-ps timescale. Influences such as the binding of a small molecule or protein interaction partner can shift the conformational equilibrium as indicated by the differences between the blue and red curves by stabilizing one and/or destabilizing another conformation. (B) Scheme of physiologically relevant timescales (cyan boxes) of protein motions. Movements that take place on these timescales are indicated by arrows above and relevant methods which can probe dynamics on respective timescales are indicated with arrows below. The figure was adapted from Henzler-Wild and Kern[40] and Boehr et al.[49]

1.3 Loop dynamics in enzyme catalysis

Somewhere in the middle of the timescale of molecular movements in proteins are the rotations of amino acid side chains and movement of small loops. Quite obviously, the rotamers of catalytically active amino acid side chains are of central importance for enzyme catalysis, since their orientation towards the substrate molecule(s) determines if reactions, such as protonations, can take place and if important interactions can be formed.

The role of loop conformations is not always so readily apparent. Still, in a number of enzymes it has been observed that loops proximal to the active site play an important role in catalysis and their role is reasonably well understood for some cases. Especially enzymes with the $(\beta\alpha)_8$-barrel (or TIM-barrel after its first member with known three dimensional structure triose phosphate isomerase) fold have provided intriguing case studies linking loop dynamics and enzyme catalysis. The $(\beta\alpha)_8$-barrel fold is probably the most common fold of proteins in general and enzymes in particular. About 10 % of all proteins with known structure contain at least one domain of this fold and reactions from 5 of the 6 EC classes have been found to be catalyzed by $(\beta\alpha)_8$barrel enzymes.[54–58] One of the reasons for the versatility of this fold is probably that it shows a structural separation of the so-called activity pole and stability pole. The $(\beta\alpha)_8$-barrel fold consists of alternating β-strands and α-helices (Fig. 4A), which are arranged in a central β-barrel surrounded by the α-helices (Fig. 4B). The stability pole is found at the C-terminal end of the β-strands and the activity pole on the opposite side, the N-terminal end of the β-strands. The eight-fold repetition of β-strand and α-helix leads to the presence of eight connecting loops, the βα-loops, which form the active site in most $(\beta\alpha)_8$-barrels and are highly variable in sequence.[59,55] For these reasons, the $(\beta\alpha)_8$-barrel fold is believed to be the most versatile fold for enzyme catalysis and has thus been used as a scaffold for several *de novo* enzyme design studies.[60,17,18] Also, enzymes of this fold have provided valuable insights into the connection between catalysis and loop motions.[60–63] Since protein stability is mainly provided by the stability pole, the active site containing the βα-loops has a relatively large mutational freedom which is advantageous for the evolution of new functions.

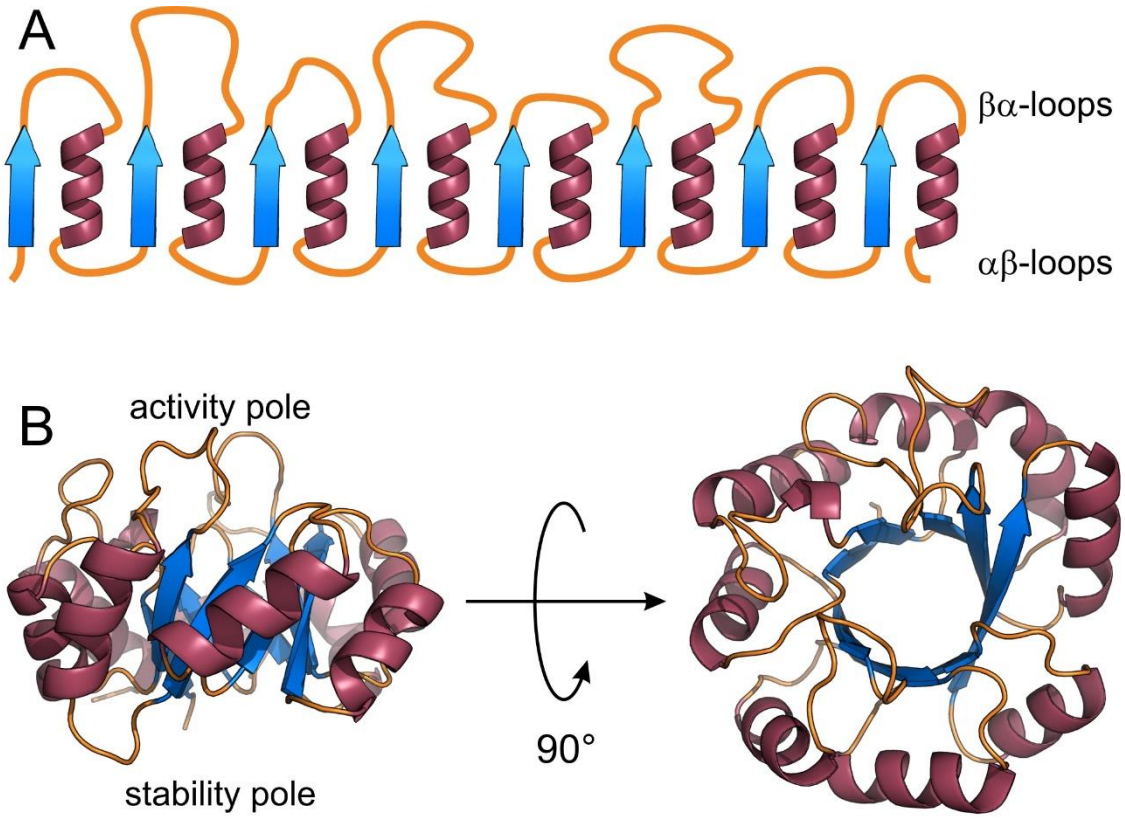

Fig. 4: The $(\beta\alpha)_8$-barrel fold. (A) Outline of secondary structure elements. The fold is made up of eight repetitions of one β-strand and one α-helix each, which are connected by βα-loops of different lengths and short αβ-loops. (**B**) Outline of tertiary structure. The C-terminal activity pole contains the βα-loops, which form the catalytic centre. The N-terminal stability pole is formed by the usually short αβ-loops.

The significance of active site loop movements for catalysis has been demonstrated for three different $(\beta\alpha)_8$-barrel enzymes, one from glycolysis (TIM) and two from amino acid biosynthesis (TrpC, HisA):

The βα-loop connecting β-strand 6 and α-helix 6 (active site loop 6) in TIM has long been thought to be a simple "lid" for the active site, which shields the bound substrate from bulk solvent and thus lowers the dielectric constant, enabling general base catalysis of a glutamate residue.[64] A recent study found, however, that the loop can adopt several conformations and that already slight displacement in the completely closed conformation leads to disruption of catalysis. This example highlights that loops can play an important role in catalysis without carrying residues actually being involved in the chemical transformation step.[65]

Indole glycerol phosphate synthase (TrpC) is an enzyme involved in tryptophan biosynthesis. TrpC from *Saccharolobus solfataricus* (until recently *Sulfolobus solfataricus*), a thermophilic archaeon growing optimally at 80 °C, shows significantly reduced catalytic activity at ambient temperatures when compared with homologues from mesophilic organisms. This has been shown to be the result of a relatively rigid active site loop 6, which only gains the proper mobility at higher temperatures and leads to product release becoming rate limiting at low temperatures. The catalytic rate can also be enhanced by mutagenesis which renders the loop more flexible.[66]

HisA from *Salmonella enterica*, an enzyme from histidine biosynthesis, catalyses the isomerisation of N'-[(5'-phosphoribosyl)-formimino]-5-aminoimidazole-4-carboxamide ribonucleotide (ProFAR) to N'-[(5'-phosphoribulosyl)-formimino]-5-aminoimidazole-4-carboxamide ribonucleotide (PRFAR). It has been observed in several crystal structures with bound ProFAR that the active site loops 1, 2, 5 and 6 can adopt two distinct conformations. In the

open conformation, no interactions with the substrate molecule are present indicating that initial binding of ProFAR is independent of the loops. However, in the closed conformation, the loops move the substrate into a more product-like conformation and therefore into the optimal substrate orientation for catalysis.[67]

An example of an enzyme with a different fold is lactate dehydrogenase (LDH), which catalyses the reversible interconversion of lactate and pyruvate with the help of the NAD(H) cofactor. In this enzyme, catalysis is strongly regulated by opening and closing of an active site loop (residues 98 to 110).[68] The loop is essential for the chemical conversion, since it excludes water from the active site and optimises its conformation for catalysis. This is facilitated by the essential residue R109 within the loop, which directly coordinates the substrate molecule and is critical for catalysis of LDH due to its electrostatic interactions with the catalytic residue H195.[69]

1.4 Allostery

The activity of enzymes within a cell can be tuned on several distinct levels. First of all, the amount of active enzyme can be controlled by regulation of transcription of its gene, translation and degradation of the respective mRNA and protein degradation.[70] However, these processes consume a lot of energy and are comparatively slow. It is for this reason that enzymes are often also regulated on the activity level, for instance by product inhibition to prevent overproduction or by the availability of the substrate.[71]

In many cases, enzymes are regulated by a process called allostery. This term was introduced by Monod and colleagues and describes an effect on the functional site of a protein that is exerted by binding of an effector to the so-called allosteric site, which distant to the functional site.[72] These allosteric effects can be transmitted over distances from a few Å to 30 Å or even more. A typical example for allosteric regulation is the inhibition in a so-called feedback mechanism.[73,74] This regulatory tool is used to ensure that if the final product of a biosynthetic pathway is available in sufficient amount, the pathway is effectively shut down to allow the usage of the educts in other syntheses. While allosteric effectors are usually small molecules, ions or protein interaction partners, other effects such as external factor like light, post-translational modifications and mutations can exert their influence allosterically, as well.[75] The structural paths within a protein along which the allosterically coupled sites are connected are known as allosteric pathways.[76]

Since the term allostery is rather general, several types are distinguished. The first examples of allosteric behaviour were discovered in oligomeric binding proteins, which often show so-called positive cooperativity (Fig. 5A). For instance, the binding of an O_2 molecule to one subunit of tetrameric hemoglobin induces a high affinity state, which is transmitted to the other three subunits of the complex via an allosteric mechanism.[77] The counterpart to positive cooperativity is negative cooperativity (Fig 4A), in which the binding of one ligand reduces affinity for further ligand binding. Cooperativity in binding leads to characteristic alterations of the macroscopic binding behaviour (Fig. 5B), which can be beneficial for the specific requirements of an organism. Cooperativity has been described mathematically by several researchers, the most popular and widely known equation is however the Hill-equation.[78] The binding affinity of proteins can of course also be influenced by other allosteric effectors, such as 2,3-bisphosphoglycerate and bicarbonate in hemoglobin.

Enzymatic activity can also be allosterically activated or inhibited. Since both substrate binding and chemical turnover contribute to the efficiency of an enzyme, K-type and V-type allostery are distinguished. K-type allostery refers to an effect on the K_M value of the enzyme, i.e. substrate binding (Fig. 5C), while V-type allostery refers to an influence the velocity of catalysis.[79] Fig. 5D demonstrates how the steady-state kinetics of an enzymatic reaction are changed by the different types of allostery.

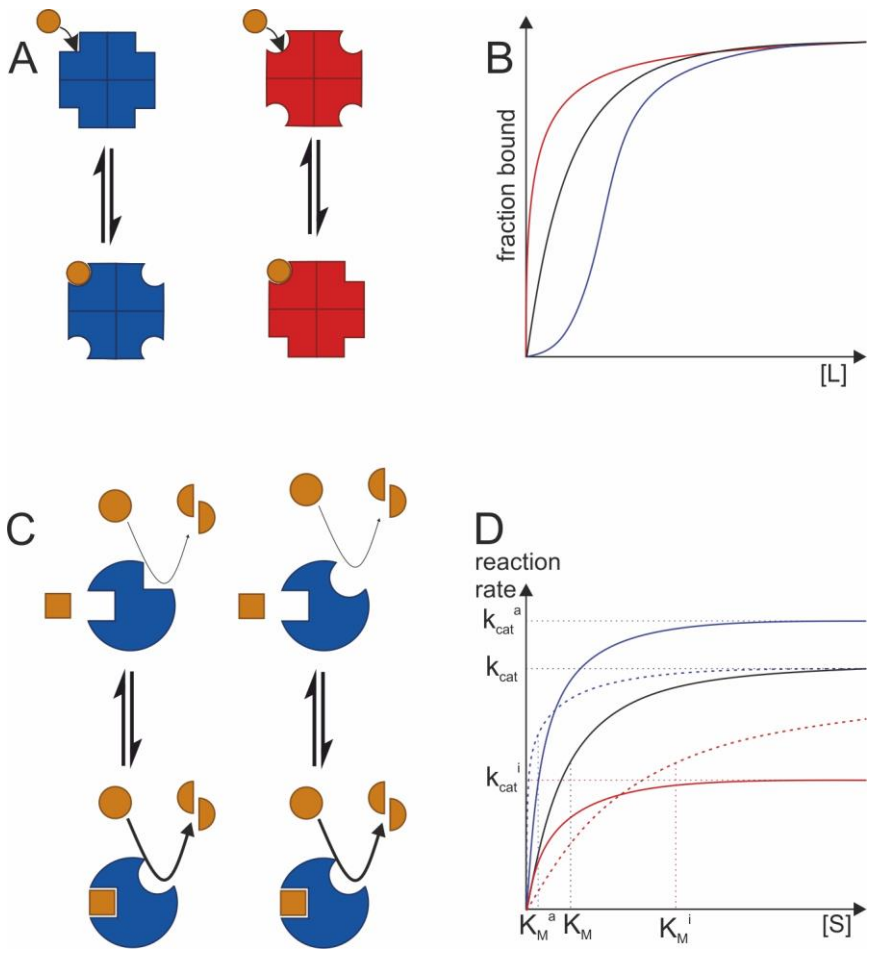

Fig. 5: Simplified allosteric models. (A) Schematic representation of a binding protein complex showing positive (blue) and negative (red) cooperativity in ligand binding. In positive cooperativity, binding of the ligand (orange) to a low affinity binding site induces a high affinity state in all subunits, whereas in negative cooperativity the high affinity for the ligand is reduced in all binding sites upon binding to the first site. **(B)** Binding curves resulting for a binding with positive (blue), negative (red) or no (black) cooperativity. **(C)** Schematic representation of an enzyme (blue) showing K-type (left) or V-type (right) allosteric activation. Binding of the effector (orange square) induces a higher affinity for the substrate (orange circle) for K-type activation. In V-type activation, the substrate binding is unaffected, and increase in activity is achieved by an increase in catalytic rate. Both kinds of activation lead to a higher net activity (indicated by a bold reaction arrow). **(D)** Michaelis-Menten kinetics for different kinds of allosteric behaviour. Activation (blue lines) is achieved by increasing the turnover number k_{cat} to k_{cat}^{a}(V-type, solid line) or lowering the K_M value to K_M^{a} (K-type, dashed line). Similarly, an enzyme can be inhibited (red lines) by lowering k_{cat} to k_{cat}^{i} (V-type, solid line) or increasing K_M to K_M^{i} (K-type, dashed line).

The view on the mechanistic basis of allostery has changed drastically over the years since the discovery of this effect and many aspects are still under considerable debate.[80,81] The atomistic details of allostery are based on different principles, depending of the protein in question. Some studies found a series of conformational rearrangements responsible for the observed allosteric effect with a defined allosteric pathway. A good example of allostery that is explained well by these observations is the afore mentioned cooperative oxygen binding in haemoglobin. This conformational change is transmitted via the F-helix, which is pulled towards the O_2 binding site and thus mediates the change to the neighbouring subunit.[82] Other studies suggest that in some systems the transmittance of the allosteric signal is based on the change in protein dynamics. For example, the negative cooperativity of the catabolite activator protein is driven by protein motions between the binding sites for cyclic AMP in the two subunits.[83]

1.5 Glutamine amidotransferases

A good example of allosteric communication between two subunits of an enzyme complex is the family of glutamine amido transferases (GATases). These bienzyme complexes are of central importance for the incorporation of nitrogen atoms into biomolecules.[84–86] After becoming bio-available by nitrate reduction or dinitrogen fixation, nitrogen is generally used in the form of ammonia to synthesize alanine, aspartate, glutamate or glutamine. From these molecules it can be transferred to other molecules, e.g by transaminases.

In every reaction catalysed by a GATase, a nitrogen atom is incorporated into a substrate molecule by transfer of ammonia from glutamine.[87] To this end, glutamine is hydrolysed in the glutaminase subunit (or domain), producing glutamate and ammonia. The ammonia is then channelled through an intermolecular tunnel to the active site of the synthase subunit (or domain) where it reacts with a substrate molecule specific for each GATase. This channelling effectively avoids unproductive diffusion of ammonia into the cytoplasm and protonation by solvent. GATasas are allosterically regulated in that substrate binding in the synthase subunit stimulates the hydrolysis of glutamine in the glutaminase subunit to avoid unproductive glutamine turnover.[88,89]

GATases are grouped into two unrelated classes according to the catalytic residues used in the glutaminase subunit. Class I GATases possess a glutaminase with the α/β hydrolase fold and a catalytic Glu-His-Cys triad. In contrast, class II GATases belong to the family of N-terminal nucleophile hydrolases and accomplish catalysis via a conserved N-terminal Cys residue.[86,90] Class I GATases are involved in various biosynthetic processes and in accordance with the diversity of the substrates, the synthase subunits adopt a wide variety of folds and possess very different catalytic mechanisms.[91–95] The glutaminase mechanism (Fig. 6), however, is common to all class I glutamine amidotransferases. It relies on the nucleophilic attack of the catalytic cysteine residue in its thiolate form on the carboxamide carbon of glutamine. The reactive thiolate form is stabilized by the neighbouring histidine, whose positive charge is in turn stabilized by a glutamate residue. The reaction progresses via an oxyanion to a thioester intermediate, which is hydrolysed in a similar reaction, which shows a second oxyanion intermediate. Both oxyanion states are stabilized by amides from protein backbone known as the oxyanion hole. The initial establishing of the charged state of the catalytic cysteine and histidine is possibly a result of direct deprotonation of the cysteine by the histidine, but might also be pre-established previous to glutamine binding.

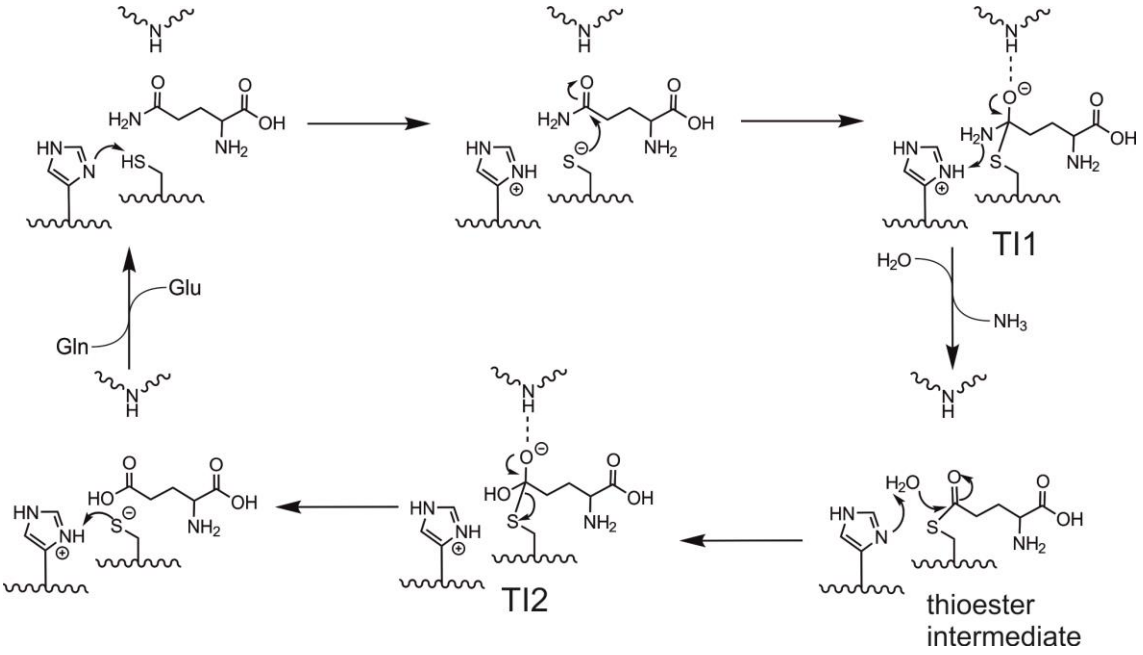

Fig. 6: Common glutaminase mechanism of class I glutamine amido transferases. Starting from the top left corner, the reaction starts with the deprotonation of the catalytic cysteine by the catalytic histidine residue (it is also possible that the protonation states are pre-established by solvent). The thiolate anion can then attack at the glutamine carboxamide carbon (top middle) leading to the first tetrahedral oxyanion intermediate (TI1, top right corner), which is stabilized by at least one protein backbone amide termed the oxyanion hole. Protonation of the leaving ammonia leads to the formation of a thioester intermediate (bottom right corner). This thioester is removed in a hydrolysis reaction similar to the first half-reaction. The attack of a water molecule results in the formation of a second tetrahedral oxyanion intermediate (TI2, bottom middle), the resolution of which leads to the final formation of glutamate. The figure was adapted from Thoden et al.[95].

1.6 Imidazole glycerol phosphate synthase

Imidazole glycerol phosphate synthase (ImGPS) is a part of the enzymatic pathway of *de novo* histidine biosynthesis.[96] It belongs to class I GATases and catalyses the fifth step of the pathway, the formation of the histidine imidazole ring, by turning over the substrate PrFAR to imidazole glycerol phosphate (ImGP) and 5-aminoimidazole-4-carboxamide-ribotide (AICAR).[97] ImGP is further processed to histidine and AICAR is salvaged in purine biosynthesis. Crystal structures of ImGPS enzymes from different organisms show that the synthase subunit HisF adopts a $(\beta\alpha)_8$-barrel fold and the glutaminase subunit HisH the α/β hydrolase fold typical for class I GATases (Fig. 7).[98] These two subunits are found to form a bi-enzyme complex in bacteria, while in eucaryotes, they are fused into a single polypeptide chain called His7.[96,97,99]

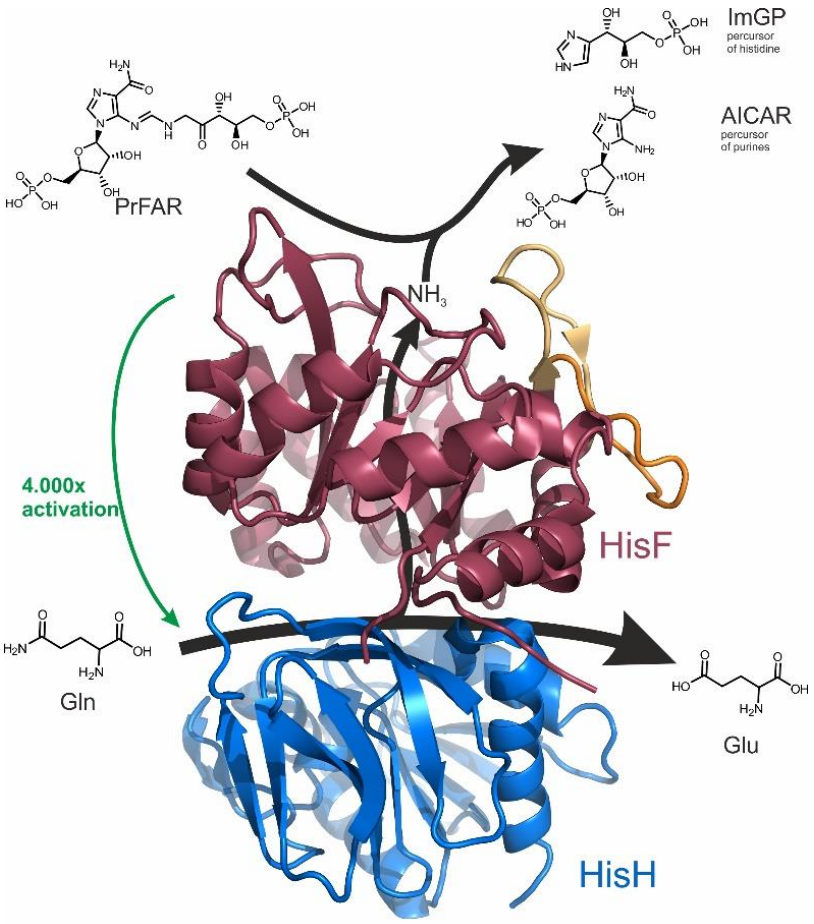

Fig. 7: The imidazole glycerol phosphate synthase form *T. maritima*. The synthase (or cyclase) subunit HisF (red) turns over the substrate PrFAR to ImGP and AICAR. ImGP is further processed into histidine and AICAR is salvaged in purine biosynthesis. The ammonia necessary for the reaction is generated by the glutaminase subunit HisH (blue). To avoid unproductive glutamine hydrolysis, HisH glutaminase activity is strongly activated upon PrFAR binding in HisF. The ammonia is shielded from solvent to prevent loss or protonation by means of channelling through a hydrophobic channel. The position of HisF loop1 is shown for the open (from PDB-ID 1VH7, orange) and closed (from PDB-ID 1GPW, beige) conformations.

The reaction catalyzed by the cyclase subunit HisF is quite complex, showing steps typical for a C-N ligase, C-N lyase and C-N cycloligase. The catalytic amino acids have been identified to be two aspartate residues in the enzyme from *Thermotoga maritima* and a plausible reaction mechanism based on general acid-base catalysis has been proposed (Fig. 8).[100] The reaction of the glutaminase has been confirmed to rely on the conserved triad Glu-His-Cys.[101] While the glutaminase reaction in HisH is strictly dependent on the presence of the HisF subunit, it was shown that the HisF subunit is also fully functional in isolated form when supplied with an external ammonia source such as ammonium salts at high pH.[100]

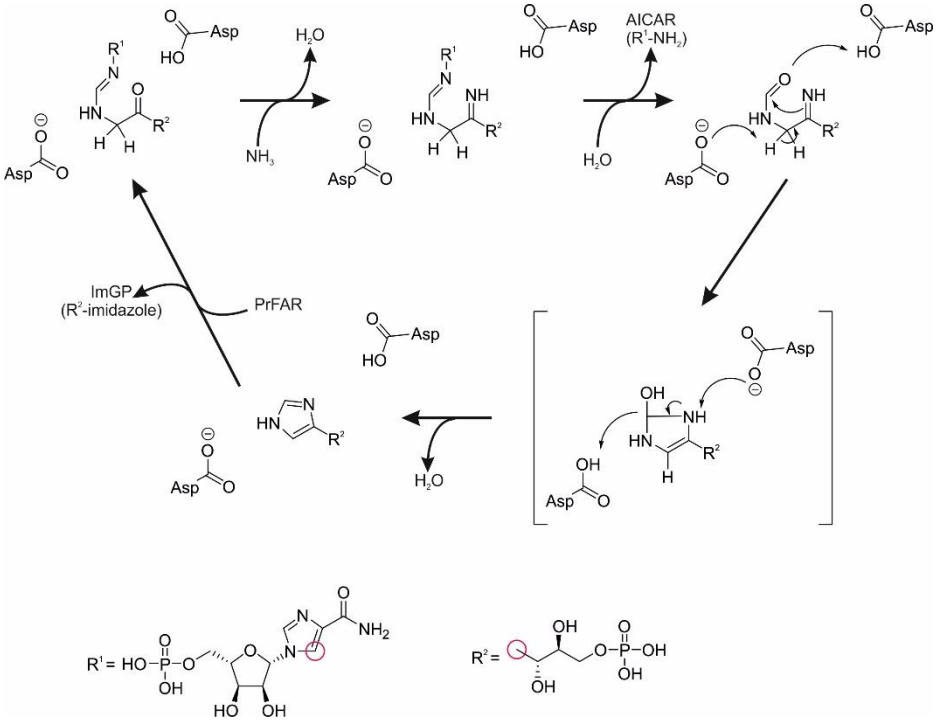

Fig. 8: Catalytic cylce of HisF. The reaction is initiated by the nucleophilic attack of ammonia at the carbonyl carbon of PrFAR under the formation of an imine. Subsequently, AICAR is cleaved of by spontaneous hydrolysis. The resulting aldehyde is subject to a nucleophilic attack by the imine and the ensuing cyclisation reaction is facilitated by two aspartate residues. After elimination of a water molecule, the imidazole ring is formed to yield the product ImGP. For clarity, the AICAR and glycerol phosphate portions of PrFAR are abbreviated as R^1 and R^2, respectively. The atoms at which R^1 and R^2 are attached to the rest of the molecule are marked with red circles. The figure was adapted from Beismann-Driemeyer and Sterner.[100]

A striking characteristic of ImGPS is that its glutaminase subunit HisH is strongly activated in a V-type manner by the cyclase subunit HisF upon PrFAR binding and is almost inactive without this allosteric activation.[97,100] Although all GATases show allosteric behaviour to minimize unproductive glutamine hydrolysis, the 4000-fold activation observed in ImGPS is the largest effect that has been observed in any GATase to date. Several hypotheses have been proposed to explain this phenomenon at the atomic level. For instance, studies on the nature of the allosteric signal revealed that there is a correlation between molecular motions on the ms timescale in the HisF subunit and the activity of the HisH subunit, suggesting that the allosteric signal is transmitted via these motions.[102] The authors concluded that the transmittance of this flexibility leads to the breaking of a hydrogen bond to allow the amide of V51 to turn into the HisH active site to form the oxyanion hole.[103,102,104] In another study it was found that the mutation of two large HisH residues in proximity to the HisH active site (Y138 and K181) to alanine leads to a high basal HisH activity. It was suggested that the unblocking of the active site allows ammonia to exit the active site more easily, which leads to the observed rate enhancement.[105] As of yet, the exact conformational nature of the active state of HisH is not known, structural data only being available in absence of allosteric activators. While there is a structure of the yeast enzyme with the HisF substrate PrFAR, this complex was formed by soaking and the authors state that the observed conformation is not likely to be the final and active conformation.[106] It is thus still not clear which exact molecular changes take place in the HisH active site to achieve allosteric activation. Recent NMR studies showed that ImGPS adopts two distinct conformations, one of which is assumed to be the active conformation.[107] The conversion between the two states is in the same range of seconds, which is similar to that of k_{cat} of the reaction, suggesting that this conformational change might be rate limiting overall. Interestingly, the active conformation is only adopted in the presence of both a HisF substrate analogue and the HisH substrate glutamine.

1.7 $\beta_1\alpha_1$loop in HisF from *T. maritima*

The $(\beta\alpha)_8$-barrel enzyme HisF protein from *T. maritima* possesses a relatively long and flexible active site $\beta_1\alpha_1$-loop (loop1), which is located between β-strand 1 and α-helix 1. It has been observed in previous research that this loop has a profound effect on ImGPS function.[108] Deletion of the loop leads to a drastic reduction in HisF activity.[108] Also, a highly conserved lysine residue (K258, corresponding to K19 in ImGPS from *T. maritima*) located in this loop has been shown to be of relevance for activity in the yeast enzyme.[106] It was suggested that loop 1 exists in two conformations, the so-called open and closed conformations as observed in several crystal structures of the *T. maritima* enzyme.[109,58] Recently, fluorescence resonance transfer (smFRET) single molecule measurements showed that loop1 indeed exists in an equilibrium of at least two conformations also in solution. The distances measured via smFRET match the open and closed conformations observed in crystal structures very well.[110] However, while binding of the substrate PrFAR appeared to populate the closed conformation, the analysis of several HisF mutants did not yield a clear correlation between the amount of a certain conformation and catalytic activity.

Also, loop1 from HisF has been ascribed a role in allosteric communication with HisH. It has been observed that the loop shows higher flexibility in the full ImGPS complex when compared with the isolated HisF protein.[100] However, the role of loop1 in allostery has not yet been studied in further detail.

2 Scope of this thesis

ImGPS is an essential bi-enzyme complex from histidine biosynthesis. Despite extensive studies, the complex reaction the ImGPS catalyses is still not well understood. Also, the mechanism of allosteric communication remains enigmatic. Since it has been observed in other enzymes that active site loops can play a crucial role in their function and this has also been demonstrated for ImGPS by the deletion of HisF loop1, this thesis aims to promote the understanding of the ImGPS catalysis by more detailed analysis of the relationship of the conformational dynamics of HisF loop1 and ImGPS function. For this purpose, one target is to gain detailed kinetic information on the individual steps of catalysis, as well as on the conformations that loop1 adopts in solution and its dynamical behaviour. A more detailed knowledge of ImGPS catalysis will help to better understand the complex relationship of protein dynamics, allostery and enzyme catalysis.

To deepen the understanding of the influence of loop1 on ImGPS function, an extensive mutational analysis was performed to identify essential amino acid residues. Furthermore, the conformation and flexibility of loop1 was analysed by a combination of several methods, including NMR and electron paramagnetic resonance (EPR).

In order to put the functional implications of loop1 mutations into a relationship with the reaction mechanism, HisF catalysis was analysed by means of rapid mixing fluorescence spectroscopy. For this purpose, a spectroscopic signal of ligand binding was established by the incorporation of an unnatural fluorescent amino acid and the influence of the label on catalysis was tested. On the basis of this data insights into the microscopic rate constants of the wild-type HisF reaction were gained, as well as the influence of loop1 by analysis of two HisF variants with altered loop dynamics.

Finally experiments were performed to gain insight on the allosteric activation of HisH. This included the characterisation of allosterically impaired variants and a spectroscopic approach to measure conformational changes. Also, experiments on the molecular mechanism of HisH activation were performed and are discussed in the context of existing hypotheses as well as a novel proposal.

3 Materials and Methods

3.1 Materials

3.1.1 Appliances and multi-use materials

Item	Model	Manufacturer
Autoclave	Series EC Stream Sterilizer	Webeco, Selmsdorf
Cell density meter	Ultrospec 10	GE Healthcare, München
Centrifuges	5810R 5414R 5415D Avanti J-26 XP	Eppendorf, Hamburg Eppendorf, Hamburg Eppendorf, Hamburg Beckmann Coulter, Krefeld
Chromatography system	Äkta prime Äkta start Äkta purifier 10	GE Healthcare, München
Chromatography column	HisTrap FF crude 5 ml Mono Q 5/50 GL Supderdex 75 HiLoad 26/600	GE Healthcare, München
Fluorescence spectrometer	FP-6500	Jasco GmbH, Groß-Umstadt
Glass pipettes and other glassware		Fisher Scientific, Schwerte Novoglas, Bern, Switzerland Schott, Mainz
Gel electrophoresis system (agarose)		Hoefer Pharmacia Biotetch, USA
Gel electrophoresis system (PAGE)	Mighty small II Multi Gel Caster	Hoefer Pharmacia Biotetch, USA
Heat-block thermostat	HBT-2 131	HLC, Bovenden
Incubator		Binder GmbH, Tuttlingen
Microliter pipettes	Research	Eppendorf, Hamburg
Nanopore water system	Ultrafree-20	Milipore, Eschborn
Imaging System	Multi-Doc-It digital	UVP Inc., USA
NMR spectrometer	Advance-800	Bruker, USA
PCR cyclers	Mastercycler personal Mastercycler EP gradient	Eppendorf, Hamburg
pH meter	Level1	Inolab, Weilheim
Pipetting robot for crystallisation screens	Mosquito LCP	TTP Labtech, Melbourn, UK
Quartz cuvettes		Hellma GmbH & Co KG, Müllheim
Scales	MC1 PL3000 SI-114	Satorius, Göttinger Mettler Toledo, Gießen Denver Instrument, Göttingen
Shaking incubators	Ceromat H Multitron	Braun Biotech, Melsungen Infors HT, Bottmingen, Switzerland
Ultrasonic system	Branson Sonifier 250 D	Heinemann, Schwäbisch Gmünd
UV-vis spectral photometer	V650 V750 Nanodrop One	Jasco GmbH, Groß-Umstadt Thermo Fisher Scientific Inc., USA
UV-Vis Biospectrometer		Eppendorf, Hamburg

3.1.2 Single use items

Item	Manufacturer
Easy Xtal plates	Qiagen, Hilden
Centrifugal filter devices (Amicon Ultra)	Miliproe, USA
Dialysis tubing Visking, 27/32, 14 kDa	Roth GmbH & Co, Kralsruhe
Disposable Syringes Omnifix ®, 50, 10, 5, 2.5 and 1 ml	B. Braun Biotech, Melsungen
Dialysis tubing Visking, 27/32, 14 kDa	Roth GmbH & Co, Karlsruhe
Laboratory film Parafilm M	Pechiney, USA
NAP5 and NAP10 columns	GE Healthcare, München
Nitrile gloves	Roth GmbH & Co, Karlsruhe
Nitrocellulose filters (Ø 13 mm)	Milipore, Eschborn
Pasteur pipettes	Hirschmann, Ebermannstadt
PCR tubes 0.2 ml	Peqlab, Erlangen
Pertri dishes 94/16	Greiner bio-one, Nürtingen
Pipette tips	Sarstedt, Nümbrecht
Plastic cuvettes 1ml	Sarstedt, Nümbrecht
Plastic tubes, 15 ml and 50 ml	Sarstedt, Nümbrecht
Reaction vessels 1.5 ml and 2 ml	Sarstedt; Nümbrecht
Syringe filters, pore sizes 0.2 µm and 0.45 µm	Renner GmbH, Daunstadt

3.1.3 Chemicals

All chemicals used had the highest available purity and were purchased form the following vendors:

Amersham Pharmacia Biotech	Freiburg
Applichem GmbH	Darmstadt
Bio 101 Inc.	Carlsbad, USA
Biorad Laboratories	München
Biozym	Hess. Oldendorf
Bode Chemie	Hamburg
Boehringer Mannheim	Mannheim
Carl Roth GmbH Co. KG	Karlsruhe
Cayman Chemicals	Ann Arbor, USA
Difco	Dreieich
Fluka	Neu-Ulm
GE Healthcare	Mümchen
Gerbu Biotechnik GmbH	Gailberg
Gibco/BRL	Eggestein
Iris Biotech GmbH	Marktredwitz
Merck	Darmstadt
MP Biochemicals	Illkirch, France
National Diagnostics	Simerville, USA
Oxoid	Wesel
Roche Diagnostics	Mannheim
Serva	Heidelberg
Sigma Aldrich	Deisenhofen

3.1.4 Kits

Kit	Manufacturer
Bradford reagent	Biorad Laboratories, München
GeneJET Plamid Minprep Kit	MBI Fermentas, St-Leon-Rot
GeneJET Gel Extraction Kit	MBI Fermentas, St-Leon-Rot
Morpheus II crystallisation screen	Molecular dimensions, UK
ProPlex crystallisation screen	Molecular dimensions, UK

3.1.5 Enzymes

Enzyme	Manufacturer
BsaI restriction endonuclease	NEB, Frankfurt am Main
Glutamate dehydrogenase	Merck, Darmstadt
Glutamate oxydase	Merck, Darmstadt
Horseradish peroxidase (HRP)	Merck, Darmstadt
NdeI restriction endonuclease	NEB, Frankfurt am Main
Phusion DNA polymerase	NEB, Frankfurt am Main
Q5 DNA polymerase	NEB, Frankfurt am Main
TEV protease	In huose production
HisA (from *T. maritima*)	In house production
T4 DNA ligase	MBI Fermentas, St-Leon-Rot
XhoI restriction endonuclease	NEB, Frankfurt am Main

3.1.6 Bacterial strains

***E. coli* Turbo** (NEW ENGLAND BIOLABS, Frankfurt a. M.)

F' *proA*$^{+}$*B*$^{+}$ *lacI*^{q} *Δ(lacZ)M15/fhuA2 Δ(lac-proAB) glnV gal R(zgb-210::Tn10)* Tet^{s} *endA1 thi-1 Δ(hsdS-mcrB)*

E. coli Turbo cells are T1-phage resistant. As the *rec*A function of the strain is intact, *E. coli* Turbo cells grow fast and form visible colonies after 8 h incubation at 37° C.

***E. coli* BL21-Gold (DE3)** (Agilent Technologies)
*hsd*S *gal* [λ cl *ts*857 *cnd*1 *hsd*R17 *rac*A1 *end*A1 *gyr*A96 *thi*1 *rel*A1] *E. coli* BL21(DE3)
E. coli BL21-Gold (DE3) cells carry a gene for T7 RNA polymerase on their chromosome, which is used for gene expression in pET systems. *E. coli* BL21-Gold (DE3) are improved versions of BL21 cells. Derived from *E. coli* B, these expression strains naturally lack the Lon protease, which can degrade recombinant proteins. In addition, these strains are engineered to be deficient for a second protease, the OmpT protein.

***E. coli* BL21-CodonPlus(DE3)-RIPL** (Stratgene)

F^- *ompT hsdS*(r_B^- m_B^-) *dcm*$^+$ *Tet*^{r} *gal* λ(DE3) *endA Hte* [*argU proL Cam*^{r}] [*argU ileY leuW Strep*/*Spec*^{r}]

E. coli BL21-CodonPlus(DE3)-RIPL cells carry a gene for T7 RNA polymerase on their chromosome, which is used for gene expression in pET systems. *E. coli* BL21-Gold (DE3) are improved versions of BL21 cells. Derived from *E. coli* B, these expression strains naturally lack the Lon protease, which can degrade recombinant proteins. In addition, these strains are engineered to be deficient for a second protease, the OmpT protein. This strain carries a plasmid encoding for the tRNA synthethases of rare tRNAs with rare condons to improve translation of genes that have a suboptimal codon usage for expression in *E. coli*.

3.1.7 Plasmids

Genes inserted into the multiple cloning site (MCS) of pET vectors (plasmids for expression by T7 RNA Polymerase) are transcribed by the RNA-polymerase of the phage28 T7.[111] The expression of genes takes place in special *E. coli* strains, which carry a chromosomal copy of the T7 RNA polymerase. The expression of the T7 RNA polymerase gene proceeds under the control of the *lac*UV5 promotor operator and is induced by the addition of IPTG. The gene for the *lac*-repressor (*lac*I), which is required for suppression of gene expression in the absence of induction, is located on the plasmid and is constitutively expressed.

The plasmid pET28_BsaI was modified for cloning with the restriction enzyme BsaI in a golden gate cloning procedure.[112,113] It carries an N-terminal $(His)_6$-tag and was further modified by the insertion of a TEV cleavage site, which allows for the proteolytic removal of the $(His)_6$-tag.[114] The final vector is named pET28_BsaI_TEV in this work. The plasmid confers a kanamycin resistance. The vector pET21a encodes a C-terminal $(His)_6$-tag and also confers a kanamycin resistance.

The pEVOL plasmid is used for the production of proteins labelled with a non-canonical amino acid incorporated via the amber stop codon suppression method.[115,116] It carries two copies of the gene for the aminoacyl-tRNA synthetase for the specific amino acid, one under the control of the constitutive glnS promoter and one under the araBAD promoter, which can be induced by arabinose. Additionally, the plasmid encodes the tRNA with the anti-codon recognizing the amber stop codon and confers a chloramphenicol resistance.

Plasmid	**gene**
pET28_BsaI_TEV	wild-type and all mutants of *hisF* and *hisH* wild-type and all mutants
pET21a	*hisA* from *T. maritima*
pEVOL	*mjTyrRS-CouA*[117]

3.1.8 Oligodeoxynucleotides

Vector specific amplification and sequencing primers

Oligonucleotide	Sequence (5' → 3')	use
T7 promoter	TAATACGACTCACTATAGGG	sequencing, colony PCR
T7 terminator	GCTAGTTATTGCTCAGCGG	sequencing, colony PCR
pEVOL ORF1-fwd	CGGATCCTACCTGACGC	sequencing
pEVOL ORF1-rev	TGATGACCGGGAGCTCAC	sequencing
pEVOL ORF2-fwd	GTTAGATTATCAATTTTA AAAAACTAACAG	sequencing
pEVOL ORF1-rev	CCTACAAAAGCACGCAAACTC	sequencing

Construction of pEVOL-CouA

Oligonucleotide	Sequence (5' → 3')	use
pEVOL ORF1 ex fwd	AAAAAAGGTCTCCTAAGCG AGAGTAGGGAACTGC	Cloning of CouA-RS into pEVOL
pEVOL ORF1 ex rev	AAAAAAGGTCTCACATGAG ATCTAATTCCTCCTGTTAGCC	Cloning of CouA-RS into pEVOL
pEVOL ORF2 ex fwd	AAAAAAGGTCTCCTAAGTG CAGTTTCAAACGCTAAATTGCC	Cloning of CouA-RS into pEVOL
pEVOL ORF2 ex rev	AAAAAAGGTCTCACATGTGG GATTCCTCAAAGCGTAAAC	Cloning of CouA-RS into pEVOL

Amplification and mutagenesis primers of *hisF*

Oligonucleotide	Sequence (5' → 3')	use
tmHisF fwd	AAAAAAGGTCTCCCATGC TCGCTAAAAGAATAATC	Cloning of *hisF* into pET28_BsaI_TEV
tmHisF rev	AAAAAAGGTCTCACTTAC AACCCCTCCAGTCTC	Cloning of *hisF* into pET28_BsaI_TEV
tmHisF I7A fwd	GCGGCGTGTCTCGATGTG AAA	Introducing of mutation I7A
tmHisF I7A rev	TATTCTTTTAGCGAGCATA TGG	Introducing of mutation I7A
tmHisF C9S fwd	AGCCTCGATGTGAAAGAC GG	Introducing of mutation C9S
tmHisF C9S rev	CGCGATTATTCTTTTAGCG A	Introducing of mutation C9S
tmHisF R16A fwd	GCGGTGGTGAAGGGAACG AACTTCGAA	Introducing of mutation R16A
tmHisF R16A rev	ACCGTCTTTCACATCGAGA CACG	Introducing of mutation R16A
tmHisF V18A fwd	GCGAAGGGAACGAACTTC GAAAAC	Introducing of mutation V18A
tmHisF V18A rev	CACACGACCGTCTTTCAC	Introducing of mutation V18A
tmHisF K19A fwd	GCGGGAACGAACTTCGAA AACCTCAGG	Introducing of mutation K19A

tmHisF rev	K19A	CACCACACGACCGTCTTTC AC	Introducing of mutation K19A
tmHisF fwd	G20A	GCGACGAACTTCGAAAAC CTCAGGGAC	Introducing of mutation G20A
tmHisF rev	G20A	CTTCACCACACGACCGTCT TTCA	Introducing of mutation G20A
tmHisF fwd	G20P	CCGACGAACTTCGAAAACC TCAGGGAC	Introducing of mutation G20P
tmHisF fwd	T21G	GGCAACTTCGAAAACCTCA GGGACAGCG	Introducing of mutation T21G
tmHisF rev	T21G	TCCCTTCACCACACGACCG TCTTT	Introducing of mutation T21G
tmHisF fwd	T21P	CCGAACTTCGAAAACCTCA GGGACAGCG	Introducing of mutation T21P
tmHisF fwd	N22A	GCGTTCGAAAACCTCAGGG ACAGCGGT	Introducing of mutation N22A
tmHisF rev	N22A	CGTTCCCTTCACCACACGA CC	Introducing of mutation N22A
tmHisF fwd	F23A	GCGGAAAACCTCAGGGAC AGCGGTG	Introducing of mutation F23A
tmHisF rev	F23A	GTTCGTTCCCTTCACCACA CGAC	Introducing of mutation F23A
tmHisF fwd	F23V	GTGGAAAACCTCAGGGAC AGCGGTG	Introducing of mutation F23V
tmHisF fwd	F23I	ATTGAAAACCTCAGGGAC AGCGGTG	Introducing of mutation F23I
tmHisF fwd	F23M	ATGGAAAACCTCAGGGACA GCGGTG	Introducing of mutation F23M
tmHisF fwd	F23L	CTGGAAAACCTCAGGGACA GCGGTG	Introducing of mutation F23L
tmHisF fwd	E24P	CCGAACCTCAGGGACAGCG GTGATC	Introducing of mutation E24P
tmHisF rev	E24P	GAAGTTCGTTCCCTTCACCA CACG	Introducing of mutation E24P
tmHisF fwd	E24C	TGCAACCTCAGGGACAGC	Introducing of mutation E24C
tmHisF E24C fwd	F23A	GCGTGCAACCTCAGGGACA	Introducing of mutations F23A and E24C
tmHisF E24C	G20P	CCGACGAACTTCTGCAACC TCAGGGAC	Introducing of mutation G20P and E24C
tmHisF fwd	D28A	GCGAGCGGTGATCCTGTCG AACTGG	Introducing of mutation D28A
tmHisF rev	D28A	CCTGAGGTTTTCGAAGTTC GTTCC	Introducing of mutation D28A
tmHisF fwd	G30A	GCGGATCCTGTCGAACTG GGAAAGTTCTATT	Introducing of mutation G30A
tmHisF rev	G30A	GCTGTCCCTGAGGTTTTCG AAGTTC	Introducing of mutation G30A
tmHisF fwd	G30P	GCGGATCCTGTCGAACTG GGAAAGTTCTATT	Introducing of mutation G30P
tmHisF fwd	Y39F	TTTTCCGAAATTGGAATA GACGAACTCGTT	Introducing of mutation Y39F
tmHisF rev	Y39F	GAACTTTCCCAGTTCGAC AGGATC	Introducing of mutation Y39F

tmHisF V48A fwd	GCGTTTCTGGATATCACC GCGTCC	Introducing of mutation V48A
tmHisF V48A rev	GAGTTCGTCTATTCCAAT TTCGGA	Introducing of mutation V48A
tmHisF I52A fwd	GCGACCGCGTCCGTTGA GA	Introducing of mutation I52A
tmHisF I52A rev	ATCCAGAAAAACGAGTT CGTC	Introducing of mutation I52A
tmHisF D98E fwd	GAAAAGGTGAGCATAAA CACGG	Introducing of mutation D98E
tmHisF D98E rev	CGCACCACGGAGAAT	Introducing of mutation D98E
tmHisF K132amber fwd	TAGAGAGTGGATGGAGA GTTC	Introducing of amber codon
tmHisF K132amber rev	GGTGAAGACCATGAACT CT	Introducing of amber codon
tmHisF S144G fwd	GGCGGAAAGAAGAACA CGGGCATA	Introducing of mutation S144G
tmHisF S144G rev	GTAGGTGAAGACCATGA ACTC	Introducing of mutation S144G
tmHisF K146A fwd	GCGAAGAACACGGGCAT ACTTCT	Introducing of mutation K146A
tmHisF K146A rev	TCCGGAGTAGGTGAA GACCA	Introducing of mutation K146A
tmHisF Δ146 fwd	TGCATCTATCGCCACG	Deletion of K146
tmHisF Δloop5 fwd	GGAAACACGGGCATA CTTCTGAG	Deletion of Y143 and K146
tmHisF Δloop5 rev	GGAGGTGAAGACCAT GAACTCTC	Deletion of Y143 and K146
tmHisF L169A fwd	GCGACCAGTATCGAC AGAGAC	Introducing of mutation L169A
tmHisF L169A rev	CAGGATCTCTCCTGC TC	Introducing of mutation L169A
tmHisF H228A fwd	GCGTTCAGAGAGATC GACGTGAGAGAAC	Introducing of mutation H228A
tmHisF H228A rev	AAAGACAGAAGCCG CAAGGGC	Introducing of mutation H228A
tmHisF F229A fwd	GCGAGAGAGATCGA CGTGAGAGAACTGA	Introducing of mutation F229A
tmHisF F229A rev	GTGAAAGACAGAAG CCGCAAGG	Introducing of mutation F229A

Amplification and mutagenesis primers for *hisH*

Oligonucleotide	Sequence (5' → 3')	use
tmHisH fwd	AAAAAAGGTCTCAGATG CTCGCTAAAAGAATAATC	Cloning of *hisH* into pET28_BsaI_TEV
tmHisH rev	AAAAAAGGTCTCACGAG CTATCGCCGGGACAAC	Cloning of *hisH* into pET28_BsaI_TEV
tmHisH TEV-linker fwd	ATGCGCATTGGTATTATT AGC	Introduction of a two amino acid linker between HisH and TEV cleavage site
tmHisH TEV-linker rev	GCCCATCGCGCCCTGAA AATAAAGATTCTCG	Introduction of a two amino acid linker between HisH and TEV cleavage site
tmHisH delta loop1 fwd	GGCGGCAACATGAATC TGTATCGCGGAGTG	Deletion of residues 10 and 13 of HisH
tmHisH delta loop1 rev	AACAGAGATTATTCCG ATCCTCAT	Deletion of residues 10 and 13 of HisH
tmHisH V51P fwd	GTCCGGGTCATTTTGG TGAAGGTATG	Introduction of the mutation V51P
tmHisH V51P rev	CAGGAATAAACAGCA GATCATAC	Introduction of the mutation V51P
tmHisH H53A fwd	GTGCGTTTGGTGAAG GTATGCG	Introduction of the mutation H53A
tmHisH H53A rev	CAACACCAGGAATA AACAG	Introduction of the mutation H53A
tmHisH C84S fwd	AGCCTGGGTATGCAGC TGC	Introduction of the mutation C84S
tmHisH C84S rev	AACACCAACAACATAA CGTTC	Introduction of the mutation C84S
tmHisH C84A fwd	GCGCTGGGTATGCAGC TGC	Introduction of the mutation C84A
tmHisH Y136amber fwd	TAGTATTACTTTGTTCA TACCTATCGTG	Introduction of an amber stop-codon at position 136
tmHisH Y136amber rev	GCCGTTCGGAAAGG	Introduction of an amber stop-codon at position 136
tmHisH Y138A fwd	GCGTTTGTTCATACCTA TCGTGCC	Introduction of the mutation Y138A
tmHisH Y138A rev	ATAATAGCCGTTCGGA AAGG	Introduction of the mutation Y138A
tmHisH H178A fwd	GCGCCGGAAAAAAGC AGCAAA	Introduction of the mutation H178A
tmHisH H178A rev	AAACTGAAAACCCAG AATACG	Introduction of the mutation H178A
tmHisH K181A fwd	GCGAGCAGCAAAATT GGTCGTAAAC	Introduction of the mutation K181A
tmHisH K181A rev	TTCCGGATGAAACTG AAAACC	Introduction of the mutation K181A
tmHisF H178A K181A fwd	GCGCCGGAAGCGAG CAGCAAA	Introduction of the mutations H178A and K181A

3.1.9 Size and weight markers

The size of DNA fragments in agarose gels was estimated with the help of the GeneRuler 1bk DNA Ladder Plus (MBI Fermentas, St. Leon-Rot). The size of proteins in SDS PAGE gels was approximated with the Unstained Protein Molecular Weight marker Plus (MBI Fermentas, St. Leon-Rot).

3.1.10 Buffers and solutions

If not explicitly states otherwise, all buffers and solutions and solutions were prepared with MILIPORE water. Buffers were filtered through a 0.22 µM filter and stored at room temperature unless stated otherwise.

3.1.10.1 Work with *E. coli*

Antibiotics

Antibiotics were stored at -20°C long term and at 4°C short term.

Ampicilin (1000 x):	150 mg/ml ampicillin (sodium salt) in H_2O
Kanamycin (1000 x):	75 mg/ml kanamycin in H_2O
Chloramppheniсol (1000 x):	30 mg/ml chloramphenicol in 100% EtOH

IPTG stock	1M IPTG in H_2O, storage at -20°C
5 x M9$^-$ Salts	64 g $Na_2HPO_4 \cdot 7\ H_2O$, 15 g KH_2PO_4, 2,5 g NaCl, 5,0 g NH_4Cl, in H_2O, autoclaved
TFB I buffer:	100 mM KCl, 50 mM $MnCl_2$, 30 mM KOAc, 10 mM $CaCl_2$, 15% Glycerol. All stocks of the respective components were stored at room temperature and the buffer was freshly prepared before each use.
TFB II buffer:	100 mM Tris/HCl pH 7,0, 10 mM KCl, 75 mM $CaCl_2$. All stocks of the respective components were stored at room temperature and the buffer was freshly prepared before each use.

Cultivation media

For sterilization, media were autoclaved for 20 min at 121°C and 2 bar. For selective media the antibiotics were added after autoclaving and cooling of the media.

Lysogeny broth (LB-medium)	0.5 % (w/v) yeast extract, 1% (w/v) NaCl, 1% (w/v) tryptone
LB agar	LB medium with 1.5% (w/v) bacto-agar
Terrific broth (TB) medium	2.4 % (w/v) yeast extract, 0.5% (w/v) glycerol 1.2% (w/v) tryptone
TB phosphate buffer	0.17 M KH_2PO_4, 0.72 M K_2HPO_4
SOB medium	0.5% (w/v) yeast extract, 0.05% (w/v) NaCl, 2.0% (w/v) tryptone after autoclaving 10 mM $MgSO_4$, 10 mM $MgCl_2$ und 2,5 mM KCl (passed through a 0.2 µm filter) were added.
SOC medium	SOB medium with addition of 10 mM glucose after autoclaving
$M9^-$ medium	750 ml H_2O, 200 ml 5 x $M9^-$ salts, 2 ml $MgSO_4$ (1 M), 0.1 ml $CaCl_2$ (1 M), 20 ml glucose (20% w/v)
^{15}N-$M9^-$ medium	$M9^-$ medium with $M9^-$ salts containing $^{15}NH_3$ instead of $^{14}NH_3$

3.1.10.2 Work with DNA

PCR dNTP stock (10 mM)	dNTP, 2mM each (N = A, T, C and G), dissolved in H_2O, stored at -20°C

3.1.10.3 Agarose gel electrophoresis

Agarose (1%)	5 g agarose were suspended in 500 ml 0.5 X TBE buffer, boiled until the agarose was dissolved and stored at 60°C
Ethidium bromide stock	10 mg/ml ethidium bromide in H_2O
Sucrose staining solution	60% (w/v) sucrose, 0.1% (w/v) bromphenol blue, 0.1% (w/v) xylencyanole FF dissolved in 0.5 x TBE
TBE buffer (5 x)	445 mM boric acid, 12.5 mM EDTA, 445 mM Tris (resulting pH: 8.15)

3.1.10.4 Work with proteins

HisF storage buffer	50 mM Tris/HCl pH 7.5, 100 mM NaCl
HisH storage buffer	50 mM KP pH 7.5, 100 mM NaCl
IMAC buffer A	50 mM Tris/HCl pH 7.5, 300 mM NaCl, 10 mM imidazole
IMAC buffer B	50 mM Tris/HCl pH 7.5, 300 mM NaCl, 500 mM imidazole
Reverse IMAC buffer	50 mM Tris/HCl pH 7.5, 300 mM NaCl

3.1.10.5 SDS polyacrylamide gel electrophoresis (SDS-PAGE)

Ammonia persulfate (APS) stock	10% (w/v) APS in H_2O. storage at -20°C
Coomassie staining solution	0.2 % (w/v) Coomassie brilliant blue G250 and R250, 50% (v/v) EtOH, 10% (v/v) acetic acid. Storage protected from light.
SDS-PAGE separating gel buffer	0.4% (w/v) SDS, 1.5 M Tris/HCl pH 8.8
SDS-PAGE collecting gel buffer	0.4 % (w/v) SDS, 0.5 M Tris/HCl pH 6.8
SDS-PAGE running buffer	0.1 % (w/v) SDS, 0.025 M Tris, 0.2 M glycine (resulting pH: 8.5)
SDS-PAGE sample buffer	2% (w/v) SDS, 10% (w/v) glycerol, 5% (v/v) β-mercaptoethanol, 0.01% (w/v) bromophenol blue, 1.25 M Tris/HCl pH 6.8

3.1.11 Software and web-based tools

Äkta Unicorn Version 5.01	GE Healthcare
Microsoft Office 2016	Microsoft
Citavi 6.3.0.0	Swiss Academic Software GmbH
Corel Draw 19.1.0.419	Corel
ChemDraw professional 16.0	CambridgeSoft
PyMOL 2.1	Schrödinger
SigmaPlot 12	SYSTAT Software
CLC main workbench 8.0	Qiagen
Spectra manager	Jasco
ProtParam	Expasy.org
NEB TM calculator	NEB.com

3.2 Methods

Preparation of lab ware, buffers and solutions

All glassware was baked for 4 h at 200 °C. All heat stable solutions as well as single use items such as pipet tips were autoclaved at 121 °C and 2 bar for 20 min. Heat labile solutions were prepared in stock solutions and passed through a syringe filter with a pore size of 0.22 µm or through filter membrane with a pore size of a 0.2 µm by the application of a vacuum. Buffers used for gel filtration or stopped-flow experiments were degassed for at least 30 min in an exsiccator. Buffers containing volatile components such as ammonia were degassed by sonication in a water bath for at least 30 min.

3.2.1 Microbiological methods

3.2.1.1 Cultivation of *E. coli* strains

All *E. coli* strains were cultivated at 37 °C while being shaken at 140 rpm (1 l and 0.6 l cultures) or 220 rpm (5, 50, 100 and 250 ml cultures), respectively. Unless stated otherwise, LB medium was used for cultivation. To select strains harbouring plasmids, the medium was supplemented with the adequate antibiotic (150 µg/ml ampicillin, 30 µg/ml chloramphenicol, 75 µg/ml kanamycin) by addition of a filter-sterilized, 1000-fold concentrated stock solution. For selection of single clones, cultures were plated on LB agar plates containing the respective antibiotic and incubated at 37 °C over night to obtain single colonies. For short term storage, plates and suspensions were sealed and stored at 4 °C.

3.2.1.2 Preparation of chemically competent *E. coli* cells[118]

To prepare *E. coli* cells for transformation of plasmids, 500 ml SOB medium was inoculated with an over night culture of the respective strain to an OD_{600} of 0.1. The culture was incubated at 37 °C and 220 rpm until an OD_{600} of 0.6 was reached. The culture was subsequently kept on ice for 15 min and harvested in 15 ml tubes by centrifugation (EPPENDORF Centrifuge 5810R, 400 rpm, 10 min, 4 °C). The supernatant was discarded and the bacterial pellet resuspended in ice-cold TFB I buffer. The cells were pelleted again under the same conditions as above. The supernatant was discarded and the resulting bacterial pellet suspended in 10 ml ice-cold TFB II buffer. Immediately afterwards, the cell suspension was transferred into 1.5 ml reaction vessels in aliquots of 100 µl each on ice and frozen at -80 °C.

3.2.1.3 Transformation of chemically competent *E. coli* cells

An aliquot of chemically competent cells was thawed on ice and a total of about 100 ng of plasmid DNA were added to the suspension. After a 20 min incubation on ice, the cells were subjected to a heat shock at 42 °C for 60 s and subsequently cooled on ice for another 5 min. For development of the antibiotic resistance, 900 µl of LB medium were added to the cell suspension and the cells were incubated for 1 h at 37 °C in an incubation shaker at 220 rpm. Finally, an appropriate dilution was plated on LB agar plate containing the appropriate antibiotic(s) or the transformation culture was used to inoculate a larger culture.

3.2.2 Molecular biology methods

3.2.2.1 Isolation and purification of plasmid DNA from *E. coli*

Plasmid amplification was performed using the strain *E. coli* turbo. Plasmid DNA was isolated by the use of a mini preparation kit from FERMENTAS (GeneJET Plasmid Miniprep Kit). For this purpose, cells 5 ml of and over night culture were harvested by centrifugation (EPPENDORF Centrifuge 5810R, 400 rpm, 10 min, 4 °C). The plasmid isolation was carried out following the instructions provided by the manufacturer. The DNA was eluted from the silica columns with 50 µl of sterile deionized water and stored at -20 °C.

3.2.2.2 Determination of DNA concentration

The concentration of DNA solutions was determined using a NanoDrop One photometer by measuring the absorbance at 260 nm. According to Lambert-Beer's law, assuming a $^{0.1\%}A_{260}$ of 20 cm^2mg^{-1} and a path length of 1 cm, a solution of 50 ng/µl double-stranded (ds) DNA shows an absorbance of 1. Therefore, the DNA concentration can be calculated by the following equation (1):

$$c_{dsDNA} = \frac{A_{260} \cdot 50}{1000} \quad \textbf{(1)}$$

The following measures were taken as quality control of the DNA preparation: There should not be a measurable absorbance above 300 nm and the ratio A_{260}/A_{280} should be at least 1.8.

3.2.2.3 Agarose gel electrophoresis

Linear dsDNA fragments were separated by agarose gel electrophoresis according to their length. Bands of DNA can be made visible under UV light by the addition of ethidium bromide, a fluorescent dye that intercalates with DNA bases.[119] For preparation of agarose gels, about 25 ml of a 1% agarose solution, previously stored at 60 °C, was supplemented with 0.2 µl ethidium bromide solution per ml agarose solution, was cast into a gel chamber and a comb was inserted to create loading pockets. After cooling to room temperature, the gel was covered with 0.5 x TBE buffer and the comb removed. The DNA samples were mixed with DNA loading dye and pipetted into the loading pockets. The electrophoresis was carried out at a voltage of 200 V for 20 min. The negatively charged DNA molecules migrate towards the anode and this migration is impeded to different extents according to the size of the DNA fragments. The DNA fragments were detected under UV light (λ = 302 nm) and documented using the Multi-Doc-It Digital imaging system. To estimate the size of the fragments, 5 µl of GeneRuler 1 kb Plus DNA ladder (FERMENTAS) was applied a pocket of the gel to compare migration lengths.

3.2.2.4 Isolation of linear DNA fragments from agarose gels

The desired DNA fragment was excised from the agarose gel using a clean scalpel under UV light (λ = 302 nm) and transferred into a clean 1.5 ml reaction vessel. The extraction was done using the GeneJET Gel Extraction Kit (FERMENTAS) according to the instructions provided by the manufacturer. The DNA was eluted using 20 – 40 µl of sterile, deionized water and stored at –20 °C.

3.2.2.5 Enzymatic manipulation of DNA

Cleavage of dsDNA with restriction endonucleases

For specific cleavage of dsDNA Type II endonucleases were applied, which recognize a specific palindromic sequence (Sambrook, 1989; Wilson and Murray, 1991). The cleavage results in single stranded overhangs (sticky ends) which carry 3' hydroxyl and 5' phosphate ends. For preparative cleavage for subsequent ligation, 2 µg of DNA or the entire purified PCR product and 2 µg of target vector DNA were treated with 20 U of each restriction enzyme in a total volume of 50 µl at 37 °C for 2 h. The fragments were purified by agarose gel electrophoresis (chapter 3.2.2.3) for before ligation (see below).

Ligation of DNA fragments

For ligation DNA fragments of the target vector and the gene insert, digested with the appropriate restriction enzymes, were mixed in an approximate 1:3 (vector:insert) ratio and supplemented with 1 U T4 Ligase (FERMENTAS) in a total volume of 20 µl in the buffer provided by the manufacturer. The mixture was incubated at RT overnight and subsequently, chemically competent *E. coli* cells were transformed (chapter 3.2.1.3) with the ligation mixture.

Golden Gate cloning

The synthetic *hisH* gene optimized for *E. coli* codon usage was cloned into a derivative of pET28 containing a TEV cleavage site for the removal of the hexa-histidine tag that was modified with BsaI restriction sites to allow for golden gate cloning.[112] The synthetic gene also carried BsaI restriction sites. 100 ng plasmid DNA were mixed in a 1:3 ratio (vector : insert) and supplemented with 20 U BsaIHF (NEB) and 400 U T4 Ligase (NEB) in ligase buffer (provided by the manufacturer) in a total volume of 50 µl. To account for the different temperature optima of the restriction enzyme and the ligase, the reaction was performed in a thermal cycler as follows

	step	**temperature (°C)**	**duration**
1.	Initial restriction	37	10 min
2.	Ligation	18	5 min
3.	Restriction	37	5 min
4.	Final restriction	37	10 min
5.	Heat inactivation	65	10 min
6.	Hold (cooling)	4	∞

Steps 2-4 were repeated 50 times

Amplification of DNA fragments by polymerase chain reaction (PCR)

PCR is used to amplify specific DNA fragments *in vitro*.[120,121] For this purpose, the DNA is subjected to cycles of denaturation, hybridization (annealing) of synthetic DNA oligonucleotides that flank the DNA sequence of interest (primers) and enzymatic DNA polymerization (elongation of the primers). This leads to an exponential increase in the amount of target DNA with each cycle. PCR was performed in a total volume of 50 µl in a thermal cycler (lid temperature 110 °C). A standard PCR mixture contained 1-100 ng template DNA, 2.5 U DNA polymerase, 0.2 mM dNTP mix and 1 µM of each primer in the appropriate reaction buffer provided by the manufacturer for the respective DNA polymerase used. A standard PCR protocol was as follows:

	step	temperature (°C)	duration
1.	Initial denaturation	95	3 min
2.	Denaturation	95	30 s
3.	Annealing	T_A	30 s
4.	Elongation	72	30 s/kb
5.	Final elongation	72	10 min
6.	Hold (cooling)	4	∞

Steps 2 to 4 were repeated 30-35 times.

The melting temperature (T_M) was calculated using the web tool NEB TM calculator. The annealing temperature (T_A) was set to be 1 °C higher than the lower T_M of the two primers. If the standard conditions did not yield a suitable PCR product, the optimal T_A was determined using a temperature gradient in a gradient cycler (EPPENDORF Mastercycler gradient), using several separate reaction set-ups at temperatures ranging from 50 °C to 70 °C.

Colony PCR

For verification of the ligation process, colonies resulting from a transformation after ligation were screened for the correct length of insert. To this end, single colonies were picked with a pipette tip and a small quantity of cells was transferred to a 20 µl PCR reaction mixture for GoTaq polymerase as described in above.

Site directed mutagenesis

In order to exchange or delete amino acids in HisF or HisH enzymes, their respective genes were modified on the nucleotide level. The method used here is a modified protocol after the Phusion Site-directed mutagenesis kits by Finnzymes (Thermo Fisher Scientific). For the exchange of nucleotides, the primers were designed such that the 5’ ends anneal back-to-back, leading to an amplification of the entire plasmid. The nucleotide changes were incorporated in one of the primers. These primers were used in a standard PCR reaction using Phusion polymerase. The resulting PCR product was purified via an agarose gel. The purified, linearized plasmid was cyclized in a standard ligation reaction, with the addition of polynucleotide kinase. *E. coli* turbo cells were transformed in a standard transformation procedure (chapter 3.2.1.3) with the resulting mutated plasmid.

DNA sequencing

The correct sequence of all cloned genes and all introduced mutations was verified by Sanger sequencing. The sequencing was performed by the company Seqlab (Göttingen). Samples for sequencing contained approximately 600 ng Plasmid DNA and 2 µM of sequencing primer in a total volume of 15 µl. The sequencing results were analysed with the program CLC main workbench (Qiagen).

Gene synthesis

The *hisH* gene was optimized for *E. coli* codon usage using the web service of the company GeneArt (Thermo Fisher Scientific, Regensburg). The gene was designed to carry a BsaI restriction site on both ends to allow for golden gate cloning (chapter 3.2.2.5) and was delivered as a linear fragment (GeneArt Gene String). Also, the gene encoding for the aminoacyl-tRNA synthethase for the incorporation of the unnatural amino acid CouA (chapter 3.2.4.3) was designed in a similar fashion for cloning into the plasmid pEVOL.

Construction of pEVOL-pCouA

For the incorporation of the unnatural amino acid L-(7-hydroxycoumarin-4-yl) ethylglycine (CouA) the plasmid pEVOL-pAzF (Chin et al. 2002) was modified to carry the gene for aminoacyl-tRNA synthethase that was optimized to attach CouA to a tRNA recognising the amber STOP codon (Wang et al. 2006). Since both systems use the orthogonal tyrosyl system of *M. janaschii*, an exchange of the region encoding for the tRNA was not necessary. For the exchange of the first copy of the gene, the plasmid was amplified with primers flanking the gene, carrying BsaI restriction sites for golden gate cloning. The synthetic gene also carried these restriction sites, creating matching sticky ends for ligation. The insertion of the gene was done by golden gate cloning. The second copy of the gene was exchanged in a similar fashion, with primers matching the flanking regions. Both exchanges were verified by sequencing.

3.2.3 Protein biochemistry methods

3.2.4 Gene expression and heterologous protein production

3.2.4.1 Production of unlabelled protein

For purification of unlabelled proteins, 4 l LB medium, supplemented with the appropriate antibiotics, were inoculated to an OD_{600} of 0.1 with an overnight culture of *E. coli* BL21Gold (DE3) carrying the respective plasmid. The cultures were incubated at 37 °C and 140 rpm until they reached an OD_{600} of 0.6 to 0.8, at which point gene expression was induced by the addition of 1 mM IPTG. Cells were grown at 20°C overnight. Cells were harvested by centrifugation (Beckmann Coulter Avanti J-26SXP, JLA-8.1000, 20 min, 4000 rpm, 4 °C). The cells were resuspended in IMAC buffer A (chapter 3.1.10) and lysed by sonication (Heinemann Branson sonifier W-250D, 3 min in 2 s intervals, 65% pulse intensity, 0 °C). The solution was cleared of cell debris by centrifugation (Beckmann Coulter Avanti J-26SXP, JA-25.50. 30 min, 14000 rpm, 4 °C) and the supernatant used for further processing.

3.2.4.2 Production of labelled proteins for NMR spectroscopy

Isotopically labelled HisH (with 13C in the ε-position of Histidine) and HisF (^{15}N labelling) were expressed in D_2O-based M9 minimal medium at 20-25 °C over night in *E. coli* BL21-CodonPlus(DE3)-RIPL cells (Stratagene). Expression was induced by addition of 1 mM IPTG at an OD_{600} of 0.6-0.8. For ^{15}N labelling of HisF 0.5 g/l $^{15}NH_4Cl$ was used. Specific. For histidine labelling 100 mg/l Ring-2-^{13}C labelled histidine (Cambridge Isotope Laboratories) was used. Labelled histidine was added 1 h prior to induction.

3.2.4.3 Production of proteins carrying the unnatural amino acid CouA

For purification of CouA containing proteins, 6 l LB medium were supplemented with the appropriate antibiotics and inoculated with an overnight culture of *E. Coli* BL21Gold (DE3) harbouring the appropriate plasmid encoding the gene of interest and pEVOL-pCouA to an OD_{600} of 0.1. Cultures were incubated at 37 °C and 140 rpm until they reached an OD_{600} of 0.6 to 0.8. Cells were harvested by centrifugation (Beckmann Coulter Avanti J-26SXP, JLA-8.1000, 20 min, 4000 rpm, 4 °C) and resuspended on 600 ml TB medium. This culture was incubated at 37 °C and 140 rpm until it reached an OD_{600} of 10. Subsequently, the expression of the aminoacyl-tRNA synthethase gene was induced by addition of 0.2% arabinose and CouA was added to a final concentration of 0.45 mM. For variants of HisH, IPTG was added for induction of *hisH* expression, for variants of HisF, no IPTG was added and expression was accomplished solely by "leaky" expression of the pET system. The cells were harvested, lysed and further treated as described in chapter 3.2.4.1.

3.2.4.4 Protein purification

As purification steps, heat incubation, nickel affinity chromatography, reverse nickel affinity chromatography and preparative size exclusion chromatography were used. If size exclusion chromatography was not the final purification step, the buffer was exchanged by dialysis. Solutions of purified proteins were concentrated by ultrafiltration (Amicon 10 kDa cut-off, Millipore), flash frozen in liquid nitrogen and stored at -80 °C.

Heat incubation

For HisF variants, the crude extract was subjected to 70 °C for 15 min in a water bath. Aggregates of host proteins were removed by centrifugation (Beckmann Coulter Avanti J-26SXP, JA-25.50. 30 min, 14000 rpm, 4 °C). The supernatant was used in further purification steps.

Immobilized metal chelate chromatography (IMAC)

IMAC takes advantage of the specific and reversible interactions between histidine residues in proteins and immobilized metal ions. The column consists of a sepharose matrix, which is modified covalently with an iminodiacetic acid (IDA)-type chelator. IDA coordinates divalent metal ions such as Ni^{2+}, Cu^{2+} or Co^{2+}. The coordination site not occupied by the chelator can bind to nitrogen or sulphur atoms. In this work, HisF and HisH proteins were genetically fused to an N-terminal His_6-tag containing a tobacco etch virus (TEV) protease cleavage site for specifically removing the His_6-tag. The raw extract was filtered through a 0.45 µm syringe filter and afterwards directly passed through a HisTrap FF crude column (GE Healthcare, CV = 5 ml, pressure limit: 0.5 MPa) with an Äkta chromatography system (GE Healtcare). Bound protein was eluted from the column with free imidazole, which competes with the histidine residues for the coordination site of the nickel ions. IMAC purifications were performed according to the following protocol:

Flow rate	5 ml/min
Equilibration	5 CV IMAC buffer A
Sample application	25 – 80 ml expression cells homogenized in IMAC buffer A
Washing	10 CV IMAC buffer A
Elution	15 CV, gradient 0 – 75 % IMAC buffer B
Purging	10 CV IMAC buffer B
Flushing	10 CV H_2O
Storage of the column	in 20 % EtOH

The entire chromatographic process was monitored by following the absorbance at 260 nm and 280 nm. The fractions were analysed by SDS-PAGE (chapter 3.2.5.2) and the fractions containing target protein in acceptable purity were pooled and used in further purification steps.

Proteolytic cleavage of N-terminal His_6-tags and reverse IMAC

After IMAC purification (chapter 3.2.4.4), the N-terminal His_6-tag was removed by proteolytic cleavage with TEV protease. This highly specific cleavage leaves two amino acids (GH) for HisF protein and four amino acids (GAMG) for HisH proteins N-terminal of the starting methionine. To this end, TEV protease was added to the pool of elution fractions as produced from IMAC and the imidazole removed by dialysis against 5 l of reverse IMAC buffer A overnight. The resulting protein solution was again passed through a HisTrap FF crude column (GE Healthcare). All protein molecules that have been cleaved, e.g. the target protein, does not bind to the column again and is to be found the flow-through. All non-cleaved target protein, the cleaved His_6-tag peptides as well as the TEV protease, which also carries a His_6-tag, bind to the column and are thus removed. Reverse IMAC purification steps were conducted according the following protocol:

Flow rate	5 ml/min
Equilibration	5 CV reverse IMAC buffer A
Sample application	Protein solution
Washing	10 CV reverse IMAC buffer A
Elution	15 CV, gradient 0 – 75 % IMAC buffer B
Purging	10 CV reverse IMAC buffer A
Flushing	10 CV H_2O
Storage of the column	in 20 % EtOH

The fractions were analysed by SDS-PAGE (chapter 3.2.5.2) and all flow-through fractions containing target protein in acceptable purity were pooled.

Preparative size exclusion chromatography (SEC)

The principle of SEC can be understood as a reverse molecular sieve. The mobile phase passes through a porous material at a constant flow rate. Small molecule in the mobile phase can diffuse into the pores while larger molecules are excluded from them. As a result, the larger molecules effectively travel through a smaller volume than the small molecules and elute from the column earlier. This allows for both complete buffer exchange of protein solutions as well as the separation of proteins by their size. In this work, proteins were separated on Superdex 75 columns (HiLoad 26/600, 320 ml, GE Healthcare) using an Äkta prime chromatography system (GE Healthcare). For HisF proteins, 50 mM Tris/HCl pH 7.5 was used and for HisH protein 50 mM KP pH 7.5. Proteins were loaded via a 10 ml super loop and eluted with 1.2 CV of the respective buffer at a flow rate of 1.5 ml/min (back pressure: max. 0.38 MPa). Fractionation was started at the beginning of the elution and the progress of the elution was monitored by observation of the absorbance at 280 nm. Fractions were analysed by SDS-PAGE (chapter 3.2.5.2) and fractions containing target protein in acceptable purify were pooled.

Buffer exchange by dialysis

For buffer exchange or to remove salt or imidazole from a protein solution, dialysis was performed for at least 4h against an at least 1000-fold excess of the desired buffer. For HisH proteins still carrying a His_6-tag, this was performed at RT. The used dialysis tubing (Visking) had a molecular cut-off of 14 kDa to retain proteins, while substances with low molecular weight can pass through the membrane freely.

Concentrating of protein solutions

Protein solutions were concentrated by ultrafiltration using Amicon Ultra centrifugal filter devices (Millipore, cut-off: 10 kDa for HisF and HisH monomers, 30 kDa for ImGPS complexes). The filtration was achieved by centrifugation (Eppendorf Centrifuge 5810R, 4000 rpm, 4 °C) according to the instructions provided by the manufacturer

Synthesis of ProFAR and PrFAR

Because PrFAR is labile and can hydrolyse spontaneously,[97] it was synthesized from ProFAR *in situ* with HisA from *T. maritima*.[100] ProFAR is more stable that PrFAR and can be stored at –80 °C.[54] ProFAR was synthesized from ATP and PRPP,[122] the starting compounds of histidine biosynthesis, using ATP-phosphoribosyltransferase (HisG) and phosphoribosyl-ATP phosphoribosyl-ATP pyrophosphohydrolase:phosphoribosyl-AMP cyclohydrolase (HisIE) from *E. coli* in an enzymatic reaction. The reaction mixture consisted to 6 mg ATP, 12 mg PRPP and 15.2 mg$MgCl_2$ in a total volume of 10 ml of 50 mM Tris/Ac pH 7.8. The reaction was initiated by addition of ca. 2 mg HisG-IE (in 50 mM KP pH 7.5, 2.5 mM EDTA and 1 mM DTT) under vigorous stirring. Spectra (200 to 400 nm) were recorded at regular intervals to observe the reaction progress by the characteristic increase in absorbance at 290 nm due to the production of ProFAR. When no further increase in absorbance at 290 nm could be observed ProFAR was isolated from the reaction mixture via anion exchange chromatography on a Poros HQ-20 column (CV: 7.9 ml). The column was previously equilibrated with 50 mM ammonium acetate pH 8.0. ProFAR was eluted with a linear gradient of ammonium acetate (0-1 M over 12 CV, fractionation in 4 ml fractions). ProFAR concentration was determined by its absorbance at 300 nm (ε_{300} = 6069 $M^{-1}cm^{-1}$,).[97] Purity was estimated by the ratio A_{290}/A_{260}, with values between 1.1 and 1.2 being assumed as optimal.[123] Fractions with pure ProFAR were flash frozen in liquid nitrogen and lyophilized. All steps were carried out under exclusion of light.

For applications that needed excluded *in situ* synthesis of PrFAR, such as stopped-flow kinetic measurements, PrFAR was synthesized from ProFAR. To this end, ProFAR was dissolved in 50 mM Tris/HCl, pH 7.8 and after the addition of 4 µM HisA from *T. maritima* incubated for 45 min at room temperature. PrFAR was isolated from the reaction mixture by anion exchange chromatography on a Poros HQ-20 column (CV: 7.9 ml). PrFAR was eluted with a linear gradient of 1 M Tris/HCl pH 7.8 over 12 CV. Since PrFAR shows the same spectroscopic properties as ProFAR, concentration and purity were estimated as described for ProFAR. PrFAR was not stable during lyophilisation and was therefore stored in solution. The fractions from purification containing PrFAR were pooled and flash frozen in liquid nitrogen and stored at –80°C.

3.2.5 Analytical methods

3.2.5.1 Determination of protein concentrations via absorption spectroscopy

Aromatic amino acids (Trp, Tyr and Phe) and also disulphide bonds absorb UV-light of wavelengths between 250 and 300 nm. The molar extinction coefficient at 280 nm (ε_{280}) can be calculated form the amino acid composition (equation (2)).[124]

$$\boldsymbol{\varepsilon_{280} = \sum Trp \cdot 5500 + \sum Tyr \cdot 1490 + \sum Cys \cdot 125} \quad \textbf{(2)}$$

Using Lambert-Beer's law, the protein concentration can be determined by the absorbance at 280 nm (equation (3))

$$\boldsymbol{A_{280} = \varepsilon \cdot c \cdot d} \quad \textbf{(3)}$$

$$\boldsymbol{c = \frac{A_{280}}{\varepsilon \cdot d}}$$

A280	absorbance at 280 nm
c	concentration [M]
d	pathlength [cm]
ε_{280}	molar extinction coefficient at 280 nm

Absorbance spectra were recorded between 220 and 700 nm. The maximum absorbance of protein solutions should be a 278 nm and for pure protein the ration A_{280}/A_{260} should be at least 1.8. Above 300 nm there should not be any absorbance, as this is an indication of protein aggregation.

3.2.5.2 SDS-polyacrylamide gel electrophoresis (SDS-PAGE)

When subjected to the detergent sodium dodecyl sulphate (SDS), proteins are denatured and negatively charged proportionally to their mass due to SDS binding to hydrophobic parts of the polypeptide chain in a ratio of one molecule of SDS per 1.4 amino acid residues. Since the net charge of the proteins can be neglected, this results in an approximately uniform mass to charge ratio. Consequently, the electrophoretic mobility is determined only by the sieve effect of the polyacrylamide gel. As described by Laemmli, the migration speed of a protein is inversely proportional to the logarithm of its molecular mass.[125] SDS gels were prepared according to the composition shown in Table 1.

Table 1: Composition of gels for SDS-PAGE

	Separation gel (12.5%)	**Stacking gel (6%)**
Separation/stacking gel buffer	19.5 ml	7.38 ml
Acrylamide-SL	26.2 ml	5.9 ml
Water	31.58 ml	15.95 ml
TEMED	0.089 ml	0.029 ml
APS (10%)	0.195 ml	0.089 ml

Samples were mixed 1:4 with 5 x SDS-PAGE sample buffer or 1:1 with 2 x SDS-PAGE sample buffer and incubated at 95°C for 5 min. 5-20 µl of sample were loaded into the gel pockets and electrophoresis of proteins performed at 50 mA (constant) and 300 V (maximum) for 35 min. Gels were stained by swaying them for 10 min in SDS-PAGE staining solution, the detection limit for protein bands being 200-500 ng protein per mm^2. Excess dye was removed by repeated washing with deionized water and heating in a microwave oven.

3.2.5.3 Fluorescence Titration

The CouA residues incorporated into proteins change their fluorescence properties in different microenvironment.[117,126] Therefore, changes in fluorescence can be used as a binding signal for ligands. For the determination of binding affinity of CouA-labelled HisH (HisH Y136CouA), the protein was titrated with wild-type HisF. The corrected fluorescence signal was plotted against the HisF concentration and the resulting curves were fitted to a quadratic function describing the dissociation constant (equation (4)):

$$F = F_0 + \frac{1}{2}(F_{max} - F_0) \cdot \left(1 + \frac{L_0+K_D}{E_0} - \sqrt{\left(1 + \frac{L_0+K_D}{E_0}\right)^2 - 4 \cdot \frac{L_0}{E_0}}\right) \quad \textbf{(4)}$$

F	measured fluorescence intensity
F_0	initial fluorescence intensity
F_{max}	fluorescence intensity at saturation
L_0	concentration of HisF
E_0	concentration of HisH

HisF K132CouA was used to study ligand binding to HisF. It was titrated with the HisF substrate PrFAR as well as the reaction products ImGP and AICAR. For these titrations, 1 µM labelled HisF was titrated in 50 mM Tris/HCl pH 7.5 with the respective ligand. Since the addition of ligands did not show any significant change in signal when titrated against free CouA and show no fluorescence on their own, the data were only corrected for dilution of HisF. The change in fluorescence was plotted against the concentration of the titrated ligand and fitted with a simple hyperbolic fit to determine the dissociation constant (equation (5)).

$$\Delta F = \cdot \frac{F_{max} \cdot L_0}{K_D + L_0} \quad \textbf{(5)}$$

ΔF	measured difference in fluorescence intensity
F_{max}	fluorescence intensity at saturation
L_0	concentration of ligand

3.2.5.4 Steady-state enzyme kinetics

For functional characterization of generated protein variants, state-state enzyme kinetics was performed. The measured reactions were cyclase activity (both ammonia-dependent and glutamine-dependent) and glutaminase activity. If both subunits were present, the subunit whose reaction was not observed was added in access to ensure correct concentration of the observed subunit and full complex formation. All kinetic measurements were carried out at 25 °C.

Ammonia dependent HisF (cyclase) activity

Although physiologically, ImGPS is a bienzyme complex in which the ammonia necessary for the reaction is generated by the hydrolysis of glutamine, HisF is also fully functional as a stand-alone enzyme, when supplied with free ammonia. The reaction progress was followed by the decrease of absorbance at 300 nm ($\Delta\varepsilon_{300}$ PrFAR-AICAR = 5637 $M^{-1}cm^{-1}$).[97] As PrFAR is quite labile, the more stable precursor ProFAR was added to the reaction mixture and was turned over *in situ* to PrFAR by addition of HisA from *T. maritima*. As source of ammonia, 100 mM NH_4Ac were added. According to the Herdeson-Hasselbach equation, at pH 8.5 this results in a concentration of free ammonia of roughly 17 mM, which constitutes saturation.[100] Typical reactions conditions were:

50 mM	Tris/Ac pH 8.5
100 mM	NH_4Ac
1-30 µM	ProFAR
0.5 µM	HisA

The reaction was observed in the absence of HisH. Reactions were started by the addition of 0.05 to 10 µM HisF. From the initial slopes, reaction rates were calculated, normalized to HisF concentration and plotted against the PrFAR concentration. The values for k_{cat} and K_M^{PrFAR} values were determined by fitting the data points to the Michaelis-Menten equation.

Glutamine dependent cyclase activity

The glutamine dependent turnover of PrFAR is the physiological reaction of ImGPS. In this case, the glutaminase HisH hydrolyses glutamine to glutamate. The resulting ammonia is channelled through an intra-molecular channel to the active site of HisF, where it reacts with PrFAR. The reaction progress was followed as described above for ammonia-dependent cyclase activity. Generally, glutamine was added to saturation (10 mM) and kinetics measured in dependence of PrFAR concentration. Typical reaction conditions were:

50 mM	Tris/HCl pH 7.5
10 mM	glutamine
1-30 µM	ProFAR
0.5 µM	HisA
2-11 µM	HisH

The reaction was initiated by addition of 1-10 µM HisF. Catalytic parameters were determined as described above.

Glutaminase activity

The glutaminase subunit of ImGPS, HisH, catalyses the hydrolysis of glutamine to glutamate and ammonia. Since the hydrolysis of glutamine does not yield a spectroscopic signal, coupled enzymatic reaction assays were used. Both used detection systems are based on the turnover of generated glutamate. Since there is a small quantity of glutamate as an impurity in commercially available glutamine, all reactions were incubated 1 h at 25 °C before the start by the addition of HisH.

Glutamate dehydrogenase assay

Glutamate dehydrogenase oxidises glutamate to α-ketoglutarate and ammonia. The cofactor needed for this reaction is NAD^+, which is reduced to NADH. This leads to a spectroscopic signal and the reaction progress can be observed by the absorbance increase at 340 nm (ε_{340} = 6220 $M^{-1}cm^{-1}$). Since NAD^+ binds to HisF with a low affinity and also induces a low allosteric activation, basal activity cannot be measured in this assay and activity was only measured with the addition of the allosteric activator ProFAR.

Glutamate oxidase assay

To reliably measure the basal glutaminase activity as well as the fully activated activity, a glutaminase assay for ImGPS has to be free of NAD^+. Therefore, in this work a assay base on glutaminase oxidase (GOX) was used. This assay is a modified protocol of one developed for high-throughput screenings.[127] In this assay the oxidation of glutamate to oxoglutarate and ammonia is carried out without a NAD^+ cofactor. As a by-product of this reaction, H_2O_2 is generated. This in turn is reduced by horseradish peroxidase (HRP) which can then use chromogenic substrates as final electron acceptor. The main difference to the high-throughput assay is the HRP substrate. Instead of the fluorophore AmplexRed, Phenol and 4-amino antipyrine (AAP) were used to make the assay feasible for larger assay volumes.
After the initial incubation, the reaction was started by the addition of 0.05-35 µM HisH. Reaction progress was monitored by observing the increase in absorbance at 505 nm (ε_{505} = 6400 $M^{-1}cm^{-1}$) in a 96-well plate format using a Tecan infinite M200 Pro plate reader. The progress curves showed a characteristic lag phase and the slope for determining the reaction rate was fitted to points in the following linear phase. Reaction rates were normalized with the HisH concentration and plotted against the concentration of glutamine if full kinetics were measured. Typical reaction conditions were:

20 mM	Tris/HCl pH 7.0
0.1 - 10 mM	glutamine
0 or 70 µM	ProFAR
20 mU/ml	GOX
1 U/ml	HRP
1 mM	phenol
1 mM	AAP
1 – 36 µM	HisF
0.05 – 35 µM	HisH (start)

This assay was also used for the determination of the pH dependency of the HisH reaction. For these experiments, the buffer system was changed to Bis-Tris/HCl (20 mM) in order to ensure comparability between different pH values. Linearity of this coupled enzymatic assay under the used conditions was tested for standard conditions (Fig. 9) as well as at different pH values (Fig. 10). The latter demonstrated that this assay can be used between pH 5.6 and pH 9.2.

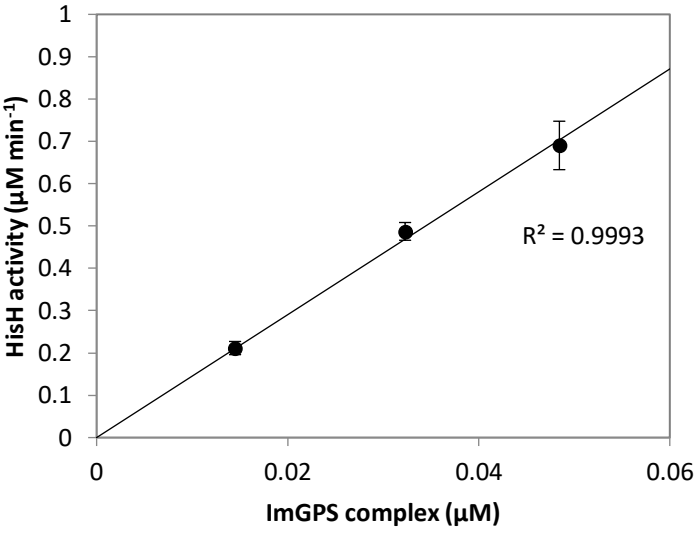

Fig. 9: Test of linearity of the GOX assay. Different concentrations of wild-type ImGPS were assayed in 20 mM Tris/HCl pH 7.0, 10 mM glutamine, 70 µM ProFAR for glutaminase activity to demonstrate the suitability of the assay in this range of activity. The turnover was calculated from the maximal slope of raw data. The linear increase of activity with the HisH concentration shows that the activity of auxiliary enzymes is not limiting under these conditions. Error bars indicate the standard error of a technical triplicate measurement.

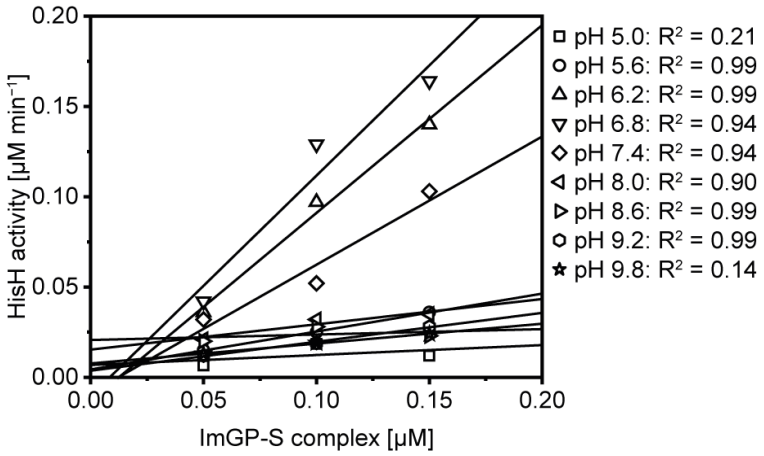

Fig. 10: Test of linearity of the GOX assay at different pH values. The suitability of the GOX based assay was tested by measuring HisH activity at different pH values (100 mM CHC buffer). The useful pH range of the assay was determined to be 5.6 to 9.2.

3.2.5.5 Transient binding kinetics

Transient binding kinetics of the HisF substrate PrFAR as well as the reaction products ImGP and AICAR was measured with an Applied Photophysics stopped-flow apparatus at 25 °C. For usual binding experiments, both the enzyme and ligand containing solutions were prepared in two-fold concentrated stocks, which were filled into the syringes of the device and incubated for 5 min to ensure temperature adjustment of the samples. CouA fluorescence was excited with a xenon lamp (367 nm) and the fluorescence measured with a 400 nm cut-off filter. All transients were measured at least 10 times and averaged. All measurements were performed with the pressure hold option, since pressure release led to a fluorescence artefact. Fitting of single transients was performed with the software supplied by the manufacturer of the machine. Global fitting analysis for determination of the kinetic mechanism of HisF was performed with the program DynaFit.[128]

3.2.5.6 Protein crystallization and structure determination by X-ray diffraction

Structure determination was performed in collaboration with Chitra Rajendran (group of Prof. Christine Ziegler, Institute of Biophysics and Physical Biochemistry, University of Regensburg). For crystallization of HisF protein variants, all proteins were concentrated to about 20 mg/ml using Amicon Ultra centrifugal devices (Millipore, 10 kDa cut-off). First, crystals of the wild-type protein were grown in a previously determined condition using Qiagen EasyXtal 15 well plates.[58] These crystals were used to perform micro seeding. For this purpose, crystals were harvested from drops and placed in a reaction tube containing 50 µl of reservoir solution and a plastic bead. The suspension was mixed vigorously with a vortex mixer for 1 min and the resulting seeding solution was diluted in a serial dilution with reservoir solution. A drop containing 1 µl of the concentrated HisF variant (about 20 mg/ml) and 1 µl of a seeding solution was set up in a Qiagen EasyXtal 15 well plate. For the variant G20P this procedure was not successful and a new screen (Morpheus II Screen, Molecular dimensions) was carried out using 400 nl drops (200 nl reservoir plus 200 nl protein solution). This screen was pipetted with a mosquito pipetting robot (SPT Labtech) in Greiner Bio One 96-well plates. The crystals for structure determination were taken directly from this screen.

For crystallization of ImGPS complexes, the respective HisH and HisF protein were mixed in a 1:1 molar ratio and any excess monomeric protein was removed by SEC (S75 column ART, Äkta prime GE Healthcare) in 10 mM Tris/HCl pH 8.0 and concentrated to at least 25 mg/ml. using a Amicon Ultra centrifugal device (Millipore, 30 kDa cut-off). Afterwards, a screening of conditions was performed with the commercially available ProPlex Eco screen (Molecular Dimensions) using 400 nl drops (200 nl reservoir plus 200 nl protein solution). This screen was pipetted with a mosquito pipetting robot (SPT Labtech) in Greiner Bio One 96-well plates. Initial hits were optimized by slightly varying precipitant solution, pH or additive concentrations depending on the particular condition in 15-well plates (EasyXtal tool, Qiagen).

Data sets were collected using synchrotron radiation from the Swiss Light Source (SLS), Switzerland at beamline PXIII and PXI. Data collection was done at cryogenic temperature. Data were processed using XDS,[129] and the data quality was assessed using the program PHENIX.[130] Structures were solved by molecular replacement with MOLREP within the CCP4i[131] suite using PDB-ID 1THF[58] or PDB-ID 1gpw[109] as search model for isolated HisF proteins or ImGPS complexes, respectively. Initial refinement was performed using REFMAC.[132] The model was further improved in several refinement rounds using automated restrained refinement with PHENIX[130] and interactive modelling with Coot.[133]

3.2.5.7 Nuclear magnetic resonance spectroscopy

To measure the effects of allosteric HisH activation by either the activating ligand ProFAR or constitutive activity inducing mutations, several different nuclear magnetic resonance (NMR) experiments were performed. All NMR experiments were done in cooperation with Dr. Jan-Philip Wurm (group of Prof. Dr. Remco Sprangers, Institute of Biophysics and Physical Biochemistry, University of Regensburg).

All NMR measurements were performed on 600 MHz and 800 MHz Bruker Avance NEO spectrometers equipped with triple resonance cryoprobes. Size exclusion buffer was used for NMR measurements of the ImGPS complex, whereas for HisF the buffer consisted of 50 mM KCl, 10 mM MES, 1 mM EDTA, pH 6.8. 5 % D_2O was added to both buffers. Protein concentrations of 50-150 uM and 250-350 uM were used. The backbone amide resonance assignment of HisF was published previously.[134] All spectra were processed with Topspin 4.0 and analysed with Sparky.[135]

4 Results and Discussion

4.1 Investigation of the influence of flexibility on HisF catalysis

Already early in the investigation of the ImGPS from *Thermotoga maritima* it has been observed in limited tryptic proteolysis experiments that the $\beta_1\alpha_1$loop (loop1) is the most flexible element of the cyclase subunit HisF.[100] Furthermore, the deletion of loop1 led to a reduction in k_{cat} of 1000-fold[108]. However, an understanding of the individual role of specific residues, motions or defined conformations of loop1 is still lacking. Therefore, in this thesis, the properties of loop1 were studied in more detail. In addition to loop1, other parts of the HisF active site were studied in order to get a more complete picture. These are structural elements that potentially interact with loop1 (α-helices 1 and 8') as well as the only other elongated active site loop, the $\alpha_5\beta_5$loop (loop5).

4.1.1 Mutagenesis studies on HisF loop5

Before studying loop1 in detail, it was first analysed if loop5 also plays an important role for HisF catalysis. This loop shows the same conformation in all available HisF and ImGPS structures. Strikingly, loop5 also adopts the same conformation in the homologous ImGPS enzyme His7 from yeast (e.g. PDB codes 1OX4 or 1OX5). Therefore, it appears that in contrast to loop1, loop5 adopts one stable conformation. Nevertheless, sequence analysis shows that the only residues that are conserved in this loop are the ones in positions 144, 145 and 146 (numbering according to HisF from *T. maritima*). While in most HisF proteins, positions 144 and 145 contain glycine residues (serine and glycine in HisF from *T. maritima*, respectively), position 146 is occupied by positively charged amino acids, usually arginine (lysine in HisF from *T. maritima*). The sequence conservation implies a functional role of these residues. Indeed, the sidechains of K146 and S144 point towards the active site of HisF and might interact with PrFAR (Fig. 11).

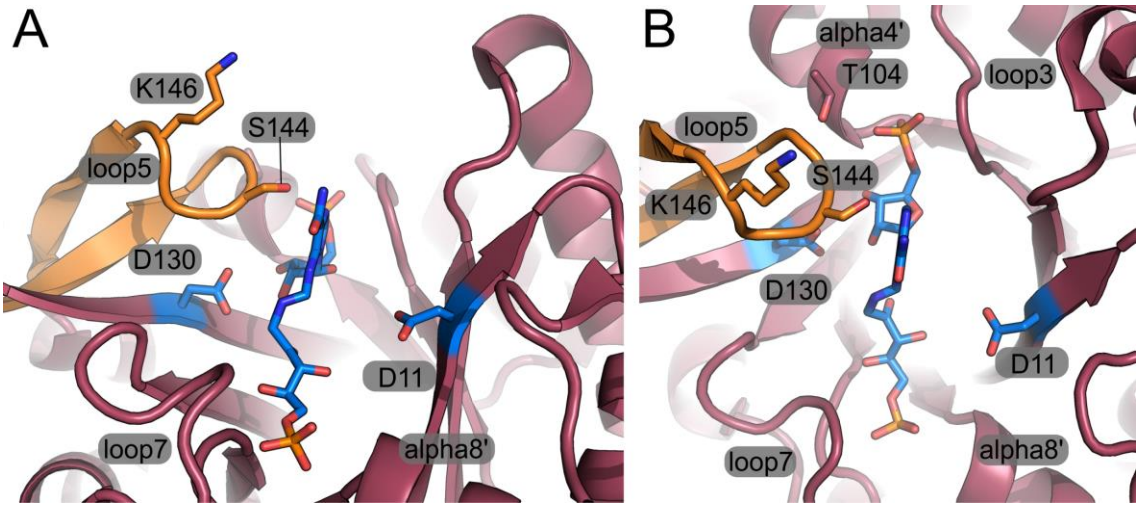

Fig. 11: Residues in loop5 analysed by mutagenesis. HisF is shown in red (PDB code 1VH7). The binding position of PrFAR was approximated by an overlay with the PrFAR-bound structure of yeast His7, which is depicted in blue (PDB code 1OX5). **(A)** Side view of the HisF active side. **(B)** Top view of the HisF active site. Loop5 is highlighted in orange. For orientation, the catalytic residues D11 and D130 are shown as blue sticks. PrFAR is bound mainly via its two phosphate groups, one binding between loop3 and α-helix 4', assisted by the side chain of T104, which is situated within α-helix 4' (shown as sticks), the other one between loop7 and α-helix 8'. The mutated residues K146 and S144 are also shown sticks. The figure illustrates how the catalytic residue D130 is covered by loop5 and how loop5 comes into close proximity to the PrFAR molecule which could result in interactions that assure its correct orientation for catalysis.

To test the impact of K146 and S144 on catalysis, the two residues were mutated. K146 was mutated to alanine and S144 to glycine, since this is the consensus for HisF proteins. The effect of both mutations S144G and K146A was tested for the ammonia dependent HisF activity. In this assay, the activity is observed via the difference in absorption at 300 nm of the substrate PrFAR and the products AICAR and ImGP. The reaction was carried out with isolated HisF proteins in the presence of ammonium chloride at pH 8.5 to provide free ammonia as a second substrate in saturation. It turned out that both mutations did not significantly affect K_M^{PrFAR} or k_{cat} (Table 2). It can therefore be assumed that neither side chain has an important functional role.

Table 2: Steady-state kinetic parameters of HisF variants with mutations in loop5 at 25 °C

HisF variant	k_{cat} (s^{-1})	K_M^{PrFAR} (µM)	k_{cat}/K_M ($M^{-1}s^{-1}$)
wild-type	2.4 ± 0.2	4.5 ± 0.5	5.3 x 10^5
S144G	3.0 ± 0.1	3.9 ± 0.6	7.7 x 10^5
K146A	1.6 ± 0.01	4.0 ± 0.7	4 x 10^5
ΔK146	0.24 ± 0.02	23 ± 4	0.1 x 10^5
Δloop5	0.04 ± 0.001	38 ± 2	926

Activity was monitored in the presence of 100 mM ammonium chloride at pH 8.5. All errors are standard errors from technical triplicates.

The fact remains that this loop appears to be structurally highly conserved and its close proximity to the catalytic residue D130 makes it likely that loop5 plays an important role in HisF catalysis. The structural conservation of loop5 despite its low conservation on the sequence level indicates that the conformation, rather than specific amino acid side chains, is responsible for this role. The two glycine (or serine) residues are most likely necessary for the loop to be able to adopt the tight hairpin conformation. To assess the importance of the structural integrity of loop5, its structure was disrupted by deletion of specific residues. Two variants were constructed, ΔK146, since the residue was observed not to be of functional relevance and Δloop5, in which residues Y143 and K147, which show no significant sequence conservation, were deleted in addition to K146. S144 and G145 were not deleted to maintain the hairpin conformation. The deletion of residues in loop5 led to an increase in K_M^{PrFAR} as well as a reduction of k_{cat} in the ammonia-dependent HisF activity (Table 2).

These data suggest that loop5 is involved in both binding and chemical turnover of PrFAR. The role in binding could be based on direct interaction via hydrogen bonds of the backbone of loop5 with PrFAR or a modulation of the phosphate binding site between loop3 and α-helix 4'. The latter contains the highly conserved residue T104 (Fig. 11B), which has been shown to be of central importance for PrFAR binding.[104,136]

The influence on the k_{cat} might be the result of the proximity of loop5 to D130. Loop5 covers D130 (Fig. 11), creating a hydrophobic environment. This might be beneficial for the acid/base catalysis of HisF, which requires the catalytic aspartate residues D11 and D130 to undergo protonation as well as deprotonation.[100] For the reaction to occur at physiological pH, this generally requires a higher pK_a value than observed for an aspartate residue that is exposed to solvent, which can be facilitated by creation of a hydrophobic environment.[137] To fully interpret the role of loop5 for D130, a more detailed knowledge of the catalytic mechanism of HisF is needed, including the determination of which aspartate residue is involved in which step of catalysis and the confirmation whether either of these steps is rate-limiting for the overall reaction rate. In the context of this thesis, which focuses on the influence of loop dynamics on catalysis, loop5 appears to be of little relevance, since it seems not to be flexible. Rather, it supports HisF catalysis by maintaining one stable conformation. The mechanistic implications will be discussed in greater detail in chapter 4.1.10.

4.1.2 Identification of key residues within loop1

In contrast to loop5, conformational flexibility has been observed for loop1.[100] The first step in the detailed analysis of loop1 was to identify functionally important residues within the loop by mutagenesis. To narrow the search for important residues in loop1, a multiple sequence alignment of 1307 ImGPS sequences (compiled by Dr. Kristina Straub, group of Prof. Rainer Merkl, University of Regensburg, Institute of Biophysics and Physical Biochemistry) was used to identify conserved residues. The sequence of loop1 was defined as residues 19 to 30, as suggested in previous studies.[108] Thus the sequence starts with the highly conserved K19, which was already found to be of functional relevance in His7 from yeast.[106] Loop1 contains several other highly conserved positions, most notably G20, F23 and G30, which show almost 100 % conservation.

Residues in loop1 with a conservation of >50% were mutated (Fig. 12A). Most positions were mutated to alanine in the classical sense of an alanine scanning (positions 19, 20, 22, 23 26, 27, 28 and 30). Since one of the key objects of study is the flexibility of loop1, additional mutations were introduced. The branching of side chains at the beta-position is known to restrict conformational freedom.[138] Since position 21 exclusively contains beta-branched amino acids (V, I and T) in all HisF sequences, T21 was mutated to glycine to introduce a maximum of flexibility. Moreover, to reduce loop1 flexibility, proline was introduced at different positions. For one, the highly conserved glycine residues at positions 20 and 30 were replaced since sequence conservation indicates that high conformational freedom at these positions might be of functional relevance. Finally, two arbitrarily chosen positions (T21 and E24) were mutated to proline to test for the implications of rigidifying loop1 at other positions. The only residue that was excluded from this study although it shows a high sequence conservation was S29, since the consensus amino acid is alanine followed by valine and isoleucine. This makes the functional relevance of the serine, present in the studied enzyme from *T. maritima*, unlikely.

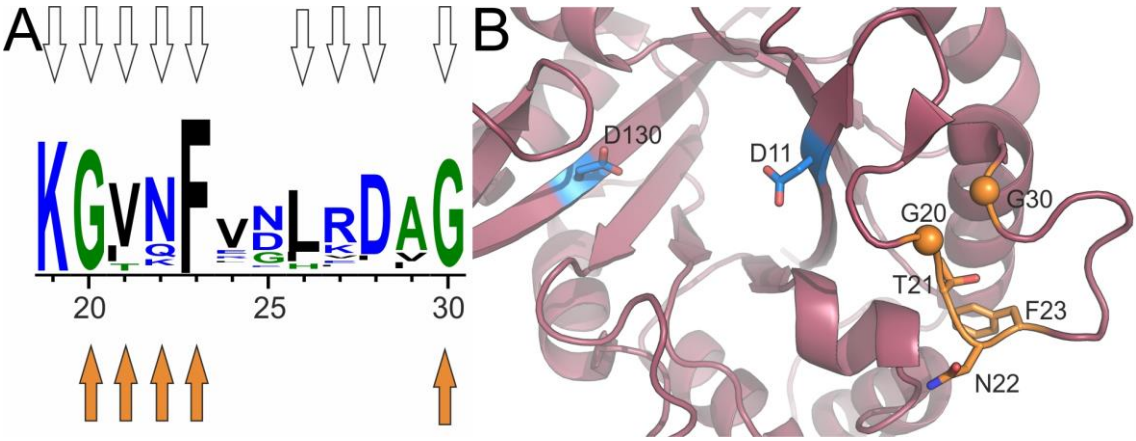

Fig. 12: Mutational analysis of single residues in loop1 of HisF. (A) Residues were selected for mutagenesis based on their conservation as represented by the sequence logo, which is based on 1307 HisF sequences. Numbering is according to the sequence of HisF from *T. maritima*. The size of the letters indicates the respective bitscore value, which reflects the relative abundance of the residue in the used alignment, but also takes into account the general frequency of the respective amino acid in all proteins (infrequently used amino acids getting higher bitscores). Residues with conservation greater than 50 % were chosen for mutagenesis (empty arrows). Residues with a significant influence on HisF catalysis are marked with orange arrows. **(B)** The functionally relevant residues are shown as orange sticks in the top view onto the HisF active site (loop1 in the open conformation, PDB-code 1VH7). The positions of G20 and G30 are indicated by spheres at the position of their respective Cα atoms. For orientation, the catalytic residues D11 and D130 of HisF are shown as blues sticks.

The influence of the individual mutations was assessed by measuring the ammonia dependent HisF reaction. The results showed that the mutations G20A, T21G, N22A, F23A and G30A had a significant effect on catalysis, underscoring the functional importance of loop1 (Table 3). The corresponding wild-type residues are highlighted in Fig. 12B. Most striking is that for all variants, the influence on the K_M^{PrFAR} value is negligible whereas k_{cat}-values tend to be decreased significantly

Table 3: Steady-state kinetic parameters of HisF variants with mutations in loop1 at 25 °C

variant	k_{cat} (s^{-1})	K_M^{PrFAR} (µM)	k_{cat}/K_M ($M^{-1}s^{-1}$)	k_{cat} wt/mut	K_M wt/mut	k_{cat}/K_M wt/mut
wild-type	2.4 ± 0.2	4.5 ± 0.5	5.3 x 10^5	1	1	1
K19A	1.1 ± 0.1	6.1 ± 1.8	1.8 x 10^5	2.2	0.7	1.5
G20A	2.2 ± 0.1 x 10^{-2}	2.1 ± 0.2	1.0 x 10^4	109	2.1	53
G20P	n.d.	n.d.	n.d.	n.d.	n.d.	n.d.
T21G	1.8 ± 0.1 x 10^{-2}	5.0 ± 0.8	3.6 x 10^3	133	0.9	148
T21P	n.d.	n.d.	n.d.	n.d.	n.d.	n.d.
N22A	2.9 ± 0.2 x 10^{-1}	8.4 ± 1.7	3.5 x 10^4	8.3	0.5	15
F23A	5.5 ± 0.4 x 10^{-3}	6.8 ± 1.3	8.1 x 10^2	436	0.7	658
E24P	n.d.	n.d.	n.d.	n.d.	n.d.	n.d.
L26A	1.1 ± 0.03	2.0 ± 0.3	5.5 x 10^5	2.2	2.3	1
D28A	2.4 ± 0.1	4.5 ± 0.9	5.3 x 10^5	1	1.9	1
G30A	1.0 ± 0.1 x 10^{-1}	3.7 ± 1.3	2.7 x 10^4	24	1.2	20
G30P	n.d.	n.d.	n.d.	n.d.	n.d.	n.d.

Activity was monitored in the presence of 100 mM ammonium chloride at pH 8.5. All errors are standard errors from a technical triplicate measurement; n.d.: activity not detectable

Mutations D28A and L26A showed little to no effect. Surprisingly, although its relevance was observed in His7,[106] also the mutation K19A had only a low impact on HisF activity. The conservation of these residues might thus have another functional reason, such as an involvement in allosteric communication with the glutaminase subunit HisH, which will be further discussed in chapter 4.2.2.

With an 8-fold decrease of k_{cat}, the mutation N22A showed a moderate influence. However, the role of N22 is not obvious. Both in structures showing an open and a closed loop conformation, N22 does not interact with any other protein residues. At this point, it can therefore only be speculated that it might be involved in a transient interaction with either protein or the substrate during the catalytic cycle.

Mutations that can be assumed to influence the flexibility of loop1 have a significantly higher impact on the catalytic rate of HisF. The mutations G20A, T21G and G30A reduced the k_{cat} 24 to 133-fold. The comparison of structures showing an open and a closed loop conformation demonstrates that the two glycine residues are situated at the sites at which loop1 bends between the two conformations, suggesting that G20 and G30 facilitate the exchange between the two states (Fig. 13A). The 133-fold reduction in k_{cat} caused by the mutation T21G indicates that while flexibility is needed, it has to be restricted, at least in certain structural elements, as well. Since most HisF proteins have a valine or isoleucine at this position, it appears unlikely that the hydrogen bonds formed by the threonine hydroxyl group with the backbone of S29 and F23 (Fig. 13B) are of particular importance. The effect on catalysis is even more drastic for mutations in which proline was introduced into the loop (G20P, T21P, E24P and G30P). For all of these variants the activity was reduced below the detection limit (no significant turnover within 10 min with 10 µM HisF and 100 µM PrFAR). This indicates that flexibility is indeed essential for loop1 to carry out its function.

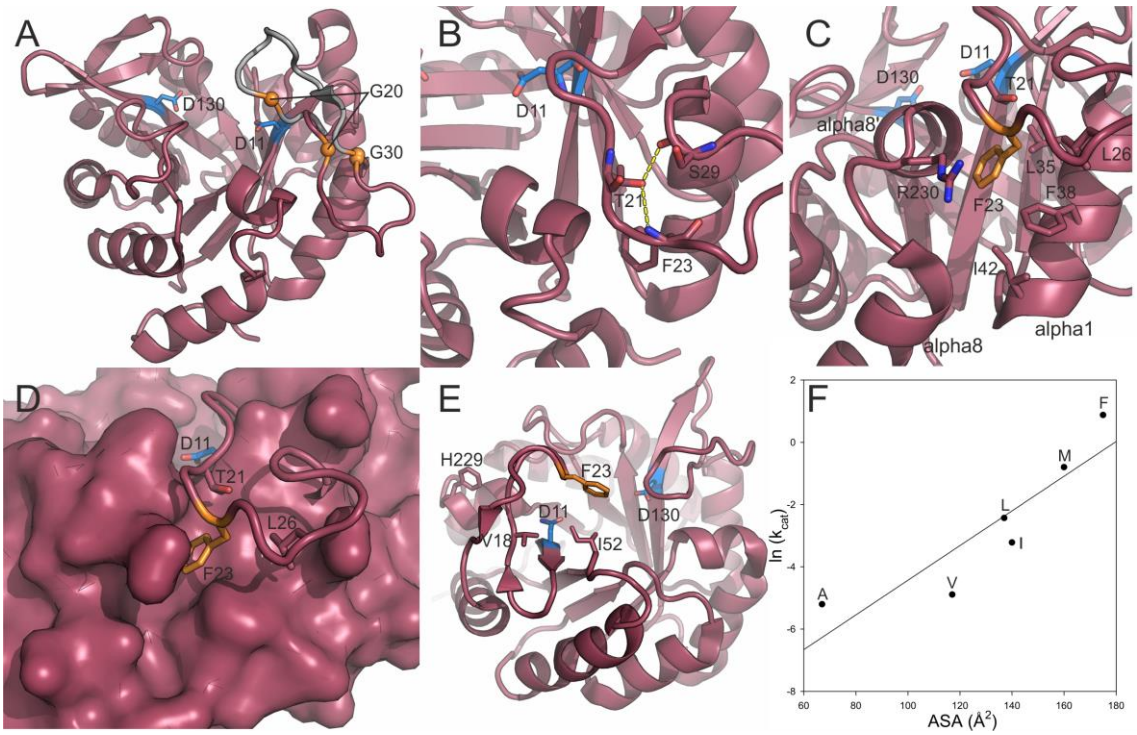

Fig. 13: Structural and mutational analysis of key residues in HisF loop1. (A) G20 and G30 (Cα atoms as orange spheres) are positioned at the hinge points of loop1 when comparing the open (red, PDB code 1VH7) and the closed conformation (grey, PDB code 1GPW, chain A). **(B)** T21 forms two hydrogen bonds with the backbone of S29 and F23, which might stabilize the open conformation. **(C)** The crucial residue F23 binds to a hydrophobic pocket in the open conformation. This pocket is formed by L35, F38 and I42. Residues that possibly also contribute to the pocket are T21 and L26 within loop1 as well as R230 in α-helix 8'. **(D)** The hydrophobic pocket around F23 in the open conformation in surface representation. **(E)** A potential second interaction site of F23 in the closed conformation is the hydrophobic patch formed by V18 and I52, which directly flank the catalytic residue D11. **(F)** The natural logarithm of the k_{cat} values of HisF variants with differently sized hydrophobic residues in position 23 shows a linear correlation with the accessible surface area (ASA) of the respective amino acid side chain.

The most pronounced effect of the alanine variants demonstrated the mutation of F23 with a 436-fold reduction of k_{cat}. An analysis of available crystal structures shows that in the open conformation, the side chain of F23 is buried in a hydrophobic pocket between α-helices 1, 8 and 8' (Fig. 13 C and D). In the closed conformation, it points toward the active site and is exposed to solvent. In this conformation, the residues V18 and I52 are in proximity and could possibly form a hydrophobic interaction surface for F23 (Fig. 13E). Thus, F23 appears to be a hydrophobic plug, which anchors certain conformations of loop1. To further analyse the role of this hydrophobic plug, several hydrophobic amino acids with increasing ASA (V, L, I, M) were inserted into position 23 by mutagenesis. The HisF activity of these variants was measured in the ammonia-dependent assay. While the K_M^{PrFAR} was not influenced by the mutations, the natural logarithm of the resulting k_{cat} showed a linear dependency on the accessible surface area of the side chain in position 23 (Fig. 13F). This observation has implications for the formulation of a kinetic model including the conformational transition of loop1 (see chapter 4.1.9).

4.1.3 Identification of key residues in the vicinity of loop1

The results presented in chapter 4.1.2 demonstrate the significance of loop1 for catalysis, with F23 being of particular importance. The experiments presented in this chapter are aimed at identifying and functionally characterizing residues that can interact with F23 or are in proximity of the interaction sites of F23 and are thus connected to its function.

Candidate residues for interaction with F23 need to be hydrophobic and located close to loop1 in order to be able from relevant contacts with F23. Residues that fit these criteria are V18, I52 and F229 (Fig. 13E), which are located in β-strand 1', the $\beta_2\alpha_2$-loop (loop2) and α-helix 8', respectively. Interestingly, V18 and I52 directly flank the catalytic residue D11. There is a gap in between the two residues into which F23 could bind, which would put it in direct vicinity of D11.

To test the role of these three residues, they were mutated to alanine and the resulting variants were tested for ammonia-dependent HisF activity (Table 4). Measurements on the variants V18A and I52A were carried out by Leon Babel.[139]

Table 4: Steady-state kinetic parameters of HisF variants with mutations in the vicinity of loop1 at 25 °C

HisF variant	k_{cat} (s^{-1})	K_M^{PrFAR} (µM)	k_{cat}/K_M ($M^{-1}s^{-1}$)
wild-type	2.4 ± 0.2	4.5 ± 0.5	5.3×10^5
V18A	0.21 ± 0.02	5.8 ± 1.4	3.6×10^4
Y39F	1.0 ± 0.03	1.9 ± 0.2	5.3×10^5
I52A	0.06 ± 0.005	7.1 ± 1.7	8.5×10^3
H228A	0.19 ± 0.01	4.2 ± 0.8	4.5×10^4
F229A	1.9 ± 0.2	3.1 ± 1.2	6.1×10^5

Activity was monitored in the presence of 100 mM ammonium chloride at pH 8.5. Errors are standard errors from a technical triplicate measurement

The mutation F229A did not lead to a significant reduction of HisF activity. The variants V18A and I52A on the other hand showed a 12-fold and 40-fold decrease in k_{cat}, respectively, which indicates a role in HisF function. This could be the result of the interaction with F23, but it is also conceivable that the two residues alone create a suitable, hydrophobic surrounding for D11 to facilitate catalysis. A hydrophobic environment leads to a preferential protonation of the carboxyl group, which is most likely necessary for D11 to carry out its catalytic function. This will be discussed in further detail in chapter 4.1.10. To conclusively determine whether V18 and I52 interact with F23, more detailed structural data of the closed conformation is needed.

In the following, the conserved residues Y39 and H228 in the vicinity of loop1 were also mutated. To avoid the creation of a large gap between α-helices 1 and 8, Y39 was mutated to phenylalanine to remove the hydroxyl group, which could be involved in important interactions. H228 was mutated to alanine. While the variant Y39F only showed a 2.4-fold decrease in HisF activity, the k_{cat} of HisF H228A was reduced 12-fold. Structural analysis of HisF showed that both Y39 and H228 are involved in a network of hydrogen bonds (Fig. 14A). In the structure of wild-type HisF (PDB code 1VH7), the imidazole ring of H228 forms a hydrogen bond with the carbonyl oxygen of the backbone of C9, a direct neighbour of D11. The other nitrogen atom of the side chain of H228 is hydrogen bonded to the hydroxyl group of Y39. A conformational change in α-helix 8' can induce the release of H228 from this hydrogen bond network (Fig. 14). This change can be observed in several crystal structures to be induced by phosphate binding between loop7 and α-helix 8' (e.g. HisF K19A, see chapter 4.1.4). Phosphate binding results in a contraction of loop7 and α-helix 8', which leads to movement of the functionally highly important residues T21 and F23. These observations may indicate that the hydrogen bond between H228 and C9 is functionally relevant and that Y39 stabilizes the relevant conformation of H228. This is in agreement with the fact that mutation of H228 has a greater effect on HisF activity than mutation of Y39.

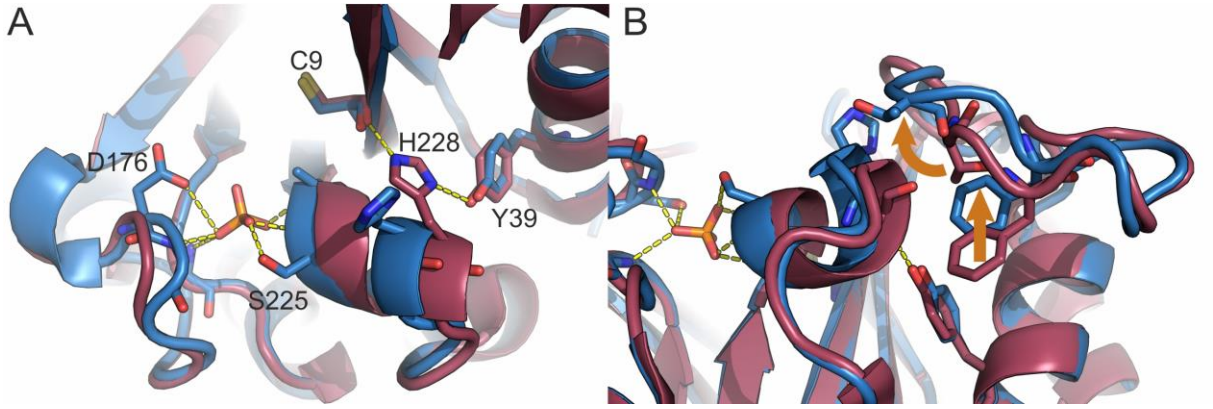

Fig. 14: Residues in the proximity of loop1 involved in conformational changes. The figure shows a comparison of the structure of wild type HisF (PBD code 1VH7, red) and the structure of HisF K19A (blue), which has an additional phosphate ion bound. **(A)** In wild-type HisF, the residue H228 forms a hydrogen bond with Y39 and the backbone of C9 without a bound phosphate. The structure of HisF K19A demonstrates how loop7 and α-helix 8' contract with a phosphate bound and H228 is released from its hydrogen bonds. Loop1 was removed for a clear view. **(B)** The side view demonstrates how loop1 conformation changes with a bound phosphate ion. The side chain of F23 moves out of the hydrophobic pocket and the side chain of T21 flips out, most likely leading to a destabilized open loop conformation (motions indicated by orange arrows).

4.1.4 Analysis of the impact of loop1 mutations on HisF structure

For further insight on the nature of the structural changes and functional implications of the introduced mutations, three-dimensional structures of HisF variants were solved by X-ray crystallography in cooperation with Dr. Chitra Rajendran (University of Regensburg, Institute of Biophysics and Physical Biochemistry). Crystals could be obtained for the variants K19A, G20P, T21P, F23A, Y39F and H228A. For all of these variants, the structures were solved. The data collection and processing statistics are summarized in Table Appendix 1. Except for some subtle differences in loops 1 and 2, particularly at the site of each mutation, the solved structures show little difference to the available structures of wild-type HisF (Fig. 15A). In all variants, loop1 adopts the open conformation. Since most variants were crystallized with high concentrations of phosphate as precipitant (1.2 M), in all structures except that of HisF G20P both phosphate binding sites are occupied. The slight shift in loop1 conformation already discussed in chapter 4.1.3 could also be observed for these structures. Also, there are some slight variations in the conformation of loop2. In the HisF variants K19A, Y39F and H228A, no further changes of significance were detected. HisF G20P, T21P and F23A show the greatest conformational distortions in loop1 (Fig. 15B, C and D, respectively). The most notable difference is the missing electron density of residues 20-24 in HisF F23A, which indicates an increase in loop1 flexibility.

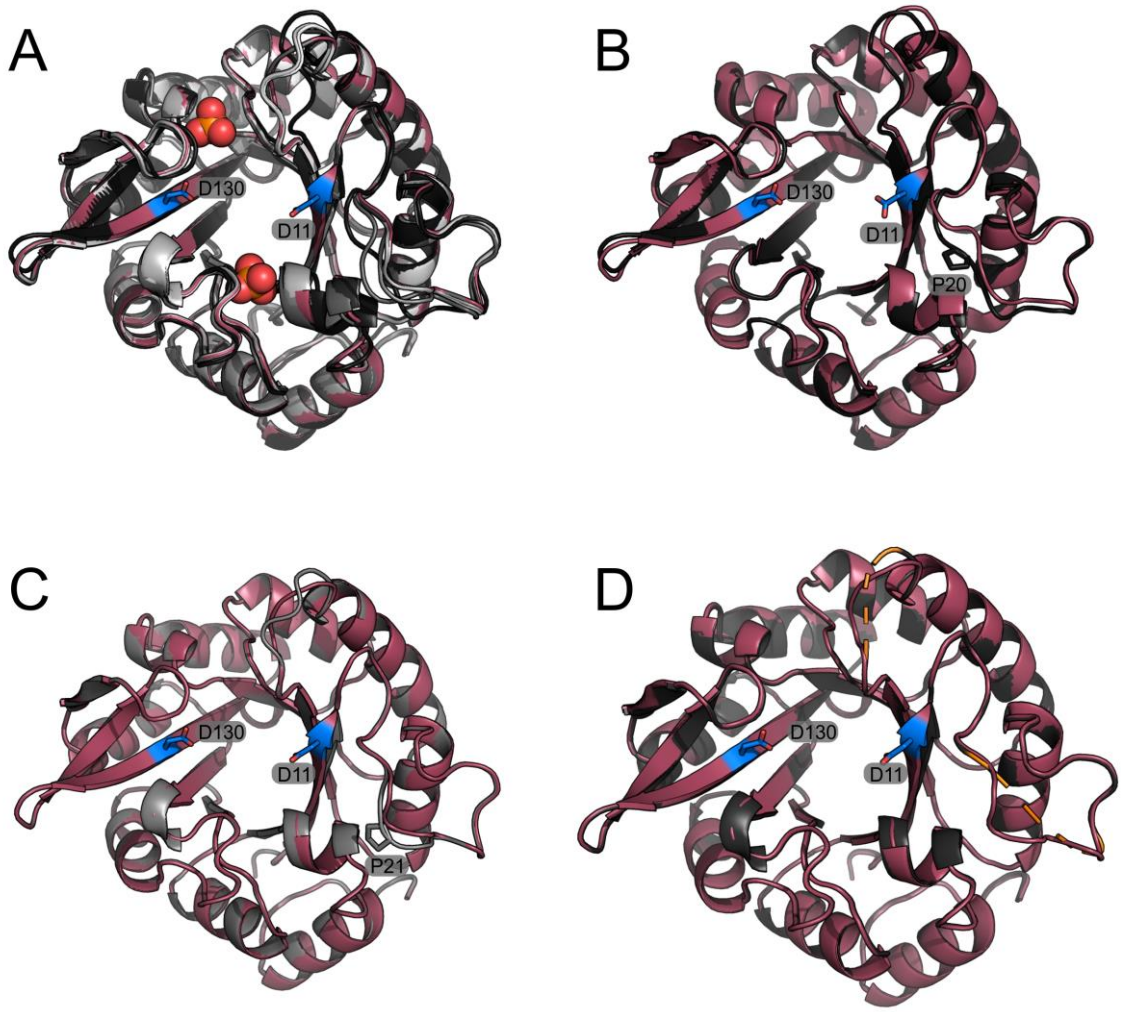

Fig. 15: Structural comparison of HisF loop1 variants. (A) Structural alignment of all solved loop1 variants (different shades of grey) with the "wild-type" structure of HisF T21S (red, PDB code 1THF). For orientation, the catalytic residues D11 and D130 are shown as blues sticks. The structures are overall very similar. In all variants, loop1 adopts the open conformation. **(B)** The structure of HisF G20P (dark grey) was aligned with wild-type HisF (red, PDB code 1VH7), because both structures do not contain phosphate ions, which lead to changes in α-helix 8' and loop1. The proline introduced into loop1 does not allow for the conformation observed in wild-type HisF. **(C)** HisF T21P (grey) shows a similar effect as HisF G20P. The conformation of loop1 is slightly distorted when compared to "wild-type" HisF (red). **(D)** HisF F23A (dark grey) is structurally very similar to "wild-type" HisF (red). The mutation apparently led to an increase in the flexibility of both loop1 and loop2, since in both loops electron density for respective residues is missing (stretches of missing residues indicated by dashed orange lines).

Taken together, all mutations do not lead to a significant change of the HisF structure. Considering the current comprehension of HisF catalysis, the solved structures cannot explain the extreme effect of the mutations G20P, T21P and F23A on HisF activity. This implies that the mutations have an effect which differs from a permanent conformational change. Instead, some mutations suggest that the conformational flexibility of loop1 might be crucial for catalysis.

4.1.5 Analysis of loop1 flexibility

In this chapter, the connection of loop1 flexibility and HisF catalysis will be addressed. For experiments assessing the relevance of loop1 flexibility, two mutations within loop1 which show a strong effect on HisF activity and are anticipated to have opposite effects on loop1 flexibility were chosen for a more detailed analysis: i) The mutant F23A was used as a model for increased loop flexibility since this mutations leads to part of the loop not being resolved in the crystal structure; ii) The mutation G20P was chosen, since the exchange of glycine to proline is assumed to have the greatest rigidifying effect on loop flexibility.

As a qualitative test of loop flexibility, limited proteolysis with trypsin was performed. This method is based on the observation, that the rate of proteolytic cleavage is dependent on the conformational flexibility of the protein.[140] Flexible regions of proteins are more often in unordered states that are exposed to the solvent and are thus accessible for proteases. In experiments with wild-type HisF, it could be observed that the protein is generally very resistant against limited proteolysis by trypsin, but is cleaved in one position, R27 in loop1.[100] In a repetition of this experiment, it could be observed that it requires approximately 250 min to cleave about 50 % of wild-type HisF. HisF G20P is cleaved much slower, showing only slight proteolysis after 250 min. HisF F23A possesses a much more accessible loop1, since 50 % cleavage is observed already after 25 min and cleavage is completed after 250 min (Fig. 16A). This result confirms that loop1 flexibility is indeed decreased for the variant G20P and increased for the variant F23A. Remarkably, the addition of the substrate analogue ProFAR (70 µM) did not change susceptibility to proteolysis (data not shown).

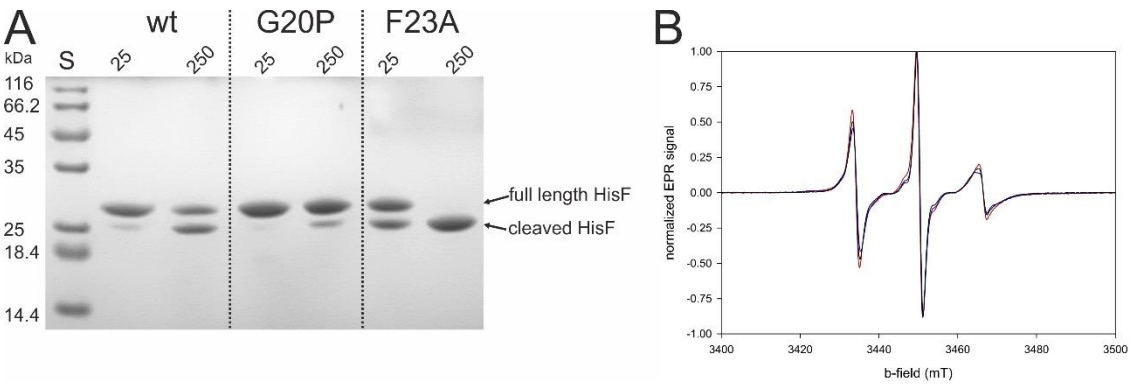

Fig. 16: Limited proteolysis and EPR spectra of HisF variants with different loop1 flexibility. (A) Limited proteolysis with trypsin shows that wild-type HisF was cleaved to ~50% over the course of 250 min. In the same timeframe, HisF G20P is cleaved only to a small extent, while HisF F23A is cleaved completely. **(B)** EPR spectra were recorded in 50 mM Tris/HCl pH 7.5 with 100 µM protein. All proteins carry the mutations necessary for site specific labelling (C9S and E24C). Curves show the spectra of HisF with no further mutation (black), with F23A (red) and G20P (blue). All spectra are typical for a dynamic element as expected for a loop, however containing a more static component. Curves were fitted with application of the Redfield-theory to gain an indication as to the differences in ns motions. All experiments were carried out at 25 °C.

For a quantitative analysis of loop1 flexibility, electron paramagnetic resonance (EPR) spectroscopy was performed in cooperation with Dr. Magdalena Schumacher (group of Prof. Heinz-Jürgen Steinhoff, University of Osnabrück). EPR observes the spin resonance of an unpaired electron in a magnetic field. This method is sensitive to the rotation of the molecule carrying the unpaired electron and a rotational correlation time (RCT) can be calculated for the recorded spectra, which is an indicator for the mobility of the monitored molecule. Since the rotational correlation times of proteins are approximately 10-100 ns, only movements faster than this can be observed because slower effects are masked by the protein rotation. Loop movements

span a relatively large range of timescales, depending on the size of the loop and the observed movement. Thus, it is possible, that loop motions are slower or faster than the protein rotation. However, the rotational freedom of amino acid side chains within a loop is strongly dependent on whether the loop is ordered or disordered, since ordered states strongly reduce their conformational freedom. Thus, EPR spectroscopy should give a good measure of the flexibility of loop1.

For EPR measurements on loop1 the mutations C9S and E24C were introduced. These mutations were necessary to ensure the site specific labelling of loop1 via disulphide chemistry. While these mutations led to a decrease in activity, the k_{cat}/K_M of 6 x 10^4 $M^{-1}s^{-1}$ (5.36 x 10^4 $M^{-1}s^{-1}$ in wild-type HisF) indicates that this variant is still a good model of an active HisF enzyme.[110]

Analysed HisF variants were labelled with the spin label (1-Oxyl-2,2,5,5-tetramethylpyrroline-3-methyl)methanethiosulfonate (MTSSL). Experiments were carried out with the C9S E24C double mutant as well as with HisF variants that additionally carry the mutations G20P or F23A, respectively.

EPR measurements revealed that for all three variants loop1 is flexible, as indicated by the narrow peaks of the EPR spectra (Fig. 16B). Slight differences could be observed in the shape of the spectra. The peaks differ in amplitude and width, which is indicative of a change in molecular dynamics. Calculation of the RCT using the Redfield theory[141] revealed that loop1 dynamics indeed changed as previously hypothesised. For the wild-type HisF model, the RCT is 1.82 ns. The mutation G20P led to a decrease in loop dynamics, indicated by an increased RCT of 2.02 ns. The mutation F23A on the other hand led to a decrease in the rotational correlation time to 1.52 ns, indicating a more flexible loop. The addition of 200 µM PrFAR did not change the EPR spectra of any of the HisF proteins significantly (data not shown). This indicates no significant change in loop1 dynamics upon substrate binding, which is in agreement with the observation made in limited proteolysis experiments.

The results from both proteolysis and EPR spectroscopy show that the introduction of the activity impairing mutations G20P and F23A leads to a disruption of the loop dynamics observable in wild-type HisF. There is no indication that substrate binding induces a change in the dynamics of loop1.

4.1.6 Localization of loop1 in solution

Recent smFRET measurements confirmed the existence of two conformations of loop1 in solution, which matches the observation of an open and a closed conformation made in crystal structures.[110] However, no clear correlation between the existence and population of either conformation with the catalytic performance of the respective HisF variant was observed. A reason for this might lie in the FRET methodology. Due to experimental requirements as well as optical properties, FRET labels are rather large molecules with a molecular weight of over 1 kDa. The modification of a flexible loop with such a molecule undoubtedly changes the loop dynamics and could also shift the conformational equilibrium via unintended interactions of the labels. These effects are reduced with smaller labels. Additionally, FRET measurements only give a distance measure and several separate measurements with labels at different positions are needed to gather structural information as to where the observed loop lies relative to the rest of the protein.

To gather more detailed structural information on loop1 in solution an orthogonal method to smFRET was applied. The method used here was paramagnetic relaxation enhancement (PRE). Similar to EPR spectroscopy, PRE uses chemical labelling with a molecule that carries an unpaired electron (spin label). Since an unpaired electron possesses a paramagnetic moment, it has an influence on observed signals in an NMR spectrum. The influence of the unpaired electron on the magnetic field leads to an increase in the rate of relaxation of nuclear spins that are in

proximity. Thus, the time in which the signal can be recorded is decreased, leading effectively to a decrease in signal strength up to complete eradication. The strength of this effect is strongly dependent on the distance between the spin label and respective atom, allowing for distance approximations of NMR active atoms to the spin label. However, in a flexible element such as loop1, one has to consider that signal strength is also dependent on the amount of time the label is in proximity of the respective residue. Thus, the observed PRE effects are only an approximation of the loop position and do not give quantitative distance information. Protein samples for these measurements were prepared by Alisa Ruisinger[110] and measurements were performed by Dr. Jan-Philip Wurm (group of Prof. Remco Sprangers, University of Regensburg, Institute of Biophysics and Physical Biochemistry).

For PRE measurements, a 4-Maleimido-2,2,6,6-tetramethyl-1-piperidinyloxy (M-TEMPO, Fig. 17A) spin label was introduced into loop1 at position 24, using the same variant as for EPR experiments (HisF C9S E24C). The introduction of the mutations C9S and E24C lead to a perturbation in the chemical shift of several residues distributed over the entire protein when compared to a spectrum of wild-type HisF (Fig. Appendix 1), which highlights that loop1 exerts an influence on the entire protein. ^{15}N-labelled HisF C9S E24C was chemically modified with M-TEMPO and the PRE was recorded for ^{1}H-^{15}N signals in TROSY spectra. As a control, the spin label was reduced with ascorbate, eliminating the free radical and thus its paramagnetic properties. This leads to re-emergence of previously attenuated peaks and shows whether the observed attenuation is really the result of the spin label or is a result of mutagenesis or chemical modification. For all HisF variants used, the attenuated signals reappear after reduction, showing that the observed PRE is a reliable measure for the proximity of the label to the respective backbone amides (Fig. Appendix 2).

The distribution of PRE effects in the wild-type HisF model shows that most amides affected by the spin label lie at the C-terminal ends of α-helices 1, 8 and 8' (Fig. 17B). Particularly strong PRE values are observed for α-helix 8' around F229 and the $\alpha_1\beta_2$-loop around G43. This pattern shows unambiguously that in solution, most of the HisF molecules adopt an open loop conformation very similar to the one observed in crystal structures, which is in good agreement with smFRET data.[110] There are slight changes in peak intensity in residues S144, D176 and G202 in loops 5, 6 and 7, respectively. This could be an indication that the spin label is close to these positions when adopting a lesser populated conformation, which would be in agreement with the closed conformation previously identified in crystal structures in the presence of HisH (for instance PDB code 1PGW). Overall, these data, combined with the data from smFRET experiments, confirm the assumptions made on the basis of crystal structures: loop1 almost exclusively adopts the open conformation.

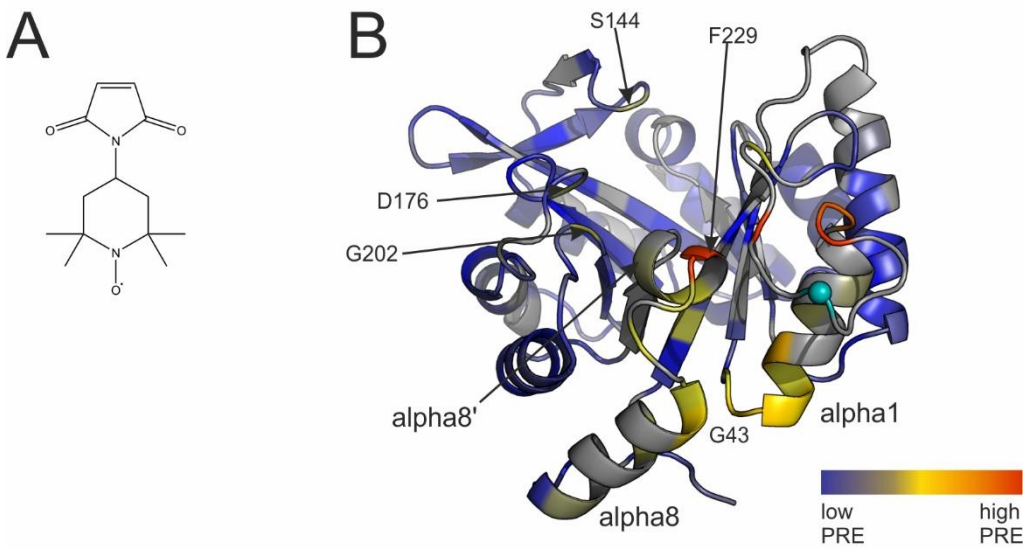

Fig. 17: PRE of HisF backbone amides induced by M-TEMPO labelling. (A) Chemical structure of M-TEMPO. **(B)** Cartoon representation of the wild-type HisF structure (PDB-code 1VH7) coloured according to the measured relative peak integrals observed in H^1N^{15}-TROSY spectra. The applied range is from 0 to 1.12 (maximum observed relative value) and is colour coded red (low values, high PRE) via yellow to blue (high values, low PRE). Grey colouring signifies a change in chemical shift of the respective residue relative to wild-type HisF caused by mutations made for labelling. These residues cannot be assigned to a specific signal without further experiments. The position of the M-TEMPO spin label is marked by a cyan sphere at the position of the Cα of C24. The distribution of signals affected by the M-TEMPO label clearly indicates that the main conformation of loop1 is the open conformation, as shown, or at least similar to, the conformation shown in this structure.

To determine whether a significant shift from the closed towards the open conformation can be observed upon substrate binding, the measurements were repeated in the presence of 300 µM ProFAR. The addition of ProFAR led to further chemical shift perturbations, accompanied by a strong peak broadening over the entire spectrum. The peak broadening upon ProFAR binding is not observed in wild-type HisF and thus appears to be an artefact of the mutations C9S and E24C introduced for labelling. Thus, these data cannot reliably be taken for the determination of loop1 conformations. However, the amide signal of G43 could still be identified and this particular signal was strongly attenuated, demonstrating that a large portion of the protein molecules still adopts the open conformation.

For the detection of changes in conformation introduced by mutagenesis, the PRE experiments were repeated for two HisF variants carrying either of the two mutations G20P or F23A in addition to the mutations necessary for labelling (C9S E24C). Both mutations led to further alterations in the chemical shift of several residues and reduced the number of available signals for loop localization. In F23A, the signal of G43 and D233 ($\alpha_1\beta_2$-loop and α-helix 8, respectively) showed significant PRE, indicating that loop1 in HisF F23A also mainly adopts an open conformation (Fig. Appendix 3A). Also, K179 showed a slight signal reduction, which indicates the existence of the open conformation of this mutant. The variant G20P showed a similar pattern, with a significant PRE for residues G43 (and its two direct neighbours), I232 and K238 (α-helix 8 and 8', respectively), indicating that here, too, the main conformation is the open state (Fig. Appendix 3B). It should be kept in mind, that especially in HisF F23A and HisF G20P, this might be due to the lack of a proper assignment of signals. Just as in HisF C9S E24C, the addition of ProFAR led to further changes in the spectrum, although the peak broadening effect was much smaller. The signal of G43 could again be taken as an indicator that there is still a significant population of the open conformation for both variants. Hence, also the PRE experiments with HisF G20P and HisF F23A show that loop1 is almost exclusively in the open conformation.

Unfortunately, both the introduction of cysteines for attachment of spin labels and the addition of the substrate analogue ProFAR results in limited data quality, restricting their information

content. In order to improve this, one could perform the backbone assignments of the mutants which would lead to better structural information for these proteins. The most useful change however would be to avoid the two mutations currently introduced for labelling altogether, since they have several disadvantages: They reduce the HisF activity, they lead to significant chemical shift perturbations and they induce an artefact that causes significant peak broadening upon ProFAR binding. It would be conceivable to use an unnatural amino acid (UAA), such as p-ethynylphenylalanine or p-propargyloxyphenylalanine, which could then be coupled with an azide modified TEMPO spin label. This method would eliminate the necessity for the mutation of C9, which has a detrimental effect on HisF activity.[100,110] However, the incorporation of UAAs is usually accompanied by a significant loss in protein yield. This is problematic for NMR experiments, since not only are relatively high amount of protein needed, but expression also has to take place in minimal medium to allow for isotopic labelling, which in turn most likely reduces the efficiency of UAA incorporation.

4.1.7 Analysis of loop1 mutations on induced fit

To detect structural changes in HisF introduced by substrate binding, ^{1}H-^{15}N-TROSY spectra of ^{15}N-labelled HisF proteins were recorded in the presence and absence of the substrate analogue ProFAR. In wild-type HisF, ProFAR induces the emergence of a new set of peaks (Fig. 18A). These signals are quite weak and do not replace the signals of the apo state. This is a clear indication of the emergence of a second HisF conformation upon ProFAR binding (induced fit), which is in equilibrium with the conformation of the apo state. Since these spectra do not give additional structural information, at this point it cannot be determined whether these two conformations correspond to the open and closed conformation of loop1.

Interestingly, the emergence of this second set of signals is not observed for the HisF variants F23A and G20P (Fig. 18B and C, respectively). This suggests that the induced fit is eliminated by these two mutations, which implies a functional relevance of loop1 for this conformational change. This will be discussed further in chapter 4.1.8.3.

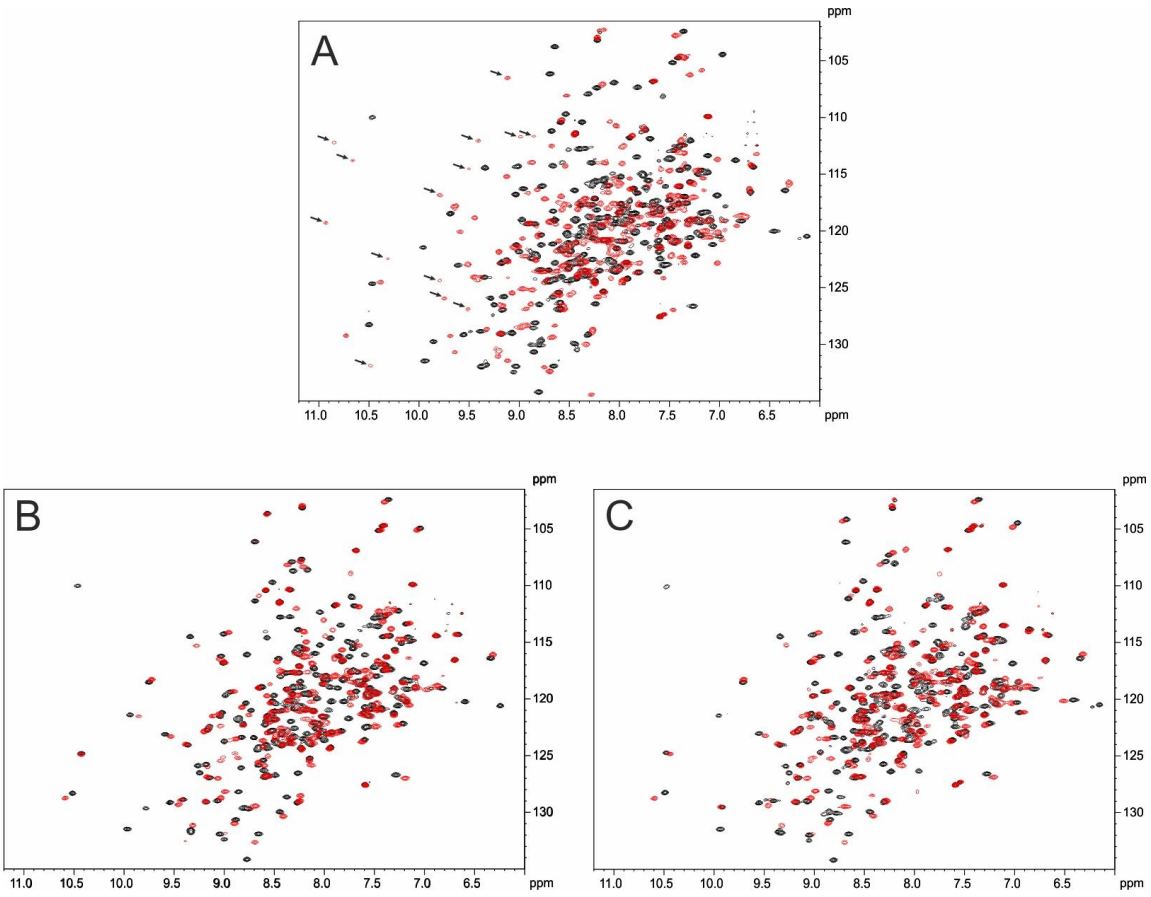

Fig. 18: NMR spectra of HisF variants with different loop flexibility. The spectra show the chemical shift distribution of HisF proteins in the apo state (black) and in the presence of 300 µM ProFAR (red). **(A)** wild-type HisF. The binding of ProFAR induces the emergence of weak signals not present in the apo state (examples indicated by black arrows). These additional signals are not observed in HisF F23A **(B)** and HisF G20P **(C)**.

4.1.8 Studies on the microscopic rate constants of ligands binding to HisF

A major target of this work is to determine the correlation between the enzymatic activity and the conformational dynamics of loop1. For this purpose, it is essential to have detailed kinetic knowledge of the HisF reaction beyond the commonly determined steady-state kinetics in order to correlate rates of specific steps of the reaction with conformational motions. Two very important steps are substrate binding and product release, which are often connected to active site loop dynamics.[61–64] Microscopic rate constants for binding and dissociation of substrate and product molecules can be determined by stopped-flow spectroscopy. This method, however, depends on a change in the spectroscopic properties of one interaction partner after binding. Previous work was based on the fluorescence of W156 for the determination of equilibrium dissociation constants for the substrate PrFAR.[142] In control experiments with free tryptophan, it became evident that the addition of PrFAR, its analogue ProFAR or the reaction product AICAR quenches the tryptophan fluorescence unspecifically (Fig. Appendix 4). Because this kind of effect is strongly dependent on the microenvironment of the tryptophan molecule or residue, subtraction of a control with free tryptophan is not sufficient for correction. Therefore, for stopped-flow experiments with HisF another spectroscopically active sensor was needed. In this work, the unnatural, fluorescent amino acid L-(7-hydroxycoumarin-4-yl)ethylglycine (CouA) was used.[117] Its hydroxycoumaryl moiety shows spectroscopic properties that are very suitable for binding experiments. The main advantage of this UAA is that it absorbs and emits light at higher wavelengths than PrFAR, which makes it less susceptible to quenching (Fig. 19A). The high quantum yield of 0.63 should furthermore lead to a good spectroscopic signal and the strong

Stokes-shift ensures a good separation of the fluorescence signal and the scattering signal of excitation light.[117] Finally, CouA shows a high sensitivity to environmental factors such as dielectric constant, hydration and pH,[143,144] which is caused by the protonation equilibrium of the 7-hydroxy group of the coumaryl moiety. Deprotonation results in a shifted absorption maximum (370 nm, c, instead of 340 nm, p, Fig. 19A and B). This leads to a drastic change in fluorescence intensity depending on the wavelength used for excitation. Since in general, protonation reactions are considered to be very fast (>10^5 s^{-1})[145] and the maximum rates that can be observed in stopped-flow experiments are about two orders of magnitude slower than this,[146] it is very unlikely that this reaction leads to any limitations for rate measurements. In fact, if fluorescence is excited at either absorption maximum of the protonated or charged form of CouA, a shift in protonation will directly impact the fluorescence intensity because of the change in absorbance. This can generate a strong signal for binding experiments.

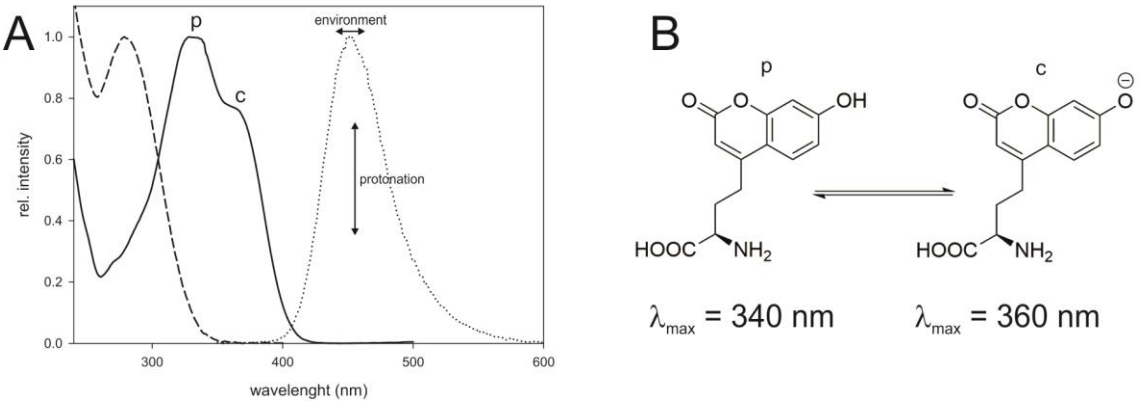

Fig. 19: Spectroscopic properties of CouA. (A) Absorbance spectrum of PrFAR (dashed line), absorbance of free CouA (solid line) and fluorescence of free CouA (dotted line) recorded in 50 mM Tris/HCl pH 7.5. The spectra have been normalized to the respective maximum. Double arrows indicate the change in fluorescence upon a change in the environment of CouA: the horizontal arrow shows the shift of the maximum to higher or lower wavelength, the vertical arrow indicates that by altering the protonation, the fluorescence intensity is changed due to a change in magnitude of absorption, depending on the wavelength used for excitation. **(B)** Equilibrium of CouA between protonated (p) and charged (c), which influences the absorption spectrum of CouA as shown in (A).

4.1.8.1 Evaluation of CouA as a probe for ligand binding to HisF

For incorporation of CouA into HisF, the amber STOP-codon suppression method was used as published by the Schultz group.[117] For this purpose the gene of the corresponding aminoacyl-tRNA synthethase, optimized by directed evolution for CouA incorporation, was cloned into the vector system pEVOL,[147] which carries two copies of the aminoacyl-tRNA synthethase gene and the gene for the tRNA carrying the TAG-anti-codon. The amber STOP-codon was introduced into the *hisF* gene by site directed mutagenesis (chapter 3.2.2.5), and modified HisF was produced by heterologous gene expression in *E. coli* in medium containing saturating concentrations of CouA (0.45 mM). The resulting protein was purified as described in chapter 3.2.4.4.

For ligand binding experiments, K132 in HisF was chosen because it is positioned in the elongated β-strand 5 (Fig. 20). This position is in the periphery of the active site and CouA incorporation should not interfere with ligand binding. However, the CouA residue should be close enough to sense the presence of the ligand and generate a spectroscopic signal.

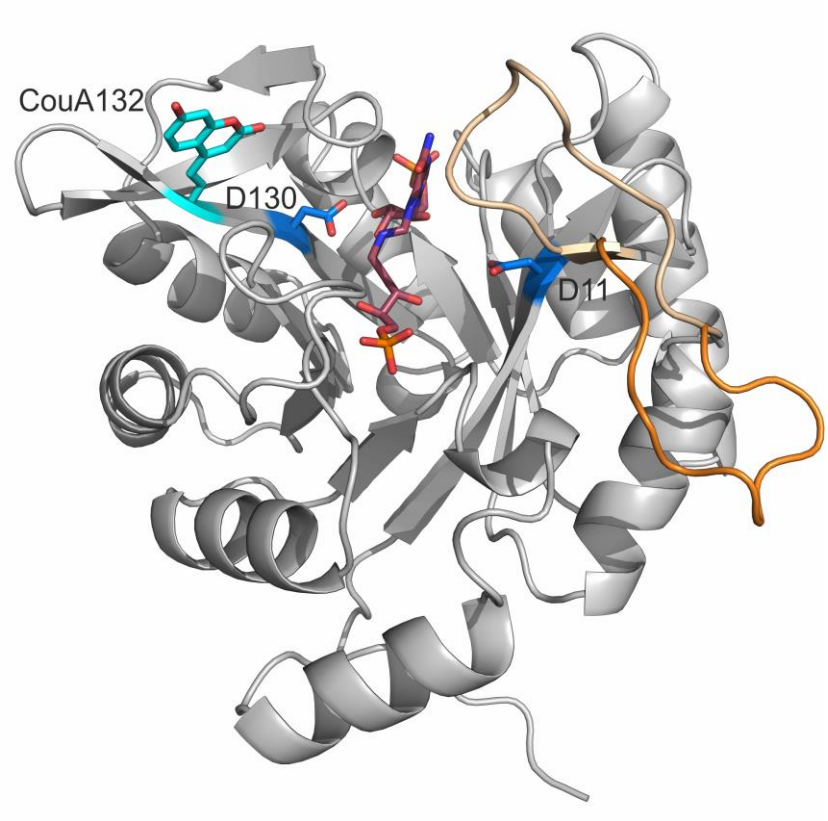

Fig. 20: Labelling of HisF with CouA in position 132 for measurements of ligand binding.. CouA (cyan sticks) was incorporated *in silico* using YASARA into the structure of wild-type HisF (PDB-code 1VH7). Position 132 was chosen due to its proximity to the binding site of PrFAR (red sticks, super-positioned from the complex structure of yeast His7, PDB-code 1OX5). The position is opposite to the flexible loop1, which is shown in the open (orange ribbon) and closed (beige ribbon, super-positioned from the structure of the full ImGPS complex, PDB-code 1GPW) conformation. For orientation, the catalytic residues D11 and D130 are shown as blue sticks.

Purified HisF K132CouA was analysed by SDS-PAGE and the resulting gel was imaged under UV-light observing CouA fluorescence and after Coomassie staining (Fig. 21A). The SDS-PAGE shows that the protein is > 90 % pure and has the same molecular weight as the wild-type protein. Some impurities could be detected, but these are most likely products of proteolytic cleavage of HisF K132CouA, since they also contain CouA and are detected via their fluorescence under UV light. The protein exhibits the absorption maximum of a regular protein at 280 nm and additionally shows the absorption of CouA (maxima at 340 and 370 nm) as well as the corresponding fluorescence properties with an emission maximum at 450 nm (Fig. 21B).

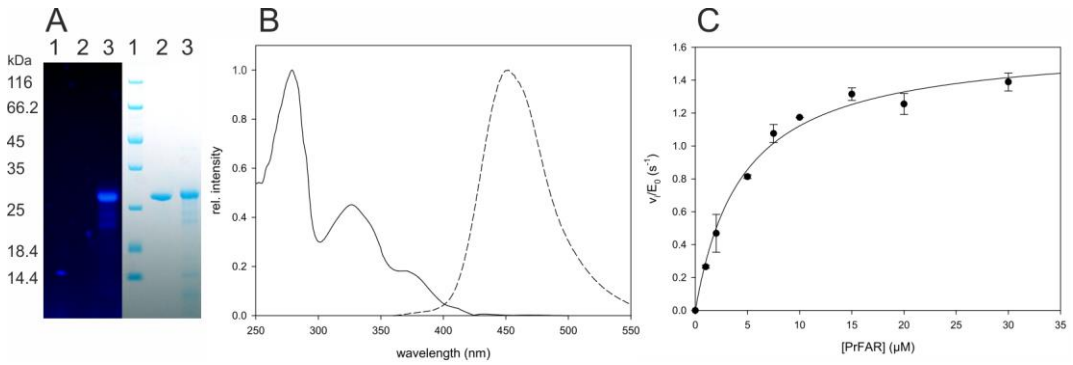

Fig. 21: Overview of the biochmical properties of HisF K132CouA. (A) SDS-PAGE under UV-light (left hand side, 366 nm illumination) and after Coomassie staining (right hand side). Both the molecular weight standard (lane 1) and wild-type HisF (lane 2) do not show fluorescence, while HisF 132CouA (lane 3) clearly fluoresces. **(B)** Absorbance (solid line) and fluorescence (dashed line) spectra of HisF K132CouA, normalized to the respective maximum. **(C)** Steady state kinetics of the ammonia-dependent PrFAR turnover of HisF 132CouA. Activities were monitored in the presence of saturating ammonia concentrations (100 mM ammonium chloride at pH 8.5) at 25 °C. Data points were recorded as technical triplicates with standard deviation as error bars. The line represents a fit to the Michaelis-Menten equation which yielded a k_{cat} value of 1.5 s^{-1} and a K_M^{PrFAR} value of 4.1 µM, in good agreement with values for the wild-type protein.

To verify that the incorporation of CouA at position 132 does not disturb the function of HisF, steady-state kinetics of PrFAR turnover in the ammonia-dependent cyclase assay were measured (Fig. 21C). The resulting k_{cat} of 1.5 ± 0.1 s^{-1} and K_M^{PrFAR} of 4.1 ± 0.9 µM are almost identical to those of wild-type HisF (2.4 s^{-1} and 4.5 µM for k_{cat} and K_M^{PrFAR}, respectively, see Table 3). Thus, HisF K132CouA is a suitable model for wild-type HisF and is referred to as "wild-type" in the following measurements. All other variants are only referred to by their respective mutation, the CouA moiety residing in position 132 if not explicitly stated otherwise.

4.1.8.2 Determination of equilibrium dissociation constants of HisF ligands

To test whether the incorporation of CouA gives a suitable signal for ligand binding and whether binding is impaired in HisF containing CouA, equilibrium titrations were performed in a fluorescence spectrometer for the substrate PrFAR and reaction products ImGP and AICAR. Control titrations against free CouA did not yield a signal beyond the dilution, demonstrating that the quenching effect observed for tryptophan is not present for CouA.

The addition of the ligands to wild-type HisF led to a decrease in fluorescence intensity. The resulting difference in fluorescence was plotted against the ligand concentration and fitted with a hyperbola to determine the dissociation constants (Fig. 22). The resulting values are 1.1 µM, 2.2 mM and 1.1 mM for PrFAR, AICAR and ImGP, respectively. These data are in good agreement with those resulting from ITC and/or NMR experiments (0.5 µM for PrFAR by ITC, 1.5 mM for AICAR by NMR and 0.5 mM for ImGP by ITC).[148] Intriguingly, the apparent dissociation constant for ImGP is lowered to 40 µM (approximately 26-fold) in the presence of 5 mM AICAR. Likewise, the apparent dissociation constant for AICAR is reduced to 274 µM (approximately 8-fold) in the presence of 1 mM ImGP. These findings indicate a significantly higher stability of the ternary complex (HisF:ImGP:AICAR) compared with the respective binary complexes (HisF:ImGP and HisF:AICAR). It should be kept in mind that due to the limited access to the two products they could not be supplied in saturating concentrations, the exact values for formation of the ternary complex should therefore be viewed with caution. It can be assumed that the K_D values for formation of the ternary complex would further decrease with saturating concentrations of the respective second product. For the second HisF substrate, ammonia, no binding signal could be observed, indicating that either no binding occurs in the absence of PrFAR or that no significant signal change is caused by ammonia binding.

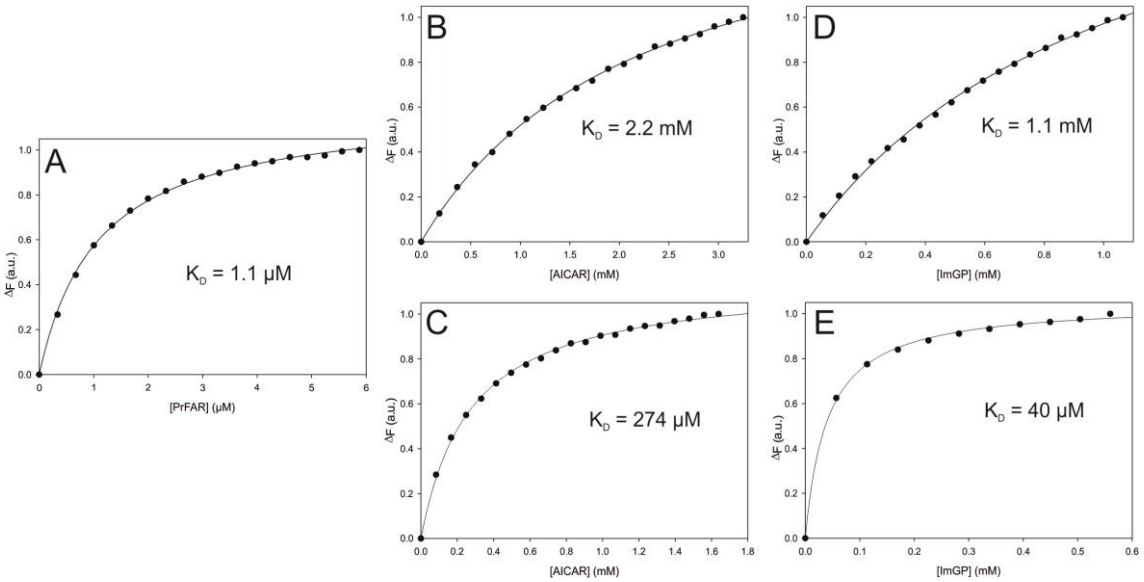

Fig. 22: Equilibrium fluorescence titration of HisF ligands to wild-type HisF at 25 °C. 1 µM HisF was titrated with the respective ligand in 1.5 ml 50 mM Tris/HCl pH 7.5 in a fluorescence spectrometer under constant strirring. The fluorescence signal was corrected for HisF dilution and normalized to the highest value measured. The data was fitted with a simple hyperbolic equation to determine the dissociation constant. Titrations are shown for the ligands PrFAR **(A)**, AICAR in the absence **(B)** and presence of 1 mM ImGP **(C)** and ImGP in the absence **(D)** and presence **(E)** of 5 mM AICAR.

4.1.8.3 Binding rate of the substrate PrFAR

With a suitable detection method in place, the PrFAR binding rate was determined by following the CouA fluorescence in a stopped-flow spectroscopy apparatus. The excitation wavelength was set to 367 nm, as the used xenon lamp exhibits a high intensity at this wavelength and the absorbance maximum of CouA (370 nm) is also close to this wavelength, ensuring a strong signal. The fluorescence was monitored with a cut-off filter of 400 nm, which allows for the detection of almost the complete fluorescence emission of CouA and should exclude all scattered excitation light.

PrFAR binding led to a strong decrease in fluorescence intensity, as expected from the equilibrium titrations. The binding transients consisted of two phases, a fast phase with high negative amplitude and a slow phase with low and positive amplitude. Accounting for these two phases, the transients could be described well with double exponential fits (Fig. 23A). The second, slow phase shows a quite low rate constant (~0.05 s^{-1}). Since this would be unusually slow for ligand binding, the fast phase was assumed to represent PrFAR binding. In the first instance, the substrate binding mechanism was evaluated by plotting observed rate constants (k_{obs}) as a function of PrFAR concentration. However, the slow phase could not be fitted adequately with double exponential fits for low PrFAR concentrations due to its low signal amplitude. Thus, to assess the binding velocity, the first phase of the transients (up to the time of 1 s) was fitted with a single exponential decay function, which describes this phase reasonably well (Fig. 23B). The resulting observed rates (k_{obs}) and amplitudes were plotted against the PrFAR concentration (Fig. 23C and D, respectively). The k_{obs} value shows a hyperbolic dependence on the PrFAR concentration, which is typical for a binding equilibrium with a subsequent conformational equilibrium (induced fit). While quantification of the conformational change is not possible from this analysis, it can be taken as a qualitative indication which agrees with the observation of a second phase in the transients. The amplitude of the fast phase also follows a hyperbolic increase with the PrFAR concentration and was used to determine the equilibrium dissociation constant of PrFAR of 1.5 µM, which is in good agreement with the equilibrium titration data (1.1 µM).

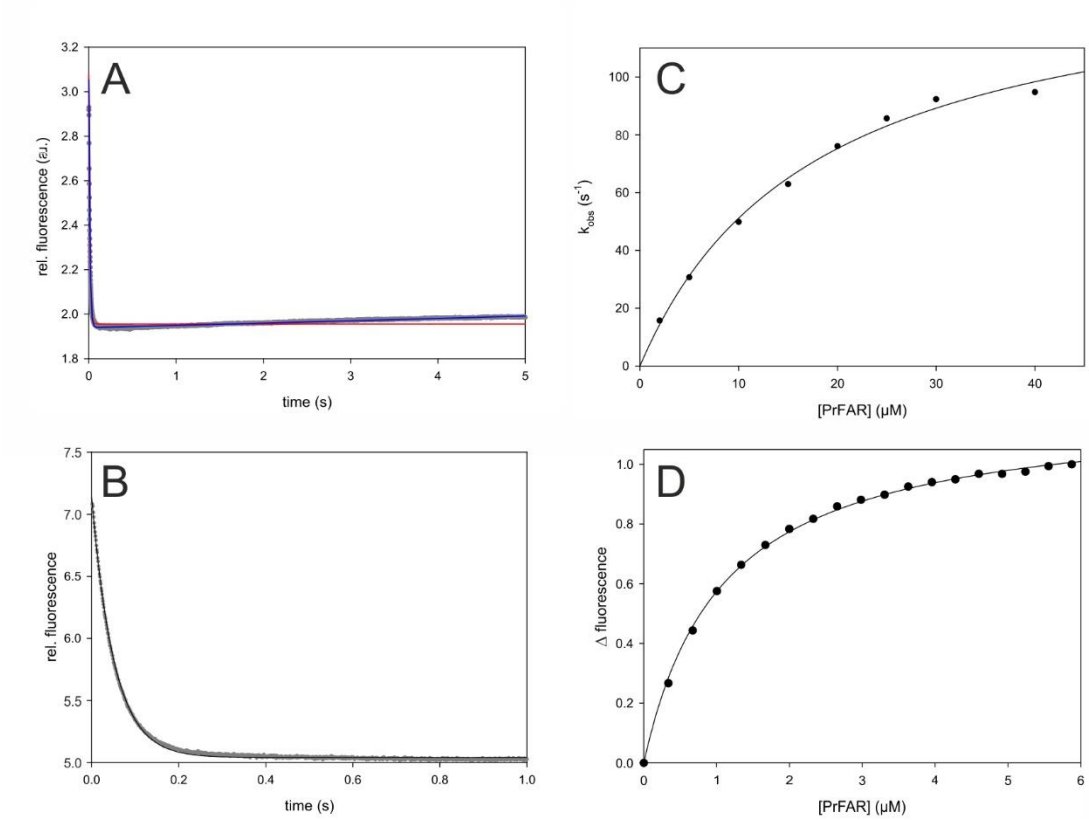

Fig. 23: PrFAR binding to wild-type HisF as observed in stopped-flow experiments at 25 °C. PrFAR binding was observed by the change in fluorescence of the CouA residue (λ_{ex} = 367 nm, λ_{em} > 400 nm). **(A)** Transient of PrFAR binding (40 µM) to HisF. After the initial fast binding phase, a second, slow phase can be observed. A single exponential fit (red line) only describes the binding phase, while a double exponential fit (blue line) describes both phases. **(B)** The fast phase of the transients (0 – 1 s) was fitted to single exponential function (black line). **(C)** Secondary plot of the observed pseudo first order binding rate k_{obs} against the PrFAR concentration follows a hyperbolic trend indicative of an induced fit conformational change. **(D)** The amplitude of the pseudo-first order binding yields a hyperbolic binding curve, the derived K_D value is 1.5 µM.

To gain more detailed kinetic information, the data was fitted globally to a kinetic mechanism accounting for binding and a conformational using the program DynaFit.[128] Since fits to mechanisms assuming a simple binding or a conformational equilibrium before PrFAR binding (conformational selection) did not yield useful results, a conformational equilibrium after PrFAR binding was assumed (induced fit, Scheme 1).

E = HisF
S = PrFAR

Scheme 1: Kinetic model of PrFAR binding to HisF

This is in accordance with the observation of the hyperbolic shape of the secondary plot of k_{obs} against the PrFAR concentration. According to this fit, the binding rate of PrFAR to HisF k_1 is 4.3 $\mu M^{-1}s^{-1}$ and the dissociation rate k_{-1} is 3.9 s^{-1} (Table 5). The macroscopic dissociation constant K_D calculated from these values is 0.91 µM, which is in agreement with the values from both equilibrium titration (1.1 µM, Fig. 22) and secondary plot analysis of the amplitudes of the binding transients (1.5 µM, Fig. 23C). However, due to the following conformational equilibrium, which influences the macroscopically observed K_D, a comparison of these values has to be viewed carefully.

Table 5: Kinetic parameters for PrFAR binding to HisF from global fit analysis

parameter	value ± standard error
k_1	4.32 ± 0.012 $\mu M^{-1}s^{-1}$
k_{-1}	3.89 ± 0.022 s^{-1}
k_2	0.061 ± 0.002 s^{-1}
k_{-2}	0.37 ± 0.015 s^{-1}
r_{EP}	−32.2 ± 0.06 a.u.
r_{E*S}	−25.7 ± 0.14 a.u.

Response coefficients r_{EP} and r_{E*S} are the measure for difference in fluorescence of the respective complex to free HisF. a.u.: arbitrary units

The rate constants k_2 and k_{-2} in the global fit analysis are the result of the second, slow phase observed in the binding transients. Due to the absence of ammonia, no PrFAR turnover takes place. Thus, the binding transients would be expected to follow a single exponential decay in the case of a simple bimolecular binding. The second phase detected in the PrFAR binding transients must thus represent a conformational change in HisF.

The rate limiting step derived from global fit analysis (k_2 = 0.061 s^{-1}) is much slower than the rate observed in steady-state PrFAR turnover (k_{cat} = 2.4 s^{-1}). The reason for this discrepancy is not clear at the moment. This observation indicates that either the observed conformational change is not necessary for HisF catalysis or the mechanism is in fact more complicated than the assumed model. This will be discussed further in chapter 4.1.9.

To test for the influence of loop1 mutations on the microscopic binding rate constants, the experiments were also conducted for HisF G20P and HisF F23A. For both variants, the secondary plots do not follow a hyperbolic form as the wild-type, but instead show a linear dependency of k_{obs} on the PrFAR concentration (Fig. 24). This behaviour is indicative of a simple bimolecular binding reaction. Additionally, the second, slow phase in the binding transients could not be detected for the two variants. It can thus be surmised that the two variants do not undergo the induced fit motion observed for wild-type HisF, which agrees with observations made in NMR experiments (chapter 4.1.7).

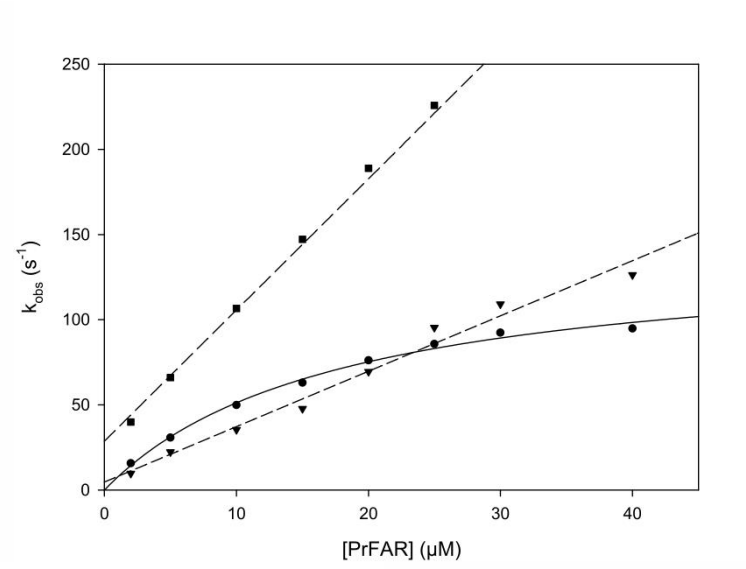

Fig. 24: Comparison of rates of PrFAR binding to HisF proteins with different loop1 dynamics at 25 °C. Pseudo first order rates of PrFAR binding to wild-type HisF (dots) follow a hyperbolic trend (solid line). The rates of PrFAR binding to F23A (triangles) and G20P (squares) follow a linear trend (dashed lines).

The two mutations F23A and G20P have been shown to alter loop1 dynamics as well as to decrease the catalytic rate. The results from PrFAR binding kinetics show that the change in loop1 dynamics results in the disruption of the observed conformational changes induced by substrate binding. These data clearly indicate that the observed conformational motions for wild-type HisF are not only closely connected to loop1 but are of great importance for catalysis as well.

It is reasonable to assume that there might be even more conformational changes that are not detected in these experiments (e.g. motions with $k > 1000\ s^{-1}$) and that some, but not all motions might have an impact on HisF catalysis. The elimination of the induced fit in catalytically impaired loop1 variants clearly shows that loop1 plays an important role in this induced fit motion and that the motion is beneficial for catalysis. This would be in agreement with the hypothesis according to which loop1 adopts the closed conformation in response to PrFAR binding. However, results from PRE and smFRET experiments suggest that the open loop1 conformation is the main conformation, regardless of ligand binding.[110] In conclusion, it can only be stated that PrFAR binding leads to profound conformational changes in HisF. Moreover, these motions are clearly connected to the catalytic cycle, but further experiments are needed to unravel the complex interplay of defined conformations and motions.

4.1.8.4 Binding of the reaction products AICAR and ImGP

An event that is often rate limiting in enzymatic reactions is the dissociation of the reaction product. Thus, binding reactions of the HisF products ImGP and AICAR were analysed in stopped-flow experiments as well. Although the equilibrium titrations indicated a fluorescence signal for the binding of the products ImGP and AICAR, no binding or dissociation transients could be observed for either substance (Fig. 25). This can be explained by the low binding affinity. Consequently, comparatively high concentrations of ligand had to be used in order to approach saturation, which, in the case of a pseudo first order binding reaction, leads to high values of the observed rate constant k_{obs}. This causes the binding or dissociation to be completed during the dead time of the measurement (about 1-2 ms).

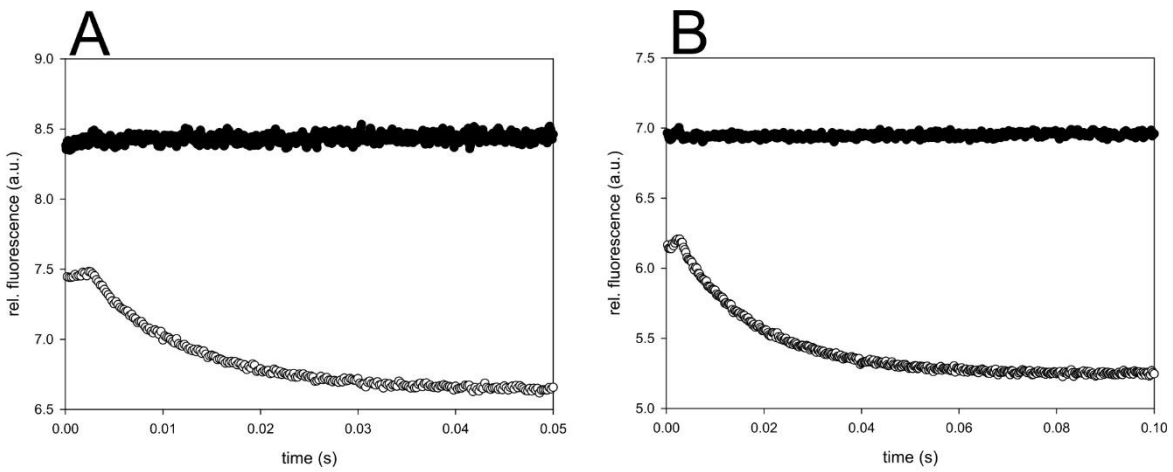

Fig. 25: Binding transients of wild-type HisF for AICAR and ImGP at 25 °C. (A) Binding of 2 mM AICAR to 0.25 µM HisF in the absence (dots) and presence of 0.3 mM ImGP (circles). **(B)** Binding of 0.2 mM ImGP to 0.25 mM HisF in the absence (dots) and presence of 2 mM AICAR. Both HisF reaction products bind and dissociate too fast to be observed in a stopped flow experiment. Addition of the other product slows down the binding and dissociation rates so that reproducible binding transients were observed. Experiments were carried out by 1:1 mixture of HisF and the reaction products in 50 mM Tris/acetate pH 8.5.

When both products were present, reproducible dissociation transients could be observed (Fig. 25). This demonstrates that the binding and dissociation rates are decreased for both ImGP and AICAR when the second product is present. In the equilibrium titrations, it was observed that both products increase the binding affinity for the other ligand. Considering this in the context of the measurements of dissociation kinetics, this increase in affinity is probably mainly caused by a decreased rate of dissociation.

For mathematical analysis with the global fitting program DynaFit,[128] four separate datasets were collected. In each of these data sets, the concentration of either ImGP or AICAR was kept constant and the concentration of the other was varied. Two data sets were collected for a 10-fold dilution of the pre-formed HisF:ImGP:AICAR complex with buffer to observe dissociation. The other two data sets were collected of a 1:1 mixture of HisF with a solution containing both ImGP and AICAR in order to observe binding. These data were fitted to different kinetic models of the product release mechanism of HisF. The two models giving the best fits are an ordered sequential model in which ImGP leaves the active site first and a random sequential model, i.e. either reaction product can leave the active site first (Scheme 2). Interestingly, an ordered sequential model with AICAR dissociating first does not give reasonable fitting results. Thus it was not further considered for the following analysis.

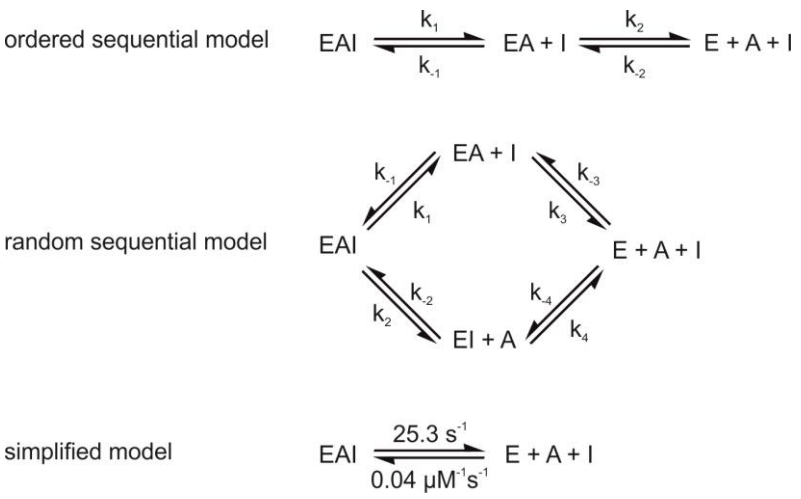

E = HisF
A = AICAR
I = ImGP

Scheme 2: Kinetic models for the dissociation of ACIAR and ImGP from HisF

For both kinetic mechanisms, the dissociation rates are fast compared to the k_{cat} of the ammonia dependent HisF reaction (k_{cat} = 2.4 s^{-1}, Table 6). The slowest first order rate constant is that of ImGP dissociation from the ternary complex in the random sequential model (k_1). Nevertheless, with a value of 25.3 s^{-1}, this rate is over 10 times larger than k_{cat}. From this, it can be deduced that product release is not rate-limiting for the HisF reaction.

Table 6: Kinetic parameters from global fit analysis for dissociation of AICAR and ImGP from HisF

parameter	value ordered sequential model	value random sequential model
k_1	41.9 ± 0.9 s^{-1}	25.3 ± 1 s^{-1}
k_{-1}	1.3 ± 0.04 $\mu M^{-1}s^{-1}$	2.13 ± 0.16 $\mu M^{-1}s^{-1}$
k_2	384 ± 11 s^{-1}	90.4 ± 2.5 s^{-1}
k_{-2}	0.22 ± 0.002 $\mu M^{-1}s^{-1}$	0.077 ± 0.003 $\mu M^{-1}s^{-1}$
k_3	n.a.	108 ± 10 s^{-1}
k_{-3}	n.a.	0.044 ± 0.002 $\mu M^{-1}s^{-1}$
k_4	n.a.	30.4 ± 0.4 s^{-1}
k_{-4}	n.a.	0.18 ± 0.003 $\mu M^{-1}s^{-1}$
r_{EA}	n.a.	-0.00003 ± 1.4 a.u.
r_{EI}	n.a.	-16.7 ± 0.2 a.u.
r_{EIA}	-23.8 ± 0.06 a.u.	-30.3 ± 0.2 a.u.

Response coefficients r_{EA}, r_{EI} and r_{EIA} are the measure for difference in fluorescence of the respective complex to free HisF. n.a.: not applicable, a.u.: arbitrary units; errors are standard errors form global fit analysis

The dissociation of ImGP is slower than that of AICAR in both models. Binding of ImGP on the other hand appears to be faster than that of AICAR. These observations are in agreement with the lower dissociation constant measured for ImGP in equilibrium titrations (chapter 4.1.8.2).

According to the equilibrium titrations shown in Fig. 22, both the binding of AICAR and ImGP lead to a change in fluorescence irrespective of the presence of the other reaction product. The simplification of a single response coefficient was used in the fit of the ordered sequential model because the use of two separate coefficients led to one value approaching zero. The random sequential model demonstrated a similar behaviour. While generally, the data is described quite well, the response coefficient for the dissociation of AICAR becomes very small with a high error. In both cases, this is most likely the result of the significantly faster dissociation of the second product, which is not properly represented in the raw data and is thus not fitted reliably.

Overall it is difficult to determine which of the kinetic models presented above actually applies here. However, both models offer the opportunity to gain information on the kinetics of the HisF reaction. In both models, the first dissociation event is slower than the second one but lies in the same order of magnitude. This agrees with the observations of very fast dissociation (no observable transients) and lower affinity to HisF for both products in the absence of the other. Since the second dissociation event is very fast, the kinetic model of product dissociation can be simplified as a pseudo-concerted dissociation of both reaction products (Scheme 2). In this simplified model, the net rates are assumed to correspond to the lowest rates measured. These are the formation or dissolution of the HisF:AICAR:ImGP complex for binding and dissociation, respectively.

It should be noted that the binding rates for AICAR and ImGP appear deceptively small ($\leq 0.2\ \mu M^{-1}s^{-1}$) due to the used concentration unit of µM. In the measurement conditions, mM concentrations were used. For instance, for the AICAR binding, this translates to theoretical k_{obs} values of roughly 400 s^{-1}. However, since PrFAR concentrations can be assumed to be low in a physiological setting and the products will be further processed and will not accumulate, product inhibition is not likely to play any role in HisF function.

4.1.8.5 PrFAR binding observed in the presence of ammonia

To observe the binding signal during catalysis, ammonia was added to the sample solutions in stopped-flow binding experiments. In agreement with the equilibrium titrations, the binding of ammonia on its own could not be observed. Hence, in the presence of both PrFAR and ammonia, only PrFAR binding can be detected. Binding transients were very similar to those of PrFAR binding observed without ammonia. The secondary plot of k_{obs} against the PrFAR concentration shows the same hyperbolic trend with and without ammonia, with a maximum k_{obs} of approximately 100 s^{-1} (Fig. 26).

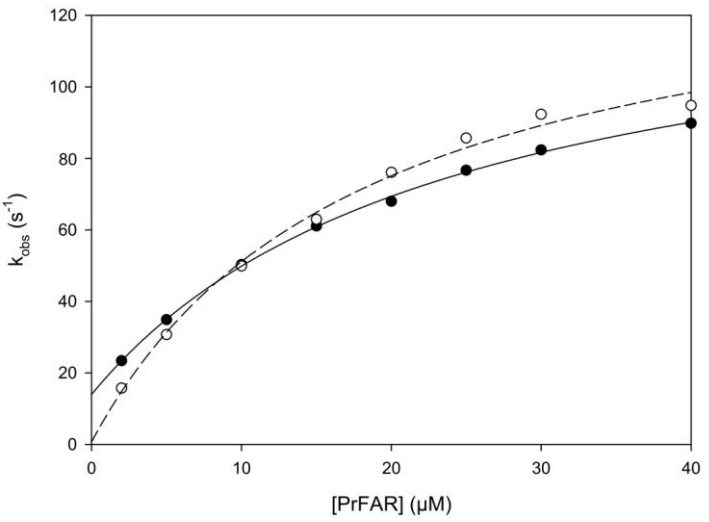

Fig. 26: PrFAR binding rates in the presence and absence of ammonia at 25 °C. PrFAR binding rates are only slightly changed when binding experiments are carried out in the presence of ammonia (dots and circles represent measurements in the absence and presence of 17.5 mM ammonia, respectively).

In order to determine whether ammonia binds previous to PrFAR and influences its binding, three experimental set-ups were tested. Ammonia was added once to the syringe containing PrFAR, once to the syringe containing HisF and once to both syringes. In the case that ammonia binds first and influences the binding of PrFAR, a change in the binding transients would be expected. However, the binding transients were almost identical in all three scenarios (data not shown). A sequential ordered binding mechanism with ammonia binding first is thus very unlikely.

These findings show that ammonia binding is most likely very fast. The two scenarios of a defined ammonia binding site or the transient binding of ammonia with immediate reaction cannot be distinguished with these measurements. Since ammonia binding appears to be fast (not rate limiting) and cannot be further defined, its binding can be simplified as a transient binding during catalysis for the formulation of a kinetic model of the HisF reaction (Scheme 3).

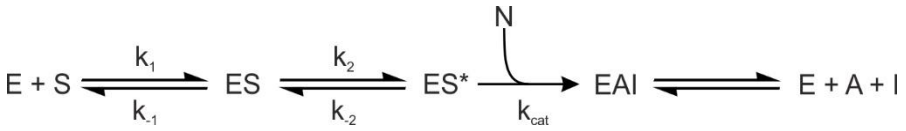

E = HisF
S = PrFAR
N = NH_3
A = AICAR
I = ImGP

Scheme 3: Simplified kinetic model of the HisF reaction assuming transient ammonia binding.

Further implications for a kinetic model of the entire ammonia dependent HisF reaction will be discussed in chapter 4.1.9.

4.1.9 Kinetic model of the entire ammonia-dependent HisF reaction

In order to formulate a complete kinetic model for the reaction catalysed by HisF, it is useful to first revisit the key conclusions that can be drawn from the results presented in the previous chapters, since the model has to agree with all available data. Concerning the binding of PrFAR and the dissociation of AICAR and ImGP, it could be observed that neither of these steps is rate limiting for the overall reaction (chapters 4.1.8.3 and 4.1.8.4, respectively). Ammonia binding could not be observed experimentally, neither spectroscopically nor indirectly in the kinetic analysis. Ammonia binding does not change PrFAR binding significantly and happens most likely very fast and transiently during the chemical reaction (chapter 4.1.8.5). Thus, the rate limiting step has to be either of chemical or conformational nature. Since there is no detailed kinetic information on different steps in the chemical catalysis, this step has to be simplified in the kinetic model as a single step.

With the binding, dissociation and chemical events covered, the conformational change that has been detected in several experiments is the remaining element in the formulation of a kinetic model. There is no experimental indication that the conformational changes in HisF occur in more steps than one. Therefore, the simplest case should be assumed, which is that there is only one defined conformational step to be considered in the kinetic model. Considering all possible scenarios involving one conformational step, this change can occur in four different kinds of mechanisms (Scheme 4).

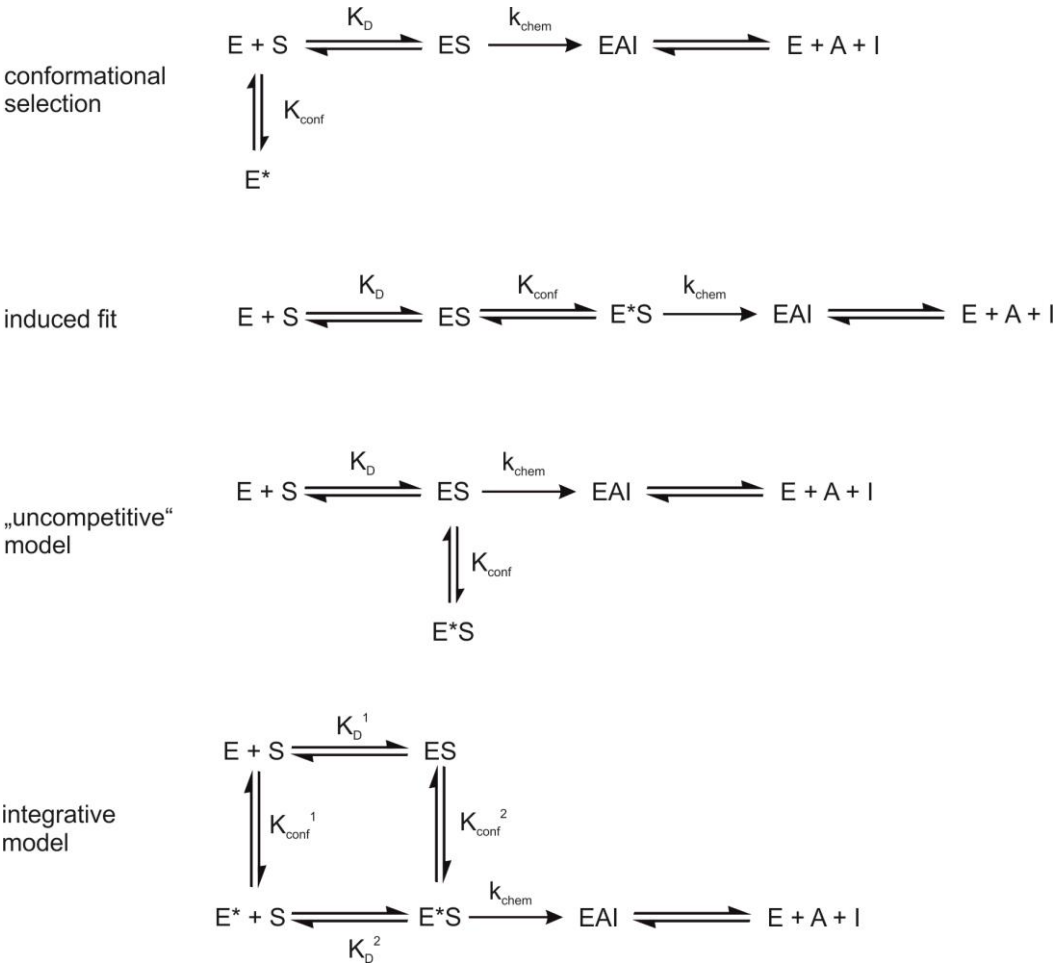

E = HisF
S = PrFAR
A = AICAR
I = IMGP

Scheme 4: Possibilities of kinetic models for the conformational change in HisF during catalysis

First of all, there are the two classical models of conformational selection and induced fit. In the former, there is an equilibrium before substrate binding, thus the active conformation is sampled by the substrate. In the latter, the conformational change is induced by substrate binding. The experimental results indicate that the conformational change in HisF happens after PrFAR binding (chapter 4.1.8.3), excluding the possibility of conformational sampling.

A simple induced fit can also happen in two varieties: The conformational change can either be the productive Michaelis complex, which is reaction competent (induced fit in Scheme 4), or be unproductive and thus "uncompetitively" reducing the reaction rate (uncompetitive model in Scheme 4). The first scenario however would suggest that the conformational change needs to be performed in order for the chemical step to become possible. The PrFAR binding analysis would then suggest that this step would have to be rate-limiting, since the determined rate constant is quite low (0.06 s^{-1}). This can clearly not be the case since k_{cat} is significantly higher (2.4 s^{-1}). In the second case, the conformational change would counteract the chemical reaction, since the conformational change leads to an unproductive enzyme-substrate complex. Thus, the reaction rate could be increased by the elimination of the conformational change. However, the variants G20P and F23A for which the conformational change is not to be observed show a severely reduced steady state rate. Finally, when incorporating the conformational step into the Michealis Menten equation (equation **(6)**), in both cases of induced fit, the K_M^{PrFAR} would be influenced along the k_{cat} in case of a change in the conformational equilibrium (equations (7) and (8), respectively). In both equations (7) and (8), K_{conf} can be found both in the term describing the observed K_M as well as the observed maximal rate v_{maxi}. However, steady-state measurements with HisF variants substantiate that this is not the case. HisF variants in general had reduced k_{cat} values but K_M values tended to remain unchanged (chapter 4.1.2). This shows that these two models clearly do not apply to the conformational change in HisF.

$$\frac{v}{v_{max_i}} = \frac{[S]}{K_{M_{app}} + [S]} \qquad \textbf{(6)}$$

$$\frac{v}{\frac{v_{max_i}}{(1+K_{conf})}} = \frac{[S]}{\frac{K_{M_{app}} \times K_{conf}}{(1+K_{conf})} + [S]} \qquad \textbf{(7)}$$

$$\frac{v}{\frac{v_{max_i}}{(1+K_{conf})}} = \frac{[S]}{\frac{K_{M_{app}}}{(1+\frac{1}{K_{conf}})} + [S]} \qquad \textbf{(8)}$$

v = reaction velocity
v_{maxi} = maximal velocity
K_{Mapp} = macroscopic K_M
K_{conf} = equilibrium constant of the conformational change
[S] = substrate concentration

Assuming a single conformational change, it can only be surmised that neither of the simple models applies and the motion can occur both before and after PrFAR binding (Scheme 4). Reformulation of the Michaelis Menten equation for this integrative model leads to an unchanged K_M^{PrFAR}, while k_{cat} is dependent on K_{conf}, which would be in agreement with available data (equation (9)). Due to transient kinetics data, this model has to underlie the following restrictions: The equilibrium constants K_{conf}^1 and K_{conf}^2 must be (at least nearly) identical, since no significant

change in the conformational equilibrium could be observed in any experiment. Thus, due to the circularity of the relationship, the affinities K_D^1 and K_D^2 for the two different HisF conformers must also be identical. This relationship does however not necessarily require the microscopic rate constants k_{conf}^1 and k_{-conf}^1 to be identical to k_{conf}^2 and k_{-conf}^2, as long as the quotient of the two pairs remains equal. The microscopic rate constants for the conformational change measured in PrFAR binding experiments (chapter 4.1.8.3) correspond to k_{conf}^2 and k_{-conf}^2, due to the induced fit type kinetic model used in fitting. k_{conf}^1 and k_{-conf}^1 cannot be determined in a straightforward manner.

$$\frac{v}{\frac{v_{max_i}}{(1+K_{conf})}} = \frac{[S]}{K_{M_{app}}+[S]} \qquad \textbf{(9)}$$

v = reaction velocity
v_{maxi} = maximal velocity
K_{Mapp} = macroscopic K_M
K_{conf} = equilibrium constant of the conformational change
[S] = substrate concentration

Taking together all available data, a complete kinetic model of the ammonia dependent HisF reaction can be formulated (Scheme 5). The chemical step, ammonia binding and the product dissociation are used in the simplified form as discussed in this chapter above, chapter 4.1.8.5 and chapter 4.1.8.4, respectively.

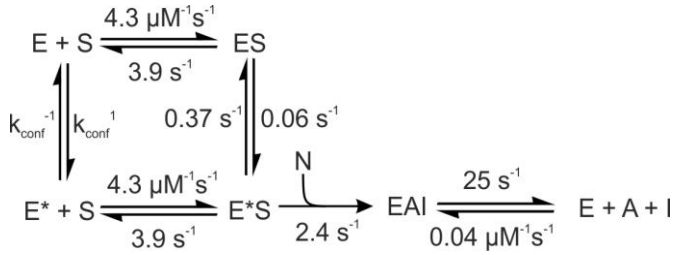

Scheme 5: Kinetic model describing the entire ammonia dependent HisF reaction

Finally, the question of the exact nature of the conformational changes during the catalytic cycle of HisF remains to be addressed. It could be observed that loop1 is of central importance both for catalytic function (chapter 4.1.2) and the observed induced-fit type conformational change observed upon PrFAR binding (chapters 4.1.5, 4.1.7 and 4.1.8.3). Whether the observed open and closed conformation of loop1 represent the active and inactive form of HisF is, at this point, however still a matter of speculation. It could be observed that loop1 exists in equilibrium between these two conformations in solution. The predominant conformation is the open conformation and the conformational equilibrium is most likely independent of the binding of PrFAR (chapter 4.1.6. and smFRET experiments of A. Ruisinger[110]). Analysis of different HisF crystal structures for example also point to a contraction of a phosphate binding site, which might increase loop1 flexibility (Fig. 14).

The correlation of the size of the accessible hydrophobic surface area of the residue in the critical loop1 position 23 (Fig. 13) is another indication of the importance of loop1 in the conformational equilibrium. Assuming a single active state of HisF which is defined by the hydrophobic interaction of F23 in loop1, the population of the active p_a state would be defined by a Boltzmann

distribution.[149] Thus, p_a would be proportional to $e^{\frac{\Delta G}{k_b T}}$, ΔG being the free energy upon formation of the active conformation. ΔG of on the other hand is proportional to the interaction surface of the two interaction partners.[150–152] This would explain the linear relationship between ln(k_{cat}) and the accessible surface area of the residue in position 23 (equations (10), (11) and (12)).

$$p_a \propto k_{cat} \propto e^{\frac{\Delta G}{k_b T}} \quad \textbf{(10)}$$

$$\Delta G \propto ASA \quad \textbf{(11)}$$

$$ASA \propto \ln(k_{cat}) \quad \textbf{(12)}$$

p_a = fraction of HisF molecule in the active conformation
ΔG = free energy change upon formation of the active conformation
k_b = Boltzmann constant
T = absolute temperature
ASA = accessible surface area of residue in position 23

It can be concluded that there is a strong correlation between integrity of loop1, the changes in its flexibility and HisF activity. This certainly suggests a direct involvement of loop1 in the critical conformational changes during the catalytic cycle. The exact structural nature of the conformational change, however, has to be the topic of further studies.

4.1.10 Evaluation of the consequences for the catalytic mechanism of HisF

The results presented in this chapter demonstrate the intricate way in which the active site loops are involved in HisF catalysis. In the case of loop5, a stable structure is needed and no side amino acid side chains are involved in its function. In contrast, loop1 needs a delicate balance between its structurally defined conformations and flexibility. The high number of loop1 residues that impact HisF catalysis when mutated highlights the central role of this loop. The steady-state catalytic parameters of the analysed variants show that its influence is different to that observed, for example, in ProFAR isomerase (HisA) or in indole glycerol phosphate synthase (TrpC). In HisA, loop closure is involved in substrate binding and in TrpC, loop flexibility controls product release.[66,67] In HisF, the effect is only on the catalytic rate k_{cat}, which shows an involvement in chemical turnover. Nevertheless, loop1 does not carry residues capable of catalysis. The residues carrying out the general acid/base catalysis are D11 and D130, which are to be found in β-strand 1 and 5, respectively.[100]

These observations strongly imply a direct link between conformations and motions of loop1 and HisF catalysis. Along these lines, it could be observed that the conformations of loop1 in crystal structures appear to exist in solution as well. Both PRE-NMR measurements as well as the recent smFRET[110] data demonstrate that the open conformation of loop1 is the most frequently adopted conformation of apo HisF in solution, but that the closed conformation exists as well. From the available experimental data, it cannot conclusively be determined how the conformational equilibrium changes upon PrFAR binding. However, the kinetic analysis of PrFAR binding in wild-type HisF as well as the variants G20P and F23A demonstrated the connection of loop1 to an induced fit type motion. Taken together, these findings support the hypothesis that loop1 changes from an open to a closed conformation after PrFAR binding. The kinetic analysis showed that several conformational changes result from PrFAR binding. The exact structural nature of the PrFAR-bound state of HisF still needs to be investigated in greater detail in order to elucidate all effects that contribute to the observed induced fit.

Loop1 is close to the catalytic residue D11 in β-strand 1. Thus, it is reasonable to assume that it exerts its influence on this residue. Since the pK_a value of aspartate residues is generally very low (< 2), the protonation required for enzymatic catalysis is facilitated by the generation of a hydrophobic environment, which stabilizes the protonated form of the aspartate side chain.[137] The environment of D11 is already relatively hydrophobic due to the flanking residues V18 and I52. Both residues have been shown to be important for HisF catalysis by mutagenesis. When loop1 is in the closed conformation, F23 might come into close proximity of these two resides. An interaction of F23 with V18 and I52 would create an even more hydrophobic environment for D11 and would shield it from solvent. In TIM, it has been shown that the closure of an active site loop leads to the shielding of a catalytic aspartate residue from solvent to favour the protonated form needed for catalysis.[64] It is likely that in HisF the same principle applies and that the formation of the closed loop1 conformation leads to protonation of D11 to facilitate its catalytic function.

Concerning its environment, a similar observation can be made for D130. It is partly covered by loop5 and only accessible to solvent from the active site. When PrFAR binds and displaces water molecules from its binding site, D130 is completely shielded from solvent. Thus, the protonated state will also be favoured for D130. This is supported by the observation that by shortening loop5 and thus exposing D130 to solvent even in the PrFAR bound state, the catalytic rate is significantly reduced.

A plausible reaction mechanism for HisF has been proposed previously.[100] Although this suggestion makes reasonable assumptions, it is partly not supported by biochemical data available today and principles observed in organic synthesis. It was assumed that the formation of the imine formed by nucleophilic attack of ammonia occurs spontaneously (Fig. 8). The formation of imines by the nucleophilic attack of ammonia or an amine on ketones progresses via a stable hemiaminal intermediate. The resolution of the hemiaminal to form the imine is generally acid-catalysed.[153] The pH of the ammonia dependent HisF reaction, however, is 8.5 to ensure a sufficient ammonia concentration, as at low pH ammonia is mostly present in the unreactive form of ammonium ions. In these conditions, spontaneous imine formation seems unlikely. A possible alternative to the spontaneous mechanism is hence that one of the aspartate residues in its protonated state catalyses the formation of the imine by acid-catalysed resolution of the hemiaminal (Fig. 27B).

The second step of HisF catalysis is assumed to be the hydrolysis of AICAR. Thus, the susceptibility for hydrolysis has to be increased as a result of the imine formation. A principle often observed in organic synthesis is that the formation of an imine has an influence on the acidity of hydrogens bound to the carbon atom at the alpha position. However, an influence on positions further than the α-carbon is generally not observed. Since the hydrolysis is assumed to occur at the gamma position from the imine, the susceptibility should not be strongly influenced by the presence of the imine. The analysis of the binding of the two HisF products in this work revealed that the presence of each product influences the binding affinity and release rate of the other and that it is more likely that ImGP leaves the active site first. The release rates were also shown not to be rate limiting, but rather the chemical turnover. If AICAR was produced and released before ImGP, this would lead to a strong increase in ImGP release rate. This in turn would result in the release of the intermediate instead of the fully formed ImGP, since the rate for chemical turnover is significantly slower than the dissociation. In the light of these new data, it appears more likely that ImGP and AICAR are produced simultaneously.

To account for the simultaneous formation of both products, instead of hydrolysis, the imidazole ring formation could be achieved by an intramolecular cyclisation reaction, catalysed by one of the two aspartate residues. This could be achieved by either base catalysis (Fig. 27C) or acid catalysis (Fig. 27D). It should be noted at this point that there has been some speculation considering the position of the double bond of the amineamide of PrFAR.[106] The amineamide is formed in the synthesis of ProFAR by phosphoribosyl-AMP cyclohydrolase.[154] Because in this

reaction, the aromatic ring of the AMP residue is broken, the double bond is initially situated between N3 and C2 of ProFAR (and thus possibly PrFAR, Fig. 27A). However, there is the possibility of tautomeric isomerisation. The current reaction mechanism is reliant on this isomerisation, because the mechanism is only possible if the double bond is between C2 and N1 of PrFAR. The alternative mechanism proposed in Fig. 27C also makes this assumption. The reaction progresses by the intramolecular nucleophilic attack of the imine nitrogen on C2 and the catalysis is performed by abstracting a proton from C1'' under the formation of a negatively charged intermediate. This intermediate is then resolved by the protonation of N3 by an aspartate, leading to the simultaneous formation of ImGP and AICAR.

A more likely mechanism, which is in fact independent of the tautomeric state of PrFAR, would assume both aspartate residues to be protonated (Fig. 27D). After imine formation, the protonation of the amineamide by the catalytic aspartate would lead to an intermediate with a delocalised positive charge on N1, C2 and N3. The reaction then progresses similar to the base catalysed mechanism with the nucleophilic attack of the imine at the amineamide carbon, which is facilitated by the positive charge. This mechanism is independent of the tautomeric form of PrFAR because the aspartate could protonate either N1 or N3, depending on which forms the double bond with C2.

The current suggestion of the catalytic mechanism of HisF assumes one of the catalytic aspartate residues to be protonated and one to be charged. This is also the case for the mechanism relying on base catalysis suggested here (Fig. 27C). However, due to the benefits of the independence of the tautomeric form of PrFAR and the facilitation of the intramolecular cyclisation by the generation of the positive charge, the mechanism based on acid catalysis (Fig. 27D) appears more likely. This would also be in agreement with the observation that shielding of both aspartate residues is beneficial for HisF catalysis.

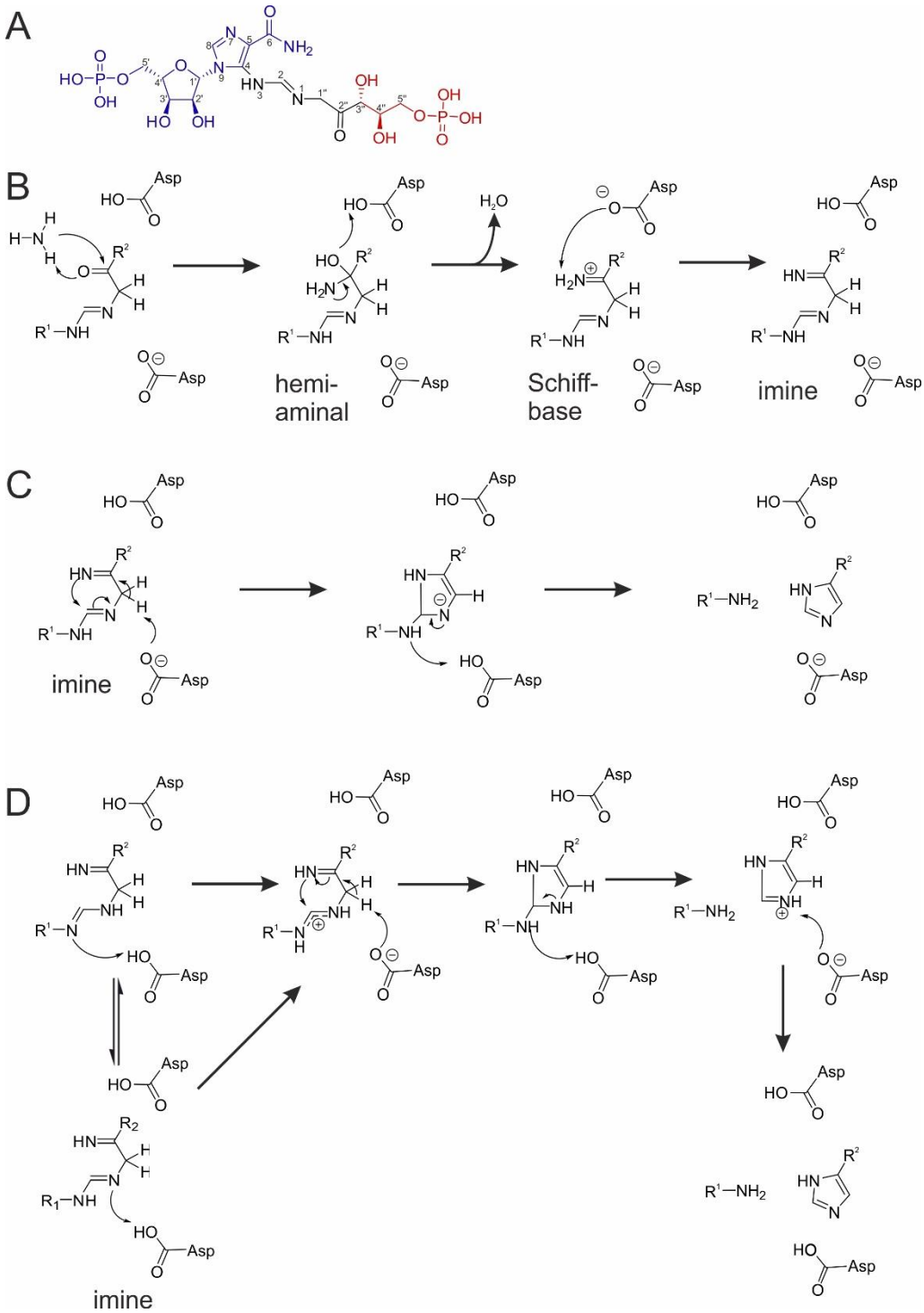

Fig. 27: New proposals for the catalytic mechanism of HisF. (A) Structure of PrFAR with numbering of the atoms according to the standard numbering of purines. For clarity, the coloured parts of the PrFAR molecule are abbreviated R^1 (blue) and R^2 (red). **(B)** The first step in HisF catalysis is assumed to be the formation of the imine intermediate. This is most likely catalysed by an aspartate residue, which protonates the leaving water molecule and can then deprotonate the Schiff-base to form the imine. **(C)** Proposal for a base catalysed formation of the imidazole ring of ImGP that progresses via a negatively charged intermediate. The charged aspartate residue deprotonates C1'', allowing the nucleophilic attack of the imine nitrogen on C2. **(D)** Proposal for an acid catalysed formation of the imidazole ring that progresses via a positively charged amineamide intermediate. For this proposal, the aspartate residue protonates either N1 or N3, which can both be double bonded to C2 due to tautomeric isomerisation. This leads to the positively charged intermediate. In this charged form, the C2 is more prone to a nucleophilic attack from the imine nitrogen.

4.1.11 Outlook

The results presented in this chapter demonstrate that the critical role of loop1 could be exerted by the transition from an open to a closed conformation. This has implications for the catalytic mechanism in that the protonation of D11 would be favoured by this to facilitate catalysis. These findings will have to be substantiated by analysing the protonation states of the catalytic residues D11 and D130. This could be achieved by quantum mechanical calculations or, since by the presence or absence of ammonia, turnover of PrFAR can be controlled, also experimentally, for instance in ^{1}H-^{1}H-TOCSY NMR experiments.

The structural knowledge of the conformations of loop1, especially of the closed conformation, still lacks sufficient detail to make definitive statements for their functional implications. This could be addressed for example by the assignment of the NMR signals of variants used for PRE measurements, which would allow for a much improved precision in the localisation of loop1 in these experiments. A method that could complement the data from PRE and smFRET experiments very well would be the determination of distances via EPR. These experiments are conducted at very low temperatures, close to absolute zero. HisF samples could be flash frozen in relevant scenarios such as in the presence of PrFAR or even during catalysis. This would prevent degradation of PrFAR both by enzymatic turnover and thermal decay. Therefore, the results from these experiments would be very reliable, which is always critical for methods that require incubation of samples at relatively high temperatures for extended periods of time.

The data on kinetic rate constants of HisF could be validated by the use of HisF variants that carry the CouA residue in other positions. Placing the CouA residue in other positions would have the added benefit that it should be sensitive to other conformational changes than when incorporated in position 132. In this way, more details of these motions could be revealed. In order to gain further insight into the microscopic rates of the complex chemical reaction catalysed by HisF, the reaction mechanism needs to be analysed in more detail. To distinguish between the proposed reaction mechanisms, it should first be clarified whether the reaction progresses via a positively or a negatively charged intermediate, which could be achieved by the use of isotopically labelled PrFAR in NMR experiments. These studies would go hand in hand with the clarification of the protonation states of the catalytic aspartate residues.

The order of dissociation of the reaction products ImGP and AICAR could possibly be clarified in more detail by repetition of the binding and dissociation experiments with different combinations of the pre-formed HisF:product complexes. Since this requires a high amount of the two substances, a chemical synthesis of ImGP would have to be established to make these experiments feasible.

Finally, it would be of great interest to do all analyses performed and suggested here on the full ImGPS complex. It is known that loop1 flexibility is influenced by the presence of HisH, but HisF catalysis is not. Inclusion of HisH into these studies would also entail the kinetic analysis of the HisH reaction and how these rates are in turn kinetically coupled with those of the HisF reaction. This naturally includes the transmittance of the allosteric signal as well as conformational changes necessary for HisH activation. The last two points will be addressed in the following chapter.

4.2 Studies on the molecular mechanism of HisH activation

The second aim of this thesis is to gain further insight into the allosteric communication between HisF and the glutaminase subunit of ImGPS, HisH. For clarity, in this chapter all residues were given a prefix, "f" signifying that the residue is found in the HisF subunit and "h" that it is part of HisH.

The molecular mechanism of allosteric signal transmission and the conformational change within the HisH active site leading to activation are still poorly understood. The allosteric signal is thought of as a "one way street", since the reaction catalysed by HisF is almost unaffected by the presence or absence of HisH and can be performed with free ammonia instead of glutamine, both by isolated HisF as well as the full ImGPS complex.[100,104] HisH activity on the other hand is strictly dependent on the presence of HisF and is strongly activated in a V-type manner (increase in k_{cat}) by PrFAR binding to HisF. The current hypothesis is that PrFAR binding induces an increase in HisF dynamics and that these conformational fluctuations are transferred to HisH. This is then assumed to lead to the breaking of a specific hydrogen bond, which allows for the correct formation of the oxyanion hole.[103,142,148]

Fig. 6 shows the established catalytic mechanism of class I glutamine amidotransferases. Specifically, the glutaminase reaction of HisH relies on the nucleophilic attack of hC84 on the carboxamide of glutamine. Whether the catalytic cysteine is deprotonated by solvent or directly by the catalytic histidine is not known at present. The second prerequisite of glutaminase catalysis is the stabilization of the negative charge on the carboxamide oxygen atom of the tetrahedral intermediates by the oxyanion hole. This facilitates both the release of ammonia and the hydrolysis of the covalent thioester intermediate. In HisH proteins, the oxyanion hole is assumed to be formed by the highly conserved h49-PGVG-52 motif. It can thus be deduced that there are only few prerequisites for HisH catalysis that can be regulated by allostery: The correct protonation state of the catalytic residues hH178 and hC84, the formation of the oxyanion hole as well as the conformational requirements for substrate binding, product release and the correct orientation of the catalytic residues for catalysis.

Before studying the molecular mechanism of HisH activation, an assay developed for high throughput screening of peptide inhibitors of ImGPS was adapted for reliable continuous measurements of HisH glutaminase activity in the absence and presence of allosteric activators.[127] Subsequently, the allosteric signal originating in HisF was studied. The effect of mutations in loop1, which has previously been shown to be allosterically connected to HisH,[100] as well mutations of residues potentially involved in signal transmittance were tested. Finally, different aspects of the molecular basis of HisH activation were examined, especially in connection with the two prerequisites for HisH activity stated above, namely the correct protonation state of the catalytic residues as well as the proper formation of the oxyanion hole.

4.2.1 Continuous measurement of HisH activity independent of NAD^+

Since glutamine hydrolysis does not generate a spectroscopically measurable change, the measurement of HisH activity generally relies on the use of coupled enzymatic assays. In most previous works, the assay used relied on the oxidation of glutamate by glutamate dehydrogenase (GDH), which uses NAD^+ as cosubstrate.[100] The concurrent reduction of NAD^+ to NADH allows for the spectroscopic observation of the reaction progress via the change in absorbance at 340 nm. While this assay is very sensitive and offers the possibility for comparing activities of different HisH variants, it has been observed that NAD^+ weakly binds to HisF.[108] This binding leads to a moderate allosteric stimulation of HisH, making a reliable determination of the basal activity impossible. Also, NAD^+ might interfere with the binding of HisF ligands with higher allosteric activation potential, lowering the final HisH activity. One alternative method to observe HisH activity is the decoupling of the glutaminase and GDH reactions in a discontinuous assay.[108] This

however leads to a tremendous increase in experimental effort as well as to a large experimental error.

In a study that aimed to identify peptide inhibitors of ImGPS, an alternative assay was developed.[127] This assay uses glutamate oxidase (GOX) for oxidation of glutamate and horseradish peroxidase (HRP) to detect the produced H_2O_2 through oxidation of a chromophore molecule. This assay was adapted here in order to improve the quality of HisH activity data and the ease of comparison of basal and allosterically activated glutamine turnover.

Steady-state glutaminase kinetics of wild-type ImGPS either in the presence of 70 µM ProFAR as allosteric activator or in the absence of any allosteric activator are shown in Fig. 28. They clearly show that this assay allows for a reliable and precise measurement of HisH activity both in the activated and the unstimulated basal state.

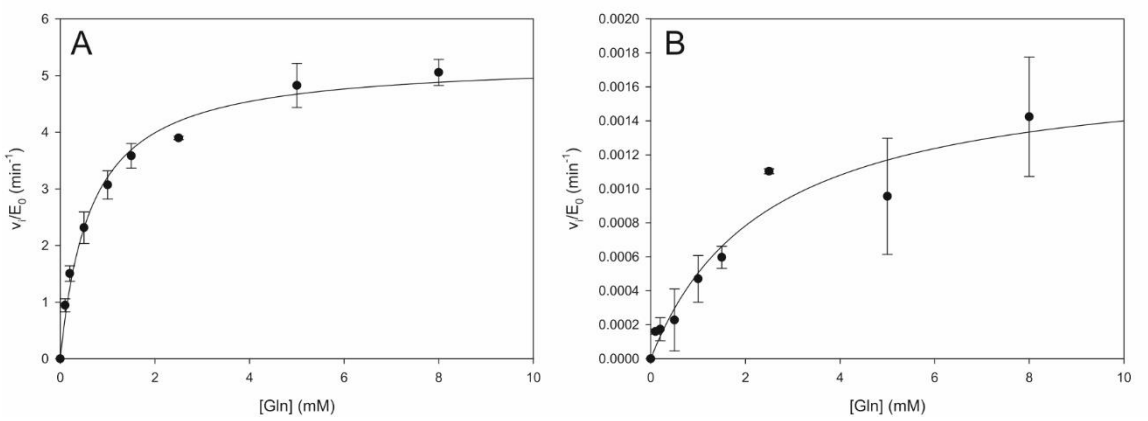

Fig. 28: Steady-state kinetic of the glutaminase reaction in wild-type ImGPS recorded with the GOX-based assay at 25 °C. HisH activity was monitored in 10 mM Tris/HCl, pH 7.0 in a volume of 100 µl in a 96 well plate by the absorbance of the quinolone dye produced by HRP at 505 nm. Reaction rates (v) were recorded with **(A)** 0.1 µM ImGPS in the presence of 70 µM ProFAR and **(B)** with 35 µM ImGPS in the absence of allosteric effectors in technical triplicates, normalized to the protein concentration (E_0) and plotted against the concentration of glutamine. The lines represent a mathematical fits of the data points to the Michealis-Menten equation.

The steady-state parameters of the ProFAR activated reaction are in good agreement with those from previous work (Table 7). In the absence of allosteric activation, the k_{cat} values is approximately 18-fold lower than the one measured in the discontinuous assay. The reason for this is most likely the higher sensitivity of the assay, since the measured value is lower than the error of the previous data. The possibility to measure several different glutamine concentrations allowed for a full Michaelis-Menten analysis of the data and hence for the determination of a K_M^{Gln} value of the basal HisH activity. This revealed that in addition of the very strong V-type activation (3,100-fold increase in k_{cat}), a relatively small K-type activation (3.8-fold reduction of K_M^{Gln}) could be observed. This led to the considerable 11,460-fold activation in the catalytic efficiency k_{cat}/K_M^{Gln} by ProFAR. Overall, these results demonstrate the usefulness of the newly adapted assay for studies on the allosteric activation of HisH.

Table 7: Steady-state kinetic parameters for the glutaminase reaction of wild-type ImGPS at 25 °C

	This work	List 2009[108]
k_{cat} (min^{-1}, basal)	0.0017 ± 0.0003	0.03 ± 0.01
K_M^{Gln} (mM, basal)	2.46 ± 0.91	n.d.
k_{cat}/K_M (M^{-1}/s^{-1}, basal)	0.012	n.d.
k_{cat} (min^{-1}, ProFAR activated)	5.28 ± 0.19	4.8 ± 0.6
K_M^{Gln} (mM, ProFAR activated)	0.64 ± 0.08	0.8 ± 0.3
k_{cat}/K_M^{Gln} (M^{-1}/s^{-1}, ProFAR activated)	137.5	100

n.d.: not determined, 70 µM ProFAR

4.2.2 Determination of the influence of HisF loop1 on HisH activation

The analysis of the allosteric communication between HisF and HisH was started with the investigation of the initial generation of the allosteric signal in HisF. As demonstrated in chapter 4.1.2, loop1 of HisF has a strong influence on HisF activity. It has also been observed previously that loop1 has an allosteric connection to HisH.[100] Loop1 is more prone to trypsin cleavage in the full ImGPS complex than in isolated HisF, which is an indication of increased flexibility. It is thus quite likely that loop1 plays a role in ImGPS allostery and is involved in initiating the stimulation signal upon PrFAR binding.

To test this hypothesis, HisF variants with mutations within or in the vicinity of loop1 (see chapter 4.1.3) were tested for the capability to stimulate glutaminase activity in HisH. To this end, the glutamine turnover of the respective ImGPS complexes was measured in the presence of the allosteric activator ProFAR (ProFAR concentration: 70 µM, measurements with variants fV18A and fI52A were performed by Leon Babel[139]). All tested mutations show an influence on the HisH activity to varying degree (Table 8).

Table 8: Allosteric activation of wild-type HisH by HisF loop1 variants at 25 °C

HisF variant	k_{cat} HisH (min^{-1})	k_{cat} wt/mut
wild-type	5.3 ± 0.19	-
fV18A	2.61 ± 0.46	2
fK19A	0.42 ± 0.26	12.3
fG20A	0.19 ± 0.01	27.9
fG20P	b.d.	> 50.000
fT21G	0.27 ± 0.05	19.6
fT21P	b.d.	> 50.000
fN22A	2.0 ± 0.14	2.7
fF23A	0.25 ± 0.20	21.2
fE24P	0.39 ± 0.13	13.6
fG30A	0.12 ± 0.05	44.2
fG30P	b.d.	> 50.000
fY39F	0.55 ± 0.04	9.6
fI52A	0.28 ± 0.04	18.9
fH228A	0.11 ± 0.08	48.2

b.d.: below detection limit, assuming a detection limit of 10^{-5} AU min^{-1} [155]

The k_{cat} of HisH was reduced 2 – 50-fold in all alanine, glycine, and phenylalanine mutations. Most of these effects were weaker than the effects of the same mutations on HisF activity (see chapters 4.1.2 and 4.1.3). For example, the variant fV18A led only to a ~2-fold decrease in k_{cat} of HisH, whereas it caused a ~11-fold reduction in k_{cat} of HisF. Likewise, the variant fF23A led only to a ~21-fold decrease in k_{cat} of HisH, whereas it caused a ~436-fold reduction in k_{cat} of HisF. As the only exception, the mutation fK19A hampered HisH stimulation 12.6-fold, while the HisF reaction was only affected 2-fold. In conclusion, the reduction of HisH activity was generally lower than the effect on HisF activity.

An interesting observation is that three of the four variants introducing proline into HisF loop1 reduced not only HisF activity below detection, but also the stimulation of HisH activity (no significant turnover within 60 min with 25 µM ImGPS, 10 mM glutamine and 70 µM ProFAR). fE24P is the only mutation which still afforded measurable HisH stimulation.

Overall, these data show that HisF loop1 is an important element in the allosteric communication in ImGPS. The missing correlation between the influence on HisF activity and HisH stimulation suggests that different conformations or motions of the loop are relevant for each of these two processes.

4.2.3 The transmittance of the allosteric signal in ImGPS

Once the binding of PrFAR to the HisF active site has generated the allosteric signal, it has to be transmitted through the HisF protein to the interface with HisH and subsequently to the HisH active site. Several studies concerned with the question how this happens exactly have been published, but no hypothesis was conclusively proven experimentally.[102,106,156,157] The current hypothesis is that instead of a chain of interacting residues, the signal is transmitted through the global ms-motions of the HisF protein.[142,148] There are however still many unanswered questions: How does this increase in molecular dynamics transfer to HisH? Which exact residues are involved and which are of central importance? Is this correlation really a sign of causality or is there a well-defined active conformation, which is simply more dynamic than the inactive conformation?

4.2.3.1 Characterization of the HisF variant fV48A

The side chain of residue fV48 contributes to the ammonia channel of HisF, in approximately the same distance from both the HisH and the HisF active sites. In a previous study, the mutation fV48A was found to result in a decreased capacity of HisF to allosterically stimulate HisH activity, suggesting that the residue is directly involved in signal transmittance.[142] It seemed rewarding to perform a detailed characterization of this variant for gaining further insight into the transmittance of the allosteric signal in ImGPS. First of all, fV48A was tested for its HisF activity and capability of activating wild-type HisH. The steady-state kinetics of the ammonia dependent HisF reaction show no significant difference when comparing fV48A to wild type HisF (Table 9). Although a previous study reported a decrease in binding affinity of fV48A for PrFAR,[142] the K_M value for PrFAR is also almost unchanged. The authors of this study measured PrFAR binding via the change in fluorescence of fW156. As explained in chapter 4.1.8.1, fW156 fluorescence is quenched unspecifically by PrFAR (Fig. Appendix 4). It is possible that the authors mistook this artefact for the binding signal. The reduced capability of fV48A to allosterically activate HisH on the other hand could be confirmed and the k_{cat} of the glutaminase reaction was decreased 15.1-fold (Table 9). This indicates that fV48 is relevant for allosteric communication, but not for HisF catalysis.

Table 9: Ammonia dependent HisF activit and HisH activation in ImGPS fI7A, fV48A and fL169A at 25 °C

ImGPS variant	k_{cat} HisF (s^{-1})	K_M^{PrFAR} HisF (µM)	k_{cat} HisH (min^{-1})
wild-type	2.4 ± 0.1	4.5 ± 0.5	5.3 ± 0.19
fI7A	1.6 ± 0.2	4.4 ± 1.0	0.5 ± 0.08
fV48A	2.4 ± 0.1	5.0 ± 1.1	0.35 ± 0.07
fL169A	3.1 ± 0.3	5.1 ± 1.1	0.26 ± 0.05

To determine whether there are significant changes in the HisF conformation that might lead to the change in HisH activation, the three-dimensional structure of fV48A was determined by X-ray crystallography. While crystallization was not successful for the full ImGPS complex, crystals could be obtained for the isolated fV48A protein. X-ray diffraction was observed to a resolution of 1.2 Å and the phases were solved by molecular replacement with the structure of "wild-type" HisF fT21S (PDB-code: 1THF). For full data collection and refinement statistics, see Table Appendix2. The structure shows very little differences to the wild type enzyme. However, changes could be observed in the side-chain conformation of residues fI7 and fL169, which are in proximity of fV48. All three residues are part of the ammonia channel. In addition to the conformation observed in wild-type HisF, both fI7 and fL169 adopt a second, alternative conformation in the variant fV48A, (Fig. 29). This indicates that these two residues have a higher degree of conformational freedom in fV48A than in wild-type HisF, which might lead to a disturbance of protein dynamics and hence, allosteric signal transmittance.

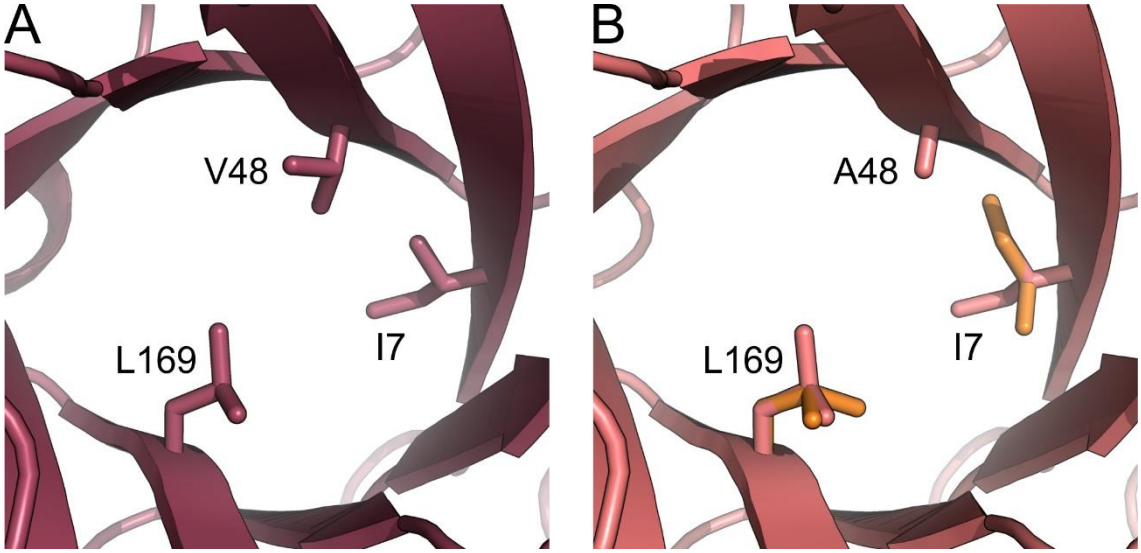

Fig. 29: Structural comparison of HisF V48A and "wild-type" HisF (fT21S). Structures of **(A)** HisF T21S (PDB-code 1THF, dark red) and **(B)** HisF V48A (light red) in cartoon representation. The region of the ammonia tunnel is shown in top-view from the HisF active site and side-chains of residues surrounding position f48 are depicted as sticks. The residues fI7 and fL169 clearly show a second conformation (orange) in the variant fV48A, one of which is not present in other HisF structures.

In order to determine whether the two identified residues are connected to the allosteric effect similar to that observed for fV48A, both positions were mutated to alanine. The respective variants were tested for HisF activity and their capability of activating wild-type HisH. In both fI7A and fL169A, much as in fV48A, HisF activity was not impaired (Table 9). However, both mutations significantly reduced capability of activating HisH similar to the 15-fold reduction observed for the mutation fV48A (approximately 10-fold and 20-fold reduction in k_{cat} for fI7A and fL169A, respectively, Table 9). These findings indicate that the flexibility and motions of residues in the hydrophobic core of HisF are correlated with the ability of HisF to activate HisH. However, the observation of greater conformational freedom seems contradictory to the conclusions drawn from observations made in NMR experiments, which indicated that allosteric activation is facilitated by an increase in HisF dynamics.

These results, especially in the light of other research that relates protein dynamics to ImGPS allostery,[142,148] highlights that conformational flexibility may play a major role in ImGPS function. While in a previous study, the residues fI7 and fL169 were noticed to be dynamic,[103] they were not considered important for allosteric communications. Even though the results presented here are based on a static crystal structure, they give a further indication of the importance of conformational dynamics in ImGPS allostery and highlight that the mechanism of transmittance is still poorly understood. Further studies will have to be conducted to identify other relevant residues and to clarify the connection between conformational dynamics in HisF and allosteric activation of HisH.

4.2.3.2 Spectroscopic detection of the allosteric communication in ImGPS

A paradigm of allostery is that the allosteric signal, which is caused by the binding of the allosteric effector, results in conformational changes at the target active site, which lead to the functional change. Since many conformational changes are relatively slow, they can become rate limiting in enzymatic reactions. It is therefore of considerable interest to measure the rates of these conformational changes.

Change in protein conformation always causes a change in the microenvironment of amino acid residues in the regions of the protein involved in this change. In spectroscopically active residues, this can result in a change in absorption and/or fluorescence properties, depending on the magnitude of the change in microenvironment and the sensitivity of the probe. Spectroscopically active residues can thus be incorporated at specific sites in order to observe the changes to this region. It is the aim of the experiments presented in this chapter to spectroscopically monitor the conformational change in the ImGPS complex upon PrFAR binding to HisF.

As a spectroscopic probe in ImGPS, the wild-typical residue hW123 has been used to quantify the binding strength of HisF and HisH,[100,158,159] since it is situated in the protein-protein interface and thus its environment changes drastically upon complex formation. As a residue in the interface, it is most likely also affected by allosteric communication. However, it is to be expected that the changes in absorbance and fluorescence are quite small. Also, as mentioned above (chapter 4.1.8.1), the unspecific quenching of tryptophan fluorescence by PrFAR makes a reliable quantification of such an effect very difficult. Residue hW123 can thus be assumed to be a poor spectroscopic probe for the intended experiments. Therefore, similar to the procedure for measuring substrate and product binding in HisF (chapters 4.1.8.2 and 4.1.8.3), the unnatural amino acid CouA was incorporated into HisH to generate a spectroscopic signal. To keep the influence on activity and complex formation to a minimum, position h136 was chosen for CouA incorporation (Fig. 30). Residue hY136 is part of the HisF/HisH interface, but is situated in its periphery. This makes a significant contribution to complex formation unlikely. Also, it is over 25 Å distant from the PrFAR binding site, making a direct sensing of PrFAR binding improbable. Finally, hY136 is not in the direct vicinity of the HisH active site, reducing the risk of a reduction in HisH activity.

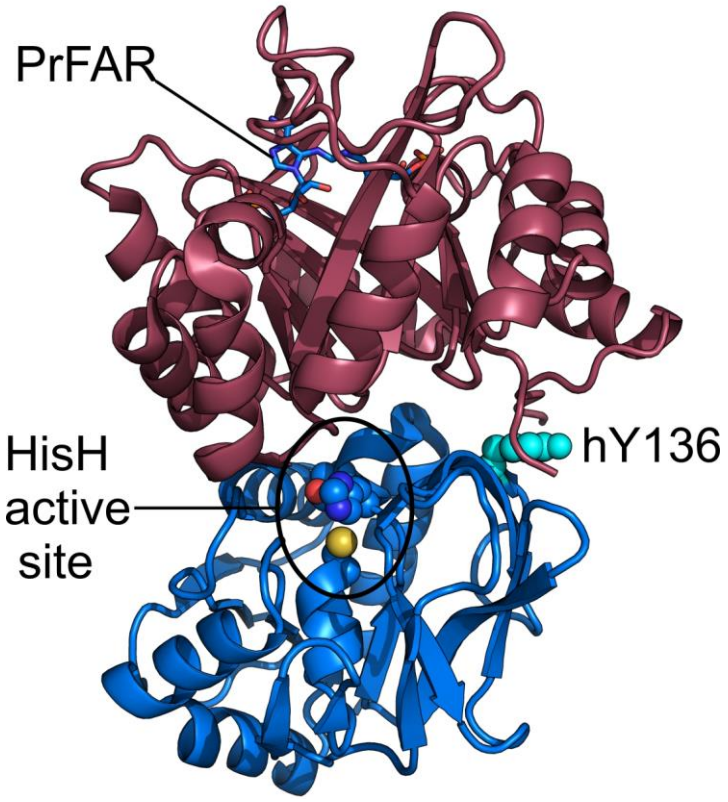

Fig. 30: Position of hY136 used for the spectroscopic observation of ImGPS allostery. The structure of wild type ImGPS is shown in cartoon representation. HisF is coloured in red, HisH in blue. hY136 (cyan spheres) is situated in the interface between HisF and HisH. It is positioned over 25 Å distant from the binding site of PrFAR (blue sticks, from an overlay with the complex structure of the PrFAR bound yeast enzyme, PDB code 1OX5) in HisF and approximately 12 Å distant from the HisH catalytic triad (blue spheres).

The variant hY136CouA was purified in comparatively low yield (approximately 1 mg/l expression culture). SDS-PAGE analysis (Fig. 31A) showed however, that the protein could be isolated with a purity of at least 90%. To ensure the formation of a functional ImGPS complex, the binding affinity between wild type HisF and hY136CouA was determined by fluorescence spectroscopy, taking advantage of the highly sensitive CouA fluorescence (λ_{ex} = 350 nm, λ_{em} = 440 nm) as a binding signal. Titration of HisF led to a significant increase in CouA fluorescence. The fit with a quadratic equation (equation (4)) shows that the dissociation constant is too low to be reliably determined (K_D < 10 nM) with the protein concentrations that had to be used here (Fig. 31B). This is in agreement with measurements performed for the wild type complex by following the hW123 fluorescence (K_D < 50 nM).[100] As a result, the impact of CouA incorporation on complex formation appears to be negligible. As a final control that the ImGPS complex is fully functional, HisH activity was measured. Glutaminase activity of ImGPS hY136CouA was determined in the presence of ProFAR as allosteric activator (70 µM). The resulting k_{cat} of 7.2 ± 0.3 min^{-1} is in good agreement with wild type activity (k_{cat} = 5.2 ± 0.2 min^{-1}), proving that the fluorescently labelled complex is fully functional and should be a suitable wild type model for further experiments.

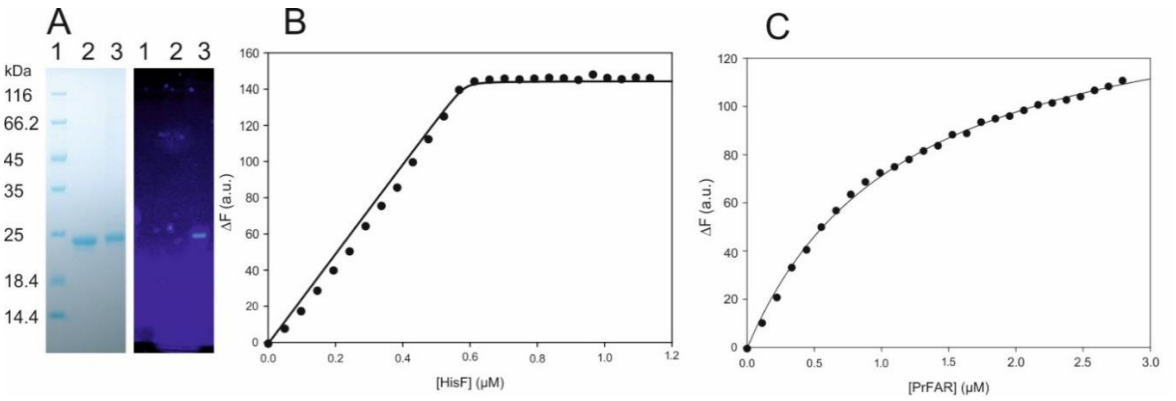

Fig. 31: Overview of the properties of HisH Y136CouA. (A) SDS-PAGE gel without staining (right hand side) under UV light (366 nm) and after Coomassie-staining (left hand side). Samples are: molecular weight standard (lanes 1), wild type HisH (lanes 2) and HisH Y136CouA (lanes 3). **(B)** Titration of HisH Y136CouA with wild type HisF monitored by changes in fluorescence (λ_{ex} = 350 nm, λ_{em} = 440 nm). The line represents a fit to a quadratic equation (see equation (4)) which showed that the dissociation constant of the complex is < 10 nM. **(C)** Titration of the HisH Y136CouA:HisF wild-type complex with PrFAR monitored by changes in fluorescence (λ_{ex} = 350 nm, λ_{em} = 440 nm). The line represents a fit to a simple hyperbolic equation (equation (5)), which yielded a dissociation constant for PrFAR binding of 1.17 ± 0.04 µM.

To test whether PrFAR binding to HisF is sensed at the protein interface by hY136CouA, PrFAR was titrated to the fully formed HisH Y136CouA:HisF complex while monitoring the CouA fluorescence (Fig. 31C). The small detected change in CouA fluorescence was plotted against the PrFAR concentration and the data fitted to a hyperbolic equation (equation (5)). This yielded an apparent dissociation constant of 1.17 ± 0.04 µM, which is in good agreement with other PrFAR binding studies that gave a K_D of 1.1 µM (chapter 4.1.8.2) and 0.45 µM.[103] This result shows that CouA at the subunit interface of ImGPS senses PrFAR binding to the active site HisF, which is located about 25 Å apart from the chromophore.

To assess the kinetics of PrFAR binding to the hY136CouA:HisF wild-type complex, stopped-flow experiments were performed under the same conditions as for isolated His K132CoA (chapter 4.1.8.3). The binding transients could be fitted well to single exponential functions, yielding the pseudo first order rate constants k_{obs} of the binding event. The secondary plot of the observed rate constants against the PrFAR concentration yielded a hyperbola (Fig. 32) similar as the one that was observed for the PrFAR titration curve of isolated HisF followed through fK132CouA (Fig. 23).

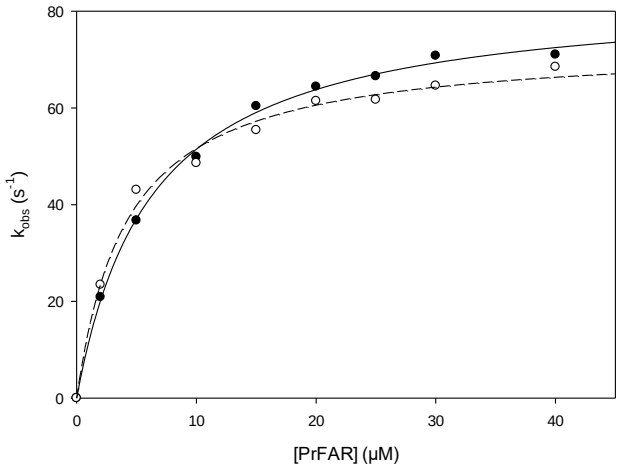

Fig. 32: Kinetic measurement of PrFAR binding to the ImGPS hY136CouA at 25 °C. Pseudo first order rates of PrFAR binding to ImGPS hY136CouA (dots) follows a hyperbolic trend (solid line). This trend is identical in the presence of 10 mM glutamine (open circles and dashed line).

The binding of the HisH substrate glutamine might also lead to conformational changes, which could in turn influence the rate of the transmission of the allosteric signal. To test for such an effect, the measurements were repeated in the presence of saturating concentrations of glutamine (10 mM). The observed rate constants were almost identical to those observed without glutamine (Fig. 32). Since it is assumed that the rate of allosteric communication is very fast, this does not necessarily mean that the rate is not influenced. However, it appears be much faster than PrFAR binding both in the presence and absence of glutamine and can thus not be determined in this experimental set-up.

Finally, the allosteric communication was observed in an ImGPS complex containing a HisF variant with reduced capability of HisH activation (cf. Table 8). The variant fF23A was chosen for this purpose, since in this variant, the induced fit type conformational change upon PrFAR binding in HisF was eliminated (chapter 4.1.8.3; Fig. 23). The use of HisF fF23A led to a linear dependency of k_{obs} on the PrFAR concentration, indicating that the binding follows a simple bimolecular mechanism (Fig. 33). Hence, these stopped flow experiments again showed a very similar trend as the data recorded for isolated HisF followed through fK132CouA (Fig. 24). That the signal can still be observed at all indicates that the conformational change that leads to the change in CouA fluorescence observed here is independent of the induced-fit motion in HisF. Since results in chapter 4.2.2 indicate that the motion of HisF loop1 is crucial for HisH activation, the conformational change followed here is most likely not the full rearrangement necessary for HisH activation. Further requirements will be discussed in chapter 4.2.4.2.

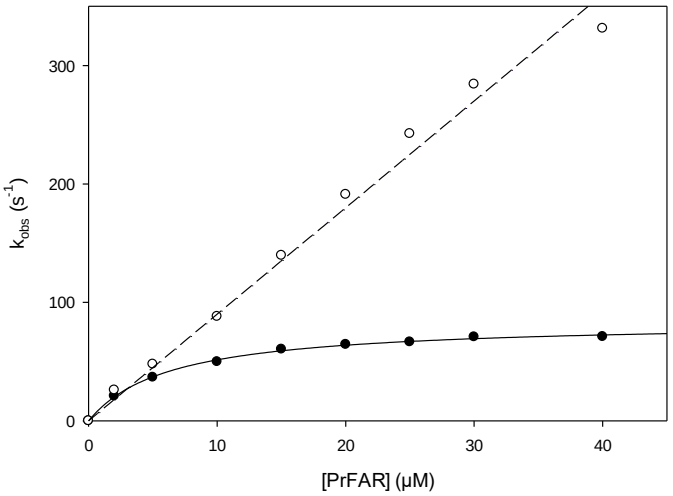

Fig. 33: Measurement of PrFAR binding to the ImGPS hY136CouA fF23A compared to ImGPS hY136CouA at 25 °C. Pseudo first order rates of PrFAR binding to ImGPS hY136CouA (dots) follows a hyperbolic trend (solid line). The rates of PrFAR binding to ImGPS hY136CouA fF23A (open circles) follows a linear trend (dashed lines).

4.2.4 Evaluation of changes in the HisH active site upon allosteric activation

Considerable effort has been made to unravel the nature of the conformational changes which happen in the HisH active site upon allosteric activation and ultimately cause the increase in catalytic activity. However, many details remain enigmatic. Therefore, one aim of this thesis is to gather more detailed information on the changes in the HisH active site in order to further the understanding of the molecular mechanism of this tightly regulated system.

As shown in Fig. 6, the catalysis of class I glutamine amidotransferases such as HisH relies on three different factors: The nucleophilic attack of hC84 on the carboxamide of glutamine, the acid/base catalysis of hH178 (deprotonation of hC84 and protonation of the leaving ammonia group) and electrostatic catalysis by stabilizing the negatively charged oxyanion intermediates. The V-type activation of HisH, i.e. the catalytic rate is increased, suggests that at least one of these three catalytic factors is changed during allosteric activation.

Two models that explain the activation of HisH on a molecular level have been proposed previously. In accordance with the requirements stated above, one model hypothesizes that the oxyanion hole is formed by the amide of hV51 within the conserved h49-PGVG-52 motif. In all available structures, this amide is turned away from the active site and engaged in a hydrogen bond with hP10. Hence, the peptide bond would have to "flip" to let the amide point towards the bound glutamine molecule.[103] This model is based on evidence from MD simulations, which suggest that the backbone of hV51 shows increased flexibility when PrFAR is bound to the HisF active site, and NMR-experiments, which demonstrated that amides of the h49-PGVG-52 motif show peak broadening in $^{1}H^{15}N$-TROSY experiments indicating increased flexibility on the µs-ms timescale.[102–104,157] Also, in some other GATases, the amide of the corresponding position of hV51 is involved in oxyanion stabilisation.[95,160] Another study found that in the crystal structure of ImGPS containing a bound glutamine (PDB-code: 3ZR4), the amide of hG52 is already positioned to interact with substrate molecule and could, hence, qualify as the oxyanion hole.[105] In combination with data from the constitutively active ImGPS hY138A hK181A, it was suggested that the reaction is actually in a constant equilibrium and activation is accomplished by the opening of the intermolecular channel, allowing ammonia to diffuse away from the HisH

active site. This implies that it is actually the release of the reaction products, which is accelerated.[105]

While the two hypotheses make reasonable assumptions, conclusive evidence for the parts of the HisH active site, which are allosterically influenced is still missing. Two factors that have hitherto not been studied in connection to allostery in ImGPS are the the nucleophilic nature of hC84 and acid/base catalysis of hH178. In order to get a more complete picture, these two points will be addressed in this chapter.

Cysteine residues are commonly occurring catalytic residues because they are particularly suited as nucleophiles (hC84 in HisH from ImGPS). The nucleophilic form of cysteine is the deprotonated thiolate. Since the pK_a value of a free cysteine in solution is above 8,[22] solvent accessible cysteines are mostly protonated at physiological pH. A very common motif in enzyme active sites is the stabilization of the negative charge of the thiolate via a positively charged histidine residue (hH178 in HisH from ImGPS). Considerable shifts in pK_a have been observed up to as much as 6.6 pH units, yielding a final pKa of 3.4.[161,162] Histidine in turn is also mostly uncharged at physiological pH, as its pK_a value is approximately 6.[22] Thus, the positive charge of catalytic histidine residues has to be stabilized by another negative charge of a strongly acidic residue. In class I glutaminases this role is carried out by a glutamate (hE180 in HisH from ImGPS). This chain of charge-stabilisation leads to a catalytic triad commonly found not only in glutaminases, but also many other enzymes such as proteases. The pivotal residue in this triad is histidine, since the glutamate residue has a very low pK_a of approximately 4 and its negative charge can be assumed to be present permanently. The cysteine deprotonation in turn is mostly dependent on the protonation state of the histidine due to the electrostatic stabilization of the negative charge. It should be noted that while histidine residues are capable of both acid and base catalysis, both of which is needed for the glutaminase reaction (Fig. 6) the expectation from other enzyme systems would be that the positively charged form of hH178 is more critical to HisH catalysis.[137,163]

In this chapter, the possibility will be explored the protonation states of hH178 and hC84 are changed upon allosteric activation and contribute to the increase in glutaminase activity of HisH. Also, the role of the amide of hV51 in forming the oxyanion hole will be examined more closely.

4.2.4.1 pH dependency of the HisH reaction

Enzymatic reactions using nucleophilic attack or acid/base catalysis involve so-called titratable groups. These can be catalytic amino acid side chains, which need to have a defined protonation state for catalysis, and chemical groups within the substrate molecule or reaction intermediates. This is particularly true for reactions using acid/base catalysis, since the protonation and deprotonation of the substrate molecule is part of the chemical mechanism. The central role of titratable groups is reflected in a strong pH-dependency of the reaction rates of the respective enzymes. If the pK_a values of catalytic HisH residues indeed change during allosteric activation, it would be expected that the pH-dependency significantly changes with different activation strength.

The pH-dependency of HisH catalysis has hitherto not been studied. This is mostly owed to the fact that the reaction is monitored in a coupled enzymatic assay detecting production of glutamate. The most commonly used auxiliary enzyme which generates a spectroscopic signal and has glutamate as substrate, is glutamate dehydrogenase (GDH). This enzyme is however also strongly pH dependent and shows only low activity at pH values lower than 8.[164] Thus, the HisH activity could not be followed at physiological pH or lower. As shown in Fig. 10, the assay using the oxidation of glutamate by GOX can be followed at a wider range from pH 5.6 to pH 9.2. Thus, the use of this assay allows the study of HisH pH-dependency.

Measurement of ImGPS glutaminase activity at different pH values were carried out by Dr. Andrea Keuttinger (Institute of Biophysics and Physical Biochemistry, University of Regensburg). To cover a broad range of pH values (6.3 to 9.0) with the same buffer system, Bis-Tris buffer (20 mM) was used. To assess the influence of different strength of allosteric activation on the observable pK_a values, measurement were performed for the basal activity as well as the ProFAR and PrFAR activated states. Under all three conditions, the reaction rate shows a bell-shaped dependency on pH (Fig. 34), as is expected for enzymes with at least two titratable groups involved in catalysis.

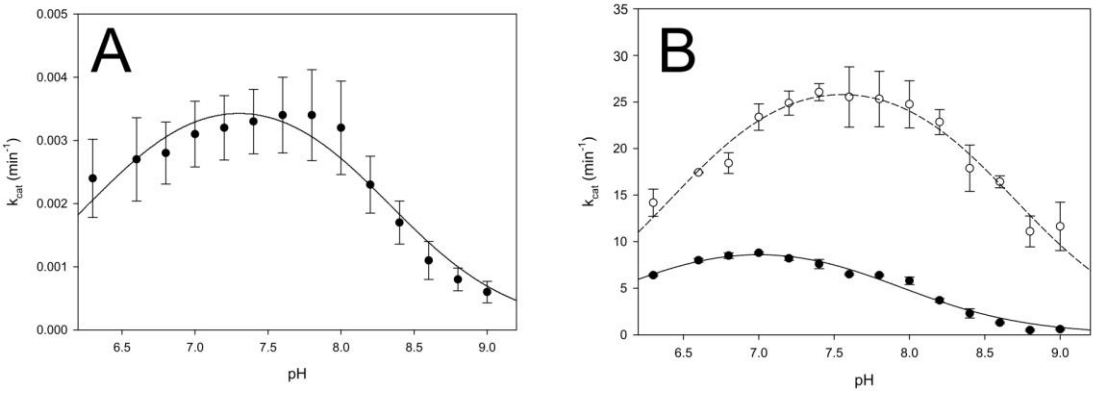

Fig. 34: pH dependency of the glutaminase reaction of wild type ImGPS at 25 °C. HisH activity was followed in the coupled assay using GOX for the oxidation of glutamate in 20 mM Bis-Tris/HCl buffer. All measurements were carried out in glutamine saturation (10 mM). Error bars represent the standard error of a technical triplicate measurement (three biological replicates for basal activity). The data were fitted to equation (13) to yield the displayed curves. **(A)** Basal activity was measured using 25 µM ImGPS. **(B)** Glutaminase activity in the presence of the allosteric activators ProFAR (70 µM, dots) and PrFAR (100 µM, circles) was measured with 0.1 µM and 0.02 µM ImGPS, respectively.

The bell-shape of the titration curve of the HisH activity is indicative of a reaction mechanism that relies on at least two different titratable groups that have opposite effects on activity when protonated. The involvement of more groups cannot be ruled out, since their effect would superpose with that of either of the first two titratable groups. In a mathematical description of this data, two macroscopic pK_a values (pK_{a1} and pK_{a2}) as well as a maximum k_{cat} ($k_{cat,max}$) can be determined using equation (13):[165]

$$k_{cat} = \frac{k_{cat,max}}{\frac{10^{-pH}}{10^{-pKa1}} + \frac{10^{-pKa2}}{10^{-pH}} + 1} \qquad \textbf{(13)}$$

The fits describe all three data sets quite well (Fig. 34). The values yielded from the fits clearly show the expected increase in $k_{cat,max}$ from basal to ProFAR- and PrFAR-activation (Table 10).

Table 10: values obtained from pH-dependency measurements of wild-type ImGPS at 25 °C

Ligand	$k_{cat,max}$ (min^{-1})	V- type activation factor	pK_{a1}	pK_{a2}	pH optimum
None (basal activity)	4.1 ± 0.3 x 10^{-3}	-	6.3 ± 0.1	8.3 ± 0.1	7.64
ProFAR	10.7 ± 0.7	2610	6.4 ± 0.1	7.9 ± 0.1	7.05
PrFAR	29.6 ± 1.0	7220	6.4 ± 0.1	8.7 ± 0.1	7.57

Errors are standard errors derived from the mathematical fit to equation (13).

According to this data, ProFAR activates HisH activity 2610-fold and PrFAR 7220-fold. As can already be seen in Fig. 34, the pH optima differ between the different strengths of activation. Interestingly, the basal activity and PrFAR-stimulated activity both have a pH optimum at approximately 7.6, while the optimum for the ProFAR-stimulated reaction is significantly lower, at 7.1. This is a direct result of shifts in the pK_a values. While pK_{a1} was quite stable at 6.4 (6.3 for the basal activity), pK_{a2} shifted between 8.3, 7.9 and 8.7 for the basal, ProFAR activated and PrFAR activated HisH reaction, respectively. To better evaluate the changes of the pK_{a2} values one has to consider that pK_a values are on a logarithmic scale. Using the Henderson-Hasselbach-equation (equation (14)), the amount of the protonated species can be calculated.[166] Assuming a physiological pH of 7.4, the titratable group associated with pK_{a1} is mainly deprotonated in all cases (90.9 % in the ProFAR and PrFAR activated states, 92.6 % for the basal activity). On the other hand, the group possessing pK_{a2} is protonated to 88.8 %, 76.2 % and 95.2 % in the basal, ProFAR activated and PrFAR activated state, respectively.

$$pH = pK_a + \log\left(\frac{[A^-]}{[AH]}\right)$$

$$\frac{[AH]}{[A^-]} = \frac{1}{10^{pH-pK_a}} \qquad \textbf{(14)}$$

If the shift in the pK_a value of a catalytic residue was the sole determinant in HisH activation, a much more pronounced difference in pK_a values and in addition a clear correlation between activation strength and the respective pK_a change would be expected. This is clearly not the case. However, the changes in pH optimum and pK_{a2} highlight that the protonation states are at least slightly tuned during the activation process.

Even though the influence of the observed pK_a values is small, the question remains to which titratable groups they can be assigned. In HisH, the most obvious candidates as titratable groups are hC84 and hH178. hC84 acts as a nucleophile, the thiolate being the more nucleophilic species of cysteine residues. Thus, for an efficient reaction, hC84 should be mainly deprotonated an it would be reasonable to assign it to pK_{a1}, since in this case it would be around 90 % deprotonated at physiological pH. The role of hH178 is more complicated, since it has both acid and base catalysis function (Fig. 6). Thus, the optimal pK_a value would be around physiological pH, which gives 50 % protonated and deprotonated species, ensuring that both reactions are performed efficiently. On the other hand, the positive charge of hH178 also stabilizes the negative charge of hC84, which would in turn stabilize the protonated state and cause an increase of the pK_a value. pK_{a2} is, depending on the strength of activation, 0.9 to 1.3 pH units higher than physiological pH and would thus represent a good trade-off for these two functions of hH178. Finally, as can be seen in Fig. 6, the nitrogen of the carboxamide group of glutamine needs to be protonated to be able to leave as free ammonia and thus also qualifies as a titratable group. For this group, a high pK_a value would be most favourable, since it would ensure protonation. Thus it might also influence the macroscopically observed pK_{a2}.

In conclusion, while the microscopic pK_a values of titratable groups play an important role in HisH activity, the macroscopically measured pK_a values observed via the k_{cat} of the HisH reaction are not strongly altered during allosteric activation. Other effects dominate of the activation mechanism to explain the more than 2000-fold activation of the k_{cat}. This could, for instance, be the correct formation of the oxyanion hole, which will be discussed in more detail in chapter 4.2.4.5.

4.2.4.2 Detection of changes in hH178 protonation during activation

In the previous chapter, it could be observed that a pKa value (pK_{a2}) of a catalytic residue changes with different activation strength. To further assess this observation and determine whether this shifted pK_a can indeed be assigned to hH178, NMR experiments were performed in cooperation with Dr. Jan-Philip Wurm (group of Prof. Remco Sprangers, Institute of Biophysics and Physical Biochemistry, University of Regensburg). For this purpose, HisH was produced with histidine residues labelled with ^{13}C at the ε_1 position. Since this is the carbon atom located between the two nitrogen atoms of the imidazole ring, its chemical shift in NMR spectra is highly sensitive to the protonation state of the respective histidine residue.[167] The signals of labelled histidine residues were recorded at physiological pH (7.4) in HMQC experiments in the presence and absence of ProFAR and/or glutamine. To avoid glutamine turnover during the experiments, measurements were performed with the ImGPS complex containing the mutation hC84S. Since HisH contains six histidine residues, the signals of the two residues inside or close to the active site (hH178 and hH53) were identified by mutagenesis (Fig. Appendix 5).

The signal of hH178 in the absence of glutamine and ProFAR showed a high chemical shift value in the ^{13}C-dimension, indicating that it is mainly deprotonated at physiological pH (Fig. 35A). Addition of either ProFAR as an allosteric activator or glutamine as the HisH substrate led to no significant change in the hH178 signal. However, when ProFAR and glutamine were added simultaneously, a significant change in chemical shift towards lower values in the ^{13}C-dimension of the signal of hH178, could be observed (Fig. 35B). This indicates that protonation of hH178 is significantly increased in the presence of ProFAR and glutamine. The signal of hH53 also shifted, but protonation was not altered significantly.

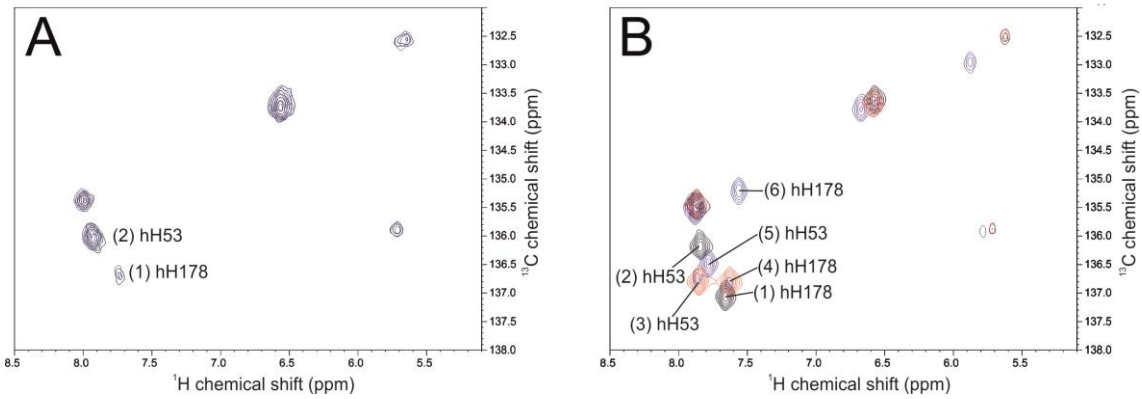

Fig. 35: NMR spectra of HisH labelled with ε^{13}C-histidine at 25 °C. To probe the protonation state of the catalytic histidine of HisH, hH178, HisH was labelled with ε^{13}C-histidine. The peak of hH178 (1) was assigned by mutation to alanine. **(A)** The spectrum of apo state (black) is virtually identical to that with 350 µM ProFAR (blue). Spectra were recorded with wild-type ImGPS **(B)** Addition of 10 mM glutamine (orange) induces small chemical shift changes to several histidine residues, including hH53 (3) and hH178 (4), probably due to the proximity of its binding site. Only after addition of a combination of glutamine and ProFAR (blue), two residues show significant changes in chemical shift. The peak with the smaller shift belongs to hH53 (5) and the one with the larger shift to hH178 (6). This shift is strong evidence for an increased protonation of hH178 in the presence of both ImGPS substrates. ImGPS complexes used for measurements with glutamine contained the mutation hC84S.

These experiments clearly demonstrate that the catalytic residue hH178 changes its protonation state upon allosteric activation of HisH. Furthermore, this confirms that hH178 is one of the titratable groups observed in the pH dependency experiments (chapter 4.2.4.1). Since the deprotonation of hC84 is dependent on the presence of the positive charge of hH178, it can be surmised that this residue, too, changes it protonation state upon binding of both products and is also one of the observed titratable groups. Due to the increase in protonation state, hH178 can be

assigned to pK_{a2}, since this is the pK_a of a titratable group for which an increased protonation is favourable for the reaction. Although the change in this pK_a value in the measurement of the pH-dependency of the glutaminase reaction was relatively small, a significant change in protonation was observed here. There are several possible explanations for this apparent discrepancy. The pK_a values measured in the pH dependency are macroscopic effects that were recorded with the overall activity as the readout. The NMR experiments specifically follow hH178 and are performed without (or very low) turnover of glutamine. In the pH-dependency, the pKa values of other titratable groups can play a role, such as that of the leaving ammonia. Furthermore, the protonation state of hH178 has to change during the course of the reaction, which will certainly influence the observed pK_a. Finally, in the substrate bound state observed in the NMR experiments, hH178 might interact with other protein residues or the glutamine molecule, which may also alter the chemical shift of hH178.

Remarkably, the observed effect is triggered by glutamine binding simultaneously with ProFAR. Usually, allostery is thought of as solely being caused by ligand binding in one site affecting another. ImGPS therefore appears to be a special case in which the substrate induced conformational change in HisH is allosterically triggered by the binding of the ligand HisF. Recent NMR studies detected a conformational change in the entire ImGPS complex which is dependent on the binding of both ProFAR and glutamine at the same time.[107] It is a reasonable assumption, that a conformation that is induced by binding of both substrates (or one analogue in this instance) constitutes the reaction competent conformation. The fact that the binding of glutamine and ProFAR to ImGPS increase the protonation of hH178, which is essential for the initiation of the glutaminase reaction, therefore support the hypothesis that conformational changes observed in other NMR experiments represent the active ImGPS conformation.[107] It remains to be determined whether the change in hH178 protonation is a direct result of this conformational change and which particular rearrangements occur in the HisH active site when the active conformation is adopted.

4.2.4.3 Study of allosteric activation and pH dependency of HisH with the inhibitor acivicin

A well-established method for gaining information on the molecular mechanism of enzymes is the use of inhibitors. For glutaminases, several inhibitors are available, some of which are so-called “suicide” inhibitors. They received their name for their property of reacting irreversibly with the catalytic residue (hC84 in the case of HisH), forming a chemically stable analogue of a reaction intermediate (in the case of HisH the thioester). Acivicin is such an inhibitor which has been used in studies with yeast His7 and *E. coli* ImGPS. It possesses an isoxazol ring substituted with a chlorine atom instead of the carboxamide group of glutamine. The leaving group is a chloride ion and the formed covalent bond with the catalytic cysteine is not cleavable by hydrolysis (Scheme 6). It is assumed that the reaction of acivicin in a glutaminase also produces a negatively charged intermediate, similar to the oxyanion during the native glutaminase reaction and is thus dependent on the proper formation of an oxyanion hole.[156]

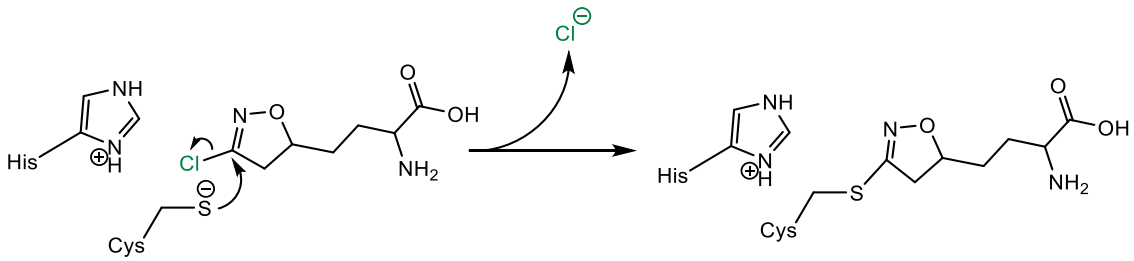

Scheme 6: Mechanism of acivicin inactivation. The glutaminase active site cysteine, in its thiolate form, nucleophilically attacks the isoxazol ring of acivicin. As a leaving group, a chloride ion is formed. The newly formed S-C-bond is stable against hydrolysis and is an analogue of the thioester intermediate of the glutaminase reaction.

In the context of this thesis, the use of acivicin offers two advantages for the study of the molecular mechanism of HisH activation: i) the reaction only progresses to the thioester analogue and ii) the leaving group is a chloride ion, which does not need to be protonated for the reaction to occur. The first point allows for the determination of the influence of activation on the first half reaction of glutamine turnover, the formation of the thioester, independent of the second half reaction, the hydrolysis of the thioester. The second property is helpful in the investigation of the pH dependency of the HisH reaction. The chloride leaving group eliminates the leaving ammonia as a putative third titratable group in the HisH mechanism and also removes the necessity of hH178 to protonate the leaving group. This leaves hH178 and hC84 as the only titratable groups that can influence activity, simplifying the analysis of pH dependency.

To assess the amount of acivicin needed for inactivation studies, acivicin was titrated into a glutamine dependent ImGPS assay following the decrease in PrFAR absorbance as signal with both PrFAR and glutamine in saturating concentrations (40 µM and 10 mM respectively). In all conditions acivicin was added in an at least 4-fold molar excess to ImGPS. This make changes in acivicin concentration over the observed time negligible, leading to conditions of pseudo first order inactivation (Fig. 36A). Under pseudo-first order conditions, the amount of active HisH and thus, active ImGPS, decreases following a single exponential decay. Since the residual ImGPS activity is directly proportional to the amount of active protein, the reaction trajectories can be fitted to a single exponential equation. The time constant constitutes the rate of inactivation $k_{inact,obs}$, which was plotted against the acivicin concentration, yielding a hyperbolic curve (Fig. 36B).

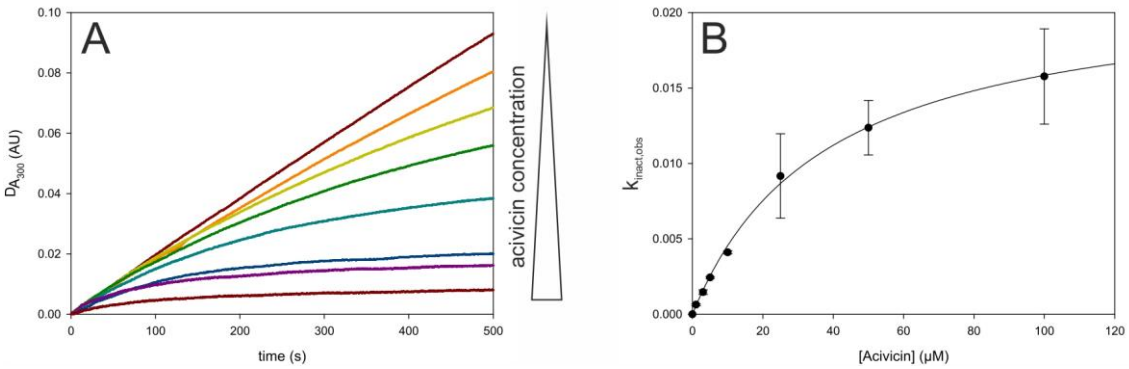

Fig. 36: Inactivation of HisH with acivicin at 25 °C. The glutamine dependent ImGPS reaction was measured in a quartz cuvette in a photo spectrometer by following the absorbance decrease at 300 nm of PrFAR to AICAR. Reaction mixtures contained 50 mM Tris/HCl pH 7.5, 40 µM PrFAR and 10 mM glutamine. ImGPS concentration was 0.2 µM to ensure at least 5-fold excess of acivicin to allow for the approximation of pseudo first order inactivation **(A)** Raw data, showing how the activity decreases over time in an exponential fashion, as expected for pseudo first order conditions. The curves were recorded in technical triplicates and fitted to a single exponential equation. **(B)** The mean values with error bar indicating the standard deviation that were obtained from fitting the raw data. The line represents a fit to a hyperbolic equation equivalent to a modified Michealis-Menten equation (equation (15)).

The inactivation kinetics describe the inhibition constant K_i and the maximal rate of inactivation k_{inact}, which are measures comparable to K_M and k_{cat} in the normal Michealis-Menten equation, respectively (equation (15)).[165]

$$k_{inact,obs} = \frac{k_{inact} \cdot [I]}{K_i \cdot \left(1 + \frac{[Gln]}{K_M^{Gln}}\right) + [I]} \qquad (15)$$

This yielded values of 38 µM for K_i and 0.022 s^{-1} for k_{inact} of the acivicin inactivation of HisH. Comparing these results with those from previous studies on yeast His7 and *E. coli* ImGPS shows that there are significant differences in the susceptibility for acivicin between ImGPS enzymes from different organisms (Table 11).

Table 11: Kinetic parameters of acivicin inactivation at 25 °C

	tmImGPS	His7	ecImGPS
K_i (µM)	38.1 ± 3.1	5.6 ± 1.1[156]	< 9[156]
k_{inact} (s^{-1})	0.022 ± 0.008	0.164 ± 0.009[156]	≥ 10[156]
k_{inact}/K_I ($M^{-1}s^{-1}$)	57.5	293[156]	≈ 10,000[156]
K_{ac} (µM, ProFAR, acivicin)	86.3 ± 26.1	-	-
K_{ac} (µM, ProFAR, Gln)	23[100]	-	430[97]

Errors are standard errors from technical triplicate measurements or taken from the respective citation. Measurements with His7 and ecImGPS at 30 °C.

To assess whether the inactivation by acivicin as a model reaction for the formation of the thioester is accelerated by the presence of an allosteric activator, a pre-incubation experiment was performed. In this experiment, 10 µM ImGPS were incubated with 200 µM acivicin and varying concentrations of the allosteric activator ProFAR. After defined time intervals, aliquots of the inactivation reaction were directly diluted 700-fold into a glutamine dependent ImGPS assay. This yielded an acivicin concentration of < 0.3 µM, making inactivation during the observed reaction time negligible (K_i = 38 µM). Due to the pseudo first order nature of the inactivation reaction, the logarithm of the observed residual activity was then plotted against the time of pre-incubation with acivicin and fitted by linear regression. This yielded pseudo first order rates of inactivation for each ProFAR concentration (Fig. 37A). These inactivation rates were plotted against the ProFAR concentration and fitted with a hyperbolic function (Fig. 37B). This fit yielded an activation constant K_{ac} of ProFAR for the acivicin inactivation of 86 ± 26 µM, which is about 3-fold higher than the activation constant for the glutaminase activity of 23 µM (Table 11).[100]

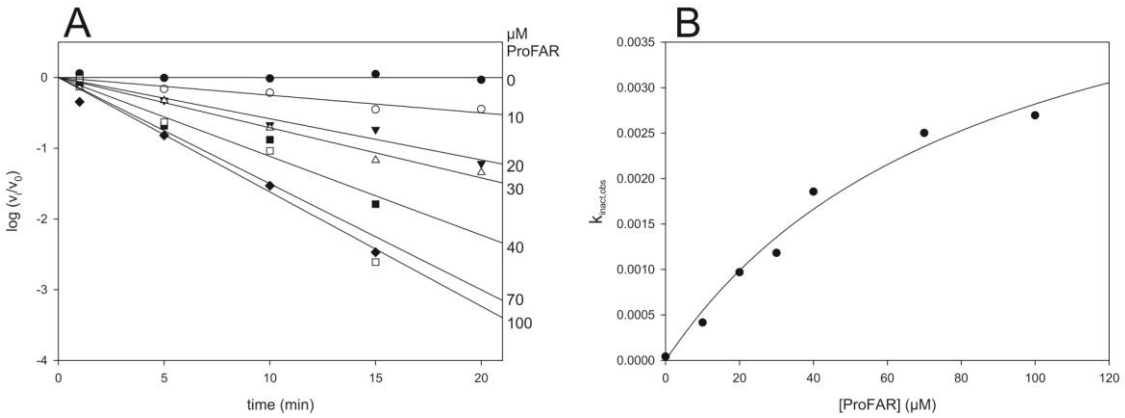

Fig. 37: Influence of ProFAR on the inactivation rate of acivicin at 25 °C. 10 µM of the fully formed ImGPS complex was incubated with 200 µM acivicin and varying concentrations of ProFAR at 25 °C in 50 mM Tris/HCl pH 7.5. After certain time intervals, aliquots were diluted 700-fold into a reaction mixture for measuring ImGPS activity (50 mM Tris/HCl, pH 7.5, 30 µM PrFAR, 10 mM Gln). **(A)** The residual activity was divided by the initial activity and the logarithm of this ratio was plotted against the incubation time. This was fitted to a linear equation, the slope signifying the pseudo first order rate constant of HisH inactivation. ProFAR concentrations are given on the right hand side of the plot. **(B)** The pseudo first order rate constant $k_{inacct,obs}$ was plotted against each ProFAR concentration used in the pre-incubation phase. The line represents a fit to a hyperbolic equation.

These data clearly indicate that ProFAR strongly accelerates the inactivation of HisH by acivicin and the strength of this effect is similar to the effect on glutamine hydrolysis. The allosteric mechanism of activating HisH glutaminase activity and acivicin inactivation therefore appear to be very similar. It can be concluded that ProFAR strongly activates the first half-reaction of glutamine hydrolysis, the formation of the thioester intermediate.

Moreover, the pH-dependency of the acivicin inactivation rate was assessed in the same experimental set-up as for the ProFAR titration, but in ProFAR saturation (100 µM) at different pH values (Fig. 38). Since the readout of activity is independent of the pre-incubation conditions, a wide pH-range of 4–9.5 could be used. The data of the acivicin inactivation shows a trend similar to glutamine turnover (Fig. 34). A bell-shaped curve typical for a reaction dependent on at least two titratable groups could be observed. The reaction could only be measured in the presence of ProFAR, since the reaction rate without allosteric activation was too low to be detected and the activation with PrFAR led to full inactivation of HisH before a measurement of residual activity could be performed.

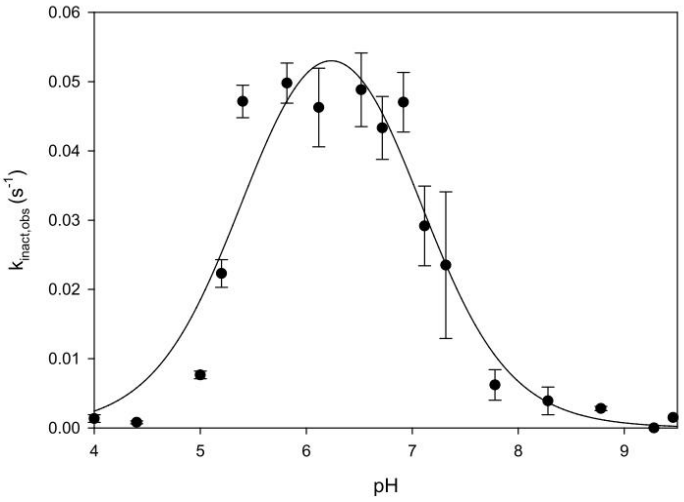

Fig. 38: pH dependency of the acivicin inactivation of HisH in the presence of ProFAR at 25 °C. The acivicin inactivation rate was determined in pre-incubation experiments at different pH values in 20 mM buffer (pH 4.0 - 5.7: acetate/acetic acid, pH 6.0–7.2: Bis-Tris/HCl, pH 7.5–9.0: Tris/HCl, pH 9.2–10.0: Glycine/NaOH) with 200 µM acivicin and 100 µM ProFAR. Rate of inactivation was determined by measurement of the glutamine dependent ImGPS reaction following the turnover of PrFAR. The error bars indicate the standard deviation of technical triplicate measurements. The data were fitted to equation (13). The pK_a values determined form the fit are 5.4 and 7.0.

Since ammonia as the third possible titratable group in the HisH reaction is not present when using acivicin, the two pK_a values calculated from the mathematical fit of the data can be assigned to hC84 and hH178, under the assumption that no other titratable groups contribute the pH-dependency of HisH activity. The calculated pK_a values are 5.4 and 7.0 for hC84 and hH178, respectively. These values are about 1 pH unit lower than those observed for the ProFAR activated glutaminase reaction (6.4 and 7.9). This might be the result of a difference in the electrostatic environment of the two residues with either acivicin or glutamine bound. Whether these differences are simply due to the change in the chemical nature of the ligand or whether they result from conformational changes induced by acivicin or glutamine binding can only be conjectured at this point. Overall, these data indicate that the pK_a values of hC84 and hH178 are determining factors in the pH dependency of the HisH reaction. That hH178 is also necessary for the inactivation reaction with acivicin highlights the central importance of the stabilization of the negative charge of hC84 for HisH activity.

4.2.4.4 The role of fD98 in the HisH glutaminase reaction

It has been observed in previous work that an aspartate residue situated in HisF (fD98) is of crucial importance to HisH activity.[105,108] In fact, a recent study showed that many, if not all, class I GATases have a conserved aspartate residue in the synthase subunit that points into the glutaminase active site and interacts with the residue next to the catalytic histidine, which corresponds to hK181 in ImGPS.[168] In ImGPS, mutation to alanine leads to a nearly complete inactivation in the position of fD98 or a great increase of basal activity in the position of hK181.[108] One hypothesis is that removal of the hK181 side chain leads to accelerated ammonia release through "unblocking" of the active site, increasing the rate of the glutaminase reaction. This is supported by the fact that the mutation of another bulky residue in the vicinity, hY138, to alanine has a similar effect and is synergistic to hK181A.[105] fD98 was thus assigned an allosteric role to transmit the activation signal via hK181 and regulating the "blockage" of the active site. However, the triple mutant ImGPS fD98A hY138A hK181A has again lower activity than the double mutant, indicating that fD98 still plays an important role in HisH activity even in the absence of the two large side chains.[108] The salt bridge between residues fD98 and hK181 is not present in the triple mutant as well as either single mutant fD98A and hK181A, which indicates that fD98 has not only an allosteric function, but also facilitates HisH activity in another way. In light of the results concerning hH178 protonation and pH dependency of the HisH reaction (chapters 4.2.4.2 and 4.2.4.3), it is conceivable that during allosteric activation, the negatively charged side chain of fD98 is brought into proximity of hH178 and/or the leaving ammonia group, increasing the respective pK_a value(s) and thus tuning the protonation state(s) in favour of the glutaminase reaction.

To test this hypothesis, fD98 was mutated to glutamate under the assumption that the elongation of the side chain might put the carboxyl group into closer proximity of hH178 and the reaction intermediates. Thus, this mutation might mimic, at least partially, the allosteric activation effect. Steady-state kinetics of the variant fD98E showed that this exchange indeed leads to a 10-fold increase of the unstimulated HisH activity without allosteric activator and a 5-fold increase with the addition of 70 µM ProFAR (Fig. 39A and B, respectively).

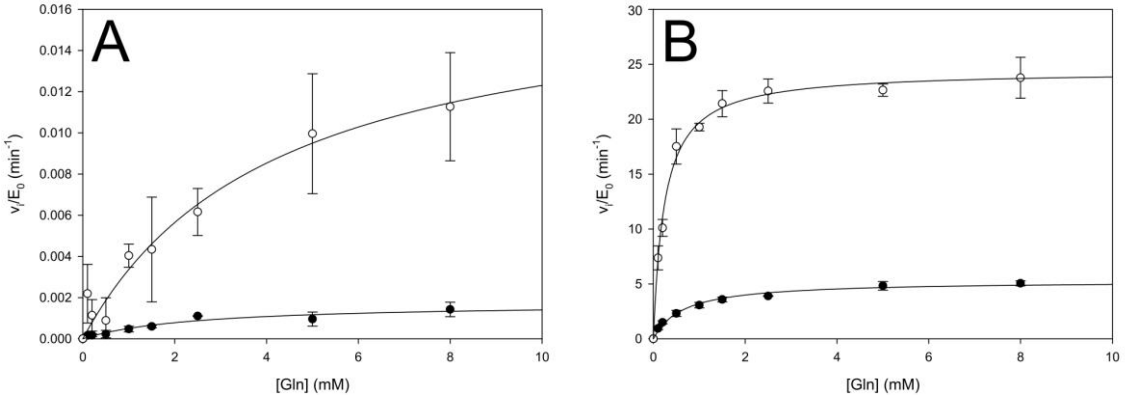

Fig. 39: Steady state glutaminase kinetics of ImGPS fD98E at 25 °C. Activity was measured in the GOX assay in 20 mM Tris/HCl pH 7.0 for wild-type ImGPS (dot) and ImGPS fD98E (empty cicles). **(A)** Without ProFAR activation, the mutation fD98E leads to an increase in k_{cat} from 1.7 x 10^{-3} min-1 to 1.75 x 10^{-2} min^{-1}, signifying a 10.3-fold change. **(B)** This factor is lowered to 4.6-fold for the ProFAR activated reaction with a k_{cat} of 5.3 min^{-1} and 24.4 min^{-1} for wild-type ImGPS and the fD98E mutant, respectively. The K_M value is similar in both variants, although it appears to be lowered by activation with ProFAR from 2.5 mM (A) to 0.64 mM (B) and from 4.2 mM (A) to 0.24 mM (B) for wild-type ImGPS and the fD98E mutant, respectively.

To elucidate the structural changes that are caused by the introduction of the mutation, the structure of HisF D98E in complex with wild-type HisH was determined by X-ray crystallography in collaboration with Dr. Chitra Rajendran (laboratory of prof. Christine Ziegler, Institute of Biophysics and Physical Biochemistry, University of Regensburg). Data collection and refinement statistics are summarized in Table Appendix3 .

The overall structure of the ImGPS fD98E contains one ImGPS complex and is very similar to that of the wild-type enzyme (all atom RMSD = 2.2 Å, PDB-code 1GPW chains A and B). However, in a closer inspection of the mutation site and its immediate surroundings, subtle changes can be observed (Fig. 40). The carboxyl group of fE98 is 1.5 Å closer to the imidazole ring of hH178 than that of fD98 in wild-type ImGPS. The HisH active site is also slightly rearranged: hH178 forms a hydrogen bond with hE180 and there is an alternative conformation observed for hC84 pointing towards hH178. These changes may give an indication that the closer proximity of the fE98 side chain indeed has a positive influence on the HisH reaction rate. However, the structural changes have to be considered with some caution due to the lower resolution of the reference structure.

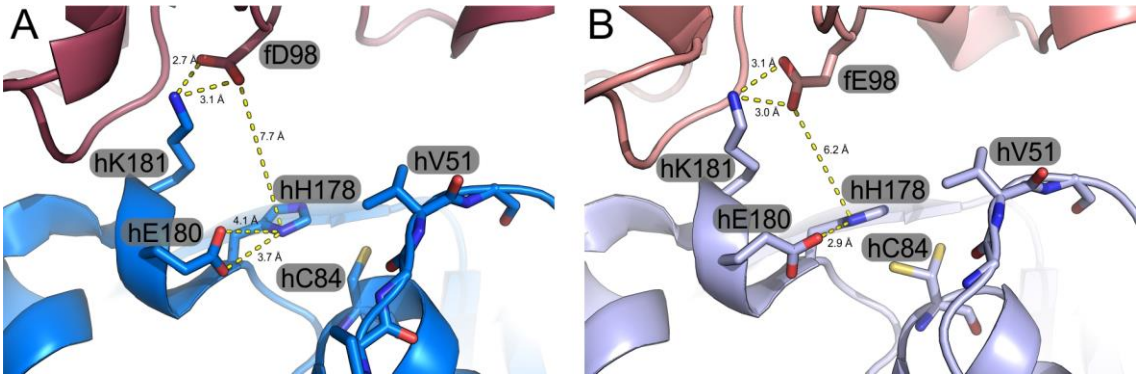

Fig. 40: Structural comparison of wild type ImGPS and ImGPS fD98E. Close-up of the interface between HisF (red) and HisH (blue) in cartoon representation. Wild type ImGPS (PDB-code 1GPW) is shown in dark colours, ImGPS fD98E is light colours. Relevant residues are shown as sticks. **(A)** In wild type ImGPS, fD98 forms a salt bridge with hK181and is 7.7 Å distant from the catalytic hH178. hC84 points towards the glutamine binding site and hE180 oriented in a way that it might form hydrogen bonds with hH178. **(B)** In ImGPS fD98E, the salt bridge of fE98 with hK181 is still present, however, hK181 is moved slightly away from the HisH active site. hE180 shows an angle of about 180° to hH178 and forms a hydrogen bond with it in a distance of 2.9 Å. hC84 adopts two alternative conformations, one pointing into the glutamine binding site as in wild type ImGPS and one pointing towards hH178. For orientation, the oxyanion strand h49-PGVG-52 of HisH is marked by the position of hV51, which shows only small differences in conformation.

In addition to the apo structure, a structure of an ImGPS complex containing the mutation fD98E with the HisH substrate glutamine and the HisF substrate analogue ProFAR could be solved (full data collection and refinement statistics in Table Appendix3). This complex additionally contained the mutation hC84S to minimize glutamine turnover. Due to the instability of ProFAR and the hydrolysis of glutamine during crystallization, both substances were added by soaking the crystals in a solution containing saturating concentrations of both substances.

Similar to the apo structure, this structure contains only one copy of the complex which has a very high similarity to wild-type ImGPS (all atom PDB-code 1GPW, RMSD = 2.2 Å chains A and B) and the apo structure (all atom RMSD = 0,77 Å). Interestingly, loop1 of HisF is not resolved completely, indicating a higher flexibility than in most other structures, such as the apo structure of ImGPS fD98E. The residues of loop1 that could be resolved indicate that loop1 adopts a mostly closed-like conformation in this structure. Electron densities could be detected for both ligands in different quality. The density for the glutamine molecule is well defined in an omit map at 1 σ (Fig. 41A). ProFAR on the other hand is only partially resolved, showing only one phosphate

with the attached ribose moiety at the site that usually binds the "AICAR part" of PrFAR (Fig. 41B). To reasonably represent the ribose moiety, the electron density of the omit map had to be lowered to 0.5 σ.

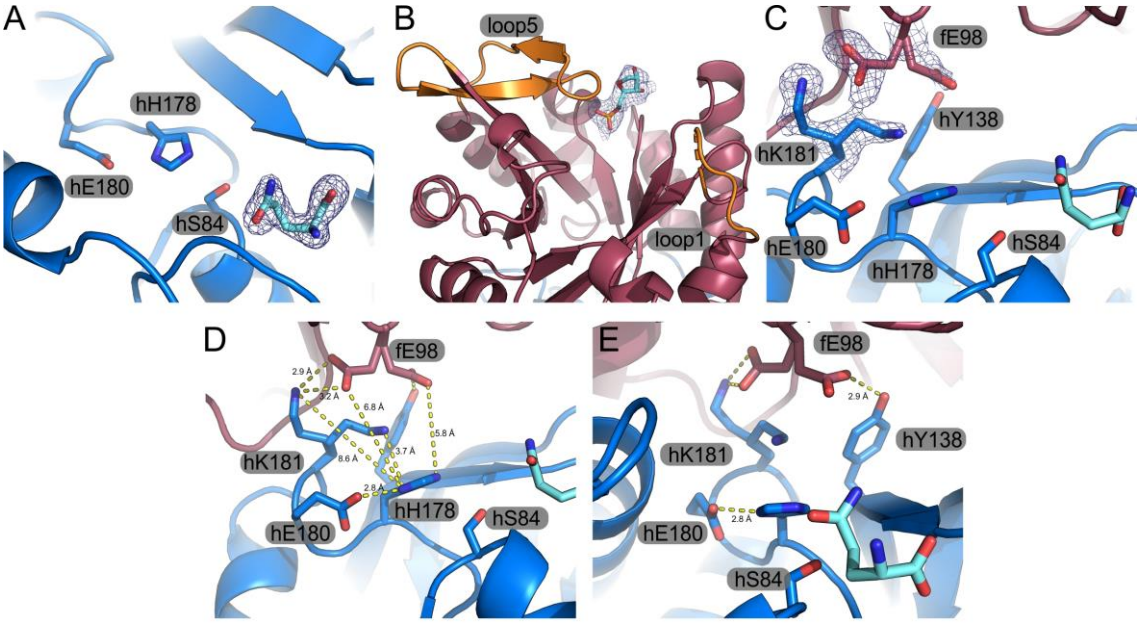

Fig. 41: Structural analysis of ImGPS fD98E hC84S with bound ProFAR and Glutamine. ImGPS fD98E hC84S is shown in cartoon representation with HisH in blue and HisF in red. **(A)** Bound Glutamine with an omit electron density at 1 σ. **(B)** Partly resolved ProFAR molecule bound at the phosphate binding site close to loop5 (orange cartoon). For orientation, loop1 is also shown in orange cartoon, the residues not resolved (19–25) are indicated by a dashed line. The electron density is from an omit map at 0.5 σ. **(C)** Residues fE98 and hK181 clearly show one additional conformation compared to other structures. The electron density is shown at 0.5 σ from an omit map. **(D)** Measurement of the distances (marked by yellow dashed lines) shows that the side chains of fE98 and hK181 are both significantly close the active site residue hH178 in their respective alternative conformations than in the previously observed conformations.**(E)** In the alternative conformation, the side chain of fE98 interacts with hY138 via a hydrogen bond (2.9 Å distance).

Interestingly, significant conformational changes can be observed for the residues fE98 and hK181. Both residues exhibit a lower quality of electron density. In an omit map at 0.5 σ, it is clearly visible that both residues can be detected not only in the identical conformation as in the apo structure of ImGPS fD98E, but also in a second, alternative conformation (Fig. 41C). Other residues are significantly closer to the catalytic hH178 in these alternative conformations compared to those observed in the apo structure (Fig. 41D, 5.8 Å for fE98 and 3.7 Å for hK181, which a reduction in distance of constitutes 1 and 2.9 Å, respectively). Another interesting observation is that in the alternative conformation, fE98 forms a hydrogen bond with the side chain of hY138 (Fig. 41E, 2.9 Å distance), a residue which also plays an important part in the process of allosteric communication as indicated by the increase in basal activity of the mutant hY138A.[105]

The structural observations made in the two ImGPS structures containing the mutation fD98E have still to be interpreted with caution. The closer proximity of the fE98 carboxyl group in the alternative conformation implicates that this electrostatic influence might be a factor in the rate enhancement observed in this mutant. The alternative conformation of fE98 might also suggest a possible role of hY138 in the activation of HisH. While a removal of this interaction by mutation would certainly not explain the increase in basal activity in ImGPS hY138A, one could speculate that this interaction is counterproductive for activity, since it holds the carboxyl group of fE98 (or fD98) relatively far from hH178. Thus, removal of this interaction possibility for fD98 would

lead to an increase in activity. This would agree with the synergy with the mutation hK181A in increasing activity, which also keeps fD98 distant from hH178.[105,108]

The incomplete binding of ProFAR indicates that the observed holo structure is not the final ternary complex and thus most likely does not contain all conformational changes necessary for activation of HisH. This is supported by the alternative conformation of hK181, in which the positively charged amino group comes in very close proximity of hH178. This clearly represents an electrostatic interaction that is detrimental to HisH activity, since it would counteract a protonation of hH178, which is essential for initiation of the glutaminase reaction.

In any case, the ligand bound structure of ImGPS fD98E hC84S indicates that considerable conformational rearrangements and/or increase in conformational flexibility are induced within the HisH active site upon allosteric activation. The latter is in agreement with previous NMR studies.[148] Taking all results of this chapter into account, there are clear indications that the residue fD98 serves in a dual role in ImGPS. On the one hand, it forms a crucial link with hK181 for allosteric communication. On the other hand, the results from steady-state kinetics combined with the structural analysis indicate that is might play a more direct part in HisH catalysis by increasing the protonation of hH178. To clarify the molecular details, such as whether the electrostatic influence is exerted solely on hH178 or also on a reaction intermediate of glutamine turnover, have to be addressed in further studies. These certainly need to contain structural studies, in which the conformational influence of the ImGPS ligands in analysed in more detail.

4.2.4.5 Investigation of the role of hV51 in forming the oxyanion hole

Stabilization of the two tetrahedral oxyanion intermediates during the hydrolysis of glutamine is certainly one of the most crucial functions performed by HisH. These chemically unstable states are stabilised electrostatically by the oxyanion hole (Fig. 6). Generally, oxyanions are stabilised by interaction with protein backbone amides.[169] The oxyanion hole is formed by different parts in their respective structures. In class I GATases, the oxyanion hole is formed by the conserved oxyanion strand (h49-PGVG-52 in ImGPS).[103,104] In some glutaminases, a second amide is involved, namely that of the residue directly neighbouring the catalytic cysteine (corresponding to hL85 in ImGPS).[160] There are two interpretations as to which amide in the highly conserved PGVG-motif in HisH forms the oxyanion hole. One hypothesis is based on observations from a crystal structure which shows that in the inactive state, the amide of hG52 is already positioned so it can form a hydrogen bond with the carboxamid of the glutamine substrate.[105] The other hypothesis states that the oxyanion hole is formed by the amide of hV51. However, this amide is turned away from the active site in all available crystal structures and forms a hydrogen bond with hP10 in the adjacent Ω-loop. The assumption is therefore that the hydrogen bond to hP10 is broken upon activation and the backbone flips into the active site. Previous studies,[100,108] as well as the experiments presented in chapter 4.2.4.1 showed that the increase in HisH activity is characterized by a strong increase in k_{cat}. Since the k_{cat} is generally associated with chemical turnover, an involvement of the oxyanion is a reasonable hypothesis. In this chapter, the role of hV51 will be explored.

Two different HisH variants were constructed in order to elucidate the role of hV51 in forming the oxyanion hole: hV51P, which effectively eliminates the amide at position h51, since in proline residues the amide is incorporated into the cyclic side chain, and hΔ10Δ13, in which hP10 and hI13 were deleted in order to shorten the Ω-loop so that it is no longer possible for hV51 to form a hydrogen bond with hP10. To characterize the effect on HisH activity, steady-state kinetic measurements were performed for the glutaminase activity of the two variants. hV51P showed a basal activity similar to wild type and 0.3 % wild type activity after ProFAR activation (11.5 fold activation, Table 12). hΔ10Δ13 on the other hand displayed a 17.6-fold increased basal activity.

Activation with 70 µM ProFAR led to a 50-fold increase in activity, yielding about 28 % wild type activity.

Table 12: steady-state glutaminase activity of HisH V51P and HisH Δ10Δ13 at 25 °C

HisH variant	k_{cat} HisH (min^{-1}) basal	k_{cat} HisH (min^{-1}) (+ 70 µM ProFAR)	activation factor
wt	$1.7 \pm 0.3 \times 10^{-3}$	5.3 ± 0.2	3,117
hΔ10Δ13	$3 \pm 0.1 \times 10^{-2}$	1.5 ± 0.1	50
V51P	$1.3 \pm 0.1 \times 10^{-3}$	$1.5 \pm 0.1 \times 10^{-2}$	11.5

In principle, a certain loss in activity compared to the wild-type HisH reaction is not surprising in both variants, since the introduced mutations are in close proximity to the active site. However, both variants are still active and provide some insight into the formation of the oxyanion hole. For instance, if the amide of hV51 was the only amide forming the oxyanion hole and the oxyanion hole formation is the only factor that activates the k_{cat} of HisH, it would be expected that the variant hV51P is completely inactive. However, the basal activity is unchanged compared to wild type and the variant is also still able to be allosterically activated. This indicates that there is at least one other amide that contributes to the oxyanion hole or the reaction can progress on the basal level without stabilization of the oxyanion intermediates. In any case, basal activity appears to not be dependent on the hV51 amide. The high reduction in k_{cat} in the ProFAR activated state suggests an important role for activation of hV51, but whether this stems from a direct involvement in catalysis or structural factors remains to be clarified.

The increase in basal activity in hΔ10Δ13 is a good indication that the weakening of the interaction of the PGVG-motif and the Ω-loop could be important for HisH activation. To elucidate if the deletion of two residues Ω-loop indeed eliminates the hydrogen bond and allows the hV51 amide to flip into the active site, the three-dimensional structure of the complex hΔ10Δ13:HisF was solved by X-ray crystallography in cooperation with Dr. Chitra Rajendran (group of Prof. Christine Ziegler, Institute of Biophysics and Physical biochemistry, University of Regensburg). The structure has a moderate resolution of 2.8 Å and contains three full ImGPS complexes (full data collection and refinement statistics in Table Appendix3). Overall, the structural similarity is very high to wild-type ImGPS (all atom RMSD = 2.2, PDB-code 1GPW, average of RMSD values of all complexes to each other), indicating no major conformational rearrangements. In two of the complexes, hV51 interacts with hG12 in the shortened Ω-loop, replacing the interaction with hP10 (Fig. 42A and B). In the third complex, no hydrogen bond formation can be observed. It should be noted that in all three complexes, the electron density for the Ω-loop is not well defined, which might be the result of an increase in flexibility by loop shortening. Otherwise, the HisH active site shows no significant conformational changes to wild-type ImGPS (Fig. 42C).

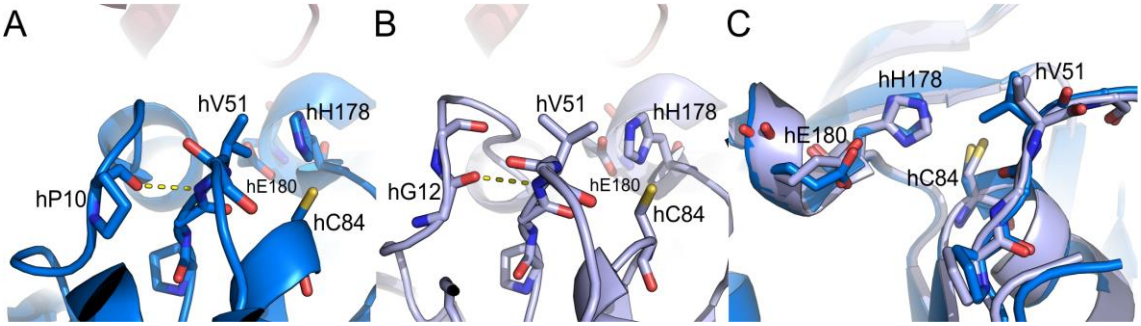

Fig. 42: Structural comparison of wild-type ImGPS with ImGPS hΔ10Δ13. The active site of wild-type HisH (dark blue) and ImGPS hΔ10Δ13 (light blue) is shown in cartoon representation. **(A)** In wild type ImGPS, the backbone amide of hV51 is hydrogen bonded (dashed yellow line) to hP10. **(B)** In ImGPS hΔ10Δ13, the deletion of two residues eliminating the possibility of forming this hydrogen bond. Instead, a replacement hydrogen bond of hV51 is formed with hG12 (numbering of wild-type HisH, residue number 10 in ImGPS hΔ10Δ13). **(C)** A structural alignment of wild type ImGPS and ImGPS hΔ10Δ13 shows that the structure of the oxyanion strand as well as the catalytic triad of HisH is not significantly altered.

There are two major conclusions that can be drawn from the results presented above: i) hV51 is likely not the only amide contributing to the oxyanion hole. Possible other candidates are hG52 and hL85. ii) hV51 is a good candidate as part of the oxyanion hole, since the weakening of the connection to the Ω-loop increases basal activity. The identification of the second oxyanion hole amide and verification of involvement of the hV51 amide need further structural data for validation.

4.2.4.6 Analysis of the relative acceleration of thioester formation and hydrolysis

The results presented in the previous chapters showed that the formation of the thioester intermediate is strongly accelerated by allosteric activation. However, the question remains whether the second half-reaction of HisH catalysis, the hydrolysis of the thioester intermediate, is also accelerated. Unfortunately, there is no method that allows for the selective monitoring of thioester hydrolysis, since this would require the trapping of HisH in this intermediate state. However, information can be gathered about the relative rate of hydrolysis compared to the rate of thioester formation by determination of the amount of enzyme that carries the thioester under steady-state conditions. Assuming that thioester hydrolysis is slower that its formation, the thioester intermediate would accumulate. Conversely, if formation is the rate limiting step, formed thioester would be hydrolysed quickly, leading to a low amount of protein carrying the covalent intermediate. Therefore, the fraction of protein carrying the thioester intermediate under steady state conditions is an indicator of the relative rate of the two half reactions.

To determine the fraction of protein carrying the thioester, ImGPS was incubated with ^{14}C-labelled glutamine, precipitated with trichloroactetic acid during steady state conditions and analysed for remaining radioactivity after filtration. For information on how allosteric activation relatively affects the rates of the two reaction steps, the experiments were carried out in the presence and absence of the allosteric activation.

In these experiments, the thioester intermediate accumulated without allosteric activation to 18.3 % in wild type ImGPS. Addition of either the substrate PrFAR or its analogue ProFAR significantly reduced this amount to 5.2 % and 1.3 %, respectively (Table 13). This observation suggests that the hydrolysis has been accelerated relative to the formation of the thioester.

Table 13: Amount of thioester intermediate of different ImGPS complexes under steady-state conditions

ImGPS complex	HisH:HisF wt	HisH:fD98E	hY138A hK181A:HisF
% thioester (basal)	18.3 ± 4.5	1.1 ± 0.5	11.9 ± 2.5
% thioester (+ProFAR)	1.3 ± 0.5	0.3 ± 0.1	16.8 ± 4.0
% thioester (+PrFAR)	5.2 ± 1.7	n.d.	n.d.

Errors are the standard deviation derived from three independent measurements. n.d.: not determined

The same experiments were conducted with two ImGPS variants that show increased basal activity, namely fD98E and hY183A hK181A. ImGPS fD98E had a strongly reduced amount of protein carrying the thioester, indicating that the hydrolysis is accelerated in this variant, as well. ProFAR addition leads to a further reduction, suggesting a similar mode of action as in wild type ImGPS. The variant hY138A hK181A on the other hand showed almost the same amount of thioester intermediate as the wild type and the addition of ProFAR even increased this amount. This indicates that for this variant, the rate of thioester formation is increased permanently and the hydrolysis cannot be accelerated so far as to become faster than thioester formation. At this point, it is difficult to interpret these results quantitatively, because this requires detailed knowledge of microscopic rate constants for binding and dissociation events as well as the chemical reaction steps.

Considering the data of the acivicin inactivation experiments, these results demonstrate that both half-reactions of glutamine hydrolysis are accelerated by allosteric activation. Since the acceleration of the thioester formation is accelerated very strongly by ProFAR and PrFAR and accumulation of thioester-bound protein is not increased, the acceleration of the hydrolysis must also be very strong. In both wild-type ImGPS and ImGPS fD98E, the hydrolysis is accelerated even more strongly than the thioester formation, because the steady-state concentration of thioester carrying enzyme is significantly reduced. The results of the variants with increased basal activity highlight that there is a delicate balance between the two reaction steps and different activating mutations or even different allosteric activators lead to subtle differences in the active site conformation and thus to a difference in activation of either step.

4.2.5 Evaluation of implications for the mechanism of HisH stimulation

The goal of the experiments presented in this chapter was to improve the knowledge of the molecular mechanism of HisH stimulation in ImGPS and to test existing hypotheses on this allosteric process. The key hypotheses concerning HisH stimulation are: i) HisH stimulation is achieved by an increase in ammonia release,[105] ii) HisH stimulation is achieved by proper formation of the oxyanion hole, namely by flipping of the amide of hV51,[102,103,148] and iii) a global increase in conformational dynamics is the allosteric signal that leads to HisH stimulation.[142,148]

The hypothesis of protein dynamics playing a role in ImGPS was supported insofar as there is clearly a connection to the highly flexible loop1 in HisF. The structural analysis of the mutant hV48A indicated that the dynamics of the HisF core exert an influence on the transmission of the allosteric signal. The hypothesis that HisH stimulation is achieved by increased release of ammonia could not be supported in this thesis. Rather, it could be shown that tuning of the protonation state of the catalytic residue hH178 plays an important role. Since the positive charge of hH178 stabilizes the negative charge of hC84, it is reasonable to assume that this protonation state is changed during activation as well. An important role in the conformational changes was also demonstrated for the residue fD98, which might be responsible for the change in protonation of hH178 and/or an increase in susceptibility for protonation of the leaving ammonia group. Indications were also found that support the hypothesis of the importance of the hV51 amide for HisH catalysis. While a second amide such as that of hG52 might be involved, hV51 is a likely

candidate for forming the ImGPS oxyanion hole. In addition, there is strong evidence of a distinct active conformation of the entire ImGPS complex. Conformational changes include and induced-fit type change in HisF loop1 as well as changes in the overall conformation of the ImGPS complex.[107] While a functional role of the increase in ImPGS dynamics cannot be discounted, it is also possible that the active conformation is simply more dynamic than the inactive conformation, leading to a correlation of dynamics and HisH activity. Fig. 43 summarizes all results and the current understanding of ImGPS allostery as well as at which points open questions remain.

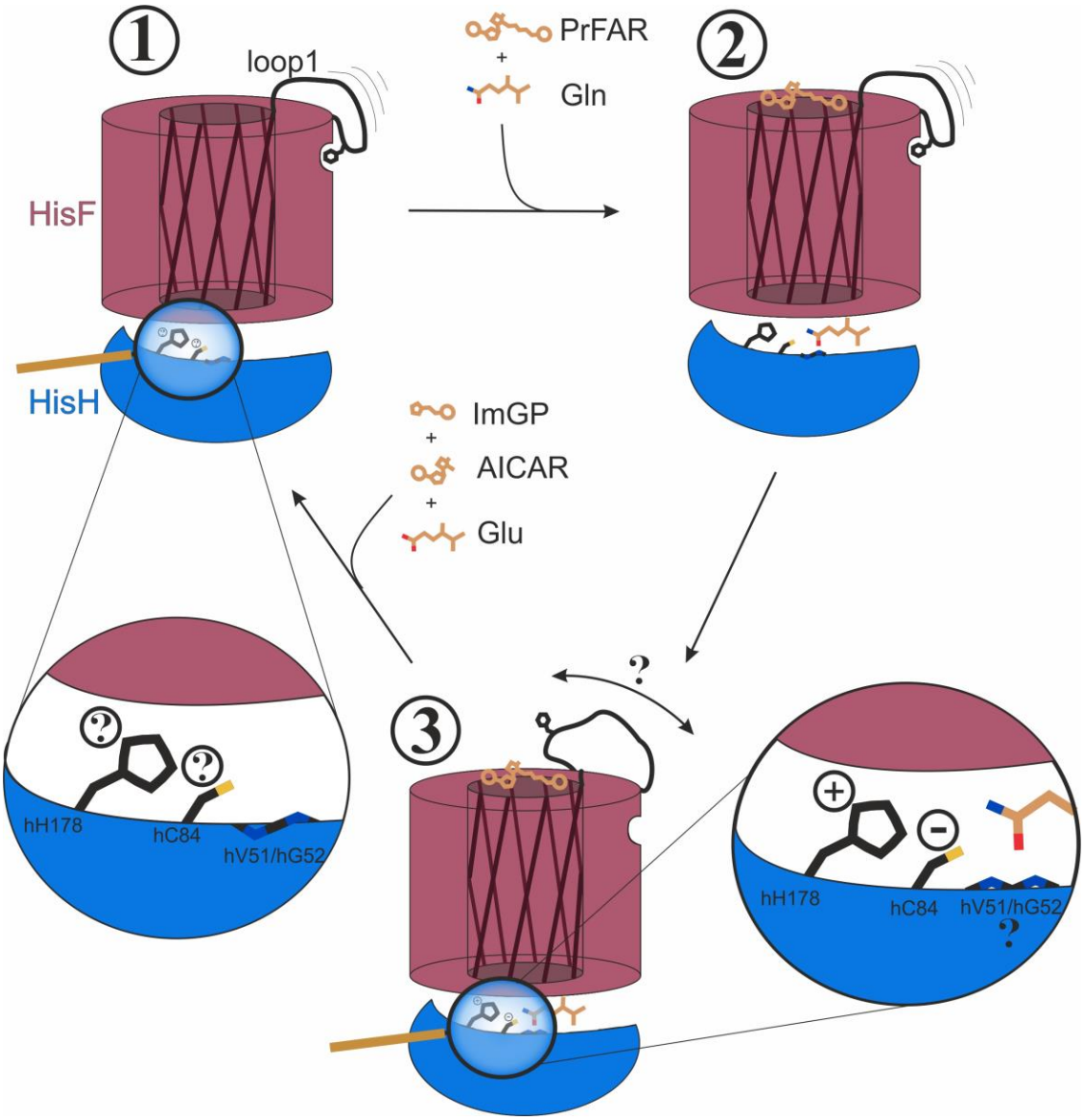

Fig. 43: Model of the current understanding of ImGPS allostery. (1) Without bound substrates, ImGPS is in an inactive state. In this state, it is not completely sure to what extent hH178 and hC84 are charged. In the oxyanion strand, the amide of hV51 is turned away from the glutamine binding site, hG52 is turned so it could interact with a binding glutamine molecule. HisF loop1 is predominantly in the open conformation. (2) Allosteric activation requires the binding of both ImGPS substrates, PrFAR and glutamine. This binding leads to the formation of the active state (3). In this state, hH178 is positively charged and hC84 is negatively charged. Which amides form the oxyanion hole is also unclear. hV51 plays an important role and might flip into the HisH active site to contribute to the oxyanion hole, but another amide might also be involved. HisF loop1 undergoes an induced-fit type conformational change. The exact conformation it adopts is yet to be determined. This conformational change facilitates both the HisF reaction as well as the allosteric stimulation of HisH. After the completion of the ImGPS reaction and the release of the reaction products ImGP, AICAR and glutamate, ImGPS returns to the inactive state.

4.2.6 Outlook

The results presented in this chapter provide valuable insights into the molecular mechanisms underlying the allosteric communication in ImGPS, but, in some ways, are only a start into a detailed investigation of this fascinating bi-enzyme complex.

For instance, loop1 of HisF, which is crucial for turnover of PrFAR in HisF, appears to also play an important role in allostery. This role should be further investigated by expanding the kinetic analysis to the complete ImGPS reaction using CouA-containing ImGPS complexes. The use of stopped-flow fluorescence spectroscopy in this context would also allow for the expansion of the kinetic model to the entire, glutamine dependent ImGPS reaction. Since in the full complex, the kinetic relationships become even more complex than in isolated HisF, CouA could be incorporated at different sites, e.g. close to the interface, close to either active site or close to loop1 in HisF. This could enable the gathering of detailed information on binding of the substrates PrFAR and glutamine and the reaction products as well as the conformational changes in the physiological setting of the complete ImGPS complex. The different residues of importance within HisF loop1 that were identified in this work and ImGPS variants carrying mutations at these positions as well as mutations in HisH such as hC84S will certainly be instrumental for future studies. Some reaction rates might also be determined in a different way. The rate of thioester hydrolysis for example could be determined in a modified set-up of the assay to determine the steady-state thioester concentration used in this thesis. Dilution of the reaction mixture with unlabelled glutamine and analysis of aliquots after defined time intervals allows for the determination of the decay rate of the thioester.[170]

The identification of the residues fI7 and fI169 as part of the allosteric network highlight that a more systematic mutational screening of HisF residues might shed further light on the mechanism of HisH activation. These studies would of course benefit greatly from more detailed structural information on the differences between the basal and activated states of ImGPS. Study of single mutations or and combinations of different activating and/or inactivating mutations in both NMR and crystallography experiments are promising for the clarification of the exact nature of the active HisH conformation. For instance, the mutation of hC84 to serine or alanine enables the study of substrate bound states and the mutation fD98E has given some insight into conformational changes during allosteric communication, which can certainly be exploited further. For structural studies, the use of ProFAR as a HisF ligand appears promising due to its higher stability as well as the fact that it is not turned over.

Concerning the observation of HisH activation by tuning of pK_a values of the active site residues in HisH, different experiments may still provide more detailed information on this phenomenon. Mutations in the HisH active site could be explored further in the respect of the pH-dependency of the HisH reaction to gain further information on the different titratable groups involved in the HisH reaction and when and how their respective pK_a values are altered. Systematic elimination of different titratable groups and study of the pH-dependency of the residual activity could improve the possible interpretation of the pH dependency of the HisH reaction. This should include not only hH178 and hC84, but also fD98 and hE180. The latter residue has largely been neglected thus far and most certainly has a profound impact on hH178 protonation. Another point that still should be addressed in the respect of pH dependency are effects on the ligand binding. It is likely that part of the differences in pH dependency of for instance the ProFAR and PrFAR activated HisH activity is also partly a result of a pH dependency of ligand binding, which may vary for the two activator molecules. The study of the differences in activation by ProFAR and PrFAR would also benefit from the measurement of pH dependency of the HisH reaction at different ProFAR concentrations (PrFAR cannot be titrated, as it is turned over during the measurement). This would allow for a more detailed description of the changes in pK_a values at different levels of allosteric activation.

5 References

1. Wolfenden, R.; Snider, M.J. The depth of chemical time and the power of enzymes as catalysts. *Acc. of Chem. Res.* **2001**, *34*, 938–945.

2. Eyring, H. The activated complex and the absolute rate of chemical reactions. *Chem. Rev.* **1935**, *17*, 65–77.

3. Kirby, A.J. Acid-Base catalysis by enzymes. *Encyclopedia of life sciences*; Wiley: Chichester, 2005; p 25529, ISBN 0470016175.

4. You, K.-S.; Oppenheimer, N.J. Stereospecificity for nicotinamide nucleotides in enzymatic and chemical hydride transfer reaction. *Crit. Rev. Biochem.* **1985**, *17*, 313–451.

5. Milton, R.D.; Minteer, S.D. Direct enzymatic bioelectrocatalysis: differentiating between myth and reality. *J R Soc Interface* **2017**, *14*.

6. Frey, P.A. Radical mechanisms of enzymatic catalysis. *Annu. Rev. Biochem.* **2001**, *70*, 121–148.

7. Fried, S.D.; Boxer, S.G. Electric fields and enzyme catalysis. *Annu. Rev. Biochem.* **2017**, *86*, 387–415.

8. Williams, R.J.P. Metallo-enzyme catalysis. *Chem. Commun. (Cambridge, U. K.)* **2003**, 1109–1113.

9. Menten, L.; Michaelis, M.I. Die Kinetik der Invertinwirkung. *Biochem. Z.* **1913**, *49*, 5.

10. Alberty, R.A.; Hammes, G.G. Application of the theory of diffusion-controlled reactions to enzyme kinetics. *J Phys Chem B.* **1958**, *62*, 154–159.

11. Wierenga, R.K.; Kapetaniou, E.G.; Venkatesan, R. Triosephosphate isomerase: a highly evolved biocatalyst. *Cell. Mol. Life Sci.* **2010**, *67*, 3961–3982.

12. Nes, W.D. Biosynthesis of cholesterol and other sterols. *Chem. Rev.* **2011**, *111*, 6423–6451.

13. Abe, I.; Rohmer, M.; Prestwich, G.D. Enzymatic cyclization of squalene and oxidosqualene to sterols and triterpenes. *Chem. Rev.* **1993**, *93*, 2189–2206.

14. Chapman, J.; Ismail, A.; Dinu, C. Industrial applications of enzymes: recent advances, techniques, and outlooks. *Catalysts* **2018**, *8*, 238.

15. Bhosale, S.H.; Rao, M.B.; Deshpande, V.V. Molecular and industrial aspects of glucose isomerase. *Microbiol. Rev.* **1996**, *60*, 280–300.

16. Houde, A.; Kademi, A.; Leblanc, D. Lipases and their industrial applications: an overview. *ABAB* **2004**, *118*, 155–170.

17. Jiang, L.; Althoff, E.A.; Clemente, F.R.; Doyle, L.; Röthlisberger, D.; Zanghellini, A.; Gallaher, J.L.; Betker, J.L.; Tanaka, F.; Barbas, C.F.; et al. De Novo Computational Design of Retro-Aldol Enzymes. *Science* **2008**, *319*, 1387.

18. Röthlisberger, D.; Khersonsky, O.; Wollacott, A.M.; Jiang, L.; DeChancie, J.; Betker, J.; Gallaher, J.L.; Althoff, E.A.; Zanghellini, A.; Dym, O.; et al. Kemp elimination catalysts by computational enzyme design. *Nature* **2008**, *453*, 190 EP -.

19. Siegel, J.B.; Zanghellini, A.; Lovick, H.M.; Kiss, G.; Lambert, A.R.; St.Clair, J.L.; Gallaher, J.L.; Hilvert, D.; Gelb, M.H.; Stoddard, B.L.; et al. Computational design of an

enzyme catalyst for a stereoselective bimolecular Diels-Alder reaction. *Science* **2010**, *329*, 309.

20. Giger, L.; Caner, S.; Obexer, R.; Kast, P.; Baker, D.; Ban, N.; Hilvert, D. Evolution of a designed retro-aldolase leads to complete active site remodeling. *Nat. Chem. Biol.* **2013**, *9*, 494–498.

21. Preiswerk, N.; Beck, T.; Schulz, J.D.; Milovník, P.; Mayer, C.; Siegel, J.B.; Baker, D.; Hilvert, D. Impact of scaffold rigidity on the design and evolution of an artificial Diels-Alderase. *Proc. Natl. Acad. Sci. U. S. A.* **2014**, *111*, 8013–8018.

22. Fersht, A. *Enzyme structure and mechanism*, 2. ed., 13. print; Freeman: New York, 1995, ISBN 0716716143.

23. Arnold, F.H. Directed evolution: bringing new chemistry to life. *Angew Chem Int Ed Engl.* **2018**, *57*, 4143–4148.

24. Kohen, A. Role of dynamics in enzyme catalysis: substantial versus semantic controversies. *Acc. of Chem. Res.* **2015**, *48*, 466–473.

25. Berman, H.M.; Coimbatore Narayanan, B.; Di Costanzo, L.; Dutta, S.; Ghosh, S.; Hudson, B.P.; Lawson, C.L.; Peisach, E.; Prlić, A.; Rose, P.W.; et al. Trendspotting in the Protein Data Bank. *FEBS Lett.* **2013**, *587*, 1036–1045.

26. DePristo, M.A.; Bakker, P.I.W. de; Blundell, T.L. Heterogeneity and inaccuracy in protein structures solved by X-ray crystallography. *Structure* **2004**, *12*, 831–838.

27. Rupp, B. *Biomolecular Crystallography: Principles, Practice, and Application to Structural Biology;* CRC Press, 2009, ISBN 9781134064199.

28. Søndergaard, C.R.; Garrett, A.E.; Carstensen, T.; Pollastri, G.; Nielsen, J.E. Structural artifacts in protein-ligand X-ray structures: implications for the development of docking scoring functions. *J Med Chem* **2009**, *52*, 5673–5684.

29. Frauenfelder, H.; Sligar, S.G.; Wolynes, P.G. The energy landscapes and motions of proteins. *Science* **1991**, *254*, 1598–1603.

30. Fischer, E.; Passmore, F. Ueber kohlenstoffreichere Zuckerarten aus d. Mannose. *Ber. Dtsch. Chem. Ges.* **1890**, *23*, 2226–2239.

31. Fischer, E. Einfluss der Configuration auf die Wirkung der Enzyme. *Ber. Dtsch. Chem. Ges.* **1894**, *27*, 2985–2993.

32. Jorgensen, W. Rusting of the lock and key model for protein-ligand binding. *Science* **1991**, *254*, 954–955.

33. Rajagopalan, P.T.R.; Benkovic, S.J. Preorganization and protein dynamics in enzyme catalysis. *Chem. Rec.* **2002**, *2*, 24–36.

34. Warshel, A. Electrostatic origin of the catalytic power of enzymes and the role of preorganized active sites. *J. Biol. Chem.* **1998**, *273*, 27035–27038.

35. Warshel, A.; Sharma, P.K.; Kato, M.; Xiang, Y.; Liu, H.; Olsson, M.H.M. Electrostatic basis for enzyme catalysis. *Chem. Rev.* **2006**, *106*, 3210–3235.

36. Bruice, T.C.; Benkovic, S.J. Chemical basis for enzyme catalysis. *Biochemistry* **2000**, *39*, 6267–6274.

37. Koshland, D.E. Application of a theory of enzyme specificity to protein synthesis. *Proc. Natl. Acad. Sci. U. S. A.* **1958**, *44*, 98–104.

38. Boehr, D.D.; Nussinov, R.; Wright, P.E. The role of dynamic conformational ensembles in biomolecular recognition. *Nat. Chem. Biol.* **2009**, *5*, 789–796.

39. Hammes-Schiffer, S. Catalytic efficiency of enzymes: a theoretical analysis. *Biochemistry* **2013**, *52*, 2012–2020.

40. Henzler-Wildman, K.; Kern, D. Dynamic personalities of proteins. *Nature* **2007**, *450*, 964 - 972.

41. Austin, R.H.; Beeson, K.W.; Eisenstein, L.; Frauenfelder, H.; Gunsalus, I.C. Dynamics of ligand binding to myoglobin. *Biochemistry* **1975**, *14*, 5355–5373.

42. Agarwal, P.K.; Billeter, S.R.; Rajagopalan, P.T.R.; Benkovic, S.J.; Hammes-Schiffer, S. Network of coupled promoting motions in enzyme catalysis. *Proc. Natl. Acad. Sci. U. S. A.* **2002**, *99*, 2794–2799.

43. Eisenmesser, E.Z.; Bosco, D.A.; Akke, M.; Kern, D. Enzyme dynamics during catalysis. *Science* **2002**, *295*, 1520–1523.

44. Warshel, A.; Bora, R.P. Perspective: defining and quantifying the role of dynamics in enzyme catalysis. *J. Chem. Phys.* **2016**, *144*, 180901.

45. Kamerlin, S.C.L.; Warshel, A. At the dawn of the 21st century: is dynamics the missing link for understanding enzyme catalysis? *Proteins: Struct., Funct., Bioinf.* **2010**, *106*, 1339-1375.

46. Marino, M.; Deuss, M.; Svergun, D.I.; Konarev, P.V.; Sterner, R.; Mayans, O. Structural and mutational analysis of substrate complexation by anthranilate phosphoribosyltransferase from *Sulfolobus solfataricus*. *J. Biol. Chem.* **2006**, *281*, 21410–21421.

47. Miriam Deuß. Mutationsanalyse des aktiven Zentrums der Anthranilat Phosphoribosyltransferase aus *Sulfolobus solfataricus*. Diploma thesis, 2002.

48. Elisabeth Wöhrle. Investigation on enzyme dynamics during the catalytic reaction of anthranilate phosphoribosyltransferase by single molecule spectroscopy. Masters thesis, 2018.

49. Boehr, D.D.; Dyson, H.J.; Wright, P.E. An NMR perspective on enzyme dynamics. *Chem. Rev.* **2006**, *106*, 3055–3079.

50. Šrajer, V.; Schmidt, M. Watching proteins function with time-resolved X-ray crystallography. *J Phys D Appl Phys* **2017**, *50*.

51. *Comprehensive Biophysics;* Egelman, E.H., Ed.; Elsevier: Amsterdam, 2012, ISBN 978-0-08-095718-0.

52. Karplus, M.; McCammon, J.A. Molecular dynamics simulations of biomolecules. *Nat. Struct. Mol. Biol.* **2002**, *9*, 646–652.

53. Hollingsworth, S.A.; Dror, R.O. Molecular dynamics simulation for all. *Neuron* **2018**, *99*, 1129–1143.

54. Henn-Sax M.; Höcker B.; Wilmanns M.; Sterner R. *Divergent evolution of (ba)$_8$-barrel enzymes*, 2019.439+02:00, *382*. https://www.degruyter.com/view/j/bchm.2001.382.issue-9/bc.2001.163/bc.2001.163.xml.

55. Nagano, N.; Orengo, C.A.; Thornton, J.M. One fold with many functions: the evolutionary relationships between TIM barrel families based on their sequences, structures and functions. *J. Mol. Biol.* **2002**, *321*, 741–765.

56. Sterner, R.; Höcker, B. Catalytic versatility, stability, and evolution of the $(\beta\alpha)_8$-barrel enzyme fold. *Chem. Rev.* **2005**, *105*, 4038–4055.

57. Wierenga, R.K. The TIM-barrel fold: a versatile framework for efficient enzymes. *FEBS Lett.* **2001**, *492*, 193–198.

58. Lang, D.; Thoma, R.; Henn-Sax, M.; Sterner, R.; Wilmanns, M. Structural evidence for evolution of the β/α barrel scaffold by gene duplication and fusion. *Science* **2000**, *289*, 1546–1550.

59. Brändén, C.-I. The TIM barrel—the most frequently occurring folding motif in proteins. *Curr Opin Struct Biol* **1991**, *1*, 978–983.

60. Ochoa-Leyva, A.; Soberón, X.; Sánchez, F.; Argüello, M.; Montero-Morán, G.; Saab-Rincón, G. Protein design through systematic catalytic loop exchange in the $(\beta/\alpha)_8$ fold. *J. Mol. Biol.* **2009**, *387*, 949–964.

61. Ochoa-Leyva, A.; Barona-Gómez, F.; Saab-Rincón, G.; Verdel-Aranda, K.; Sánchez, F.; Soberón, X. Exploring the structure–function loop adaptability of a $(\beta/\alpha)_8$-barrel enzyme through loop swapping and hinge variability. *J. Mol. Biol.* **2011**, *411*, 143–157.

62. O'Rourke, F.K.; Jelowicki, M.A.; Boehr, D.D. Controlling active site loop dynamics in the $(\beta/\alpha)_8$ barrel enzyme indole-3-glycerol phosphate synthase. *Catalysts* **2016**, *6*.

63. Nestl, B.M.; Hauer, B. Engineering of flexible loops in enzymes. *ACS Catal.* **2014**, *4*, 3201–3211.

64. Malabanan, M.M.; Amyes, T.L.; Richard, J.P. A role for flexible loops in enzyme catalysis. *Curr Opin Struct Biol* **2010**, *20*, 702–710.

65. Liao, Q.; Kulkarni, Y.; Sengupta, U.; Petrović, D.; Mulholland, A.J.; van der Kamp, Marc W.; Strodel, B.; Kamerlin, S.C.L. Loop motion in triosephosphate isomerase is not a simple open and shut case. *J. Am. Chem. Soc.* **2018**, *140*, 15889–15903.

66. Schlee, S.; Klein, T.; Schumacher, M.; Nazet, J.; Merkl, R.; Steinhoff, H.-J.; Sterner, R. Relationship of catalysis and active site loop dynamics in the $(\beta\alpha)_8$-barrel enzyme indole-3-glycerol phosphate synthase. *Biochemistry* **2018**, *57*, 3265–3277.

67. Söderholm, A.; Guo, X.; Newton, M.S.; Evans, G.B.; Näsvall, J.; Patrick, W.M.; Selmer, M. Two-step Ligand Binding in a $(\beta\alpha)_8$ Barrel Enzyme: substrate-bound structures shed new light on the catalytic clyce of HisA. *J. Biol. Chem.* **2015**, *290*, 24657–24668.

68. Reddish, M.J.; Peng, H.-L.; Deng, H.; Panwar, K.S.; Callender, R.; Dyer, R.B. Direct evidence of catalytic heterogeneity in lactate dehydrogenase by temperature jump infrared spectroscopy. *J Phys Chem B.* **2014**, *118*, 10854–10862.

69. Deng, H.; Zheng, J.; Clarke, A.; Holbrook, J.J.; Callender, R.; Burgner, J.W. Source of catalysis in the lactate dehydrogenase system: ground-state interactions in the enzyme-substrate complex. *Biochemistry* **1994**, *33*, 2297–2305.

70. Cooper, G.M.; Hausman, R.E. *The cell: a molecular approach*, Seventh edition; Sinauer Associates Inc: Sunderland, Massachusetts U.S.A., 2016, ISBN 9781605355405.

71. Lopina, O.D. Enzyme inhibitors and activators. In *Enzyme inhibitors and activators*; Senturk, M., Ed.; InTech, 2017, ISBN 978-953-51-3057-4.

72. Monod, J.; Changeux, J.-P.; Jacob, F. Allosteric proteins and cellular control systems. *J. Mol. Biol.* **1963**, *6*, 306–329.

73. Pardee, A.B.; Yates, R.A. Control of pyrimidine biosynthesis in *Escherichia coli* by a feed-back mechanism. *J. Biol. Chem.* **1956**, *221*, 757–770.

74. Umbarger, H.E. Evidence for a negative-feedback mechanism in the biosynthesis of isoleucine. *Science* **1956**, *123*, 848.

75. Nussinov, R.; Tsai, C.-J.; Ma, B. The underappreciated role of allostery in the cellular network. *Annu Rev Biophys* **2013**, *42*, 169–189.

76. Perica, T.; Marsh, J.A.; Sousa, F.L.; Natan, E.; Colwell, L.J.; Ahnert, S.E.; Teichmann, S.A. The emergence of protein complexes: quaternary structure, dynamics and allostery. Colworth Medal Lecture. *Biochem. Soc. Trans.* **2012**, *40*, 475–491.

77. Perutz, M.F.; Wilkinson, A.J.; Paoli, M.; Dodson, G.G. The stereochemical mechanism of the cooperative effects in hemoglobin revisited. *Annu Rev Biophys Biomol Struct* **1998**, *27*, 1–34.

78. Stefan, M.I.; Le Novère, N. Cooperative binding. *PLoS Comput. Biol.* **2013**, *9*, e1003106.

79. Manley, G.; Rivalta, I.; Loria, J.P. Solution NMR and computational methods for understanding protein allostery. *J Phys Chem B.* **2013**, *117*, 3063–3073.

80. Motlagh, H.N.; Wrabl, J.O.; Li, J.; Hilser, V.J. The ensemble nature of allostery. *Nature* **2014**, *508*, 331 EP -.

81. Nussinov, R.; Tsai, C.-J. Allostery without a conformational change? Revisiting the paradigm. *Curr Opin Struct Biol* **2015**, *30*, 17–24.

82. Lukin, J.A.; Ho, C. The structure-function relationship of hemoglobin in solution at atomic resolution. *Chem. Rev.* **2004**, *104*, 1219–1230.

83. Popovych, N.; Sun, S.; Ebright, R.H.; Kalodimos, C.G. Dynamically driven protein allostery. *Nat. Struct. Mol. Biol.* **2006**, *13*, 831–838.

84. Mouilleron, S.; Golinelli-Pimpaneau, B. Conformational changes in ammonia-channeling glutamine amidotransferases. *Curr Opin Struct Biol* **2007**, *17*, 653–664.

85. Raushel, F.M.; Thoden, J.B.; Holden, H.M. The amidotransferase family of enzymes: molecular machines for the production and delivery of ammonia. *Biochemistry* **1999**, *38*, 7891–7899.

86. Zalkin, H.; Smith, J.L. Enzymes utilizing glutamine as an amide donor. In *Advances in enzymology and related areas of molecular biology*: *Volume 72: Amino acid metabolism ; Part A*; Purich, D.L., Ed.; Wiley: New York, 1998; pp 87–144, ISBN 9780470123188.

87. Massière, F.; Badet-Denisot, M.-A. The mechanism of glutamine-dependent amidotransferases. *Cell. Mol. Life Sci.* **1998**, *54*, 205–222.

88. Oliver, J.C.; Gudihal, R.; Burgner, J.W.; Pedley, A.M.; Zwierko, A.T.; Davisson, V.J.; Linger, R.S. Conformational changes involving ammonia tunnel formation and allosteric control in GMP synthetase. *Arch Biochem Biophys* **2014**, *545*, 22–32.

89. Raushel, F.M.; Thoden, J.B.; Holden, H.M. Enzymes with molecular tunnels. *Acc. of Chem. Res.* **2003**, *36*, 539–548.

90. Brannigan, J.A.; Dodson, G.; Duggleby, H.J.; Moody, P.C.E.; Smith, J.L.; Tomchick, D.R.; Murzin, A.G. A protein catalytic framework with an N-terminal nucleophile is capable of self-activation. *Nature* **1995**, *378*, 416–419.

91. Douangamath, A.; Walker, M.; Beismann-Driemeyer, S.; Vega-Fernandez, M.C.; Sterner, R.; Wilmanns, M. Structural evidence for ammonia tunneling across the $(\beta\alpha)_8$ barrel of the imidazole glycerol phosphate synthase bienzyme complex. *Structure* **2002**, *10*, 185–193.

92. Li, Q.-A.; Mavrodi, D.V.; Thomashow, L.S.; Roessle, M.; Blankenfeldt, W. Ligand binding induces an ammonia channel in 2-amino-2-desoxyisochorismate (ADIC) synthase PhzE. *J. Biol. Chem.* **2011**, *286*, 18213–18221.

93. Morollo, A.A.; Eck, M.J. Structure of the cooperative allosteric anthranilate synthase from *Salmonella typhimurium*. *Nat. Struct. Biol.* **2001**, *8*, 243–247.

94. Parsons, J.F.; Jensen, P.Y.; Pachikara, A.S.; Howard, A.J.; Eisenstein, E.; Ladner, J.E. Structure of *Escherichia coli* aminodeoxychorismate synthase: architectural conservation and diversity in chorismate-utilizing enzymes. *Biochemistry* **2002**, *41*, 2198–2208.

95. Thoden, J.B.; Miran, S.G.; Phillips, J.C.; Howard, A.J.; Raushel, F.M.; Holden, H.M. Carbamoyl phosphate synthetase: caught in the act of glutamine hydrolysis. *Biochemistry* **1998**, *37*, 8825–8831.

96. Alifano, P.; Fani, R.; Liò, P.; Lazcano, A.; Bazzicalupo, M.; Carlomagno, M.S.; Bruni, C.B. Histidine biosynthetic pathway and genes: structure, regulation, and evolution. *Microbiol. Rev.* **1996**, *60*, 44–69.

97. Klem, T.J.; Davisson, V.J. Imidazole glycerol phosphate synthase: the glutamine amidotransferase in histidine biosynthesis. *Biochemistry* **1993**, *32*, 5177–5186.

98. Chaudhuri, B.N.; Lange, S.C.; Myers, R.S.; Chittur, S.V.; Davisson, V.J.; Smith, J.L. Crystal structure of imidazole glycerol phosphate synthase: a tunnel through a $(\beta/\alpha)_8$ barrel joins two active sites. *Structure* **2001**, *9*, 987–997.

99. Chittur, S.V.; Chen, Y.; Davisson, V.J. Expression and purification of imidazole glycerol phosphate synthase from *Saccharomyces cerevisiae*. *Protein Expression Purif.* **2000**, *18*, 366–377.

100. Beismann-Driemeyer, S.; Sterner, R. Imidazole glycerol phosphate synthase from *Thermotoga maritima*. Quaternary structure, steady-state kinetics, and reaction mechanism of the bienzyme complex. *J. Biol. Chem.* **2001**, *276*, 20387–20396.

101. Lyons, S.D.; Sant, M.E.; Christopherson, R.I. Cytotoxic mechanisms of glutamine antagonists in mouse L1210 leukemia. *J. Biol. Chem.* **1990**, *265*, 11377–11381.

102. Lipchock, J.; Loria, J.P. Millisecond dynamics in the allosteric enzyme imidazole glycerol phosphate synthase (IGPS) from *Thermotoga maritima*. *J. Biomol. NMR* **2009**, *45*, 73–84.

103. Lipchock, J.M.; Loria, J.P. Nanometer propagation of millisecond motions in V-type allostery. *Structure* **2010**, *18*, 1596–1607.

104. Rivalta, I.; Sultan, M.M.; Lee, N.-S.; Manley, G.A.; Loria, J.P.; Batista, V.S. Allosteric pathways in imidazole glycerol phosphate synthase. *Proc. Natl. Acad. Sci. U. S. A.* **2012**, *109*, E1428-36.

105. List, F.; Vega, M.C.; Razeto, A.; Häger, M.C.; Sterner, R.; Wilmanns, M. Catalysis uncoupling in a glutamine amidotransferase bienzyme by unblocking the glutaminase active site. *Chemistry & biology* **2012**, *19*, 1589–1599.

106. Chaudhuri, B.N.; Lange, S.C.; Myers, R.S.; Davisson, V.J.; Smith, J.L. Toward understanding the mechanism of the complex cyclization reaction catalyzed by imidazole glycerolphosphate synthase: crystal structures of a ternary complex and the free enzyme. *Biochemistry* **2003**, *42*, 7003–7012.

107. Wurm, J.P. unpublished data.

108. List, F. Die Imidazolglycerinphosphat-Synthase aus *Thermotoga maritima*: Struktur, Regulation und Evolution einer Glutaminamidotransferase. doctoral disstertation; Universität Regensburg, Regensburg, 2009.

109. Douangamath, A.; Walker, M.; Beismann-Driemeyer, S.; Vega-Fernandez, M.C.; Sterner, R.; Wilmanns, M. Structural evidence for ammonia tunneling across the $(\beta\alpha)_8$ barrel of the imidazole glycerol phosphate synthase bienzyme complex. *Structure* **2002**, *10*, 185–193.

110. Ruisinger, A. Identification of active site loop conformations and analysis of their significance for enzymatic function in imidazole glycerol phosphate synthase. Master's thesis; Universität Regensburg, Regensburg, 2019.

111. William Studier, F.; Rosenberg, A.H.; Dunn, J.J.; Dubendorff, J.W. Use of T7 RNA polymerase to direct expression of cloned genes. In *Gene expression technology*; Goeddel, D.V., Ed.; Acad. Press: San Diego, Calif., 1990; pp 60–89, ISBN 9780121820862.

112. Rohweder, B.; Semmelmann, F.; Endres, C.; Sterner, R. Standardized cloning vectors for protein production and generation of large gene libraries in Escherichia coli. *BioTechniques* **2018**, *64*, 24–26.

113. Engler, C.; Kandzia, R.; Marillonnet, S. A one pot, one step, precision cloning method with high throughput capability. *PLoS ONE* **2008**, *3*, e3647.

114. Kneuttinger, A.C.; Straub, K.; Bittner, P.; Simeth, N.A.; Bruckmann, A.; Busch, F.; Rajendran, C.; Hupfeld, E.; Wysocki, V.H.; Horinek, D.; et al. Light regulation of enzyme allostery through photo-responsive unnatural amino acids. *Cell Chem Biol* **2019**.

115. Liu, C.C.; Schultz, P.G. Adding new chemistries to the genetic code. *Annu. Rev. Biochem.* **2010**, *79*, 413–444.

116. Normanly, J.; Kleina, L.G.; Masson, J.-M.; Abelson, J.; Miller, J.H. Construction of *Escherichia coli* amber suppressor tRNA genes. *J. Mol. Biol.* **1990**, *213*, 719–726.

117. Wang, J.; Xie, J.; Schultz, P.G. A genetically encoded fluorescent amino acid. *J. Am. Chem. Soc.* **2006**, *128*, 8738–8739.

118. Inoue, H.; Nojima, H.; Okayama, H. High efficiency transformation of *Escherichia coli* with plasmids. *Gene* **1990**, *96*, 23–28.

119. Sharp, P.A.; Sugden, B.; Sambrook, J. Detection of two restriction endonuclease activities in Haemophilus parainfluenzae using analytical agarose-ethidium bromide electrophoresis. *Biochemistry* **1973**, *12*, 3055–3063.

120. Mullis, K.B.; Faloona, F.A. Specific synthesis of DNA in vitro via a polymerase-catalyzed chain reaction. *Meth. Enzymol* **1987**, *155*, 335–350.

121. Saiki, R.K.; Gelfand, D.H.; Stoffel, S.; Scharf, S.J.; Higuchi, R.; Horn, G.T.; Mullis, K.B.; Erlich, H.A. Primer-directed enzymatic amplification of DNA with a thermostable DNA polymerase. *Science* **1988**, *239*, 487–491.

122. Davisson, V.J.; Deras, I.L.; Hamilton, S.E.; Moore, L.L. A plasmid-based approach for the synthesis of a histidine biosynthetic intermediate. *J. Org. Chem.* **1994**, *59*, 137–143.

123. Smith, D.W.; Ames, B.N. Intermediates of the early steps of histidine biosynthesis. *J. Biol. Chem.* **1964**, *239*, 1848–1855.

124. Pace, C.N.; Vajdos, F.; Fee, L.; Grimsley, G.; Gray, T. How to measure and predict the molar absorption coefficient of a protein. *Protein Sci.* **1995**, *4*, 2411–2423.

125. Laemmli, U.K. Cleavage of structural proteins during the assembly of the head of bacteriophage T4. *Nature* **1970**, *227*, 680–685.

126. Mendes, K.R.; Martinez, J.A.; Kantrowitz, E.R. Asymmetric allosteric signaling in aspartate transcarbamoylase. *ACS Chem. Biol.* **2010**, *5*, 499–506.

127. Josef Auburger. Identifikation von peptidischen Protein-Protein Interaktionsinhibitoren der Imidazolglycerolphosphat Synthase. Master's Thesis; Universität Regensburg, Regensburg, 2003.

128. Kuzmic, P. Program DYNAFIT for the analysis of enzyme kinetic data: application to HIV proteinase. *Anal Biochem* **1996**, *237*, 260–273.

129. Kabsch, W. Automatic processing of rotation diffraction data from crystals of initially unknown symmetry and cell constants. *J. Appl. Crystallogr.* **1993**, *26*, 795–800.

130. Adams, P.D.; Grosse-Kunstleve, R.W.; Hung, L.W.; Ioerger, T.R.; McCoy, A.J.; Moriarty, N.W.; Read, R.J.; Sacchettini, J.C.; Sauter, N.K.; Terwilliger, T.C. PHENIX: building new software for automated crystallographic structure determination. *Acta Crystallogr., Sect. D: Struct. Biol.* **2002**, *58*, 1948–1954.

131. Potterton, L.; McNicholas, S.; Krissinel, E.; Gruber, J.; Cowtan, K.; Emsley, P.; Murshudov, G.N.; Cohen, S.; Perrakis, A.; Noble, M. Developments in the CCP4 molecular-graphics project. *Acta Crystallogr., Sect. D: Struct. Biol.* **2004**, *60*, 2288–2294.

132. Murshudov, G.N.; Vagin, A.A.; Dodson, E.J. Refinement of macromolecular structures by the maximum-likelihood method. *Acta Crystallogr., Sect. D: Struct. Biol.* **1997**, *53*, 240–255.

133. Emsley, P.; Cowtan, K. Coot: model-building tools for molecular graphics. *Acta Crystallogr., Sect. D: Struct. Biol.* **2004**, *60*, 2126–2132.

134. Lipchock, J.M.; Loria, J.P. ^{1}H, ^{15}N and ^{13}C resonance assignment of imidazole glycerol phosphate (IGP) synthase protein HisF from *Thermotoga maritima*. *Biomol NMR Assign.* **2008**, *2*, 219–221.

135. Lee, W.; Westler, W.M.; Bahrami, A.; Eghbalnia, H.R.; Markley, J.L. PINE-SPARKY: graphical interface for evaluating automated probabilistic peak assignments in protein NMR spectroscopy. *Bioinformatics* **2009**, *25*, 2085–2087.

136. Amaro, R.E.; Sethi, A.; Myers, R.S.; Davisson, V.J.; Luthey-Schulten, Z.A. A network of conserved interactions regulates the allosteric signal in a glutamine amidotransferase. *Biochemistry* **2007**, *46*, 2156–2173.

137. Fersht, A. The pH dependence of enzyme catalysis. In *Structure and mechanism in protein science*: *A guide to enzyme catalysis and protein folding*; Fersht, A., Ed.; W.H. Freeman: New York, Basingstoke, 1999; pp 169–190, ISBN 0716732688.

138. Doig, A.J. Thermodynamics of amino acid side-chain internal rotations. *Biophys. Chem.* **1996**, *61*, 131–141.

139. Leon Babel. Studien zum Einfluss von loop-Dynamik auf Katalyse und Allosterie eines Bienzyme-Komplexes. Bachelor's Thesis; Universität Regensburg, Regensburg, 2018.

140. Kayode, O.; Wang, R.; Pendlebury, D.F.; Cohen, I.; Henin, R.D.; Hockla, A.; Soares, A.S.; Papo, N.; Caulfield, T.R.; Radisky, E.S. An acrobatic substrate metamorphosis reveals a requirement for substrate conformational dynamics in trypsin proteolysis. *J. Biol. Chem.* **2016**, *291*, 26304–26319.

141. Redfield, A.G. The Theory of Relaxation Processes. In *Advances in magnetic and optical resonance : advances in magnetic resonance*; Waugh, J.S., Ed.; Academic Press, 1965; pp 1–32, ISBN 1057-2732.

142. Lisi, G.P.; East, K.W.; Batista, V.S.; Loria, J.P. Altering the allosteric pathway in IGPS suppresses millisecond motions and catalytic activity. *Proc. Natl. Acad. Sci. U. S. A.* **2017**, *114*, E3414-E3423.

143. Amaro, M.; Brezovský, J.; Kováčová, S.; Sýkora, J.; Bednář, D.; Němec, V.; Lišková, V.; Kurumbang, N.P.; Beerens, K.; Chaloupková, R.; et al. Site-specific analysis of protein hydration based on unnatural amino acid fluorescence. *J. Am. Chem. Soc.* **2015**, *137*, 4988–4992.

144. Ho, D.; Lugo, M.R.; Lomize, A.L.; Pogozheva, I.D.; Singh, S.P.; Schwan, A.L.; Merrill, A.R. Membrane topology of the colicin E1 channel using genetically encoded fluorescence. *Biochemistry* **2011**, *50*, 4830–4842.

145. Wallerstein, J.; Weininger, U.; Khan, M.A.I.; Linse, S.; Akke, M. Site-specific protonation kinetics of acidic side chains in proteins determined by pH-dependent carboxyl ^{13}C NMR relaxation. *J. Am. Chem. Soc.* **2015**, *137*, 3093–3101.

146. Bagshaw, C.R. Stopped-flow techniques. In *Encyclopedia of biophysics*; Roberts, G.C.K., Ed.; Springer Berlin: Berlin, 2013; pp 2460–2466, ISBN 978-3-642-16711-9.

147. Young, T.S.; Ahmad, I.; Yin, J.A.; Schultz, P.G. An enhanced system for unnatural amino acid mutagenesis in *E. coli*. *J. Mol. Biol.* **2010**, *395*, 361–374.

148. Lisi, G.P.; Manley, G.A.; Hendrickson, H.; Rivalta, I.; Batista, V.S.; Loria, J.P. Dissecting dynamic allosteric pathways using chemically related small-molecule activators. *Structure* **2016**, *24*, 1155–1166.

149. Russell, D.K. The Boltzmann Distribution. *J. Chem. Educ.* **1996**, *73*, 299.

150. Blokzijl, W.; Engberts, J.B.F.N. Hydrophobic effects: opinions and facts. *Angew Chem Int Ed Engl.* **1993**, *32*, 1545–1579.

151. Reynolds, J.A.; Gilbert, D.B.; Tanford, C. Empirical correlation between hydrophobic free energy and aqueous cavity surface area. *Proc. Natl. Acad. Sci. U. S. A.* **1974**, *71*, 2925–2927.

152. Tanford, C. Interfacial free energy and the hydrophobic effect. *Proc. Natl. Acad. Sci. U. S. A.* **1979**, *76*, 4175–4176.

153. Ciaccia, M.; Di Stefano, S. Mechanisms of imine exchange reactions in organic solvents. *Org Biomol Chem* **2015**, *13*, 646–654.

154. D'Ordine, R.L.; Linger, R.S.; Thai, C.J.; Davisson, V.J. Catalytic zinc site and mechanism of the metalloenzyme PR-AMP cyclohydrolase. *Biochemistry* **2012**, *51*, 5791–5803.

155. Kneuttinger, A.C.; Zwisele, S.; Straub, K.; Bruckmann, A.; Busch, F.; Kinateder, T.; Gaim, B.; Wysocki, V.H.; Merkl, R.; Sterner, R. Light-regulation of tryptophan synthase by combining protein design and enzymology. *Int J Mol Sci* **2019**, *20*.

156. Chittur, S.V.; Klem, T.J.; Shafer, C.M.; Davisson, V.J. Mechanism for acivicin inactivation of triad glutamine amidotransferases. *Biochemistry* **2001**, *40*, 876–887.

157. Rivalta, I.; Lisi, G.P.; Snoeberger, N.-S.; Manley, G.A.; Loria, J.P.; Batista, V.S. Allosteric communication disrupted by small molecule binding to the Imidazole glycerol phosphate synthase protein-protein interface. *Biochemistry* **2016**.

158. Beismann-Driemeyer, S. Untersuchungen zur Struktur und Funktion des Bienzymkomplexes Imidazolglycerinphosphat-Synthetase aus *Thermotoga maritima*. doctoral dissteration; Universität zu Köln, Köln, 2000.

159. Holinski, A.; Heyn, K.; Merkl, R.; Sterner, R. Combining ancestral sequence reconstruction with protein design to identify an interface hotspot in a key metabolic enzyme complex. *Proteins* **2017**, *85*, 312–321.

160. Spraggon, G.; Kim, C.; Nguyen-Huu, X.; Yee, M.C.; Yanofsky, C.; Mills, S.E. The structures of anthranilate synthase of *Serratia marcescens* crystallized in the presence of (i) its substrates, chorismate and glutamine, and a product, glutamate, and (ii) its end-product inhibitor, L-tryptophan. *Proc. Natl. Acad. Sci. U. S. A.* **2001**, *98*, 6021–6026.

161. Pinitglang, S.; Watts, A.B.; Patel, M.; Reid, J.D.; Noble, M.A.; Gul, S.; Bokth, A.; Naeem, A.; Patel, H.; Thomas, E.W. A classical enzyme active center motif lacks catalytic competence until modulated electrostatically. *Biochemistry* **1997**, *36*, 9968–9982.

162. Harris, T.K.; Turner, G.J. Structural basis of perturbed pKa values of catalytic groups in enzyme active sites. *IUBMB life* **2002**, *53*, 85–98.

163. Lin, J.; Cassidy, C.S.; Frey, P.A. Correlations of the basicity of His 57 with transition state analogue binding, substrate reactivity, and the strength of the low-barrier hydrogen bond in chymotrypsin. *Biochemistry* **1998**, *37*, 11940–11948.

164. Hornby, D.P.; Engel, P.C.; Shin-Ichi, H. Beef liver glutamate dehydrogenase: a study of the oxidation of various alternative amino acid substrates retaining the correct spacing of the two carboxylate groups. *Int. J. Biochem.* **1983**, *15*, 495–500.

165. Copeland, R.A. *Enzymes;* John Wiley & Sons, Inc: New York, USA, 2000, ISBN 0471359297.

166. Nič, M.; Jirát, J.; Košata, B.; Jenkins, A.; McNaught, A. *IUPAC compendium of chemical terminology;* IUPAC: Research Triagle Park, NC, 2009, ISBN 0-9678550-9-8.

167. Wasylishen, R.E.; Tomlinson, G. pH-dependence of ^{13}C chemical shifts and $^{13}C,H$ coupling constants in imidazole and L-histidine. *Biochem J* **1975**, *147*, 605–607.

168. Semmelmann, F.; Hupfeld, E.; Heizinger, L.; Merkl, R.; Sterner, R. A fold-independent interface residue is crucial for complex formation and allosteric signaling in class I glutamine amidotransferases. *Biochemistry* **2019**, *58*, 2584–2588.

169. Sigala, P.A.; Kraut, D.A.; Caaveiro, J.M.M.; Pybus, B.; Ruben, E.A.; Ringe, D.; Petsko, G.A.; Herschlag, D. Testing geometrical discrimination within an enzyme active site: constrained hydrogen bonding in the ketosteroid isomerase oxyanion hole. *J. Am. Chem. Soc.* **2008**, *130*, 13696–13708.

170. Chaparian, M.G.; Evans, D.R. The catalytic mechanism of the amidotransferase domain of the Syrian hamster multifunctional protein CAD: Evidence for a CAD-glutamyl covalent intermediate in the formation of carbamyl phosphate. *J. Biol. Chem.* **1991**, *266*, 3387–3395.

6 Appendix

Table Appendix 1: Data collection and refinement statistics for the structures of HisF K19A, G20P, F23A and T21P

Protein	HisF K19A	HisF G20P	HisF F23A	HisF T21P
Wavelength (Å)	0.99	0.99	0.99	0.99
Resolution range (Å)	37.92 - 1.197 (1.24 - 1.197)	47.46 - 1.314 (1.361 - 1.314)	35.07 - 1.196 (1.239 - 1.196)	38.01 - 1.199 (1.242 - 1.199)
Space group	C 1 2 1	P 2_1 2_1 2_1	C 1 2 1	C 1 2 1
Unit cell	78.8, 44.4, 63.7, 90, 112, 90	44.3, 58.1, 82.4, 90, 90, 90	79.3, 44.2, 63.5, 90, 111.8, 90	79.5 44.4 63.9, 90, 112, 90
Total reflections	401586 (33683)	609236 (29703)	405073 (35017)	395461 (32694)
Unique reflections	59034 (5187)	49373 (3705)	62429 (5730)	63609 (6126)
Multiplicity	6.8 (6.3)	12.3 (8.0)	6.5 (6.0)	6.2 (5.3)
Completeness (%)	91.65 (81.31)	96.16 (73.49)	96.59 (89.73)	98.50 (95.76)
Mean I/sigma(I)	28.50 (4.88)	12.86 (0.93)	37.69 (8.88)	23.84 (6.31)
Wilson B-factor	11.97	19.54	12.05	8.43
R_{merge}	0.03345 (0.3501)	0.09083 (1.366)	0.02606 (0.179)	0.04658 (0.2919)
R_{meas}	0.03618 (0.3814)	0.09471 (1.461)	0.0283 (0.1962)	0.0509 (0.325)
R_{pim}	0.01365 (0.1492)	0.02639 (0.5038)	0.0109 (0.07919)	0.02014 (0.1396)
$CC_{1/2}$	1 (0.946)	0.999 (0.367)	0.999 (0.982)	0.999 (0.949)
CC*	1 (0.986)	1 (0.733)	1 (0.996)	1 (0.987)
Reflections used in refinement	58897 (5183)	49357 (3704)	62307 (5730)	63695 (6125)
Reflections used for R_{free}	2023 (178)	1999 (150)	2012 (182)	1990 (187)
R_{work}	0.1946 (0.2434)	0.1960 (0.4334)	0.1955 (0.2188)	0.2001 (0.2933)
R_{free}	0.2129 (0.2473)	0.2163 (0.4395)	0.2084 (0.2128)	0.2204 (0.3299)
CC_{work}	0.955 (0.881)	0.967 (0.663)	0.950 (0.897)	0.950 (0.788)
CC_{free}	0.938 (0.856)	0.946 (0.456)	0.906 (0.829)	0.928 (0.716)
Number of atoms	2260	2180	2245	2262
macromolecules	1949	1929	1954	1960
ligands	10	0	10	10
solvent	301	251	281	292
Protein residues	255	250	255	255
RMS (bonds)	0.005	0.006	0.005	0.005
RMS (angles)	0.85	1.15	0.79	0.78
Ramachandran favored (%)	96.81	98.79	96.41	96.81
Ramachandran allowed (%)	2.79	1.21	3.59	3.19
Ramachandran outliers (%)	0.40	0.00	0.00	0.00
Rotamer outliers (%)	0.00	0.48	0.00	0.00
Clashscore	5.31	4.37	6.54	7.53
Average B-factor	17.18	24.08	17.96	13.35
macromolecules	15.90	22.91	16.88	12.21
ligands	14.40	-	14.00	10.04
solvent	25.56	33.08	25.62	21.12

Statistics for the highest resolution shell are shown in parentheses.

Table Appendix2: Data collection and refinement statistics for the structures of HisF Y39F, V48A and H228A

Protein	**HisF Y39F**	**HisF V48A**	**HisF H228A**
Wavelength (Å)	0.99	0.99	0.99
Resolution range (Å)	37.97 - 1.198 (1.241 - 1.198)	35.18 - 1.197 (1.239 - 1.197)	38.02 - 1.199 (1.242 - 1.199)
Space group	C 1 2 1	C 1 2 1	C 1 2 1
Unit cell	79.5, 44.3, 63.5, 90, 111.9, 90	79.5, 44.3, 63.8, 90, 112, 90	79.6, 44.4, 64, 90, 112, 90
Total reflections	407485 (35010)	407827 (35614)	390335 (31914)
Unique reflections	59272 (5358)	64855 (6196)	59212 (5203)
Multiplicity	6.9 (6.5)	6.3 (5.5)	6.6 (6.0)
Completeness (%)	91.84 (84.22)	99.56 (96.47)	91.14 (81.19)
Mean I/sigma(I)	24.01 (7.23)	39.00 (14.45)	18.16 (8.90)
Wilson B-factor	10.12	9.10	7.03
R_{merge}	0.04715 (0.2115)	0.02752 (0.1023)	0.07756 (0.2065)
R_{meas}	0.05107 (0.2301)	0.02994 (0.1134)	0.08429 (0.227)
R_{pim}	0.01937 (0.08936)	0.01162 (0.04746)	0.03251 (0.09239)
$CC_{1/2}$	0.999 (0.978)	0.999 (0.992)	0.995 (0.966)
CC*	1 (0.994)	1 (0.998)	0.999 (0.991)
Reflections used in refinement	59214 (5357)	64632 (6196)	59103 (5194)
Reflections used for R_{free}	2011 (180)	1989 (197)	1985 (169)
R_{work}	0.1880 (0.2020)	0.1870 (0.2047)	0.1940 (0.2507)
R_{free}	0.2043 (0.1905)	0.1978 (0.2241)	0.2093 (0.2549)
CC_{work}	0.956 (0.908)	0.954 (0.902)	0.945 (0.826)
CC_{free}	0.946 (0.941)	0.933 (0.900)	0.944 (0.766)
Number of atoms	2283	2283	2313
macromolecules	1959	1958	1955
ligands	10	10	10
solvent	314	315	348
Protein residues	255	255	255
RMS (bonds)	0.005	0.005	0.005
RMS (angles)	0.80	0.78	0.76
Ramachandran favored (%)	96.81	96.41	96.81
Ramachandran allowed (%)	3.19	3.59	3.19
Ramachandran outliers (%)	0.00	0.00	0.00
Rotamer outliers (%)	0.00	0.00	0.00
Clashscore	5.78	6.29	6.04
Average B-factor	14.90	13.45	12.57
macromolecules	13.59	12.13	11.06
ligands	12.06	10.06	9.86
solvent	23.21	21.82	21.13

Statistics for the highest-resolution shell are shown in parentheses.

Table Appendix3 Data collection and refinement statistics for the ImGPS complex structures

Protein Complex	ImGPS fD98E	ImGPS fD98E hC84S + ProFAR/Gln	ImGPS h310Δ13
Wavelength (Å)	0.99	0.99	0.99
Resolution range (Å)	43.36 - 1.486 (1.539 - 1.486)	45.69 - 1.784 (1.848 - 1.784)	47.27 - 2.811 (2.912 - 2.811)
Space group	P 2_1 2_1 2_1	P 2_1 2_1 2_1	P 3_2
Unit cell	76.4, 76.6, 86.7, 90, 90, 90	75.312 76.596 86.941 90 90 90	94.5, 94.5, 166.3, 90, 90, 120
Unique reflections	83160 (8207)	48477 (4719)	40292 (3967)
Wilson B-factor	18.70	28.66	78.89
Reflections used in refinement	82925 (8205)	47031 (4265)	40292 (3967)
Reflections used for R_{free}	1988 (198)	1956 (172)	2014 (199)
R_{work}	0.2274 (0.3558)	0.1834 (0.3386)	0.1759 (0.2843)
R_{free}	0.2513 (0.3793)	0.2190 (0.3820)	0.2420 (0.3510)
Number of non-hydrogen atoms	4059	3854	10456
macromolecules	3510	3530	10456
ligands	4	23	
solvent	545	301	
Protein residues	446	448	1339
RMS(bonds)	0.007	0.006	0.009
RMS(angles)	1.23	0.77	1.18
Ramachandran favored (%)	97.27	97.51	91.40
Ramachandran allowed (%)	2.51	2.27	6.34
Ramachandran outliers (%)	0.23	0.23	2.26
Rotamer outliers (%)	0.26	0.00	0.36
Clashscore	9.33	6.48	16.75
Average B-factor	27.19	34.59	91.50
macromolecules	25.83	33.92	91.50
ligands	23.88	45.86	-
solvent	35.98	42.42	-

Statistics for the highest-resolution shell are shown in parentheses.

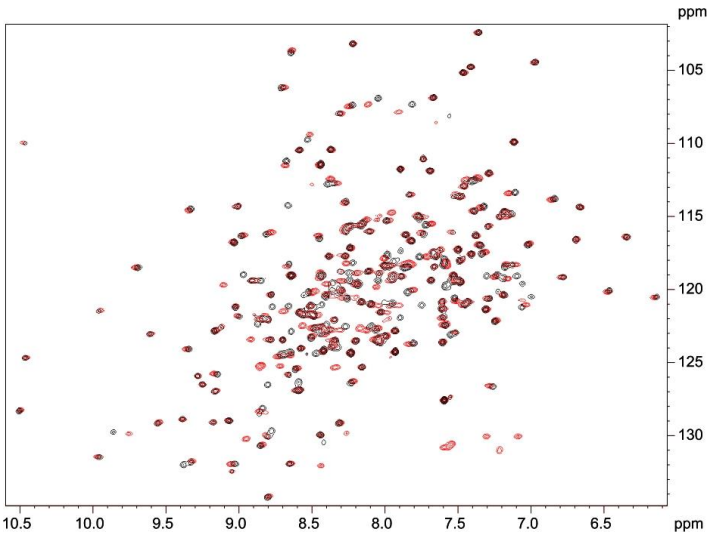

Fig. Appendix 1: H^{1}-N^{15}-TROSY Spectra of wild-type HisF and HisF C9S E24C. The direct comparison of the spectra of wild-type HisF (black) and HisF C9S E24C (red) shows that there are small chemical shift perturbations caused by the two mutations. This highlights that loop1 exerts an influence over the entire protein.

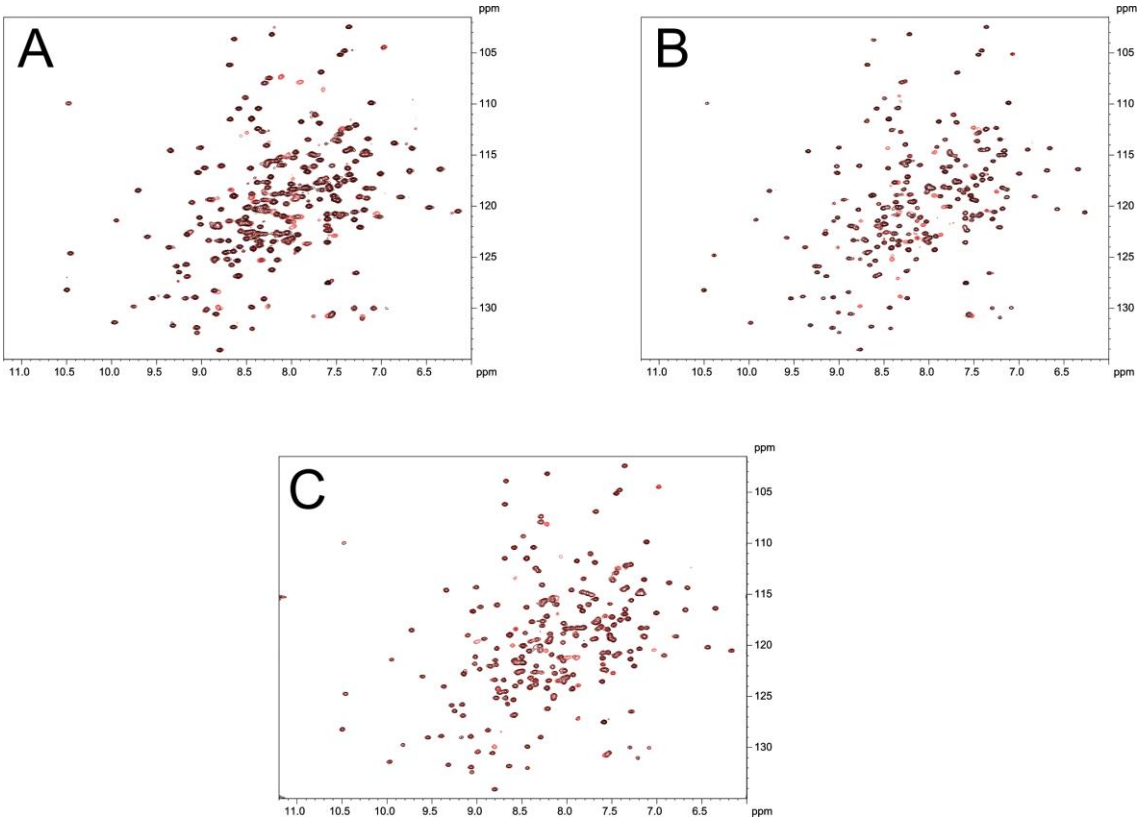

Fig. Appendix 2: Spectra of M-TEMPO-labelled HisF variants before and after reduction. Spectra were recorded in the labelled form before (black) and after (red) reduction with ascorbate. The re-appearance of missing peaks indicates that they were indeed attenuated by the proximity of the spin-label. **(A)** HisF C9S E24C (wild-type model). **(B)** HisF C9S E24C F23A. **(C)** HisF C9S G20P E24C.

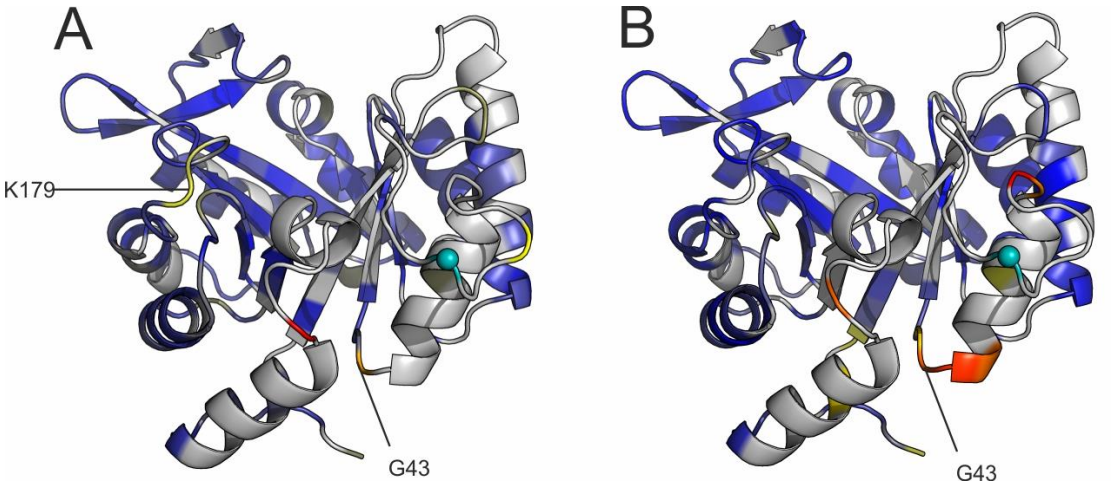

Fig. Appendix 3: PRE in HisF proteins with mutations altering loop1 dynamics. Cartoon representation of the wild-type HisF structure (PDB-code 1VH7) coloured according to the measured relative peak integrals observed in H^1N^{15}-TROSY spectra. The applied range is from 0 to 1.12 (maximum observed relative value) and is colour coded red (low values, high PRE) via yellow to blue (high values, low PRE). Grey colouring signifies a change in chemical shift of the respective residue relative to wild-type HisF caused by mutations made for labelling. These residues cannot be assigned to a specific signal without further experiments. The position of the M-TEMPO spin label is marked by a cyan sphere at the position of the Cα of C24. PRE measured for **(A)** HisF C9S E24C F23A and **(B)** HisF C9S G20P E24C.

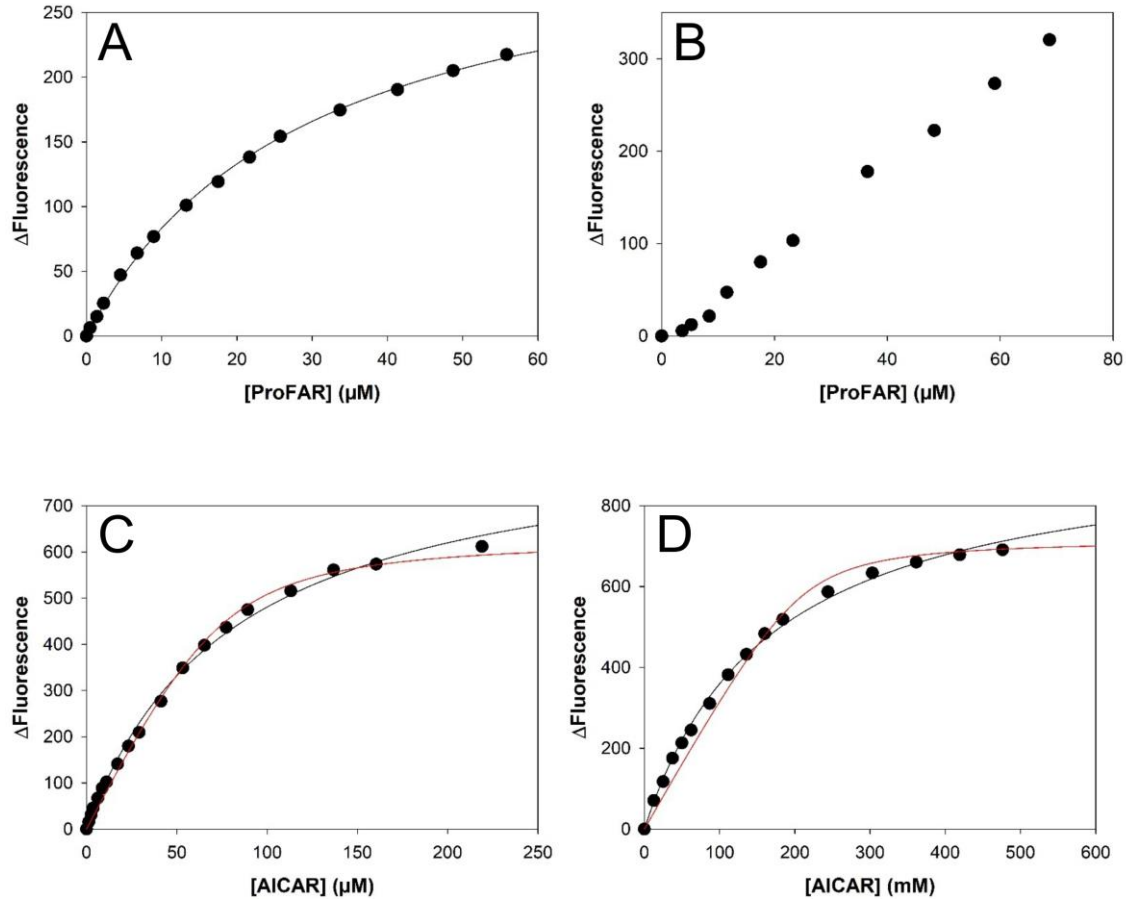

Fig. Appendix 4: Fluorescence titrations using HisF residue W156 as probe. All measurements were carried out in 50 mM Tris/acetate pH 8.5 with 10 µM HisF wild-type or free tryptophan. Fluorescence was excited with light with a wavelength of 295 nm and emission followed at 327 nm. Data were corrected for dilution and plotted against ligand concentration in the cuvette. Red lines represent a fit to equation (4), black line a fit to equation (5). **(A)** Titration of HisF with ProFAR. **(B)** Titration of free tryptophan with ProFAR. **(C)** Titration of HisF with AICAR. **(D)** Titration of free tryptophan with AICAR.

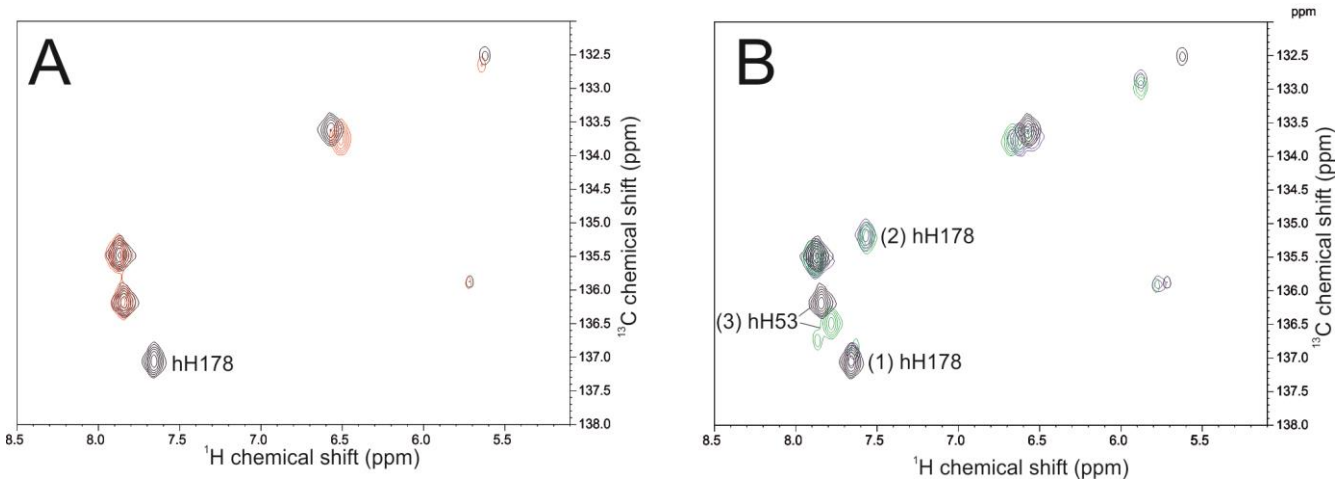

Fig. Appendix 5: Identification of NMR peaks of labelled histidine residues in HisH by mutation. (A) Comparison of HQSC spectra of ImGPS with the mutations C84S (black) and hC84S/hH178A (red) identified the labelled peak as that of hH178. (B) Comparison of HQSC spectra of ImGPS with the mutation hC84S in the apo state (black) and in the presence of ProFAR and glutamine (green) with ImGPS with the mutations hC84S and hH52A show that the peak of hH178 shits from peak (1) to peak (3), while the peak with the smaller shift (3) is that of hH52.

7 Acknowledgements

As in every scientific work, the results presented here were only possible because the experimenter, that is, me, had help from many different people. Almost none of the insights that were gained in these years of work would have been possible had I had to work on my own. For all of this help, large or small, I am deeply thankful.

First and foremost, I have to thank my mentor, Prof. Dr. Reinhard Sterner, who welcomed me into is lab without even knowing who I was. Through the years, he has always been there with good advice and a lot of patience for a project that, even after quite some time, looked like it would not produce much in the way of useful results. Most of all, I am thankful for his support of my personal way after my work in his lab. In my personal opinion, his support of all the people who have worked in his group, irrespective of their personal plans, preferences and goals and their alignment with his own, makes him an extraordinary mentor, not only in science, but in live.

A close second in people supporting this thesis is Dr. Andrea Kneuttinger, whose support was given is so many aspects that I cannot even list them all. She was my source of inspiration in the field of unnatural amino acids, which made almost half of the thesis possible in the first place. The invaluable discussions with her inspired many experiments and gave me perspective on the results. She even measured some of the data shown in this thesis herself. Finally, she provided me with incredible help in bringing all the information into a written form that other people can understand it.

A special thanks goes to Prof. Remco Sprangers and Prof. Rainer Merkl, who also were mentors of my thesis and always had good suggestions in discussions of my work.

Probably one of the most important people for the interpretation of my results was Dr. Sandra Schlee, who is the real expert on transient enzyme kinetics. Without her expertise on the mathematical analysis as well as the interpretation of the resulting values and models, gaining meaningful insights from the kinetic experiments would have been difficult indeed.

The context and some of the key conclusions of this thesis were only possible through several cooperation projects. Dr. Jan-Philip Wurm and Prof. Remco Sprangers lend their great expertise in the field of NMR spectroscopy. They also showed great patience with this project, which has taken up much time in their spectrometers even before producing usable results. Dr. Chitra Rajendran helped in solving an amazing amount of crystal structures, doing all the travelling to the synchrotron and data analysis on her own. Finally, Dr. Magdalena Schumacher and Prof. Heinz-Jürgen Steinhoff enabled the measurement on loop dynamics via EPR.

People who always get too little credit are our incredible technicians, Jeannette Ueckert, Sabine Laberer and Sonja Fuchs. Without their dedicated, highly professional and not least of all hard work, none of the projects I have witnessed would have been possible in the form they were done. Thank you for everything!

I also want to thank all the students I have had the pleasure of working with in the lab, even most of the data did not make it into this thesis. In particular, I want to thank Alisa Ruisinger, who brought the investigation of loop1 a good deal forward, and Leon Babel, who pioneered the measurements with CouA.

Finally, I want to thank everyone I have worked with in the Sterner group. Dr. Michael Schupfner was a particular help in mastering the every-day peanut-butter-jelly-time. Dr. Alexandra Holinski did some great work in topic of ImGPS and introduced me to the field, which helped my start along very much. Our bio-informatics specialists, Dr. Kristina Heyn, Julian Nazet and Leonhard Heizinger provided me with great discussions and put in a lot of work on ImGPS, none of which, unfortunately, has made it into this thesis. Sorry for that guys, but it wasn't meant to be. Dr. Florain Semmelmann was a good partner in the investigation and discussion of GATases in

general. Thanks goes to him for doing the most work for and writing the paper on the conserved aspartates in GATases as well as for valuable discussions. Finally, I want to thank everyone else that I have not mentioned by name, both present and previous members of the Sterner group for creating a great atmosphere of support and a good working environment.